INTERNATIONAL STUDIES IN

SCIENCE AND MATHEMATICS

June 2023

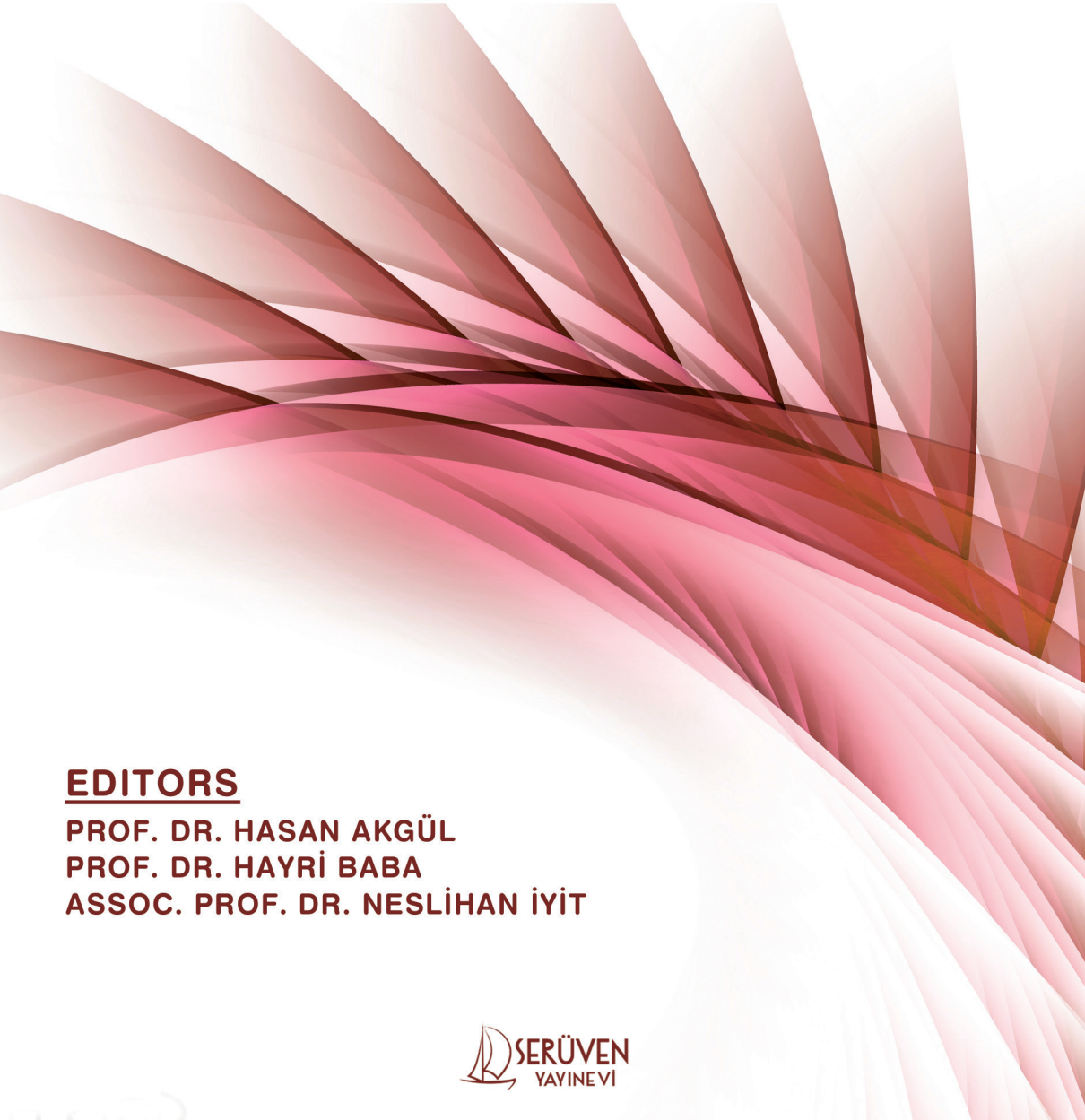

EDITORS

PROF. DR. HASAN AKGÜL
PROF. DR. HAYRİ BABA
ASSOC. PROF. DR. NESLİHAN İYİT

SERÜVEN YAYINEVİ

Genel Yayın Yönetmeni / Editor in Chief • C. Cansın Selin Temana

Kapak & İç Tasarım / Cover & Interior Design • Serüven Yayınevi

Birinci Basım / First Edition • © Haziran 2023

ISBN • 978-625-6450-60-8

Serüven Yayınevi / Serüven Publishing
Türkiye Adres / Turkey Address: Kızılay Mah. Fevzi Çakmak 1. Sokak
Ümit Apt No: 22/A Çankaya/ANKARA
Telefon / Phone: 05437675765
web: www.seruvenyayinevi.com
e-mail: seruvenyayinevi@gmail.com

Baskı & Cilt / Printing & Volume
Sertifika / Certificate No: 47083

INTERNATIONAL STUDIES IN SCIENCE AND MATHEMATICS

June 2023

Editors
PROF. DR. HASAN AKGÜL
PROF. DR. HAYRİ BABA
ASSOC. PROF. DR. NESLİHAN İYİT

CONTENTS

Chapter 1

SCIENTIFIC STUDY OF PARTICLE NAMES

Çağın KAMIŞCIOĞLU[1]

1 Ankara University, Faculty of Engineering,
Physics Engineering Department, Ankara, Türkiye
Assoc. Prof. Dr. Çağın KAMIŞCIOĞLU, ORCID:0000-0003-2610-6447

1. Introduction

Physics is the science that tries to understand, model, and explain the natural phenomena in the universe through examination, research, and observation. The science of physics is divided into various sub-branches within itself. One of them is particle physics, which has developed rapidly in recent years. Particle physics aims to understand the fundamental constituents of matter and their interactions. In other words, it is the science of the smallest particle. These are called subatomic particles. Subatomic particles combine among themselves to form the earth, stars, other planets, and eventually the entire universe. As a result of research, experiments, and investigations in this field, new information is gained about the behavior, interactions, and properties of subatomic particles. Thus, it is tried to determine what the basic components that make up the universe are, to define, reconstruct and decompose in a controlled way (Kamışcıoğlu, 2017, 2020, 2022).

The quality of the information produced in such an important area for understanding the universe and the state of the scientific language used are very important in terms of giving students scientific thinking, attitude, and behavior. As it is known, science is the body of systematic and proven knowledge with objective soundness obtained through various research and experiments. The process of producing knowledge is based on both research and experimentation. It examines the phenomena in a field through controlled research, experiment, or observation and finds the relationships between them. Based on the results obtained, theories, laws, and models are developed. These are called scientific knowledge. Various words, concepts, terms, formulas, tables, figures, pictures, etc. are used to present scientific information. Among these, words, concepts, and terms have a special importance.

A word is a sound or unit of sound or a word that has meaning. The concept is explained in the TDK Current Turkish Dictionary as “the abstract image, meaning or meaning a load of an object, event or thought in the mind”. The concept is also “the general design that covers the common features of objects or events and gathers them under a common name” (TDK, 2023). Concepts are expressed with words and have some meaningful, abstract, and scientific features. It is carefully chosen to explain a subject well and to prevent ambiguity or lack of meaning. Scientists describe research, experiments, observations, and events in the field with concepts. Therefore, the concept forms the basis of scientific studies. The term, on the other hand, is “the word that corresponds to a specific and specific concept related to a science, art, profession or a subject” (TDK, 2023). In other words, concepts specific to a branch of science are called terms.

As can be seen, words, concepts, and terms are the building blocks of scientific language. It plays an important role in the development of a branch

of science. All research, experiments, and innovations in the field are necessary to explain well to future generations. For this reason, the concepts and terms used in the branches of science should be chosen by scientific rules. In other words, it is necessary to name the objects, elements, methods, tools, and materials used in the science branch correctly. Naming has special importance in the identification process and guides the explanations. Because the given name indicates or directly characterizes the quality of the object, event, or thought it represents. A Chinese proverb says, "Correct naming is the highest science of science". In this respect, it is necessary to choose scientific words that help to understand, recognize and distinguish the relevant object, event or thought correctly in the naming process. This is also important in terms of the names given to the particles discovered in particle physics.

In this research, the question that is tried to be answered is "What names are given to the particles discovered in particle physics?". How are particle names chosen to teach future generations the knowledge, research, experiments, and developments in particle physics? What methods and techniques are used? Is there a harmony between the names of the particles and their properties? Do the names given to the particles change according to the periods? Is the choice of particle names by scientific rules? This research was born out of such a need.

2. Method

In the research, scientific resources, journals, and internet resources that can be accessed on particle physics were first searched. Various resources such as research, experiments, documents of international organizations such as CERN(Conseil Européen pour la Recherche Nucléaire), publications, reports, and physics teaching programs related to particle physics in our world have been discussed. To determine the scientific status and development of particle names, all particles discovered from 1800 to 2022 were included in the research. In this process, the names given to the particles and the explanations about the names were examined in detail from the scientific point of view.

The document analysis method, one of the qualitative research methods, was chosen for the research. Document review is a research method used to analyze the content of written documents rigorously and systematically (Wach & Ward, 2013). The research data are taken from scientific sources in the field. Since all of these were included in the study, it was not necessary to take a sample. At the stage of data collection, the names given to the particles were listed in the Word program, the explanations about the names were listed, they were divided into periods, tables related to the data were created and the findings were transferred to the tables and interpreted.

3. Findings

To determine the scientific status of particle names, the names of all particles discovered from 1800 to 2022 were examined scientifically. As a result of this analysis, four different periods formed. In the first period, it is seen that Greek names were given to the particles based on ancient understanding. In the second period, a large number of particles were discovered, and instead of naming each, they were listed alphabetically. However, the letters of the Greek alphabet are used in ordering the particles. Some are named with the sign of the letters and some with the pronunciation. Then the term "particle zoo" was used. In the third period, particle names started to change again. Daily, unusual, and exotic names were chosen with a romantic understanding. For example, particles have been given names such as strange, charm, beauty, top, bottom, up, and down. In the fourth period, particle families were created based on the family approach. Thus, a more scientific understanding was adopted in the naming process. These developments are given in Table 1 below according to the periods.

Table 1. Naming periods and approaches

Periods	Approaches	Particle Name Examples
1.Period	Ancient Approach	electron, proton, baryon…
2. Period	Alphabetical Approach	α, β, γ , Δ, μ, Φ, Σ, Λ…
3. Period	Romantic Approach	up, down, charm, strange, top, and bottom
4. Period	Family Approach	Particle families, 1. Family, 2. Family, 3. Family…

3.1. First Period: The Ancient Approach

The first period of naming studies in particle physics is seen between the years 1800-1930. Physicists living in this period generally gave Greek names to particles to be compatible with the philosophy of science. In the naming process, a relationship was established between the name given and the quality of the relevant particle, and attention was drawn to common and similar aspects (Marleau, 2007). For example, atom, electron, proton, baryon, gluon, meson, lepton, hadron, neutron, neutrino, and photon. These are briefly explained below.

Atom: The word atom, which dates back to ancient times, is derived from the word "atomos". The Greek philosopher Democritus used this word, which means indivisible in Greek, in the 5th century BC, and suggested that the atom consists of very small particles. This idea of Democritus continued to exist until the 1800s (Arnaud,2015; Crespo-Anadon, 2017).

Electron: Discovered by Joseph John Thomson in 1897. It comes from the Greek word "electros" meaning yellow amber. Amber (a fossilized resin) is easily charged with static electricity when rubbed with a cloth. Since ancient times, rubbed yellow amber was known to release electricity. Joseph John Thomson discovers the electron and creates a model in which the atom is defined as a charge-neutral entity (Crespo-Anadon, 2017; Khalatbari,2015).

Proton: Proton means "first" in Greek. It is one of the first particles described in physics. Ernest Rutherford proved the existence of the proton in 1918 and gave it this name. Proton is a nucleon. Together with the neutrons, it forms the nucleus of the atom. The electric charge is +1 inverse of the electron. The mass of the electron is 2,000 times less than that of the proton (Futura-sciences, 2023).

Baryon: Particles made up of three quarks are called baryons. The word baryon comes from the Greek "barus" meaning heavy. The three categories of particles known in the 1950s are leptons, mesons, and baryons, corresponding to the Greek words for "light", "medium" and "heavy." Baryons are heavy particles. The lightest particle of this family is the proton. A proton consists of 3 quarks, 2 u, and 1 d quark. Neutrons consist of 3 quarks, 2 d, and 1 u quark. The quarks determine the charge of the particles. The u quark has a charge of +2/3, and the d quark has a charge of -1/3 (Futura-sciences,2023; MEB, 2018).

Gluon: A gluon is a boson. The name gluon comes from the word "glue". As the name suggests, gluons, which are much stronger than other interactions, enable "gluing" quarks together with strong interaction (Futura-sciences, 2023).

Meson: Double quark groups are called mesons. Mesons were first discovered by the Japanese physicist Hideki Yukawa and named "mesotron". This word is derived from the Greek words "mesos" meaning middle and "electron". However, German physicist Werner Heisenberg, one of the important names in quantum mechanics, argued that this term is not appropriate and changed mesotrons to "meson". All mesons consist of a quark and an antiquark. Antiquarks are similar to quarks in terms of mass and spin, but their electric charge is the opposite of quarks. The symbol of the antiquark is represented by putting a line on the letters ((Futura-sciences,2023; Khalatbari,2015; MEB, 2018).

Lepton: Unlike quarks, fermions that can be found freely in nature are called leptons. Lepton is derived from the Greek word "leptos" meaning small and light (Marleau, 2007). The most well-known example of particles in this group is the electron. There are three generations of leptons, tau, muon, and electron, in order from largest to smallest by mass. Each has a corresponding neutrino. Neutrinos are uncharged and have almost no mass so they hardly interact with anything. All leptons also have antiparticles (Futura-sciences, 2023; MEB, 2018).

Hadron: A hadron is a composite particle made up of quarks. There are two types of hadrons. These are baryons and mesons. The name Hadron means "strong" in Greek. Hadrons are named so because, unlike leptons, they are particles sensitive to strong interaction (Futura-sciences, 2023).

Neutron: The neutron was discovered in 1932, its mass was close to that of a proton, but it was named a neutron because it is electrically neutral. Between leptons and baryons, there are intermediate Greek mesons such as pions (Crespo-Anadon, 2017).

Neutrino: Wolfgang Pauli discovered a new, very light, and neutral particle in 1930. He called it the neutrino. In Italian, the small neutral will be a lepton. Leptons are subject to only weak and electromagnetic forces, distinguishing them from Greek thick hadrons, which are subject to strong force (Vannucci, 2019).

Photon: Photon is a boson. It is the particle that transmits electromagnetic interaction. It is usually denoted by gamma. The modern origins of the idea of light as a particle date back to 1901. Physicist Max Planck used the expression quanta, which comes from the Latin quantum, meaning "packets of energy". The first known use of the word "photon" was made by physicist Leonard Troland, who used it in 1916 to describe a unit of illumination for the retina. Photon is derived from the Greek word phos, "light", PIE bha "to shine". The photon transmits electromagnetic interaction, light is an example of this (Futura-sciences, 2023; Symmetry Magazine, 2023).

As can be seen, most of the names given to the first-period particles come from Greek. It has been associated with the properties of particles by giving names such as small, light, heavy, medium, light, glue, strong, neutral, and yellow amber in Greek. These are known widely in the area as ancient or historical names. These names were chosen to describe the properties and masses of the particles. In the research carried out in the following years, different properties of the particles were discovered, but these names remained the same. It is still used today.

3.2. Second Term: The Alphabetical Approach

The second-period naming studies in particle physics are seen between the 1930s and 1960s. A large number of particles were discovered during this period. The newly discovered particles are listed in alphabetical order by giving the name or pronunciation of the letters. This order is again made in Greek letters. Thus, almost all Greek letters such as α, β, γ, Δ, μ, Φ, Σ, Λ… were used (Vannucci, 2019). Before long, the term "particle zoo" was coined to explain these particles with different properties, masses, and types. This expression was deprecated with the Standard Model theory in the 1970s.

3.2.1.Greek Letters: In the field of particle physics, researchers discovered many new particles between 1950 and 1960. The letters of the Greek alphabet, signs, and even the pronunciation of some Greek letters such as omega, delta, and epsilon are given. Some of these are listed below by date.

*1946/47: Discovery of pion with charged π± meson ($\pi+ \rightarrow \mu+ + \nu\mu$)

*1948: Artificial production of π+

*1949: Discovery of K+.

*1950: Discovery of the Neutral pion ($\pi\, 0 \rightarrow \gamma + \gamma$).

*1951: Discovery of the "V" events in Brookhaven, New York.

*1952: Discovery of Δ (the excited state of the nucleon).

*1955: Discovery of the antiproton $\bar{p}$.

*1956: Discovery of P violation in 60 Co atoms by Wu and Amber.

*1960/70: Discovery of hundreds of "elementary" particles (ρ, ω, K * , Δ, Ξ, ….)

*1962: Discovery of ν_μ and ν_e.

*1964: Proposal of the existence of u, d, s quarks (Techno-science, 2023).

As can be seen, many particles were discovered in the field of particle physics from 1950 to 1964, and they were usually given Greek letters. These are shown on a historical line in Table 2.

3.2.2.Particle Zoo: A surprising number of particles with different qualities and masses were found in the experiments conducted in the second period. This is called "particle zoo". In the history of particle physics, this was thought to be confusing in the late 1960s. Before the discovery of quarks, hundreds of strongly interacting particles (hadrons) were known and believed to be different fundamental particles. It was later discovered that these were not elementary particles but combinations of quarks. However, it was necessary to classify and order these particles. In particle physics, the term particle zoo was used to describe the relatively broad list of known subatomic particles, compared to the diversity of species in a zoo. The term "underground zoo" was coined by Robert Oppenheimer in 1956 VI. It was used at the Rochester International Conference on High Energy Physics and subsequently expanded (Particle_zoo,2023). This expression is also used as "particle universe or world" in some sources. In some sources, visual examples are given by associating the properties and mass of particles with animals (Arnaud, 2015). The term Particle Zoo was deprecated after the Standard Model Theory was created in the 1970s. Because it has been seen that these particles, which are in large numbers, are the result of the combination of a small number of fundamental particles. The particle zoo image is given in Figure 1 below.

As seen in Figure 1, the particles were matched with pictures of creatures such as ducks, penguins, squirrels, ants, cows, cheetahs, gorillas, and mice. Connections have been established between their properties and the properties of particles. Attention was drawn to the characteristics of various living things such as weight, lightness, and agility.

Table 2. Discovery years and names of second-period particles (Arnaud,2015).

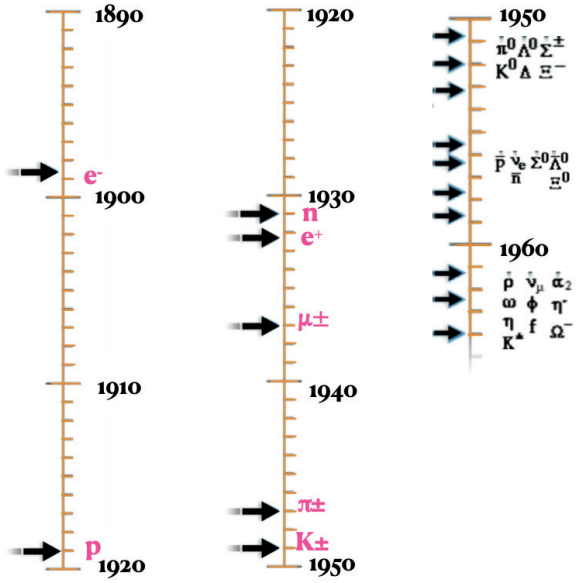

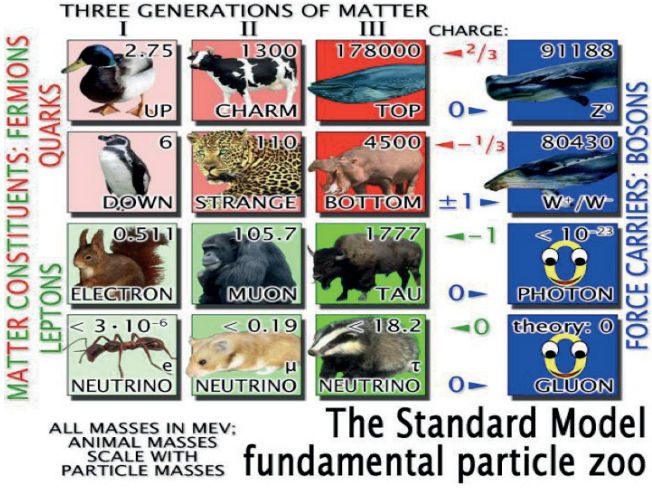

Figure 1. Particle Zoo (Arnaud,2015).

3.3. Third Period: The Romantic Approach

The third period of naming studies in particle physics emerged between the years 1960-1985. In this period, the names given to the particles began to differ from the previous ones. Instead of continuing the practices of previous years, the scientists of this period chose unusual, foreign, exotic, and easy-to-understand names in everyday language with a romantic understanding. For example, particles have been given various names such as strange, charm, beauty, top, up, down, and bottom. The fact that the newly discovered particles have different properties from the previous ones has also been effective in this naming. For this reason, different and remarkable names were preferred. These are described below.

3.3.1.Strange Particles: This name was given to explain that some particles discovered by Gell-Mann and Nishijima in the 1960s have strange and elusive properties. Later they were also called "strange particles" and "quark (s)". Over time it has become one of the fundamental particles of the standard model of particle physics. These particles were produced in copious pairs in experiments but degraded much more slowly than expected. Because of these features, they were also called "odd" to refer to their "strange" longevity. Strange particles were important for establishing the quark theory and contributed to understanding the two quarks u and d, proton (uud) and neutron (udd), and pions (anti-u, anti-d) with +2/3 and -1/3 charges (Gell -Mann, 1953; Nishijima, 1955).

3.3.2.Charm Particles: These are named "attractive, charming, beautiful, enchanted, cute, mysterious particles, charm quark(c)". It is one of the second-generation quarks along with the strange particles. It makes up the third-largest mass of all quarks. It is also one of the fundamental particles of the standard model. Charm quarks are found in hadrons, which are subatomic particles made of quarks. These were observed by some researchers in 1964, but their discovery was attributed to Sheldon Glashow, John Ipoulus, and Luciano Maiani in 1970. Glashow in this regard; "We named the particle the 'charming quark' because we were fascinated and delighted by the symmetry it brings to the subnuclear world." It means. The first charmed particle (a particle containing a charmed quark), the J/ ψ meson, was discovered by a team in 1974 (Glashow, Iliopoulos & Maiani, 1970).

3.3.3. Other Particles: Are there any other strange particles? Two families of particles are produced from quarks: mesons, which combine a quark and an antiquark, and baryons, which consist of three quarks such as a proton or neutron. Kaons exhaust their possibilities to form new mesons with the first known quarks. For baryons, an additional quark introduces a host of new connotations; the only restriction is to restore a full electrical charge. So we can imagine combinations: sud, suu, sdd, ssd, ssu, sss. He determined Λ^0, Σ^-,

Σ^0, Σ^+, Ξ^-, Ξ^0 in cosmic rays that responded to the first associations.

In the following years, a series of experiments were carried out in the field to reveal the still missing quarks. After these studies, the bottom quark (b) and top quark (t) was discovered. Today it is known that the quark list is complete. All particles are therefore treated as more or less complex relationships between six different quarks and six different quarks. Thus, the formation of atoms and molecules, that is, all ordinary matter, is explained by the particles responsible for leptons and force fields. Their discovery years are given in Table 3 below.

3.3.4.Quarks: A quark is an elementary fermion that is susceptible to strong interaction. It creates hadrons. There are six types of quarks. These are listed as up quark (u), down quark (d), strange quark (s), charm quark (c), bottom quark (b), and top quark (t). Quarks are fundamental components of matter. They come together to form hadrons, that is, baryons such as protons and neutrons (mesons made up of three quarks–and quark-antiquark pairs) (Traczyk, 2021). Quarks are fundamental particles that make up hadrons, such as protons and neutrons, and more exotic particles and states of matter, such as quark-gluon plasma. Murray Gell-Mann and George Zweig formerly called these particles "aces" (Gell-Mann, 1964; Zweig, 1964). However, later Gell-Mann called them "quarks". It is suggested that the name quark is taken from the novel by James Joyce (Finnegan's Wake) and means cheese (Futura-sciences, 2023). Gell-Mann, on the other hand, wrote the following about the quark in his book "The Quark and the Jaguar" published in 1994;

"In 1963, I first gave the word "kwork" to the basic components of the nucleon. Then, while reading James Joyce's novel Finnegan's Wake, I came across the word "quark" in the phrase "Three Quarks for Muster Mark." The number three matched perfectly with the way quarks occur in nature. Some scholars argue that the quark in Joyce's epic is derived from the German word for quark, a type of curd cheese. The German word quark was probably taken from a West Slavic word meaning "to shape". This word potentially refers to the solidification of milk and turning it into curd. However, the word quark that I use should be considered as a non-dairy particle that emerges as the main component of matter" (Gell-Mann, 1994).

Table 3. Discovery years and names of third-period particles (1960 -1990)

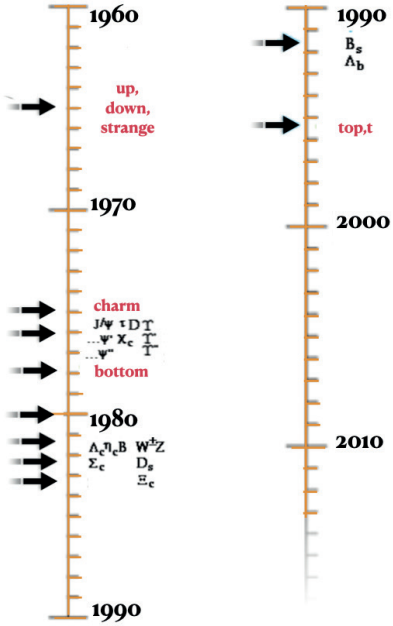

As can be seen, Murray Gell-Mann explains that the word quark does not come from the word cheese. The names and basic properties of quarks discovered in the third period in the field of particle physics are given in Table 4.

3.4. Fourth Term: The Family Approach

The fourth-period naming studies in particle physics date back to 1985. The names given to particles in the recent period have been handled with a more scientific understanding compared to the previous period. In this period, the family approach was adopted, "particle families" were formed, and newly discovered particles were placed in these families as a matrix. This process is described below.

Particle Families: Several new particles were discovered in the field of particle physics between 1800 and 2020. These were named with Greek names, letters, signs, and romantic names in previous years. However, in recent years, the idea of family has been put forward to better explain them. Thus, elementary particles are divided into three families under the name of particle families. The newly discovered particles are planned to be added to these families, such as newborn children. These three family understandings are basic parameters of the Standard Model (Arnaud, 2015).

Table 4. Quark names and properties

Quark	Symbol	Spin	Charge	Baryon Number	S	C	B	T	Mass
Up	U	1/2	+2/3	1/3	0	0	0	0	1.7-3.3 MeV
Down	D	1/2	-1/3	1/3	0	0	0	0	4.1-5.8 MeV
Charm	C	1/2	+2/3	1/3	0	1	0	0	1270 MeV
Strange	S	1/2	-1/3	1/3	-1	0	0	0	101 MeV
Top	T	1/2	+2/3	1/3	0	0	0	1	172 MeV
Bottom	B	1/2	-1/3	1/3	0	0	-1	0	4.19 MeV

Particles discovered through familial understanding are arranged in a "matrix" into three families of four particles. The families are presented in the form of a table of mathematical objects, rows, and columns. For example, for the first family, A1, A2, A3, for the last family, C1, C2… C4 is sorted. Thus, scientists wanted to make the developments about particles more understandable by choosing a new way of naming them (Khalatbari, 2015). Particle Families are shown in Figure 2.

As seen in Figure 2, all known elementary particles of matter are given together. There are three columns called "Families". The first family includes particles found around us. The two quarks (u and d) that make up the protons and neutrons in the nuclei of atoms, an electron, and the "electronic" neutrino express its relationship with the electron, etc. given way. Other families were placed in order. Thus, all particles are arranged in three families.

Some authors do not stay with only three families but also establish horizontal and vertical family ties between them. For example, Arnaud (2015) and Mansoulie (2005), "the second and third families are replicas of the first, containing particles of higher mass, the same properties as their sisters in the first column, observed in higher energy reactions, natural (cosmic rays) or artificial (accelerators)" they say (Arnaud, 2015; Mansoulie, 2005). In these statements, it was stated that the second and third families were sisters and the first family.

Michel Davier says that "the muon in the second family is an elementary particle cousin to the electron in the first family, but it is 200 times heavier and transient". Both have the same electromagnetic properties. They behave like small magnets with magnetic moments, the value of which was predicted by British Paul Adrien Maurice Dirac by combining quantum mechanics and special relativity in 1927 (Davier, 2021). As can be seen, researchers have also expressed kinship between particle families such as sister and cousin.

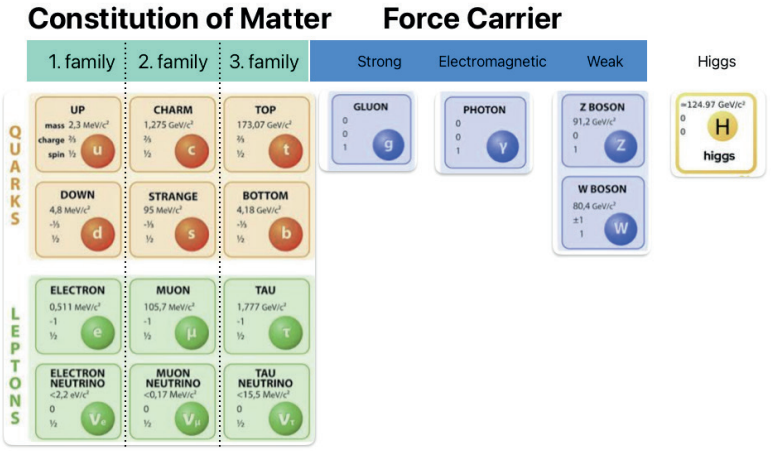

Figure 2. Particle Families

4. Conclusion

Particle physics is one of the rapidly developing branches of science in recent years. It is necessary to name the concepts and terms correctly to explain the research, experiments, and innovations in this field to future generations. Correct naming is very important to describe an event, thought, entity, or object and explain its properties. For this reason, the names given to the concepts and terms should be chosen scientifically. As it is known, concepts and terms are the cornerstones of particle physics. These make it easier to understand, learn, question, and place in the mind the developments and innovations in the field.

In this research, the names given to the particles discovered from 1800 to 2022 in particle physics were examined in detail from the scientific point of view. As a result of the examination, we came across four different periods in the naming process. In the first period, Greek names were given to particles based on the ancient approach. In Greek, names such as small, light, heavy, medium, light, and yellow amber were given and particles were associated with their properties. In the second period, many new particles were discovered and instead of naming the particles, they were listed alphabetically by giving the name or pronunciation of the letters. The letters and signs of the Greek alphabet were used in the ordering. Then, the term particle zoo was introduced and the properties of the particles were matched with the characteristics of the animals. In the third period, the old understanding of particle names has completely changed and the exotic understanding

has left its place, and the particles have been given names such as strange, mysterious, charm, and beauty. These are grouped under the name of quarks. In the fourth and last period, particle families have been created with the familial approach in order to better explain the particles. All known elementary particles are arranged in a matrix, with four particles in each family. In this process, the discovery of a surprising variety of particles and the basic understanding of the Standard Model Theory were effective. Thus, it was tried to make the particles scientifically clear, clear, and easy to understand, to determine their names by scientific rules, and to teach future generations well about research, experiments, and innovations in the field.

REFERENCES

Arnaud,N.(2015). Introduction à la physique des particules, Laboratoire de l'Accélérateur Linéaire, CNRS/IN2P3 & Université Paris-Sud.

Crespo-Anadon,J.I.(2017).Particle Physics: History of Particle Physics, Columbia University Science Honors Program Davier, M.(2021). Particle physics: will muons uncover new fundamental physics? cnrs.fr https://www.cnrs.fr › particle... adresinden erişilmiştir.

Futura-sciences (2023). Lexique de la matière : particule, fermion, gluon, quark,Higgs…,futura-sciences.com, https://www.futura-sciences.com › ... adresinden 12.02. 2023 erişilmiştir.

Gell-Mann, M.(1953). Isotopic Spin and New Unstable Particles, Physical Review, vol. 92, (3), 833. (DOI 10.1103/PhysRev.92.833, Bibcode 1953PhRv...92..833G)

Gell-Mann,M.(1964). A Schematic Model of Baryons and Mesons, Physics Letters, 8 (3), 214–215.(DOI 10.1016/S0031-9163(64)92001-3)

Gell-Mann, M.(1994). The quark and the jaguar: adventures in the simple and the complex, Publisher: New York

Glashow, S.L. Iliopoulos, J., Maiani, L. (1970). "Weak Interactions with Lepton–Hadron Symmetry". Physical Review D. 2 (7): 1285–1292. Bibcode:1970PhRvD...2.1285G. doi:10.1103/PhysRevD.2.1285

Khalatbari,A.(2015). Quark, méson, kaon... d'où vient le nom des particules, sciencesetavenir,fr/, https://www.sciencesetavenir.fr ›adesinden erişilmiştir.

Kamışcıoğlu, Ç. (2017). OPERA Dedektöründeki Nötrino-Kurşun Yüklü Akım Etkileşmelerinde Hadron Çokluk Dağılımlarının İncelenmesi, (Yayımlanmamış doktora tezi). Ankara Üniversitesi, Fen Bilimleri Enstitüsü, Ankara.

Kamışcıoğlu, Ç. (2020). Parçacık Fiziğindeki Gelişmeler ve Yönelimler, Güncel Fen Bilimleri Çalışmaları, Ankara: Akademisyen Kitabevi A.Ş.,E-ISBN 978-605-258-877-2, 1.Baskı

Kamışçıoğlu, Ç. (2022). Investigation of High School Textbooks in terms of Particle Physics. Parçacık Fiziği Açısından Lise Ders Kitaplarının İncelenmesi. The Journal of Limitless Education and Research, Sınırsız Eğitim ve Araştırma Dergisi, 7(1), 131 - 167. DOI: 10.29250/sead.1084862

Mansoulie,B. (2005). la physique des particules, La Jaune Et La Rouge,No:604,https:/ www.lajauneetlarouge.com/auteur/bruno-mansoulie-75

Marleau,L. (2007).Introduction a la physique des particules, Departement de physique de génie physique et d'optique, Université Laval, Québec, Canada

MEB (2018). Talim ve Terbiye Kurulu Başkanlığı Ortaöğretim Fen Lisesi Fizik 12.Sınıf Ders Kitabı, Ankara: Devlet Kitapları

Nishijima, K. (1955). Charge Independence Theory of V Particles, Progress of Theoretical Physics, 13 (3), p. 285 (DOI 10.1143/PTP.13.285)

Particle_zoo (2023). https://en.wikipedia.org/wiki/Particle_zoo.22 Mayıs 2023 tarihinde erişilmiştir.

Symmetry Magazine (2023) https://www.symmetrymagazine.org/article/brief-etymology-particle-physics. 20 Mayıs 2023 tarihinde erişilmiştir.

TDK (2023). Güncel Türkçe Sözlük, Ankara: TDK

Techno-science (2023). https://www.techno-science.net/glossaire-definition/Physique-des-particules. html. 20 Mayıs 2023 tarihinde erişilmiştir.

Traczyk, P. (2021). Twice the charm: long-lived exotic particle discovered, Home,CERN, https://home.cern › physics adresinden 23 mayıs 2023 te erişilmiştir.

Wach, E. & Ward, R. (2013). Learning about qualitative document analysis. https:// opendocs.ids.ac.uk/opendocs/bitstream/handle/20.500.12413/2989/PP%20InBrief%20%2013%20QDA%20FINAL2.pdf?sequence=4. 03.02.2023 tarihinde erişilmiştir.

Vannucci, F.(2019). Muons, kaons et autres leptons : comment leurs noms viennent aux particules, Fête de la science, https://www.fetedelascience.fr/ erişilmiştir.

Zweig,G.(1964). An SU(3) Model for Strong Interaction Symmetry and its Breaking, CERN Report No.8181/Th 8419.

Chapter 2

A COMPUTATIONAL (DFT) STUDY ON AN ANTI-CANCER MOLECULE: GEMCITABINE

Ahmet KUNDURACIOGLU[1]

1 Dr. https://orcid.org/0000-0002-6421-9912

Introduction / Gemcitabine in a nutshell

Gemcitabine (2',2'-difluorodeoxycytidine) is a chemotherapy drug that has been extensively studied and used in the treatment of various types of cancer. As an analog of deoxycytidine, gemcitabine interferes with DNA synthesis and disrupts cell division, leading to apoptosis in cancer cells. The effectiveness of gemcitabine in various solid tumors, including pancreatic, breast, lung, bladder, and ovarian cancers, has been well established in both preclinical and clinical studies [1-4]

However, the use of gemcitabine is not without adverse effects, including myelosuppression, nausea, vomiting, and fatigue, among others (5,6). Therefore, identifying patients who are most likely to benefit from gemcitabine treatment and optimizing the treatment regimen are crucial for its clinical success.

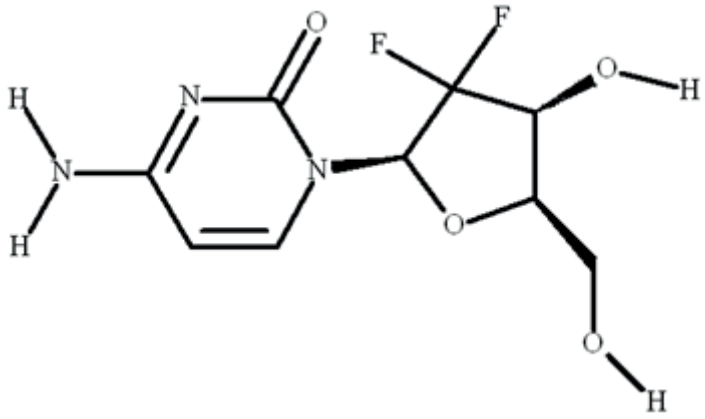

Figure 1. *Molecular formula of Gemcitabine*

In recent years, there has been significant progress in understanding the molecular mechanisms underlying gemcitabine resistance in cancer cells, which has led to the development of new strategies to overcome resistance and improve the efficacy of gemcitabine treatment [7,8].

This article aims to provide a comprehensive review of gemcitabine, including its mechanism of action, clinical applications, potential side effects, and strategies to overcome resistance. We will also discuss recent advances in the use of gemcitabine and its combinations with other therapeutic agents for the treatment of cancer.

While gemcitabine has shown promising results in clinical trials, its efficacy and toxicity can vary greatly depending on the individual patient and the specific cancer type. To better understand the mechanisms underlying

gemcitabine's effects and improve its clinical application, researchers have turned to computational analysis techniques.

Computational analysis of gemcitabine has the potential to provide valuable insights into the drug's pharmacokinetics, pharmacodynamics, and mechanism of action. Using tools such as molecular dynamics simulations, docking studies, and machine learning algorithms, researchers can predict the drug's interactions with biomolecules and identify potential targets for drug development. Additionally, computational approaches can help optimize gemcitabine dosing and predict patient response to treatment.

In this article, we review recent advances in computational analysis of gemcitabine, including studies on drug resistance, drug combination therapies, and personalized dosing strategies. We also discuss the challenges and limitations of computational methods in drug discovery and highlight the need for further integration of experimental and computational approaches. By combining these approaches, we can advance our understanding of gemcitabine's complex pharmacology and improve cancer treatment outcomes.

Computational chemistry has become an increasingly important tool in drug discovery and design, with the ability to provide valuable insights into molecular interactions and properties. In particular, density functional theory (DFT) methods have emerged as a powerful approach to model the electronic structure and properties of molecules, including drugs and their targets[9].

DFT methods offer several advantages over other computational approaches, including their ability to accurately predict the energetics and electronic properties of complex systems with reasonable computational cost. These methods have been used to study a wide range of molecular systems relevant to drug discovery, including protein-ligand interactions, drug metabolism, and drug delivery. Moreover, DFT methods have been used to design new drugs and optimize existing ones by predicting their properties and interactions with target proteins[10].

One of the main applications of DFT methods in drug discovery is the prediction of the binding affinity of a drug to its target protein. This is crucial in the development of new drugs, as it allows researchers to optimize drug structures and predict their efficacy before costly experimental testing. DFT methods can also be used to study the thermodynamics and kinetics of drug binding, providing valuable insights into the binding mechanism and potential allosteric sites.

Another application of DFT methods in drug discovery is the prediction of drug metabolism and toxicity. These methods can be used to predict the reactivity of drugs with various enzymes involved in drug metabolism, such as cytochrome P450 enzymes. This information can be used to optimize drug structures and reduce the risk of toxicity in patients [11].

Overall, computational chemistry, and DFT methods in particular, have become indispensable tools in drug discovery and design. They offer unique insights into molecular interactions and properties that can aid in the development of new drugs and the optimization of existing ones. As computational methods continue to improve, their importance in drug discovery will only continue to grow.

Calculations on Molecular Structure of Gemcitabine

Molecular structure of any molecule is defined by bond lengths, bond angles and torsion (dihedral) angles. These values are experimentally measured via single crystal X-ray diffraction method. With this method, the spatial arrangement of the atoms of a molecule can be mapped.

In this study, the experimental results of the previous crystallographic study performed by Sivalakshmidevi et al. were used [12]. In their study, the substance 2'-Deoxy-2',2'-difluorocytidine monohydrochloride (Gemcitabine hydrochloride) was investigated, which gave the closest results we could obtain for gemcitabine. Both theoretical and experimental results have been exhibited in the corresponding tables.

Table 1. *Theoretical and experimental bond lengths for Gemcitabine*

	B3LYP		HF				B3LYP		HF		
BOND	**6-31G***	**6-31G****	**3-21G**	**6-31G***	**Exp***	**BOND**	**6-31G***	**6-31G****	**3-21G**	**6-31G***	**Exp***
N3,C2	1.357	1.354	1.337	1.339	1.295	F1,C6	1.362	1.362	1.366	1.336	1.360
N1,C2	1.322	1.322	1.303	1.298	1.360	F2,C6	1.370	1.370	1.377	1.346	1.371
N1,C3	1.360	1.359	1.352	1.352	1.361	H11,N3	1.010	1.008	0.998	0.995	0.950
N2,C3	1.437	1.437	1.412	1.409	1.386	H10,N3	1.008	1.005	0.995	0.992	0.950
N2,C4	1.363	1.363	1.363	1.358	1.393	H1,C1	1.083	1.082	1.067	1.071	
N2,C5	1.463	1.462	1.447	1.449	1.449	H2,C4	1.085	1.085	1.070	1.073	
C2,C1	1.436	1.436	1.438	1.439	1.419	H9,O4	0.978	0.974	0.974	0.952	
C5,C6	1.554	1.554	1.543	1.543	1.531	H8,C9	1.103	1.103	1.084	1.088	0.950
C6,C7	1.536	1.535	1.516	1,522	1.509	H7,C9	1.096	1.096	1.079	1.083	0.950
C7,C8	1.534	1.534	1.526	1.526	1.509	H6,C8	1.099	1.099	1.079	1.086	0.950
C8,C9	1.527	1.527	1.522	1.518	1.503	H5,O3	0.969	0.965	0.965	0.947	0.940
O4,C9	1.408	1.407	1.427	1.390	1.410	H3,C5	1.097	1.098	1.078	1.082	0.950
O2,C8	1.451	1.451	1.468	1.424	1.441	H2,C4	1.085	1.085	1.070	1.073	0.950
O2,C5	1.401	1.401	1.415	1.382	1.409	H1,C1	1.083	1.082	1.067	1.071	0.950

O3,C7	1.411	1.410	1.424	1.391	1.406
O1,C3	1.228	1.228	1.222	1.203	1.233

From Table 1, some details can be noticed as in following lines.

1- The shortest N-C bond is N3-C2 bond of the –NH2 group. And N1-C2 and N1-C3 bonds are almst equal in length. It can be clearly seen that this is due to resonance. Similarly N2-Cx bonds are longer than the other N-C bonds Because they are pure single bonds.

2- The shortest O-C bond is O1-C3 as expected due to it is a double bond.

3- In two O-H groups, the O-H bonds have different lengths. O3-H5 bond is shorter than O4-H9 bond. This is because of their electronic environments.[13,14]

Table 2. *Theoretical and experimental bond angles for Gemcitabine*

	B3LYP		HF				B3LYP		HF		
BOND	**6-31G***	**6-31G****	**3-21G**	**6-31G***	**Exp***	**BOND**	**6-31G***	**6-31G****	**3-21G**	**6-31G***	**Exp***
N3,C2,N1	117.05	117.03	118.1	117.82	118.8	H10,N3,C2	121.38	122.10	122.80	122.20	120.06
N3,C2,C1	119.75	119.8	120.0	119.16	124.0	H1,C1,C2	122.56	122.60	121.90	122.40	120.44
C2,C1,C4	116.17	116.19	116.3	115.73	119.2	H1,C1,C4	121.26	121.20	121.80	121.90	120.34
N2,C4,C1	121.63	121.63	121.9	121.97	121.3	H2,C4,C1	122.24	122.20	121.90	121.90	119.38
N2,C3,N1	117.67	117.67	117.00	118.02	116.2	H2,C4,N2	116.13	116.20	116.20	116.20	119.28
C4,N2,C3	120.49	120.5	120.60	120.32	120.7	H3,C5,N2	105.76	105.80	107.60	106.10	109.70
N2,C3,O1	118.54	118.54	118.40	118.39	121.5	H3,C5,C6	107.00	106.80	107.20	106.90	109.65
N1,C3,O1	123.79	123.79	124.60	123.59	122.4	H9,O4,C9	108.71	108.80	111.40	110.60	104.00
C4,N2,C5	119.42	119.37	120.40	119.48	119.7	H8,C9,H7	107.63	107.50	108.80	107.90	109.45
C3,N2,C5	120.09	120.13	119.00	120.19	118.2	H4,C7,C8	109.61	109.50	110.00	110.40	--
N2,C5,O2	111.35	111.34	111.60	111.45	109.2	H4,C7,C6	108.18	108.10	108.80	108.20	107.77
N2,C5,C6	115.41	115.46	113.80	116.01	112.5	H5,O3,C7	108.03	108.10	111.60	110.00	106.00
C5,O2,C8	111.74	111.71	111.40	112.24	109.7	H4,C7,O3	112.66	112.90	113.90	112.40	--
O2,C8,C7	106.32	106.28	105.10	105.47	104.8	N1,C2,C1	123.2	123.20	121.90	123.00	117.30
C8,C7,C6	102.45	102.39	103.20	101.71	102.4	C3,N1,C2	120.83	120.90	122.40	120.90	125.20
C7,C6,C5	105.70	105.73	106.30	105.39	105.6	O2,C8,C9	108.42	108.40	108.40	108.80	107.50
C6,C5,O2	106.62	106.59	106.00	106.09	106.10	C7,C8,C9	115.05	115.00	114.00	115.50	114.70
O4,C9,C8	114.44	114.38	113.40	113.91	112.60	O2,C5,H6	110.63	110.80	110.70	110.10	109.63
O3,C7,C8	109.12	109.2	107.00	109.44	116.1	O3,C7,H9	112.66	112.90	113.90	112.40	107.64
O3,C7,C6	114.29	114.27	113.30	114.19	114.70	C8,C7,H9	109.61	109.50	110.00	110.40	107.82

F1,C6,F2	106.74	106.73	106.80	106.31	104.5	O2,C8,H10	108.74	108.90	109.00	109.00	109.83
F1,C6,C7	113.79	113.84	114.10	114.23	114.00	C7,C8,H10	108.53	108.50	108.60	108.60	109.93
F1,C6,C5	112.77	112.78	112.30	113.18	112.30	C9,C8,H10	109.59	109.60	111.40	109.30	109.90
F2,C6,C7	110.25	110.24	110.20	110.36	111.20	O4,C9,H11	106.98	107.10	106.40	107.10	108.76
F2,C6,C5	107.45	107.39	106.90	107.22	109.30	O4,C9,H12	112.23	112.40	112.20	111.60	108.62
H11,N3,H10	118.62	119.68	119.50	119.17	119.99	C8,C9,H11	108.09	108.00	108.40	108.40	108.71
H11,N3,C2	117.41	117.90	117.80	118.46	119.95	C8,C9,H12	107.3	107.20	107.50	107.80	108.68

When it comes to the angles, lots of factor can effect the angles such as hybridisation, electronic environments, atom types and diameters etc.

In gemcitabine Mostly the bond angles are as they were expected from their hybridisation types. For example in the first ring, the bond angles are mostly between 117° and 121°. The angles CxN2Cy are about 120° too. It is due to resonance of double bonds in the ring.

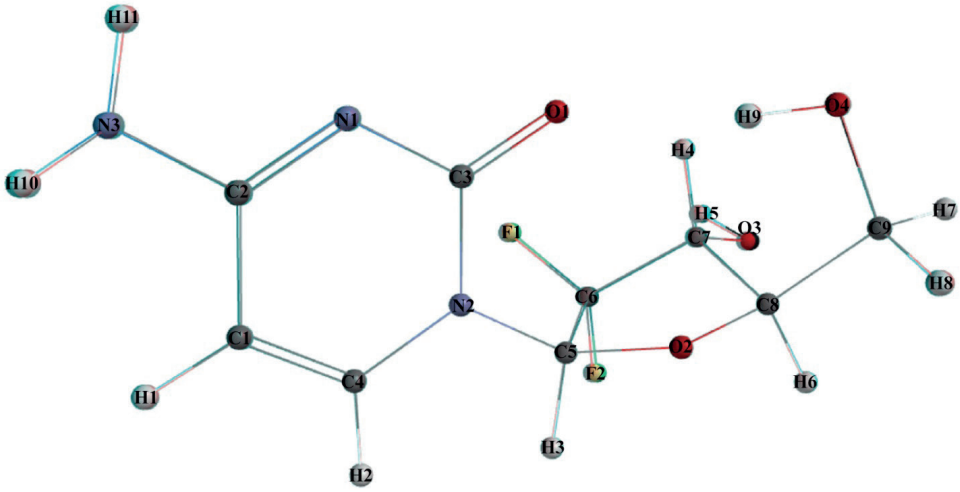

Figure 2. *Molecular structure and labeling for Gemcitabine*

Table 3. *Theoretical and experimental dihedral angles for Gemcitabine*

BOND	B3LYP		HF		EXP*	BOND	B3LYP		HF		EXP*
	6-31G*	6-31G**	3-21G	6-31G*			6-31G*	6-31G**	3-21G	6-31G*	
N3,C2,N1,C3	-178.3	-179.2	-179.8	179.9	177.6	H11,N3,C2,N1	-7.5	-2.9	0.2	1.9	---
C2,N1,C3,O1	179.0	179.1	179.8	179.5	−177.1	N3,C2,C1,H1	-1.2	-0.7	-0.3	-0.1	---
C2,N1,C3,N2	-0.9	-0.6	-0.1	-0.3	2.3	H3,C5,C6,C7	-129.2	-129.5	-129.6	-128.4	---

C2,C1,C4,N2	-0.5	-0.5	-0.6	-0.6	---	H8,C9,C8,H6	-70.6	-70.4	-76.4	-67.4	---
N3,C2,C1,C4	179.0	179.8	-179.9	-179.5	---	C8,O2,C5,C6	-6.8	-6.7	-7.1	-9.1	−14.6
N3,C2,C3,O1	0.9	-0.3	0.1	-1.1	---	C5,O2,C8,C9	146.0	146.0	-144.9	149.9	153.3
N3,C2,N2,C5	74.5	43.3	53.5	28.6	---	C4,N2,C3,O1	-179.6	-179.6	179.5	-180.0	178.4
N1,C3,O2,C8	-154.2	-154.4	-152.0	-153.7	---	C5,N2,C3,O1	0.8	0.7	1.6	1.6	12.1
C1,C4,C5,C6	-79.6	-79.5	-78.5	-80.8	---	C5,N2,C3,N1	-179.3	-179.5	-178.4	-178.6	−167.3
N2,C5,O2,C8	-133.5	-133.5	-131.4	-136.2	−136.1	C4,N2,C3,N1	0.3	0.1	-0.6	-0.2	−0.9
N2,C5,C6,C7	113.5	113.3	111.7	113.5	112.1	C3,N2,C4,C1	0.5	0.5	0.9	0.6	0.3
C4,N2,C5,C6	116.7	116.8	119.1	117.9	−71.2	C5,N2,C4,C1	-180.0	-179.9	-178.8	179.1	166.5
C3,N2,C5,O2	58.1	58.2	56.8	57.9	−147.2	C3,N2,C5,C6	-63.7	-63.5	-63.0	-63.6	95.3
O4,C9,C8,O2	-77.3	-76.9	-81.2	-72.9	−63.2	C4,N2,C5,O2	-121.5	-121.5	-121.0	-120.5	46.3
O4,C9,C8,C7	41.6	41.8	35.5	45.4	52.9	C3,N1,C2,C1	0.8	0.6	0.4	0.4	−2.8
C9,C8,C7,O3	91.7	91.6	93.6	88.7	83.1	N1,C2,C1,C4	-0.1	0.0	-0.1	0.1	1.9
C5,O2,C8,C7	21.8	21.9	22.6	25.4	30.9	N3,C2,C1,C4	179.0	179.8	-179.9	-179.5	−178.4
O2,C5,C6,C7	-10.8	-11.0	-11.3	-10.9	−7.2	C2,C1,C4,N2	-0.5	-0.5	-0.6	-0.6	−0.8
O3,C7,C6,C5	140.4	140.7	139.5	142.3	151.3	C5,C6,C7,C8	55.6	22.8	24.1	24.6	24.7
O3,C7,C8,O2	-148.3	-148.5	-147.9	-151.2	−159.2	C6,C7,C8,C9	-146.8	-146.9	-146.6	-150.2	−151.1
O3,C7,C6,F1	-95.3	-94.9	-96.2	-92.8	−85.0	C6,C7,C8,O2	-26.8	-27.0	-28.1	-30.0	−33.5
O3,C7,C6,F2	24.6	25.0	24.0	26.9	32.9	N2,C5,C6,F2	-128.8	-129.0	-130.6	-129.0	−128.2
F1,C6,C5,O2	-135.7	-136.0	-136.8	-136.4	−132.0	N2,C5,C6,F1	-11.5	-11.7	-13.8	-12.1	−12.7
F2,C6,C5,O2	107.0	106.7	106.4	106.7	112.5	F1,C6,C7,C8	146.8	147.2	-148.4	149.4	148.4
F2,C6,C7,C8	-93.3	-93.0	-91.4	-90.9	−93.7	H10,N3,C2,C1	11.8	4.3	-0.2	-3.2	---

Dihedral angles refer the torsion of the molecule or part of the molecule. In gemcitabine, first ring is almost planar with 178°-180° dihedral angles, and the second ring (with only single bonds) is twisted. The torsion angles of the second ring of the moecule are different from 10-15° to 85-90°.It should be kept in mind, 0° and 180° or 30° and 150°are the same when torsion angles are mentioned.

Electronic Properties of Gemcitabine

Molecular shape, spatial positions of the atoms are important to describe a molecule; but the other feature that is at least as important in terms of reactivity is the electronic structure. Mulliken [15] charge distribution (equation 1) is one of the most popular and oldest population analysis methods. Most software packages include this method and This is the main factor in its widespread use. Although it gives different results when different basis sets are used, it is widely used because it is easy in terms of calculation[15].

$$Vr = \sum_A \frac{Z_A}{R_A - r} - \int \frac{\rho(r')}{(r'-r)} dr' \quad (1)$$

The calculated Mulliken charge values are tabulated as Table 4 for Gemcitabine. These values can be interpreted in the shortest terms as follows:

1- Of all the carbon atoms of the molecule, only C1and C9 have negative charges.

2- The C atom with the greatest positive value is the C3 atom belonging to the carbonyl group,

3- Surprisingly, the C6 atom does not have the highest positive valence. In fact, it is seen that it exhibits a very low charge compared to C3. However, since it carries F atoms, it would be expected to have the highest positive charge.

4- All O atoms have negative charges, It is seen that the O atoms belonging to the OH groups have significantly higher negative charges than the others.

5- Although the F atoms have negative charges as expected, they showed lower charges than expected.

6- The champion of the day is N. The negative charges of N atoms were calculated to be much higher than O and Fs.

7- All H atoms exhibit positive charges as expected. It is noteworthy that there is a difference of up to two times between the charges of the H atoms.

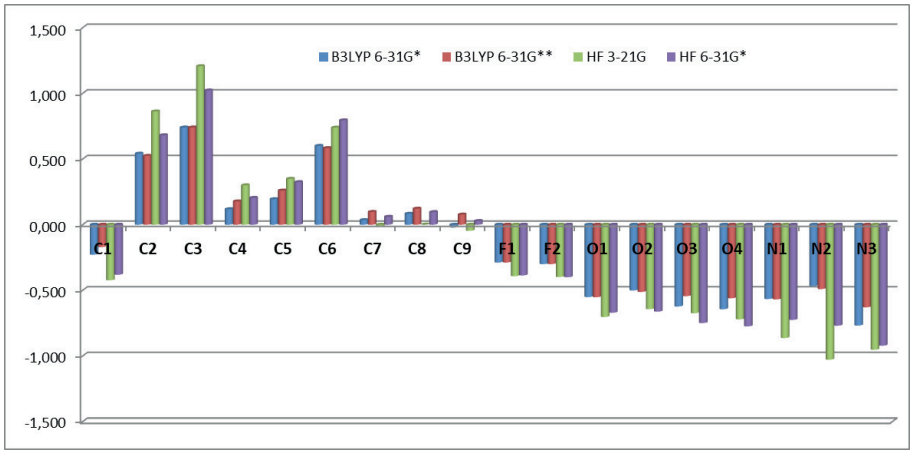

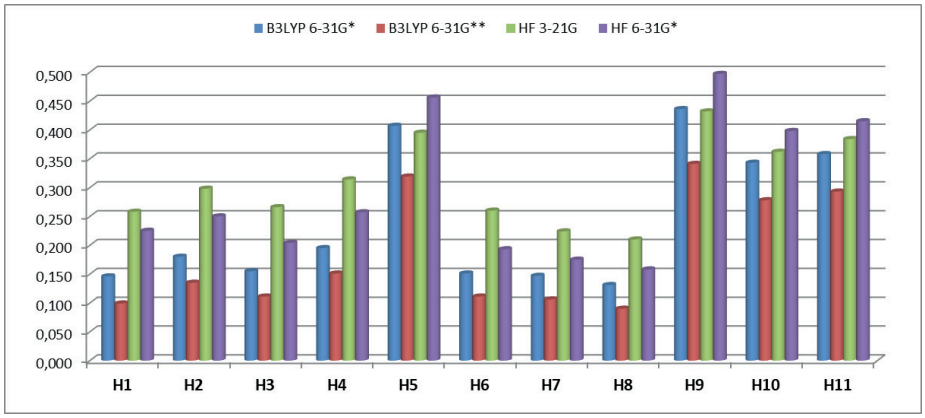

Figure 3. *Mulliken charge distribution of Gemcitabine a) C & heteroatoms, b) H atoms*

Table 4. *Theoretical Mulliken Charges values for Gemcitabine molecule*

	B3LYP		HF			B3LYP		HF	
BOND	**6-31G***	**6-31G****	**3-21G**	**6-31G***	**BOND**	**6-31G***	**6-31G****	**3-21G**	**6-31G***
C1	-0.228	-0.170	-0.423	-0.381	N1	-0.566	-0.569	-0.863	-0.725
C2	0.541	0.524	0.862	0.681	N2	-0.468	-0.490	-1.028	-0.769
C3	0.740	0.740	1.207	1.022	N3	-0.768	-0.629	-0.952	-0.921
C4	0.118	0.177	0.300	0.204	H1	0.146	0.099	0.258	0.225
C5	0.194	0.260	0.349	0.324	H2	0.180	0.135	0.298	0.250
C6	0.600	0.583	0.739	0.795	H3	0.155	0.111	0.266	0.204
C7	0.035	0.097	-0.017	0.060	H4	0.195	0.151	0.314	0.257
C8	0.083	0.122	0.001	0.096	H5	0.407	0.319	0.395	0.456
C9	-0.022	0.077	-0.046	0.028	H6	0.151	0.111	0.260	0.193
F1	-0.288	-0.288	-0.392	-0.386	H7	0.147	0.106	0.224	0.175
F2	-0.300	-0.300	-0.398	-0.400	H8	0.131	0.090	0.210	0.158
O1	-0.551	-0.552	-0.703	-0.670	H9	0.436	0.341	0.432	0.497
O2	-0.501	-0.512	-0.643	-0.662	H10	0.343	0.278	0.362	0.398
O3	-0.623	-0.544	-0.674	-0.749	H11	0.358	0.293	0.384	0.415
O4	-0.644	-0.560	-0.721	-0.774					

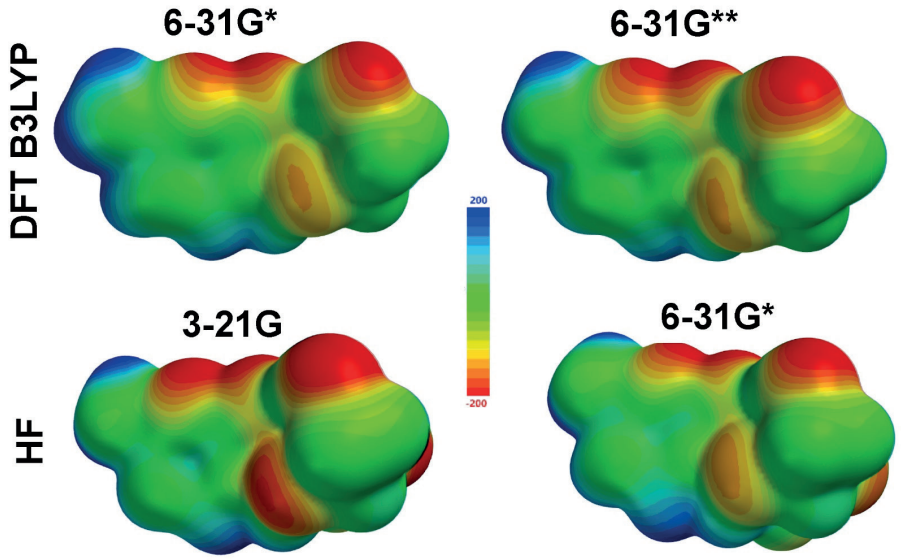

Figure 4. *Electrostatic Potential Map (ESPMap) of Gemcitabine*

Molecular orbitals analysis (HOMO-LUMO)

HOMO (Highest Occupied Molecular Orbital) and LUMO (Lowest Unoccupied Molecular Orbital) represent the energy levels of a molecule. In a certain molecule there is a gap between these two energy levels. The larger this energy gap is, the more stable the molecule and reluctant to react. HOMO&LUMO levels also determine the acidity or basicity of the molecule.

Table 5. *HOMO-LUMO Energies(eV) and ΔE values for Gemcitabine (Also see Figure 5)*

Method & Basis Set		HOMO-1	HOMO	LUMO	LUMO+1	Energy Diff. (ΔE)			λmax		
						ΔE_1	ΔE_2	ΔE_3	Calculated (Vac.)		
HF	3-21G	-10.5	-9.7	2.7	4.4	13,2	12,4	14,1	93,9	100	87.9
	6-31G*	-10.5	-9.6	2.9	4.6	13,40	12,50	14,20	92.5	99.2	87.3
DFT/ B3LYP	6-31G*	-6.7	-6.6	-1.2	0.1	5,50	5,40	6,70	225,4	229,6	185
	6-31G**	-6.7	-6.6	-1.2	0.1	5,50	5,40	6,70	225,4	229,6	185

According to calculated values, Gemcitabine is a "hard" molecule with a deep gap between HOMO&LUMO levels. The chemical hardness of a molecule can be calculated via equation 2a and also chemical softness of the same molecule can be obtained from equation 2b[16].

$$\eta=(\text{ELUMO}-\text{EHOMO}) \quad (2a)$$

$$S=1/\eta \quad (2b)$$

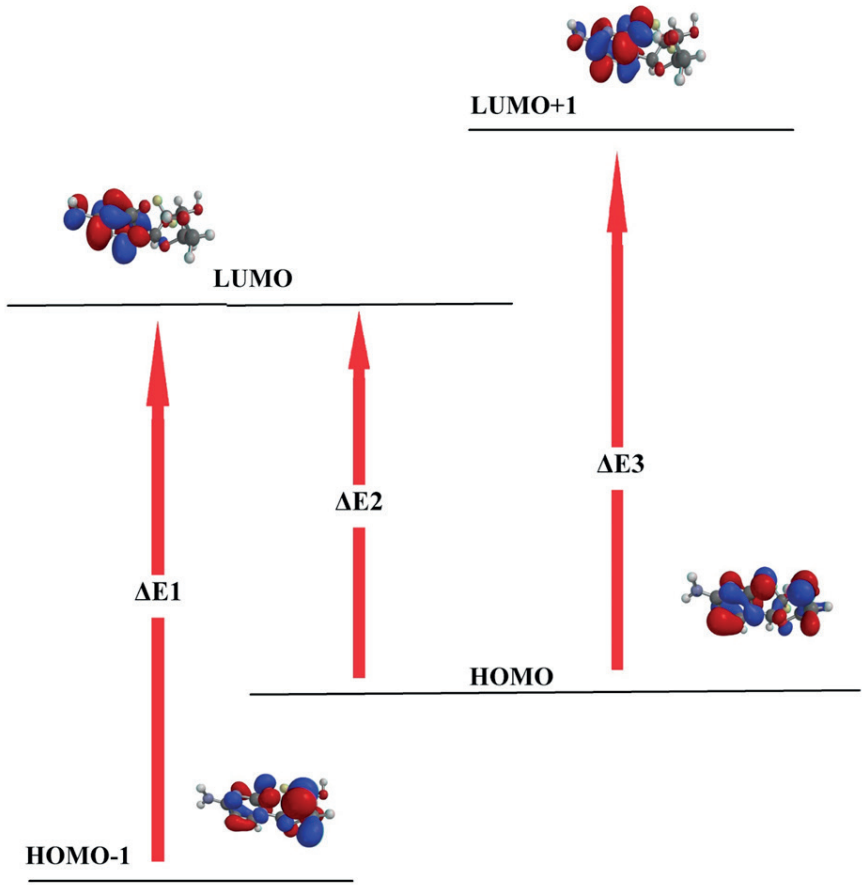

Figure 5. *Schematical illustrations of ΔE values for Gemcitabine (Also see Table 5)*

Table 6. *HOMO-LUMO Energies (eV)*

MOs	DFT B3LYP		HF	
	6-31G*	6-31G**	3-21G	6-31G*
LUMO{+1}	0.1	0.1	4.4	4.6
LUMO	-1.2	-1.2	2.7	2.9
HOMO	-6.6	-6.6	-9.7	-9.6
HOMO{-1}	-6.7	-6.7	-10.5	-10.5
HOMO{-2}	-7.0	-7.0	-11.0	-11.3
HOMO{-3}	-7.2	-7.2	-11.3	-11.5
HOMO{-4}	-7.5	-7.5	-11.7	-11.9
HOMO{-5}	-7.6	-7.6	-11.9	-12.1
HOMO{-6}	-7.9	-7.9	-12.4	-12.6
HOMO{-7}	-8.6	-8.6	-13.0	-13.3
HOMO{-8}	-8.9	-8.9	-13.4	-13.8
HOMO{-9}	-9.6	-9.6	-13.9	-13.9

NMR Spectra of Gemcitabine

When it comes to determining the molecular structure, the first methods that come to mind are H and C nmr techniques. NMR is unquestionably of great importance in molecular structure determination. Therefore, NMR information can be found for almost all known molecules in the literature. Moreover, the H and C nmr values of the molecule can be calculated with great approximation even if the NMR measurement has not been performed experimentally [17,18].

For Gemcitabine the calculated and experimental NMR values are tabulated in the Table 7. As a "one word" summary of all the tables and figures the calculated values are in a great harmony with experimental ones. Some significant peaks can briefly be interpreted as follows.

1- All H atoms are in electron-rich chemical environments that give them high shift values. This is reflected in the calculated values.

2- H5 and H9 have been calculated to give peaks on about 0.8 ppm and 3-4 ppm. But in experimental spectra as expected their peaks is not seen, which is typical for –OH groups.

3- C2, C3, C4 and C5 have given peaks at 159.74, 148.62, 144.37 and 96 ppm, respectively. Their calculated shift values are very near to experimental ones, with a difference of about (+/-)5-10 ppm. For most C atoms, the nearest calculated results are given by DFT method with B3LYP/6-31G**.

Table 7 *Calculated and experimental schift values for Gemcitabine*

ATOM	B3LYP		HF		EXP.*
	6-31G*	6-31G**	3-21G	6-31G*	
C1	91.59	87.48	84.20	85.12	
C2	166.09	155.68	153.70	165.70	159.74
C3	158.62	147.04	146.67	150.82	148.62
C4	149.05	141.37	139.90	150.17	144.37
C5	100.39	99.13	80.80	85.53	96.00
C6	125.12	127.55	112.44	110.13	
C7	71.73	72.05	61.82	62.94	
C8	85.29	85.29	73.21	73.55	
C9	62.09	61.38	50.30	54.69	
H1	4.90	6.16	5.09	5.00	
H2	6.71	7.90	7.33	7.33	
H3	4.49	5.60	4.07	4.21	
H4	5.37	6.58	5.12	4.99	
H5	0.85	1.77	0.81	0.86	
H6	3.87	4.92	3.81	3.46	
H7	3.62	4.65	3.69	3.55	
H8	3.98	5.03	3.63	3.75	
H9	3.04	4.42	3.98	2.35	
H10	3.66	5.07	3.72	3.83	3.81
H11	3.66	5.07	3.72	3.83	3.95

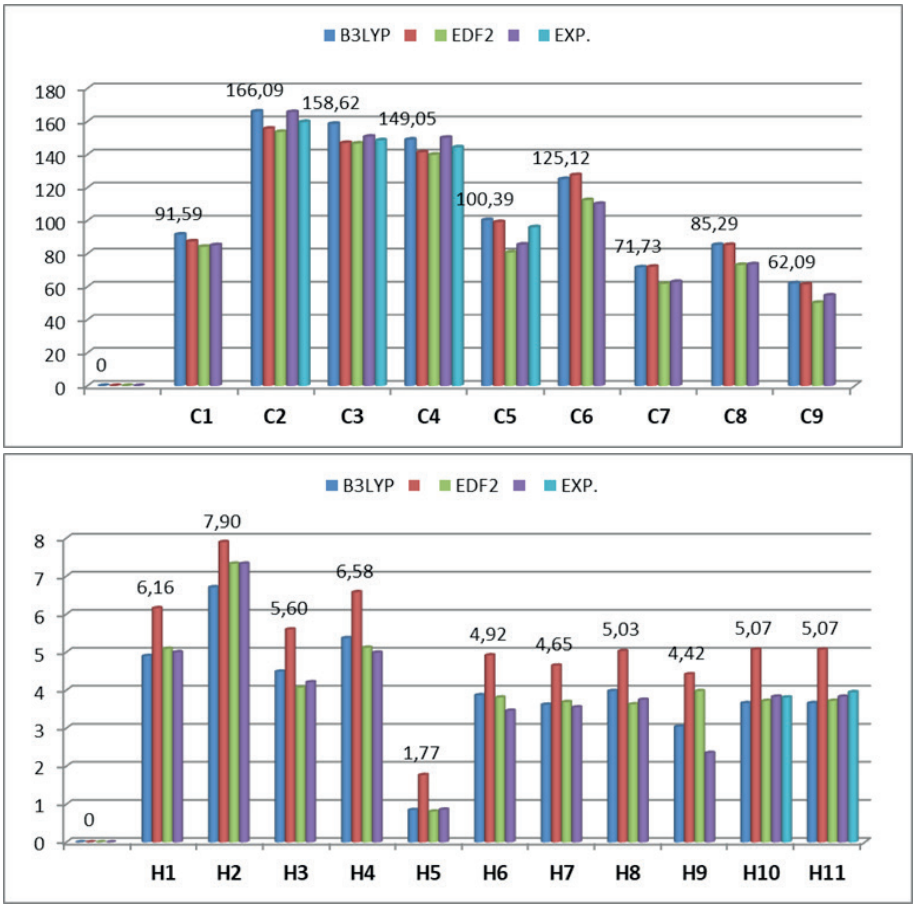

Figure 5. *^{13}C and ^{1}H NMR values for Gemcitabine*

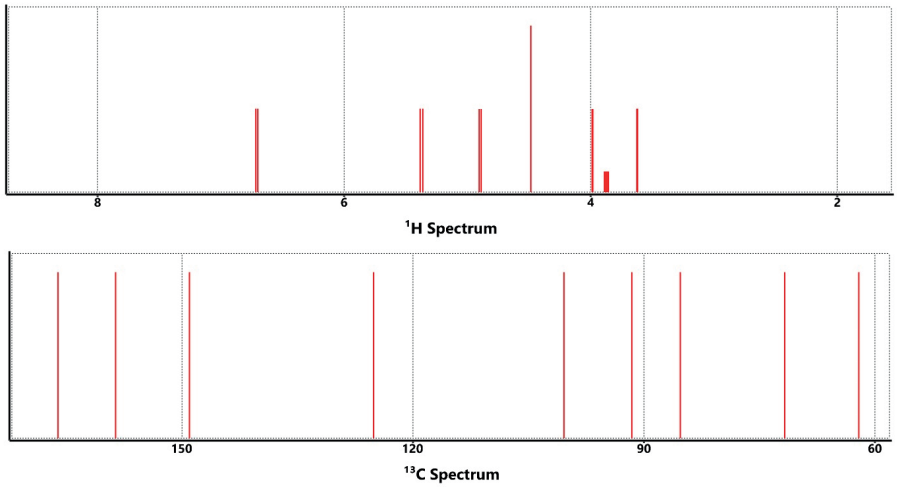

Figure 6. *Calculated ^{13}C and ^{1}H NMR spectra for Gemcitabine*

Vibrational analysis of Gemcitabine

FT-IR and FT-RAMAN spectra give information about vibrational modes of any molecule. Every vibrational mode represents a spesific molecular movement, such as stretching, rotating,

Gemcitabine (C9H11F2N3O4) has 27 atoms which create 81 vibrational modes. They exhibit rocking, swinging, stretching and every kind of motions. These movements add different spatial positions to the molecule.

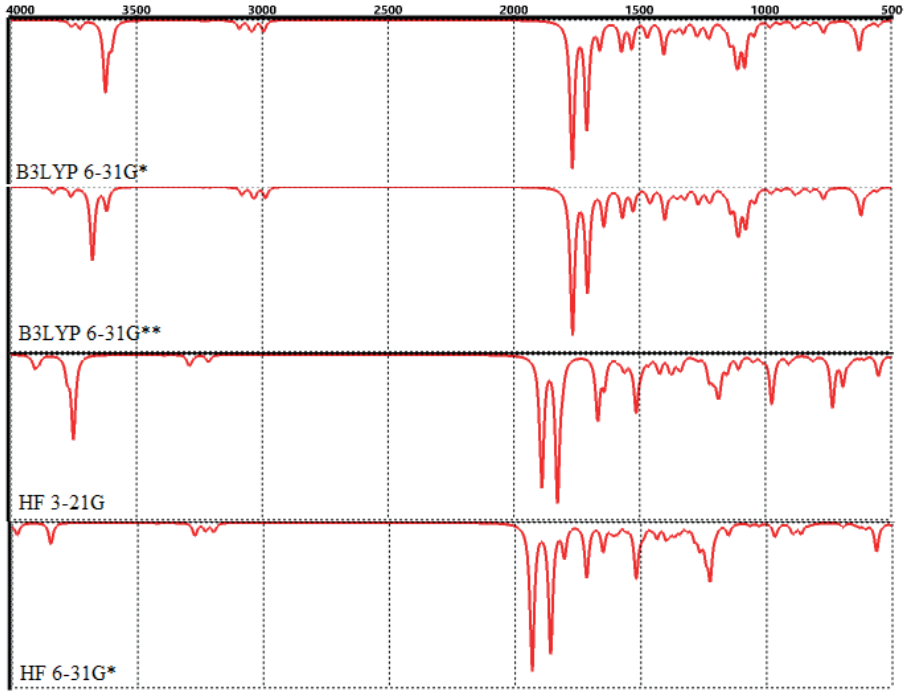

Figure 7. *Calculated FT-IR spectra for Gemcitabine*

In a short view the frequencies and their corresponding motions can be underlined briefly as follows.

1- The broad band in ~3200-3400 cm^{-1}(modes 74-78) refers to –O-H and –N-H parts of the molecule.

2- The most severe band at 1700-1800 cm^{-1} (modes 68-70) belongs to the carbonyl group's C3=O1 bond.

3- The bands about 3000 cm^{-1} (Modes 71-74) assign the C-H stretching motions.

Table 8. *Calculated Vibrational modes for Gemcitabine*

	B3LYP		HF			B3LYP		HF			B3LYP		HF	
#	6-31G*	6-31G**	321G	G-31G*	#	6-31G*	6-31G**	321G	G-31G*	#	6-31G*	6-31G**	321G	G-31G*
1	44	45	49	46	**28**	637	637	692	697	**55**	1326	1317	1420	1436
2	60	60	64	66	**29**	655	655	733	710	**56**	1330	1324	1430	1457
3	63	64	73	72	**30**	722	723	810	796	**57**	1354	1346	1464	1488
4	107	90	100	100	**31**	748	748	822	820	**58**	1365	1357	1488	1501
5	123	106	141	105	**32**	768	768	840	835	**59**	1385	1377	1497	1519
6	145	123	172	127	**33**	769	768	890	863	**60**	1404	1400	1514	1533
7	191	143	213	154	**34**	779	779	908	8888	**61**	1417	1407	1535	1559
8	198	191	222	211	**35**	824	823	934	899	**62**	1461	1450	1557	1591
9	207	207	247	226	**36**	868	867	958	958	**63**	1469	1458	1565	1606
10	217	216	254	240	**37**	885	883	975	968	**64**	1474	1466	1585	1617
11	236	236	264	259	**38**	940	938	1013	1030	**65**	1525	1510	1640	1650
12	249	248	290	270	**39**	957	959	1049	1066	**66**	1532	1526	1666	1658
13	263	262	302	290	**40**	982	978	1107	1108	**67**	1572	1569	1673	1715
14	278	277	324	297	**41**	1045	1042	1153	1152	**68**	1658	1642	1807	1804
15	303	303	342	328	**42**	1082	1074	1178	1196	**69**	1710	1707	1827	1859
16	318	317	380	338	**43**	1084	1080	1179	1203	**70**	1768	1767	1889	1932
17	350	350	400	380	**44**	1108	1105	1184	1225	**71**	2995	2987	3214	3198
18	368	369	459	404	**45**	1117	1114	1191	1241	**72**	3037	3029	3279	3230
19	419	420	500	455	**46**	1136	1136	1207	1255	**73**	3048	3038	3287	3271
20	449	449	535	491	**47**	1141	1139	1224	1266	**74**	3092	3081	3293	3275
21	493	493	551	538	**48**	1166	1162	1268	1286	**75**	3128	3119	3388	3341
22	550	556	608	563	**49**	1188	1186	1283	1316	**76**	3216	3209	3396	3406
23	563	562	627	606	**50**	1222	1217	1333	1345	**77**	3239	3236	3430	3425
24	582	582	644	615	**51**	1231	1229	1340	1365	**78**	3599	3619	3751	3846
25	596	595	661	632	**52**	1262	1256	1350	1366	**79**	3624	3675	3775	3979
26	600	599	668	647	**53**	1269	1267	1370	1386	**80**	3725	3761	3888	4039
27	627	620	683	648	**54**	1275	1270	1381	1400	**81**	3760	3833	3904	4117

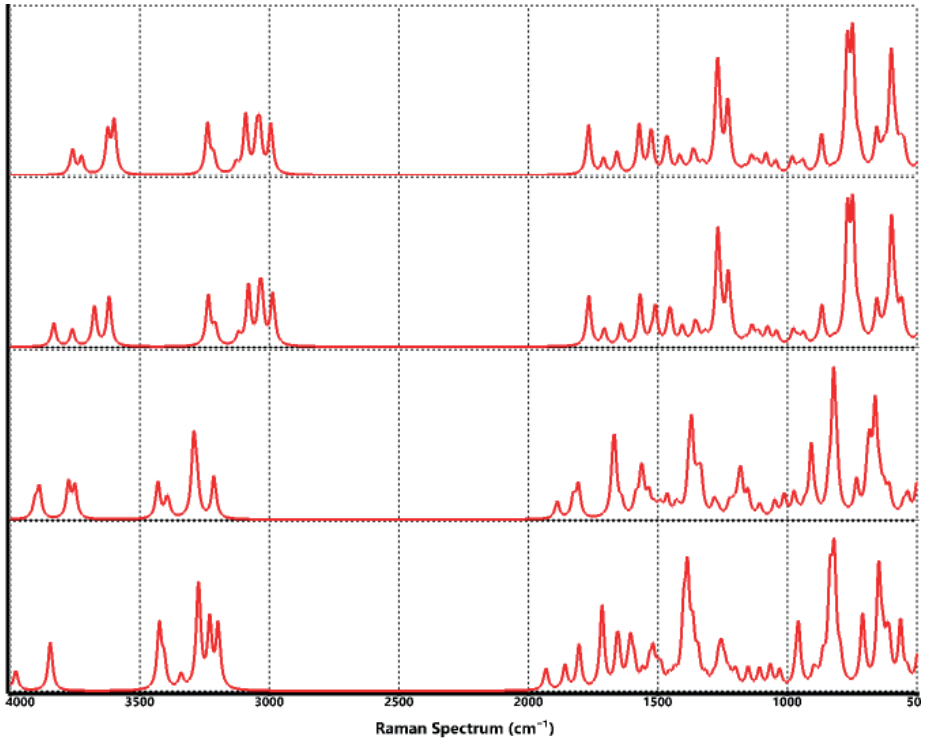

Figure 8. *Calculated FT-RAMAN spectra for Gemcitabine*

REFERENCES

1- Venkataramanan, N.S., Suvitha, A., Sahara, R. et al. Unveiling the gemcitabine drug complexation with cucurbit[n]urils (n = 6–8): a computational analysis. Struct Chem (2023). https://doi.org/10.1007/s11224-023-02133-z

2- Amrutkar M, Gladhaug IP. Pancreatic Cancer Chemoresistance to Gemcitabine. Cancers (Basel). 2017 Nov 16;9(11):157. doi: 10.3390/cancers9110157. PMID: 29144412; PMCID: PMC5704175.

3- Liu Y., Li Y., Du S., Li Fan Wang J., "Clinical Study of Anti-PD-1 Immunotherapy Combined with Gemcitabine Chemotherapy in Multiline Treatment of Advanced Pancreatic Cancer", Computational and Mathematical Methods in Medicine, vol. 2022, Article ID 4070060, 6 pages, 2022. https://doi.org/10.1155/2022/4070060

4- Kang, H., Kim, C., Kim, D., Song, J.H., Choi, M.,Choi, K., Kang, M., Lee, K., Kim, H.S., Shin, J.S., Kim, J., Han, S.B., Lee, M.Y., Lee, S.U., Lee, C.K.,Kim, M., Ko, H.J., Kuppeveld, F.J.M., and Cho, S. \Synergistic antiviral activity of gemcitabine and ribavirin against enteroviruses", Antiviral Res., 124, pp. 1-10 (2015).

5- Vicario A, Sergo V, Toffoli G, Bonifacio A. Surface-enhanced Raman spectroscopy of the anti-cancer drug irinotecan in presence of human serum albumin. Colloids Surf B Biointerfaces. 2015 Mar 1;127:41-6. doi: 10.1016/j.colsurfb.2015.01.023. Epub 2015 Jan 22. PMID: 25645751.

6- W. Bakasa and S. Viriri, "Pancreatic cancer survival prediction: a survey of the state-of-the-art," Computational and Mathematical Methods in Medicine, vol. 2021, Article ID 1188414, 17 pages, 2021.

7- Q. Jiang and W. Zhou, "Excerpt from "2019 American preventive medicine working group expert consensus: screening for pancreatic cancer"," Journal of Clinical Hepatobiliary Diseases, vol. 36, no. 1, p. 3, 2020.

8- Chashmniam, S., & Tafazzoli, M. (2018). Conformation of Gemcitabine: An Experimental NMR and Theoretical DFT Study. Scientia Iranica, 25(3), 1354-1363. doi: 10.24200/sci.2017.4602

9- Asiri, A.M., Karabacak, M., Kurt, M., and Alamry,K.A. \Synthesis, molecular conformation, vibrational and electronic transition, isometric chemical shift, polarizability and hyperpolarizability analysis of 3-(4-methoxy-phenyl)-2-(4-nitro-phenyl) acrylonitrile: A combined experimental and theoretical analysis", Spectrochimica Acta Part A., 82, pp. 444-455 (2011).

10- Dereli Ö.; Erdoğdu Y.; Güllüoğlu M.T., Study on molecular structure and vibrational spectra of (triphenylphosphoranylidene) acetaldehyde using DFT: A combined experimental and quantum chemical approach. J. Mol. Struct., 2012 1012: 105–112. DOI: https://doi.org/10.1016/j.molstruc.2011.12.040

11- Sarıkaya E.K.; Dereli Ö.; Erdoğdu Y.; Güllüoğlu M. T. Molecular structure and vibrational spectra of 7–Ethoxycoumarin by density functional

method. J. Mol. Struct. 2013, 1049: 220–226. DOI: https://doi.org/10.1016/j.molstruc.2013.06.026

12- A. Sivalakshmidevi, K. Vyas, G. Om Reddy, S. D. V. N. Sivaram, P. V. Swamy, R. Puranik, P. Sairam; 2'-Deoxy-2',2'-difluorocytidine monohydrochloride (Gemcitabine hydrochloride). Acta Crystallogr. 2003 E59, o1435-o1437

13- Jensen F. Introduction to Computational Chemistry. 2016 Chichester: Wiley..

14- Peter K., Vollhardt C., Schore N. E., Organic chemistry: Structure and function. 6th ed. 2011 Freeman&Comp. NY-US.. DOI: https://doi.org/10.1007/978-1-319-19197-9

15- Şahin Z.S.; Kaya-Kantar G.; Şaşmaz S.; Büyükgüngör O. Synthesis, molecular structure, spectroscopic analysis, thermodynamic parameters and molecular modeling studies of (2-methoxyphenyl)oxalate, J. Mol. Struct., 2015 1087:104-112 DOI: https://doi.org/10.1016/j.molstruc.2015.01.039

16- Pearson R.G. Chemical hardness and density functional theory, Chem. Sci. J., 2005 117(5): 369-377 DOI: https://doi.org/10.1007/bf02708340

17- Silverstein R.M.; Webster F.X.; Kiemle D.J. Spectrometric Identification of Organic Compounds. 7th Ed. 2005 John Wiley Sons INC.. https://doi.org/10.1002/ange.19650771675

18- Ramachandran K.I.; Deepa G.; Namboori K. Computational Chemistry and Molecular Modeling: Principles and Applications. 2008 Springer-Verlag Heidelberg. Berlin:. DOI 10.1007/978-3-540-77304-7

Chapter 3

IN SILICO GENOTOXIC AND CARCINOGENIC POTENTIAL ASSESSMENT OF PRYNACHLOR AND PROPISOCHLOR HERBICIDES

***Şefika Nur Demir*[1]**

***Ahmet Ali Berber*[2]**

1 School of Graduate Studies, Department of Biology, Çanakkale Onsekiz Mart University, Terzioğlu Campus, 17100, Çanakkale/ TÜRKİYE, sefika@stu.comu.edu.tr (Ş. Demir), https://orcid.org/0000-0003-3340-598X

2 Vocational School of Health Services, Çanakkale Onsekiz Mart University, Terzioğlu Campus, 17100, Çanakkale / TÜRKİYE, aberber@comu.edu.tr (A. Berber), https://orcid.org/0000-0002-2036-6929

1. **INTRODUCTION**

Pesticides are frequently used in agriculture to protect crops from pests, illnesses, and weeds, which can negatively affect crop productivity and quality [1]. Herbicides are the most widely used pesticides, with]47.5% of the global pesticide market accounting for almost half [2]. Chemical substances known as herbicides are employed to selectively suppress or eliminate weeds by interfering with their physiological functions. However, non-target animals, plants, people, and the environment can also be harmed by these herbicides. Herbicides have the potential to contaminate water supplies and groundwater, putting aquatic life in danger. Furthermore, it has been shown that some herbicides can harm DNA, which could result in mutations and other health issues [3,5]. Therefore, it is crucial to use herbicides carefully and follow safety guidelines to reduce the risk of these adverse effects.

Chloroacetanilide herbicides, such as acetochlor and alachlor, are widely used to control weeds in agricultural practices. These herbicides are effective against a wide variety of annual grasses and broadleaf weeds, and they work by inhibiting cell division in the target plants. Chloroacetanilide herbicides are typically applied to the soil before or immediately after planting, and they are absorbed by the roots of emerging seedlings [6,7]. Even though these herbicides have been in use for decades, there are concerns about their potential effects on human health and the environment, including their persistence in soil and water, toxicity to non-target organisms, and potential to contaminate food crops. These herbicides have been found to have genotoxic effects on living organisms. These genotoxic effects could result in adverse health outcomes like cancer, abnormal development, and reproductive issues [8]. For example, the herbicide alachlor has been shown to cause chromosomal damage in human lymphocytes, mice, and maize [7,9], while acetochlor has been found to induce cardiovascular toxicity in zebrafish [10]. Additionally, butachlor has been linked to an increased incidence of toxicity in the freshwater fish *Tilapia zillii* [11].

Prynachlor (N-but-3-yn-2-yl-2-chloro-N-phenylacetamide) and propisochlor (2-chloro-N-(2-ethyl-6-methylphenyl)-N-[(1-methylethoxy) methyl] acetamide) are two selective herbicides that belong to the chloroacetanilide family (Figure 1) [12,13]. They are commonly used to control annual grasses and broadleaf weeds in crops such as soybeans, cabbage, maize, and cauliflower. These herbicides work by inhibiting the protein content and synthesis of RNA, which are essential components of plant cell membranes [14]. Even though they are frequently used, these herbicides may have genotoxic and carcinogenic effects, but the research on this is sparse. The two most significant endpoints for evaluating the potential health risks of chemicals are genotoxicity, mutagenicity and carcinogenicity. Genotoxicity is the term used to describe a substance's capacity to damage DNA, which can

result in mutations, chromosomal aberrations, and other genetic alterations [15]. Contrarily, carcinogenicity describes a substance's capacity to result in cancer in humans or animals. Both of these endpoints are important in pesticide risk assessment because exposure to genotoxic and carcinogenic chemicals can have long-term health consequences [16].

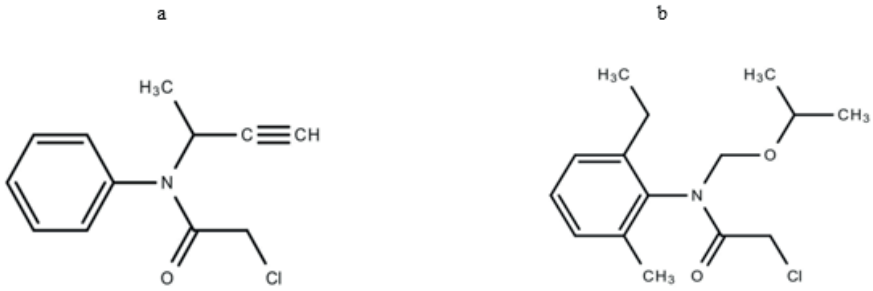

Figure 1 2D structure of a) prynachlor b) propisochlor

In silico methods have gained popularity in recent years as an alternative to traditional *in vivo* and *in vitro* assays for determining the toxicological potential of chemicals. Animal testing has traditionally been used in toxicological assessments of chemicals, which is not only costly and time-consuming but also raises ethical concerns. *In-silico* toxicity tools have become a promising alternative in recent years for evaluating the potential toxicological effects of chemicals [17, 18].

In silico toxicity tools are computer-based models that predict the toxicity of chemicals by simulating their interactions with biological systems. To estimate the potential toxicological effects of chemicals, these models use data from various sources, such as chemical structures, physicochemical properties, and biological pathways [17]. The use of these tools has the potential to significantly reduce the time and cost of toxicity testing, as well as the number of animals used in testing. Among these tools ar320e the widely used software programs Vega Hub, Toxtree (Estimation of Toxic Hazard-A Decision Tree Approach), Lazar, and Toxicity Estimation Software Tool (TEST), which allow researchers to predict the toxicity of chemicals using *in silico* models. Vega QSAR Hub is an open-source software platform that provides a variety of *in silico* toxicity prediction models, including models for acute toxicity, mutagenicity, and carcinogenicity. QSARs (Quantitative Structure-Activity Relationships) are mathematical models that forecast toxicity levels based on molecular descriptors—the physical properties of chemical structures [19]. Toxtree is another open-source software program that predicts the toxicity of chemicals using structural alerts [20]. Benigni and Bossa rules and structural alerts for genotoxic carcinogens found in the literature form the foundation of the decision tree known as Cramer rules,

which is used to evaluate potential mutagenicity [21]. Lazar is a web-based platform that integrates different toxicity prediction models and databases, allowing users to predict toxicity based on a variety of endpoints such as carcinogenicity, mutagenicity, and acute toxicity [22]. Finally, TEST was developed to allow users to easily estimate the toxicity of chemicals using QSARs methodologies. TEST can be used to predict the toxicity of chemicals in various species and endpoints, such as developmental toxicity, reproductive toxicity, and carcinogenicity [23].

These four *in silico* toxicity tools were used in this study to assess the genotoxic and carcinogenic potential of prynachlor and propisochlor herbicides. We performed a thorough analysis of these herbicides' chemical structures and compared the predictions of each tool to identify potential areas of agreement or disagreement. This study aims to contribute to the growing body of research on the use of in-silico toxicity tools for assessing chemical toxicity. The findings of this study will be useful in informing future risk assessments and regulatory decisions about the potential genotoxic and carcinogenic effects of prynachlor and propisochlor herbicides.

2. **METHODOLOGY**

2.1. **Chemical structures of herbicides**

The molecular structures of prynachlor and propisochlor were inserted to run the analysis using the Canonical Simplified Molecular Input Line Entry Specification (SMILES) system, CC(C#C)N(C1=CC=CC=C1)C(=O)CCl and CCC1=CC=CC(=C1N(COC(C)C)C(=O)CCl)C, respectively, according to the PubChem descriptors [12, 13].

2.2. ***In silico*** predictions

For the present assessment, Toxtree 3.1.0 application (available at https:// toxtree.sourceforge.net/), the quantitative structure-activity relationship (QSAR) modeling VEGA 1.2.0 software (available at http:// www.vega-qsar.eu), Lazar toxicity predictions (available at https://lazar.in-silico.ch/predict), and TEST 5.1.2 were used. The toxicity predictions were then carried out by means of existing rules, available in those softwares. The presence of a structural alert in Toxtree was associated with a positive Ames mutagenicity result. VEGA classified chemicals as mutagenic or nonmutagenic and assigned a level of reliability. Lazar provides options for selecting desired endpoints and returns result with a probability score. Finally, after selecting an endpoint in the TEST, the result is calculated based on the consensus score.

3. **RESULTS AND DISCUSSION**

In order to protect crops from pests, diseases, and weeds, pesticides are used in agriculture. However, the use of these chemicals raises questions

about the potential health risks they pose to people, non-target organisms, and the environment [24]. Weeds are typically controlled or eradicated using herbicides like chloroacetanilides that interfere with their physiological processes [25]. However, concerns have been raised about their persistence in soil and water, their toxicity to non-target organisms, and their potential to contaminate food crops. Some herbicides have also been shown to have genotoxic and carcinogenic effects, making it critical to assess the potential health risks associated with their use [26, 27]. As an alternative to conventional *in vivo* and *in vitro* assays, *in silico* toxicity tools have been created to assess the toxicological potential of chemicals.

The toxicity prediction results for the two chosen chloroacetanilide herbicides studied are shown in Table 1 using the software tools LAZAR, Toxtree, VEGA, and TEST. Potential health risks associated with the use of the two chloroacetanilide herbicides prynachlor and propisochlor in agriculture have been highlighted by the results of the toxicity prediction analysis. Table 1 shows the results of the *in silico* analysis using the software tools LAZAR, Toxtree, VEGA and TEST.

Table 1 Prediction of mutagenicity, carcinogenicity and genotoxicity of prynachlor and propisochlor with various in silico tools

Herbicide	VEGA Hub	Toxtree	Lazar	TEST
Prynachlor	mutagenic	mutagenic	mutagenic	mutagenic
	carcinogenic	carcinogenic	could not find similar substances for threshold 0.2 with experimental data in the training dataset.	
	non-genotoxic	genotoxic		
Propisochlor	mutagenic	mmutagenic	mutagenic	non-mutagenic
	carcinogenic	carcinogenic	cannot create prediction: only one similar compound for threshold 0.2 in the training set (threshold: 0.2).	
	non-genotoxic	genotoxic		

Toxtree, which classifies chemicals based on the presence of structural alerts, predicted that both prynachlor and propisochlor could potentially cause DNA damage, mutations, and cancer. In addition, indicating their potential toxicity, Toxtree classified both herbicides as “high” (class 3) toxic. These findings are consistent with previous studies that have reported the genotoxic and carcinogenic effects of chloroacetanilide herbicides.

Similarly, with consensus scores of 0.5 and 0.45 respectively, Vega Hub predicted that both prynachlor and propisochlor are mutagenic and carcinogenic. This is consistent with the results of the structural alerts predicted by Toxtree, suggesting that these herbicides have the potential to cause genetic mutations and cancer.

LAZAR, on the other hand, predicted prynachlor to have a low mutagenic potential with a probability of 0.12. Propisochlor was predicted to have a higher mutagenic potential with a probability of 0.439. This discrepancy in predictions between software tools highlights the limitations and uncertainties of *in silico* toxicity predictions, which are based solely on herbicide chemical structures and may not always accurately reflect their true toxicity.

TEST, another software tool used in this study, predicted that prynachlor would be mutagenic with a consensus score of 0.67, whereas propisochlor was predicted to be non-mutagenic with a consensus score of 0.40. This discrepancy between TEST and other software tools highlights that *in silico* toxicity predictions must be interpreted with caution and that additional experimental research is needed to support and confirm such predictions.

The results of this study are in line with the previous literature in which the genotoxic and carcinogenic effects of chloroacetanilide herbicides have been reported [28, 30]. Hill et al. (1997) [31] reported that chloroacetanilide herbicide exposure caused DNA damage and genetic mutations in human cells. Similarly, in animal studies, these herbicides induced carcinogenic effects leading to the development of tumors, as reported by Green et al. (2000) [32]. These findings support the hypothesis that prynachlor and propisochlor pose health risks through genotoxicity and carcinogenicity [25]. Furthermore, persistence of chloroacetanilide herbicides in soil and water is a concern, as it may lead to long-term environmental exposure [33].

It is important to consider the limitations of the current study. First, rather than using actual experimental data, the predictions were based on *in silico* analyses using the chemical structures of the herbicides [34]. Although these tools are widely used for the prediction of toxicity, the results should be critically evaluated and should be supported by additional experimental research to confirm the predicted genotoxic and carcinogenic effects of prynachlor and propisochlor.

Second, each of the software programs that were used in this study has its own set of limitations and assumptions. For example, Toxtree relies on the presence of structural alerts, which may not always be an accurate reflection of the true toxicity of a compound. Therefore, interpreting results based solely on *in silico* predictions should be done with caution.

Finally, the predictions from the software tools do not consider the potential synergistic or antagonistic effects that may occur when these herbicides are combined with other chemicals. In real-world scenarios, herbicides are often used in combination with other pesticides or chemicals, and their toxicity may be influenced by such interactions [35]. Therefore, further research is needed to assess the potential toxicity of prynachlor and propisochlor in realistic field conditions.

4. **CONCLUSION**

As a result of the *in silico* analysis used in this study, prynachlor and propisochlor herbicides may possess genotoxic and carcinogenic properties. Utilizing *in silico* tools helps in the development of safer and more sustainable substitutes by offering important insights into the potential toxicity of chemicals. To protect the environment, non-target organisms, and human health, it is critical to continue researching the potential health risks associated with the use of herbicides and other pesticides. To verify these predictions and evaluate the actual effects of these herbicides on human health and the environment, additional experimental studies are required.

REFERENCES

[1] Sun, S., Sidhu, V., Rong, Y. and Zheng, Y., Pesticide pollution in agricultural soils and sustainable remediation methods: a review. Current Pollution Reports. 4 (2018) 240-250. https://doi.org/10.1007/s40726-018-0092-x

[2] De, A., Bose, R., Kumar, A. and Mozumdar, S., Targeted delivery of pesticides using biodegradable polymeric nanoparticles, New Delhi: Springer India. (2014) pp. 5-6.

[3] Liman, R., Ali, M.M., Istifli, E.S., Ciğerci, İ.H. and Bonciu, E., Genotoxic and cytotoxic effects of pethoxamid herbicide on Allium cepa cells and its molecular docking studies to unravel genotoxicity mechanism. Environmental Science and Pollution Research. 29(42) (2022) 63127-63140. https://doi.org/10.1007/s11356-022-20166-5

[4] Cavas, T., In vivo genotoxicity evaluation of atrazine and atrazine–based herbicide on fish Carassius auratus using the micronucleus test and the comet assay. Food and Chemical Toxicology. 49(6) (2011) 1431-1435. https://doi.org/10.1016/j.fct.2011.03.038

[5] M. Moretti, M. Marcarelli, M. Villarini, C. Fatigoni, G. Scassellati-Sforzolini, and R. Pasquini, In vitro testing for genotoxicity of the herbicide terbutryn: cytogenetic and primary DNA damage, *Toxicology in Vitro*. 16(1) (2002) 81–88. https://doi.org/10.1016/S0887-2333(01)00092-3

[6] T. Huang, Y. Huang, Y. Huang, Y. Yang, Y. Zhao, and C. J. Martyniuk, Toxicity assessment of the herbicide acetochlor in the human liver carcinoma (HepG2) cell line, *Chemosphere*. 243 (2020) 125345. https://doi.org/10.1016/j.chemosphere.2019.125345

[7] N. H. Kumar and S. Jagannath, Cytological effects of herbicide alachlor in somatic cells of maize (Zea mays L.) and soybean (Glycine max Merrill.), *Biocatalysis and Agricultural Biotechnology.* 24 (2020) 101560. https://doi.org/10.1016/j.bcab.2020.101560

[8] Ma, X., Zhang, Y., Guan, M., Zhang, W., Tian, H., Jiang, C., Tan, X. and Kang, W., Genotoxicity of chloroacetamide herbicides and their metabolites in vitro and in vivo. International Journal of Molecular Medicine. 47(6) (2021) 1-10. https://doi.org/10.3892/ijmm.2021.4936

[9] L. Georgian, I. Moraru, T. Draghicescu, I. Dinu, and G. Ghizelea, Cytogenetic effects of alachlor and mancozeb, *Mutation Research/Genetic Toxicology*. 116(3) (1983) 341–348. doi: 10.1016/0165-1218(83)90072-1.

[10] H. Liu, T. Chu, L. Chen, W. Gui, and G. Zhu, In vivo cardiovascular toxicity induced by acetochlor in zebrafish larvae, *Chemosphere.* 181 (2017) 600–608. https://doi.org/10.1016/j.chemosphere.2017.04.090

[11] Nwani, C.D., Ama, U.I., Okoh, F., Oji, U.O., Ogbonyealu, R.C., Ibiam, A.A. and Udu-Ibiam, O., Acute toxicity of the chloroacetanilide herbicide butachlor and

its effects on the behavior of the freshwater fish Tilapia zillii. African journal of biotechnology. 12(5) 2013. https://doi.org/10.5897/AJB12.2433

[12] PubChem, "Prynachlor." https://pubchem.ncbi.nlm.nih.gov/compound/30559 ,2023 (accessed 02 March 2023).

[13] PubChem, "Propisochlor." https://pubchem.ncbi.nlm.nih.gov/compound/167454 ,2023 (accessed 02 March 2023).

[14] J. Kelton, "Herbicides: Current Research and Case Studies in Use." London, 2013.

[15] Eastmond, D.A. and Balakrishnan, S., Genotoxicity of pesticides. In Hayes' handbook of pesticide toxicology Academic Press (2010) pp. 357-380. https://doi.org/10.1016/B978-0-12-374367-1.00011-2

[16] R. Benigni, "Alternatives to the carcinogenicity bioassay for toxicity prediction: are we there yet?" *Expert Opinion on Drug Metabolism & Toxicology.* 8 (2012) 407–417. https://doi.org/10.1517/17425255.2012.666238

[17] Raunio, H., In silico toxicology–non-testing methods, Frontiers in pharmacology. 2 (2011) 33. https://doi.org/10.3389/fphar.2011.00033

[18] Zhu, F., Li, X.X., Yang, S.Y. and Chen, Y.Z., Clinical success of drug targets prospectively predicted by in silico study, Trends in Pharmacological Sciences. 39(3) (2018) 229-231. https://doi.org/10.1016/j.tips.2017.12.002

[19] E. Benfenati, A. Manganaro, and G. C. Gini, VEGA-QSAR: AI inside a platform for predictive toxicology, *PAI@ AI* IA.* 1107 (2013) 21–28.

[20] G. Patlewicz, N. Jeliazkova, R. J. Safford, A. P. Worth, and B. Aleksiev, An evaluation of the implementation of the Cramer classification scheme in the Toxtree software, *SAR and QSAR in Environmental Research.* 19 (2008) 495–524. https://doi.org/10.1080/10629360802083871

[21] R. Benigni and C. Bossa, Alternative strategies for carcinogenicity assessment: an efficient and simplified approach based on in vitro mutagenicity and cell transformation assays, *Mutagenesis.* 26(3) (2011) 455–460. https://doi.org/10.1093/mutage/ger004

[22] A. Maunz, M. Gütlein, M. Rautenberg, D. Vorgrimmler, D. Gebele, and C. Helma, Lazar: a modular predictive toxicology framework, *Frontiers in pharmacology.* 4 (2013) 38. https://doi.org/10.3389/fphar.2013.00038

[23] U.S. EPA , User's Guide for T.E.S.T. (version 5.1) (Toxicity Estimation Software Tool): A Program to Estimate Toxicity from Molecular Structure, 2020.

[24] Stanley, J., Preetha, G., Pesticide Toxicity to Fishes: Exposure, Toxicity and Risk Assessment Methodologies. In: Pesticide Toxicity to Non-target Organisms. Springer, Dordrecht, 2016, pp 411–497. https://doi.org/10.1007/978-94-017-7752-0_7

[25] S. S. Mohanty and H. M. Jena, A systemic assessment of the environmental impacts and remediation strategies for chloroacetanilide herbicides, *Journal of Water Process Engineering*. 31 (2019) 100860. doi: 10.1016/j.jwpe.2019.100860.

[26] G. U. Paul, Y. K. Marcellin, S. N. Soumahoro, and T. Albert, Health Risks of Triazine and Phenylurea Herbicides in Sediments of M'Badon Bay, Abidjan (Cote d'Ivoire), *Chemistry Africa*. 5(4) (2022) pp. 1139–1151. https://doi.org/10.1007/s42250-022-00394-5

[27] Smith-Roe, S.L., Swartz, C.D., Rashid, A., Christy, N.C., Sly, J.E., Chang, X., Sipes, N.S., Shockley, K.R., Harris, S.F., McBride, S.J. and Larson, G.J., Evaluation of the herbicide glyphosate, (aminomethyl) phosphonic acid, and glyphosate-based formulations for genotoxic activity using in vitro assays. Environmental and Molecular Mutagenesis. 64(4) (2023) 202-233. https://doi.org/10.1002/em.22534

[28] P. M. Hurley, Mode of carcinogenic action of pesticides inducing thyroid follicular cell tumors in rodents, *Environmental health perspectives*. 106(8) (1998) 437–445. https://doi.org/10.1289/ehp.98106437

[29] S. Dwivedi, Q. Saquib, A. A. Al-Khedhairy, and J. Musarrat, Butachlor induced dissipation of mitochondrial membrane potential, oxidative DNA damage and necrosis in human peripheral blood mononuclear cells, *Toxicology*. 302(1) (2012) 77–87. https://doi.org/10.1016/j.tox.2012.07.014

[30] N. Panneerselvam, S. Sinha, and G. Shanmugam, Butachlor is cytotoxic and clastogenic and induces apoptosis in mammalian cells, (1999).

[31] A. B. Hill, P. R. Jefferies, G. B. Quistad, and J. E. Casida, Dialkylquinoneimine metabolites of chloroacetanilide herbicides induce sister chromatid exchanges in cultured human lymphocytes, *Mutation Research/Genetic Toxicology and Environmental Mutagenesis*. 395(2–3) (1997) 159–171. https://doi.org/10.1016/S1383-5718(97)00163-0

[32] Green, T., Lee, R., Moore, R.B., Ashby, J., Willis, G.A., Lund, V.J. and Clapp, M.J.L., Acetochlor-induced rat nasal tumors: further studies on the mode of action and relevance to humans, Regulatory Toxicology and Pharmacology. 32(1) (2000) 127-133. https://doi.org/10.1006/rtph.2000.1413

[33] R. A. Rebich, R. H. Coupe, and E. M. Thurman, Herbicide concentrations in the Mississippi River Basin—the importance of chloroacetanilide herbicide degradates, *Science of the total environment*. 321(1–3) (2004) 189–199. https://doi.org/10.1016/j.scitotenv.2003.09.006

[34] L. G. Valerio Jr, In silico toxicology for the pharmaceutical sciences, *Toxicology and applied pharmacology*. 241(3) (2009) 356–370. https://doi.org/10.1016/j.taap.2009.08.022

[35] Tralau, T., Oelgeschlaeger, M., Guertler, R., Heinemeyer, G., Herzler, M., Höfer, T., Itter, H., Kuhl, T., Lange, N., Lorenz, N. and Mueller-Graf, C., Regulatory toxicology in the twenty-first century: challenges, perspectives and possible solutions. Archives of Toxicology. 89 (2015) 823-850. https://doi.org/10.1007/s00204-015-1510-0

Chapter 4

RECENT DEVELOPMENTS IN XANTHENE DERIVATIVES

Gönül YILDIZ[1]

Rahmi KASIMOĞULLARI[2]

1 Responsible Author, Research Assistant, Faculty of Arts and Sciences/ Department of Chemistry, Kütahya Dumlupınar University, Kütahya, Turkey, Orcid number: 0000-0002-1886-5964
e-mail: gonul.yildiz@dpu.edu.tr
2 Professor Dr., Faculty of Arts and Sciences/Department of Chemistry, Kütahya Dumlupınar University, Kütahya, Turkey,
e-mail: rahmi.kasimogullari@dpu.edu.tr

1. Introduction

Xanthene (9*H*-xanthene, (Fig. 1); is an organic compound with a closed formula of $C_{13}H_{10}O$, used in many organic reactions, and has a yellow crystalline structure [1]. It's biological [2] and pharmaceutical [3] properties increase the importance of xanthenes in organic chemistry. In addition to their anti-bacterial, anti-inflammatory, and anti-viral [4] effects, xanthene compounds, which are used as medicines, especially in the field of medicine, are also used in the photodynamic treatment of cancer, in the imaging of biomolecules in dyes, pH-sensitive fluorescence substances, and in laser technology [5].

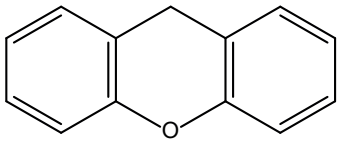

Figure 1. *Xanthene structure*

Due to all these properties, many studies have been carried out, especially for the synthesis of xanthene derivatives. Some of these are the reaction of benzaldehyde derivatives with *β*-naphthol [6], the reaction of triethyl orthoformate and aryl oxymagnesium halides [7] and the intramolecular phenyl-carbonyl ringing reaction [8]. In the synthesis of xanthene derivatives, various catalysts are used, such as $[Hbim]BF_4$ [9], Amberlite^{TM} IRA67 [10], $BF_3.OEt_2$ [11], Citric acid-DMU [12], Selectfluor^{TM} [13], [Msim]Cl [14], and $Fe_3O_4@SiO_2$-imid-PMA^n [15]. In recent studies, 1,8-dioxo-octahydro xanthene derivative compounds have been synthesized with high efficiency using effective catalysts.

Tab 1. *Synthesis of 1,8-dioxo-octahydro xanthene derivative compounds under different conditions.*

Catalyst	Reaction Conditions	Reaction Time (min)	Efficiency
UiO-66-NH_2-ILPF6$^-$-guanidine	Benzaldehyde (1 mmol), Dimedone (2 mmol), ethanol, room temperature	45 min	%95 [16]
DCDBTSD	Aromatic aldehyde (1 mmol), Dimedone (2 mmol), reflux, 90 °C	15-40 min	%80-95 [17]
n-TSA	Aromatic aldehyde (1 mmol), Dimedone (2 mmol), 90 °C	63-90 min	%83-96 [18]
$SiO_2/H_{14}[NaP_5W_{30}O_{110}]$	Aromatic aldehyde (1 mmol), Dimedone (2 mmol), water, reflux	180 min	%82-96 [19]
PEG-SO_3H	Aromatic aldehyde (1 mmol), Dimedone (2 mmol), 90 °C	30-375 min	%81-98 [20]
$SmCl_3$	Aromatic aldehyde (1 mmol), Dimedone (2 mmol), 120 °C	480-600 min	%97-98 [21]

Derivatives of xanthene are usually dyestuffs containing fluorescent, eosin, and rhodamine (Fig. 2) used as starting material [22]. In addition, the xanthene skeleton is found in natural compounds such as Gaudichaudione A, Gaudichaudione B, Allanxanthone C, and Funiculosone (Fig. 3) [23-26].

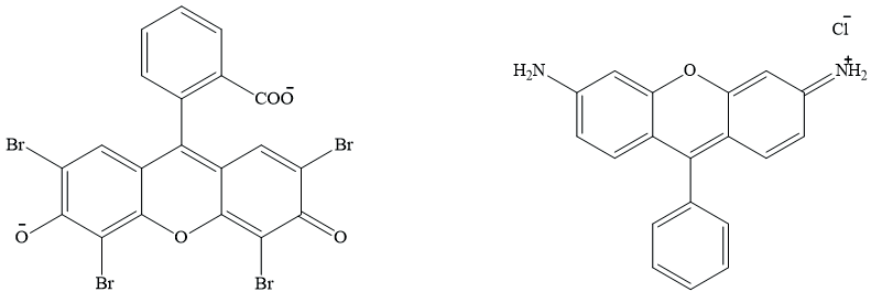

Figure 2. *Eosin ve Rhodamine Structures.*

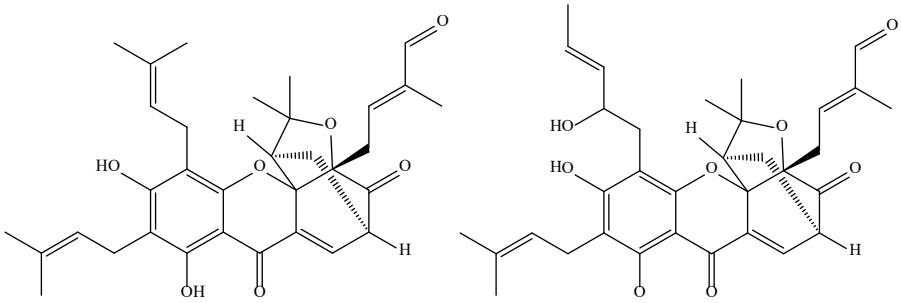

Gaudichaudione A *Gaudichaudione B*

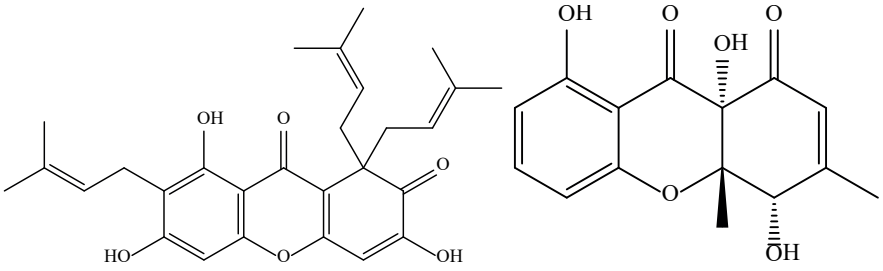

Allanxanthone C *Funiculosone*

Figure 3. *Chemical structures of some bioactive compounds, including the xanthene skeleton.*

Xanthene Synthesis Methods

Imon *et al* (2022) synthesized xanthene-derived compounds with high efficiency catalyzed by 2-aminophenol. In this study, various catalysts were used and it was determined that the most suitable catalyst was 2-aminophenol. Xanthene derivatives in the range of 70-90% yields were synthesized at 80°C in a solvent-free environment [27].

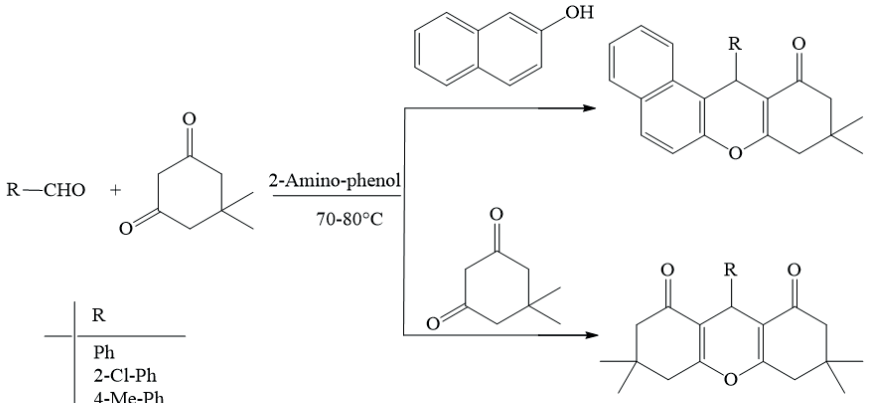

R
Ph
2-Cl-Ph
4-Me-Ph
3-Br-Ph
4-NO_2-Ph
4-Cl-Ph
3-OMe-Ph
4-OH-Ph
3-NO_2-Ph

Qareagha *et al* (2021) synthesized xanthene-derived compounds using Sg─CN, a heterogeneous acidic catalyst, in a single vessel based on benzaldehyde derivatives and the compound *β*-Naphthol [28].

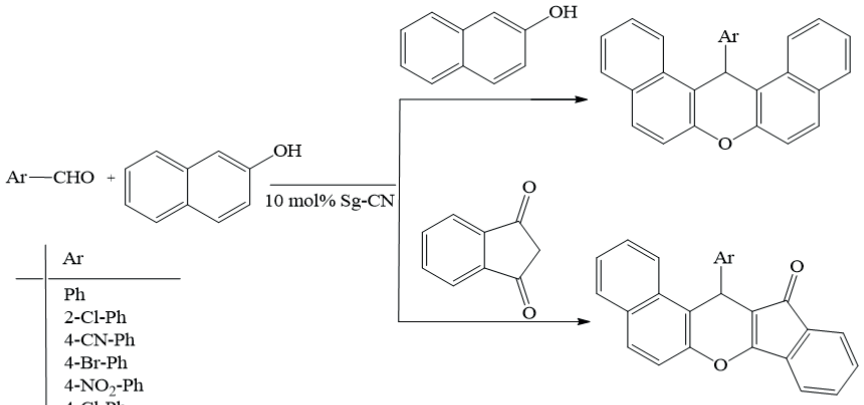

Ar
Ph
2-Cl-Ph
4-CN-Ph
4-Br-Ph
4-NO_2-Ph
4-Cl-Ph
4-OMe-Ph
4-OH-Ph
2-NO_2-Ph
3-Cl-Ph
4-Me-Ph

Cyclodextrins (CD) are cyclic maltooligosaccharides consisting of α(1-4) glycosidically bound glucose units and are used in many industrial fields such as food, medicine, cosmetics, chemicals, agriculture, and textiles. The interior of the cyclodextrins has the shape of a geometrically shaped 3D conical cylinder with a hydrophobic interior and a hydrophilic exterior [29]. Xanthene derivatives were synthesized by Mohamadpour and his team (2022) under the catalyst of *β*-Cyclodextrin, in water and in a short time [30].

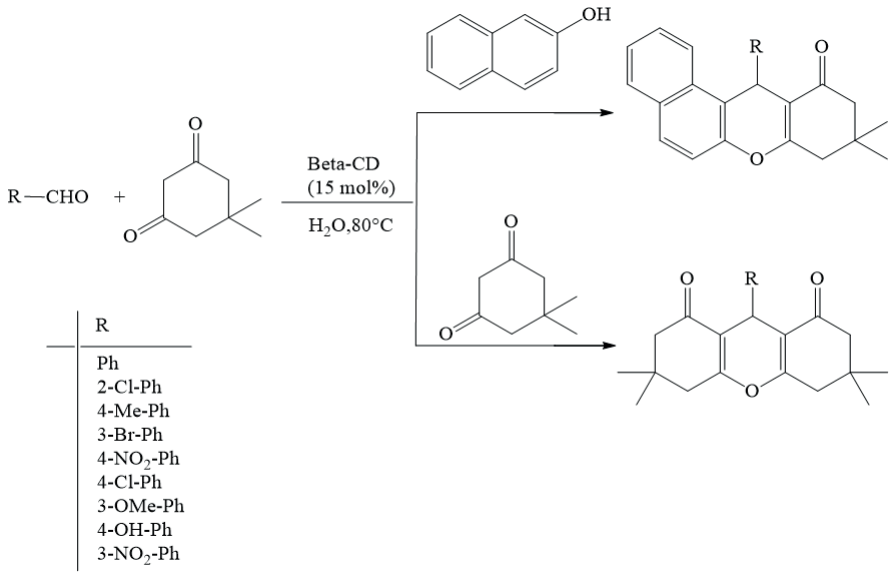

R
Ph
2-Cl-Ph
4-Me-Ph
3-Br-Ph
4-NO_2-Ph
4-Cl-Ph
3-OMe-Ph
4-OH-Ph
3-NO_2-Ph

Alsharif *et al* (2022) synthesized new benzoxanthenene derivatives using a Cu catalyst in 2-ethoxy ethanol. As a result of the Ullmann reaction, ringing took place and high yields were obtained in a short time [31].

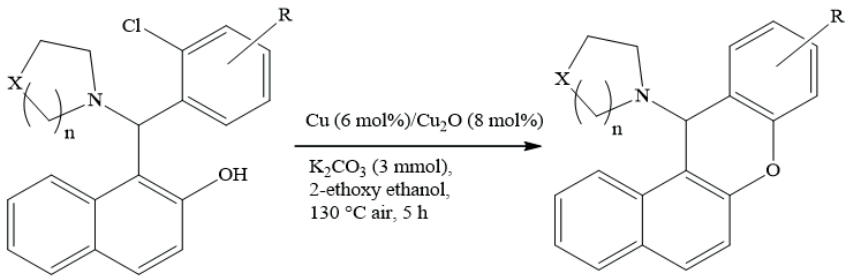

n: 1,2
X: CH_2, O
R: H, 2-MeO, 4-Me

Biological Activity of Xanthenes

Xanthenes are polycyclic compounds that can be found in a variety of physiologically important substances, including natural products [32]. Xanthene derivatives have antimicrobial [33], antiparasitic [34], antitumor [35], anticancer [36], antioxidant, anti-inflammatory [37], and antiproliferative [38] properties. It is also used in photo-dynamic processing [39] and as commercially available dyes [40].

Bhat *et al.* (2020) synthesized xanthene derivatives containing 2-chloro quinoline in a suitable single-pot container using the $[Et_3NH][HSO_4]$ catalyst. These compounds, which are formed as a result of multicomponent ringing, were evaluated for anti-tuberculosis activity *in vitro*. The 2 compounds between the synthesized compounds showed anti-tuberculosis activity [41].

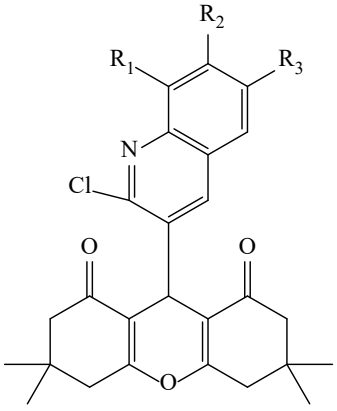

R_1	R_2	R_3
H	H	H
CH_3	H	H
H	CH_3	H
H	H	CH_3
OCH_3	H	H
H	OCH_3	H
H	H	OCH_3
Cl	H	H
H	Cl	H
H	H	Cl
H	H	F
H	H	OCH_2CH_3

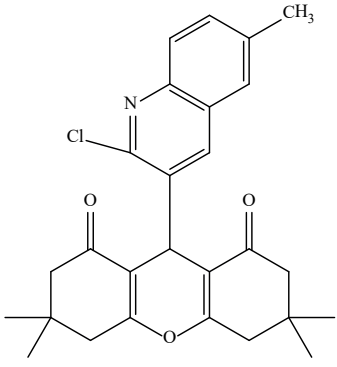

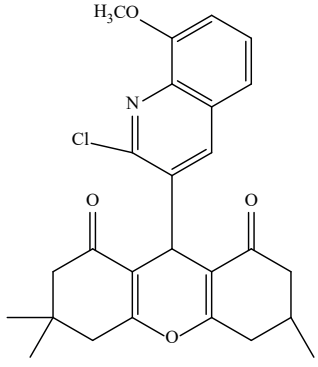

MIC values:

2.37 (μg/mL) *MTB* H37Ra	2.34 (μg/mL) *MTB* H37Ra
1.19 (μg/mL) *M. bovis* BCG	1.86 (μg/mL) *M. bovis* BCG

Lu *et al*. (2023) in a study evaluating xanthones with various substitutions at positions C-1, C-3, and C-6, found that an acetyl substitution group at position C-1 showed membrane selectivity, a higher inhibition of biofilm formation, and better antibacterial activity *in vivo* compared to other xanthones against *S. aureus* [42].

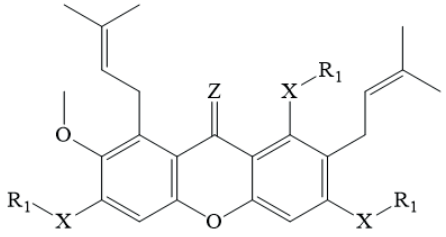

R_1	X	Z
CH_3	OCO	O
$CH(CH_3)_2$	OCO	O
Bn	O	O
H	O	H
CH_3	O	O

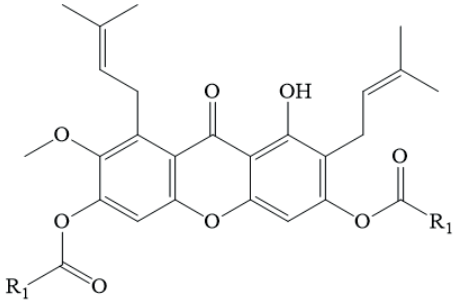

R_1
CH_3
$CH(CH_3)_2$

Lodha *et al*. (2023) reported the synthesis and biological evaluation of 9-aryl-1,8-dioxo-octahydroxanthene derivatives as antileishmanial agents. This study; confirms the prediction that some 9-aryl-1,8-dioxo-octahydroxanthene derivatives may act as an effective antileishmanial pharmacophore, inhibiting parasite TS [43].

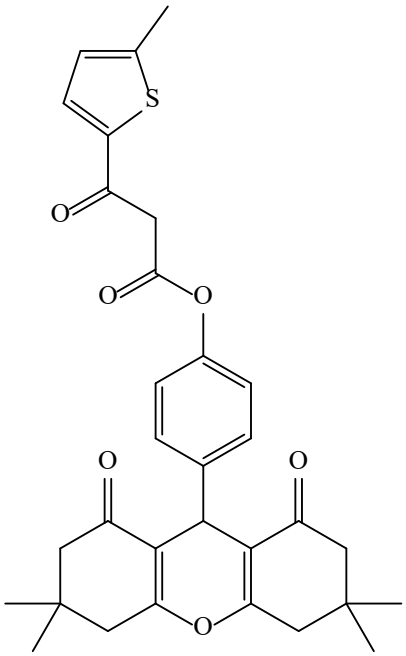

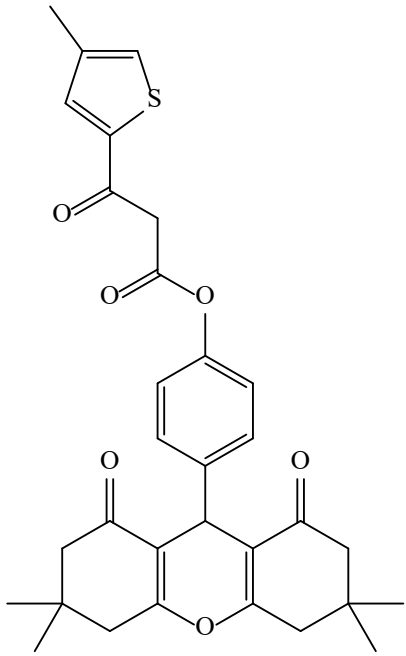

IC_{50} values: *28.08 μM* *28.21 μM*

Conclusion

To date, many collaborative teams have synthesized a large number of xanthene derivatives, tested their biological activity, and evaluated the results. In this review; general properties of xanthene structure, presentation of xanthene derivatives obtained in recent years as reactions, synthesis methods, effect of different catalysts on reaction and various biological activities are discussed. It will offer advantages for researchers who plan to study the structure of xanthene for biological activities and comprehensively understand its functions.

REFERENCES

[1] Banerjee, B. and Brahmachari, G. 2014. "Ammonium chloride catalysed one-pot multicomponent synthesis of 1,8-dioxo-octahydroxanthenes and *N*-aryl-1,8-dioxodecahydroacridines under solvent free conditions", *Journal of Chemical Research, 38*(12), 745-750. DOI: 10.3184/174751914X14177132210020

[2] Ziarani, G. M., Badiei, A. R. ve Azizi, M. 2011. "The one-pot synthesis of 14-aryl-14*H*-dibenzo [*a,j*]xanthene derivatives using sulfonic acid functionalized silica (SiO_2-Pr-SO_3H) under solvent free conditions", *Scientia Iranica*, *18*(3), 453-457. DOI: 10.1016/j.scient.2011.05.008

[3] Turgut, Z. ve Pektaş, B., 2018. "*Biyolojik aktivite içerebilecek heterohalkalı bileşiklerin tek kap yöntemi kullanarak triflat katalizörlü sentezler'*", 2. ULUSAL MARMARA ECZACILIK KONGRESİ (UMEK-2018) (pp.151). İstanbul, Turkey

[4] Smajović, A., Katica, M., Završnik, D., Veljović, E. ve Čaklovica, K. 2019. "Application of Xanten and Its Derivatives in Human and Veterinary Medicine", *Atatürk University J. Vet. Sci*.,*14*(3): 335-342. DOI: 10.17094/ataunivbd.567915.

[5] Mohammadian, N. ve Akhlaghinia, B. 2018. "Calcined oyster shell nanoparticles (COS NPs): a new, efficient and reusable catalyst for one-pot rapid preparation of 1,8-dioxo-octahydroxanthenes under solvent-free conditions", *Research on Chemical Intermediates*, *44*, 1085-1103. DOI: 10.1007/s11164-017-3153-7

[6] Hoseinzade, K., Mousavi-Mashhadi, S. A. ve Shiri, A. 2022. "An efficient and green one-pot synthesis of tetrahydrobenzo[a]xanthenes, 1,8-dioxo-octahydroxanthenes and dibenzo[*a,j*]xanthenes by Fe_3O_4@ Agar-Ag as nanocatalyst", *Molecular Diversity*, *26*(5), 2745-2759.

[7] Rajabi, F., Abdollahi, M., Diarjani, E. S., Osmolowsky, M. G., Osmolovskaya, O. M., Gómez-López, P., Puente-Sandiago, A.R. ve Luque, R. 2019. "Solvent-free preparation of 1,8-dioxo-octahydroxanthenes employing iron oxide nanomaterials", *Materials*, *12*(15), 2386. DOI: 10.3390/ma12152386

[8] Kuo, C. W. ve Fang, J. M. 2001. ''Synthesis of xanthenes, indanes, and tetrahydronaphthalenes via intramolecular phenyl–carbonyl coupling reactions", *Synthetic Communications*, *31*(6), 877-892. DOI: 10.1081/SCC-100103323

[9] Venkatesan, K., Pujari, S. S., Lahoti, R. J. ve Srinivasan, K. V. 2008. "An efficient synthesis of 1,8-dioxo-octahydro-xanthene derivatives promoted by a room temperature ionic liquid at ambient conditions under ultrasound irradiation", *Ultrasonics sonochemistry*, *15*(4), 548-553. DOI: 10.1016/j.ultsonch.2007.06.001

[10] Babu G, N., Belay, W. ve Endale, T. 2019. "Amberlite™ IRA67: A novel and efficient ion exchange resin catalyst for the synthesis of 1,8-dioxoxanthene derivatives", *Cogent Chemistry*, *5*(1), 1708160. DOI: 10.1080/23312009.2019.1708160

[11] Iniyavan, P., Balaji, G. L., Sarveswari, S. ve Vijayakumar, V. 2015. "CuO nanoparticles: Synthesis and application as an efficient reusable catalyst for

the preparation of xanthene substituted 1,2,3-triazoles via click chemistry", *Tetrahedron letters*, *56*(35), 5002-5009. DOI: 0.1016/j.tetlet.2015.07.016

[12] Li, P., Ma, F., Wang, P. ve Zhang, Z. 2013. "Highly Efficient Low Melting Mixture Catalyzed Synthesis of 1,8-Dioxo-dodecahydroxanthene Derivatives. *Chinese Journal of Chemistry*, *31*(6), 757-763. DOI: 10.1002/cjoc.201300152

[13] Poor Heravi, M. R. 2009. "Selectfluor™ promoted synthesis of 9-aryl-1,8-dioxooctahydroxanthane derivatives under solvent-free conditions", *Journal of the Iranian Chemical Society*, *6*(3), 483-488. DOI: 10.1007/BF03246525

[14] Shaterian, H. R., Sedghipour, M. ve Mollashahi, E. 2014. "Brønsted acidic ionic liquids catalyzed the preparation of 13-aryl-5*H*-dibenzo[*b,i*]xanthene-5,7,12,14(13*H*)-tetraones and 3,4-dihydro-1*H*-benzo*[b*] xanthene-1,6,11(2*H*,12*H*)-triones", *Research on Chemical Intermediates*, *40*, 1345-1355. DOI: 10.1007/s11164-013-1043-1

[15] Esmaeilpour, M., Javidi, J., Dehghani, F. ve Dodeji, F. N. 2014. "Fe_3O_4@SiO_2–imid–PMAn magnetic porous nanospheres as recyclable catalysts for the one-pot synthesis of 14-aryl-or alkyl-14*H*-dibenzo[*a,j*] xanthenes and 1, 8-dioxooctahydroxanthene derivatives under various conditions", *New Journal of Chemistry*, *38*(11), 5453-5461. DOI: 10.1039/C4NJ00961D

[16] Askari, S., Khodaei, M. M. ve Jafarzadeh, M. 2021. "Basic ionic liquid anchored on UiO-66-NH_2 metal–organic framework: a stable and efficient heterogeneous catalyst for synthesis of xanthenes", *Research on Chemical Intermediates*, *47*, 2881-2899. DOI: 10.1007/s11164-021-04439-1

[17] Khazaei, A., Abbasi, F. ve Moosavi-Zare, A. R. 2016. "Catalytic application of *N*,2-dibromo-6-chloro-3,4-dihydro-2*H*-benzo[*e*][1,2,4]thiadiazine-7-sulfonamide-1,1-dioxide as a new catalyst for the synthesis of 9-aryl-1,8-dioxo-octahydroxanthenes under neutral media", *Research on Chemical Intermediates*, *42*, 6719-6732. DOI: 10.1007/s11164-016-2492-0

[18] Amoozadeh, A., Hosseininya, S. F. ve Rahmani, S. 2018. "Nano titania-supported sulfonic acid (n-TSA) as an efficient, inexpensive, and reusable catalyst for one-pot synthesis of 1,8-dioxo-octahydroxanthene and tetrahydrobenzo[*b*]pyran derivatives", *Research on Chemical Intermediates*, *44*, 991-1011. DOI: 10.1007/s11164-017-3148-4

[19] Javid, A., Heravi, M. M. ve Bamoharram, F. F. 2011. "One-pot synthesis of 1,8-dioxo-octahydroxanthenes utilizing silica-supported preyssler nano particles as novel and efficient reusable heterogeneous acidic catalyst", *E-Journal of Chemistry*, *8*(2), 910-916. DOI: 10.1155/2011/980242

[20] Hasaninejad, A., Shekouhy, M., Miar, M. ve Firoozi, S. 2016. "Sulfonated Polyethylene Glycol (PEG-SO_3H) as eco-friendly and potent water soluble solid acid for facile and green synthesis of 1,8-dioxo-octahydroxanthene and 1,8-dioxo-decahydroacridine derivatives", *Synthesis and Reactivity in Inorganic, Metal-Organic, and Nano-Metal Chemistry*, *46*(1), 151-157. DOI: 10.1080/15533174.2014.900799

[21] Ilangovan, A., Malayappasamy, S., Muralidharan, S. ve Maruthamuthu, S. 2011. "A highly efficient green synthesis of 1,8-dioxo-octahydroxanthenes", *Chemistry Central Journal*, *5*, 1-6. DOI: 10.1186/1752-153X-5-81

[22] Belov, V. N., Wurm, C. A., Boyarskiy, V. P., Jakobs, S., & Hell, S. W. (2010). Rhodamines NN: a novel class of caged fluorescent dyes. *Angewandte Chemie International Edition*, *49*(20), 3520-3523. DOI: 10.1002/anie.201000150

[23] O. Chantarasriwong, B.D. Althufairi, N.J. Checchia, E.A. Theodorakis, Stud. Nat. Prod. *Chem. 58* (2018) 93–131.

[24] A.G. Azebaze, M. Meyer, A. Valentin, E.L. Nguemfo, Z.T. Fomum, A.E. Nkengfack, *Chem. Pharm. Bull.* 54 (Tokyo-2006) 111–113.

[25] X.M. Gao, T. Yu, F.S. Lai, Y. Zhou, X. Liu, C.F. Qiao, J.Z. Song, S.L. Chen, K.Q. Luo, H.X. Xu, *Bioorg. Med. Chem. 18* (2010) 4957–4964.

[26] S. Padhi, M. Masi, A. Cimmino, A. Tuzi, S. Jena, K. Tayung, A. Evidente, *Phytochemistry 157* (2019) 175–183.

[27] Imon, M. K., Islam, R., Karmaker, P. G., Roy, P. K., Lee, K. I., & Roy, H. N. (2022). A concise metal-free synthesis of xanthene derivatives mediated by achiral 2-aminophenol under solvent-free conditions. *Synthetic Communications*, *52*(5), 712-723. DOI: 10.1080/00397911.2022.2047730

[28] Qareaghaj, O. H., Ghaffarzadeh, M., & Azizi, N. (2021). A rapid and quantitative synthesis of xanthene derivatives using sulfonated graphitic carbon nitride under ball-milling. *Journal of Heterocyclic Chemistry*, *58*(10), 2009-2017. DOI: 10.1002/jhet.4327

[29] Ayşe, A. V. C. I., & Dönmez, S. (2010). Siklodekstrinler ve gıda endüstrisinde kullanımları. *Gıda*, *35*(4), 305-316.

[30] Mohamadpour, F. (2022). Supramolecular *β*-Cyclodextrin as a Reusable Catalyst for Xanthene Synthesis in Aqueous Medium. *Organic Preparations and Procedures International*, 1-9. DOI: 10.1080/00304948.2022.2141047

[31] Alsharif, M. A., Ahmed, N., Alahmdi, M. I., Mukhtar, S., Parveen, H., Obaid, R. J., & Almalki, A. S. (2022). Divergent synthesis of fused Benzo-xanthene and oxazine derivatives via Cu-catalyst. *Journal of Saudi Chemical Society*, *26*(6), 101568. DOI: 10.1016/j.jscs.2022.101568

[32] Robertson, L. P., Lucantoni, L., Duffy, S., Avery, V. M., & Carroll, A. R. (2019). Acrotrione: an oxidized xanthene from the roots of Acronychia pubescens. *Journal of natural products*, *82*(4), 1019-1023. DOI: 10.1021/acs.jnatprod.8b00956

[33] POUPELIN, J. P., Saint-Ruf, G., Foussard-Blanpin, O., Narcisse, G., Uchida-Ernouf, G., & Lacroix, R. (1978). Synthesis and antiinflammatory properties of bis(2-hydroxy-1-naphthyl)methane derivatives. I. Monosubstituted derivatives. *Chemischer Informationsdienst*, *9*(25). DOI: 10.1002/CHIN.197825154

[34] WATANABE, M., DATE, M., TSUKAZAKI, M., & FURUKAwA, S. (1989). Regioselective syntheses of substituted thioxanthen-and selenoxanthen-9-one

derivatives. *Chemical and pharmaceutical bulletin*, *37*(1), 36-41. DOI: 10.1248/cpb.37.36

[35] Showalter, H. H., Angelo, M. M., Berman, E. M., Kanter, G. D., Ortwine, D. F., Ross-Kesten, S. G., ... & Werbel, L. M. (1988). Benzothiopyranoindazoles, a new class of chromophore modified anthracenedione anticancer agents. Synthesis and activity against murine leukemias. *Journal of medicinal chemistry*, *31*(8), 1527-1539. DOI: 10.1021/ jm0 0403a009

[36] Davis, S., Weiss, M. J., Wong, J. R., Lampidis, T. J., & Chen, L. B. (1985). Mitochondrial and plasma membrane potentials cause unusual accumulation and retention of rhodamine 123 by human breast adenocarcinoma-derived MCF-7 cells. *Journal of Biological Chemistry*, *260*(25), 13844-13850. DOI: 10.1016/S0021-9258(17)38802-6

[37] Kim, J., & Song, J. H. (2016). Thioxanthenes, chlorprothixene and flupentixol inhibit proton currents in BV2 microglial cells. *European Journal of Pharmacology*, *779*, 31-37. DOI: 10. 1016/j.ejphar.2016.03.009

[38] Kumar, A., Sharma, S., Maurya, R. A., & Sarkar, J. (2010). Diversity oriented synthesis of benzoxanthene and benzochromene libraries via one-pot, three-component reactions and their anti-proliferative activity. *Journal of Combinatorial Chemistry*, *12*(1), 20-24. DOI: 10.1021/cc900143h

[39] Banerjee, A., & Mukherjee, A. K. (1981). Chemical aspects of santalin as a histological stain. *Stain Technology*, *56*(2), 83-85. DOI: 10.3109/10520298109067286.

[40] Yang, Y., Escobedo, J. O., Wong, A., Schowalter, C. M., Touchy, M. C., Jiao, L., ... & Strongin, R. M. (2005). A convenient preparation of xanthene dyes. *The Journal of organic chemistry*, *70*(17), 6907-6912. DOI: 10.1021/jo051002a

[41] Bhat, M. A., Al-Omar, M. A., Naglah, A. M., & Khan, A. A. (2020). $[Et_3NH][HSO_4]$-mediated efficient synthesis of novel xanthene derivatives and their biological evaluation.*Journal of Saudi Chemical Society*, *24*(5), 425-433. DOI: 10.1016/j.jscs.2020.03.006

[42] Lu, Y., Guan, T., Wang, S., Zhou, C., Wang, M., Wang, X., ... & Zhou, W. (2023). Novel xanthone antibacterials: Semi-synthesis, biological evaluation, and the action mechanisms. *Bioorganic & Medicinal Chemistry*, *83*, 117232. DOI: 10.1016/j.bmc.2023.117232

[43] Lodha, K., Wavhal, D., Bhujbal, N., Mazire, P., Bhujbal, S., Korde, A., ... & Shinde, V. (2023). Synthesis and biological evaluation of 9-aryl-1,8-dioxo-octahydroxanthene derivatives as antileishmanial agents. *Results in Chemistry*, *5*, 100943. DOI: 10.1016/j.rechem.2023.100943

Chapter 5

BIOLOGICALLY ACTIVE PYRAZOLE COMPOUNDS SYNTHESIZED BY USING DIFFERENT METHODS

Cetin Bayrak[1]

1 Dr. Öğretim Üyesi, cbk040203@gmail.com, Dogubayazit Ahmed-i Hani Vocational School, Agri Ibrahim Cecen University, Agri 04400, Turkey, Orcid number: 0000-0001-5169-7352

Introduction

Heterocyclic compounds between organic compounds are one of the fields most widely common in organic chemistry.[1] There are several five-membered aromatic rings among these compounds including such as pyrazole, isoxazole, imidazole, furan, thiophene, etc. Pyrazole scaffold is a five-member aromatic heterocycle ring that has two nitrogen atoms. [2] Pyrazole scaffolds are very attractive compounds in the synthetic and pharmaceutical chemistry fields because of their broad-scale biological properties [3] such as aldose reductase inhibition[4], antitumor, antibacterial[5], antifungal, antiviral[6], antiparasitic, anti-tubercular, insecticidal agents anti-inflammatory, anti-diabetic, anesthetic, carbonic anhydrase (CA),[7] and analgesic properties.[8] Pyrazoline compounds have also photophysical properties[9-11] Because of these properties, their synthesis became increasingly important. Some of the pyrazole-containing medicines (Figure. 1)

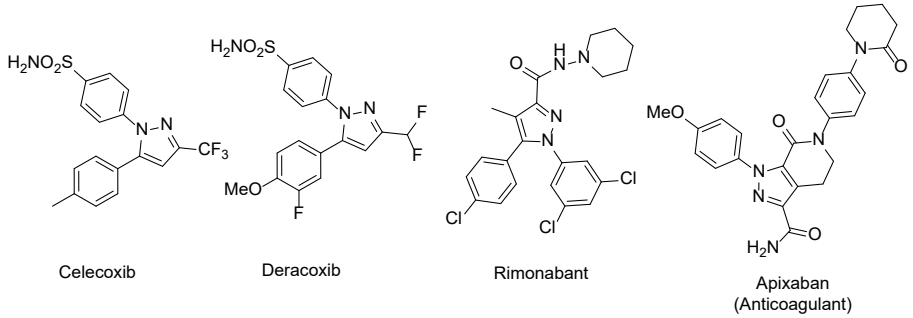

Figure 1. *FDA-approved medicines containing pyrazole*

There are a lot of methods for the synthesis of pyrazole compounds in the literature. The best well-known pyrazole synthesis is the Knorr reaction. The substituted pyrazole compounds have been obtained from the reaction of hydrazine with 1,3-dione compounds and or its derivatives (Scheme 1).[3]

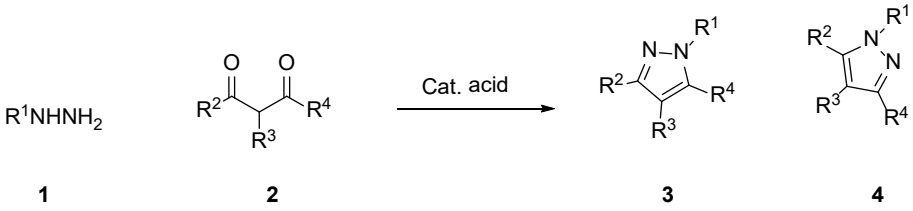

Scheme 1: *Knorr pyrazole synthesis*

Bayrak[4] reported the synthesis of pyrazole compounds from the reaction of α-β unsaturated aldehyde with phenyl hydrazine hydrate, then the DDQ was used for the oxidation of pyrazolines in the reactions (Scheme 2)

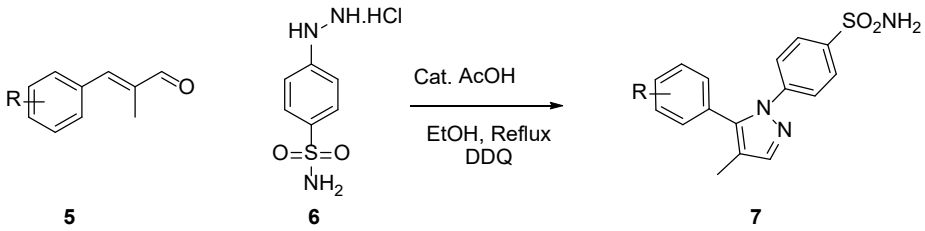

Scheme 2: *Synthesis of celecoxib derivatives pyrazoles acid-prompted*

Wang *et al* reported forming pyrazoles via hydrazone salt from the reaction of trifluoromethyl alkenone with $TsNHNH_2$. The type of solvent used in the reaction is very effective in the formation of the final product. When using H_2O as a solvent, allyl alcohol have been obtained. However, it was reported that pyrazoline compounds were formed when EtOH was used as a solvent in the reaction [12]

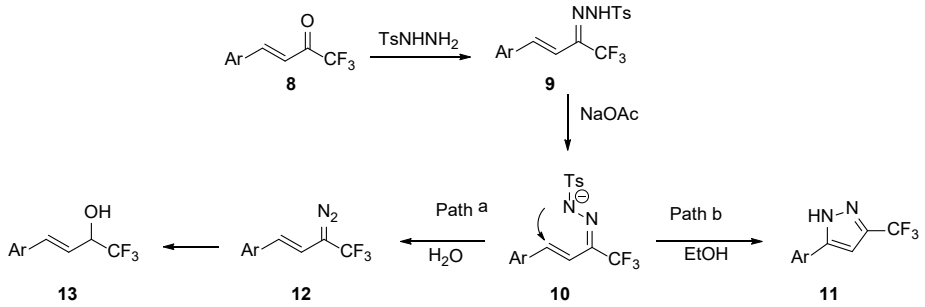

Scheme 2: *Synthesis of pyrazoles with $TsNHNH_2$*

Guo et al reported that pyrazoles synthesis of one-pot from propargylic alcohols with Bi(OTf)3-catalyzed presence of N-Iodosuccinimide(NIS). Firstly, The OH group was eliminated the presence of the Bismuth catalyst and generated intermediate A. Then in the step, the H_2O attacked to alkyne intermediate A, followed added of iodo to intermediate, and formed intermediate C. In the final step, attack of hydrazine hydrate on intermediate C gave the pyrazole **14**.[13]

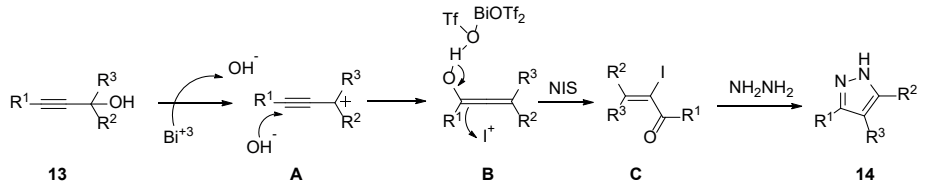

Scheme 3: *The reaction of hydrazine with propargyl alcohol by bismuth catalyst*

Pyrazoline or pyrazole compounds can be obtained from the 1,3-dipolar cycloaddition reactions. Bayrak *et al* reported the synthesis of compounds including pyrazole scaffold. They have reported obtaining two isomers from the reaction of hydrazonyl chloride with α,β- unsaturated Esther derivative.[9]

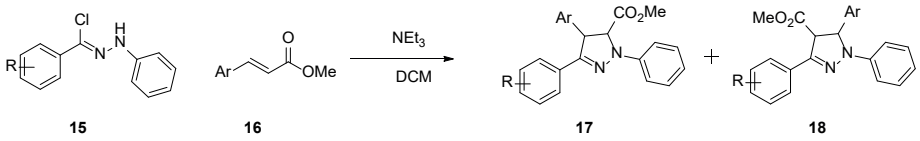

Scheme 4: *Synthesis of two isomeric pyrazoles from reaction hydrazonyl chloride with α,β- unsaturated*

Guo et al described the synthesis of pyrazole from a condensation reaction between 1,2-allenic ketone with hydrazine hydrate under mild conditions.[14]

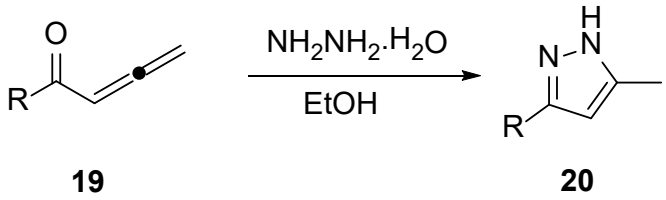

Scheme 5: *Synthesis of pyrazoles from the 1,2-allenic ketone*

The synthesizes of pyrazoles with metal-catalyzed have been investigated. Wang *et al* reported that an efficient method for the synthesis of a pyrazole between phenylhydrazine and corresponding 2,4-dione in the presence of copper salts in the acetonitrile[15]

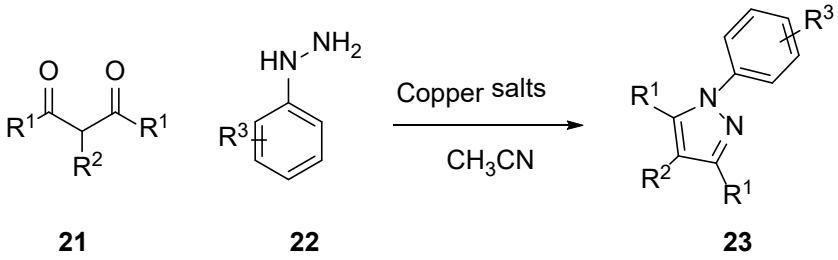

Scheme 5: *Synthesis of pyrazoles with copper salts*

Chen et al reported that pyrazole compounds have been developed from the copper-catalyzed reaction of N-tosyl hydrazone derivatives with diaryliodonium salts. N-tosyl hydrazone reacted in the presence of the base in the heat was formed intermediate A. After that, intermediate A converted

easily compounds B and C with the cyclization reaction. İn the final step, The compounds B and C gave corresponding N-arylation coupling products (**25-26**) with iodobenzene in the presence of copper acetate. [16]

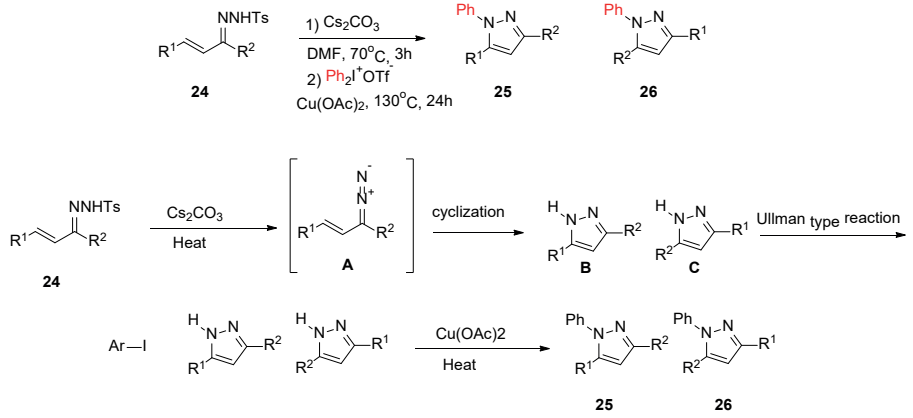

Scheme 6: *Synthesis of pyrazoles with copper acetat*

The resource iron-catalyzed pyrazole syntheses have been reported[17-21]

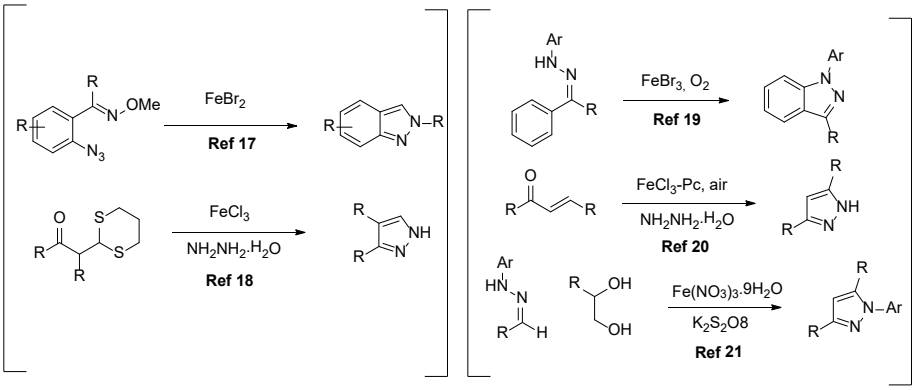

Scheme 6: *Synthesis of pyrazoles with different iron-catalyzed*

Panda *et al* also, reported iron-catalyzed one-pot regioselective pyrazole synthesis. For the synthesis of regioselective pyrazoles were used phenylhydrazine derivatives and ethylene glycol in the presence of acetylacetone (acac), $FeCl_3$, TBHP, and O_2. [22]

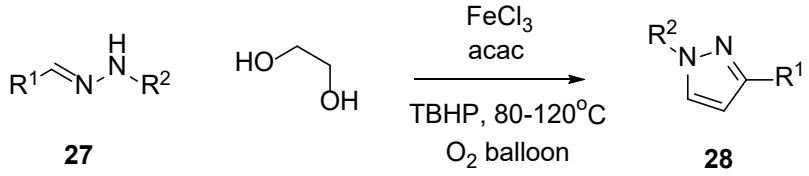

Scheme 7: *Synthesis of pyrazoles iron-catalyzed*

Schmitt *et al* has been reported the synthesis of pyrazole both in the presence of hydrogen transfer ruthenium catalyst and of a hydrogen acceptor crotonitrile.[23] When the mechanism is examined. Firstly, the Ru dihydride catalyst occurred from reacting compound **29** with crotonitrile. The O-Ru bond (A) can be formed interaction of diol **29** with the ruthenium catalyst. Dehydrogenation intermediate aldehyde B was formed from intermediate A with the help of the Ru catalyst. After that, the reaction of aldehyde B with the hydrazine gave intermediate C. Hydrogen transfer from compound C to crotonitrile gave ruthenium complex D. Finally, dehydrogenation aldehyde E and Ru dihydride species were obtained from the compound D. The pyrazole **30** was obtained from the intramolecular cycloaddition of E

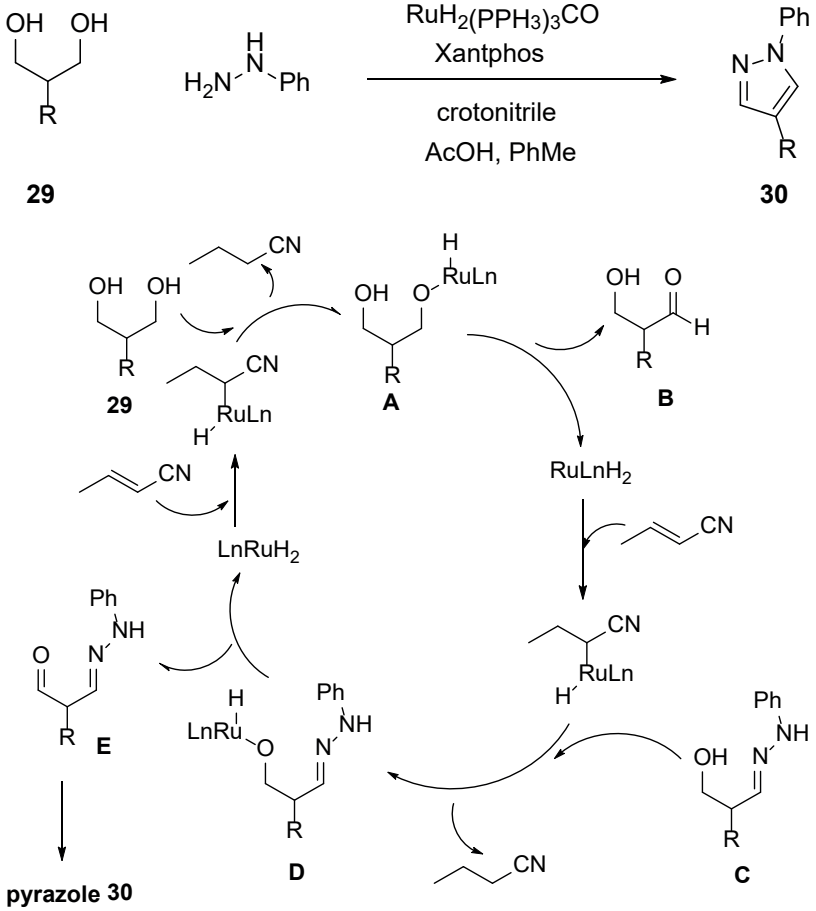

Scheme 8: *The postulated mechanism ruthenium catalyst*

The Ru catalyst forming with the combination of Ru with CBr_3F has been reported as an effective method for the synthesis of pyrazoles by Prieto *et al.*[24] Prieto et al. reported that the reaction pathway follows the RuII/RuIII redox

mechanism. lntermediate A is assumed to form with the abstraction of Br from CBr_3F by the Ru(II) complex. After that, the interaction of the hydrazone and radical A can form radical B. The result of oxidation of radical B with Ru(III) can give intermediate C and Ru(II). Subsequent, the elimination of HX from intermediate C by the presence of base would give intermediate D. ın the last step, with the removal of 1 more HX would occur pyrazole compound.

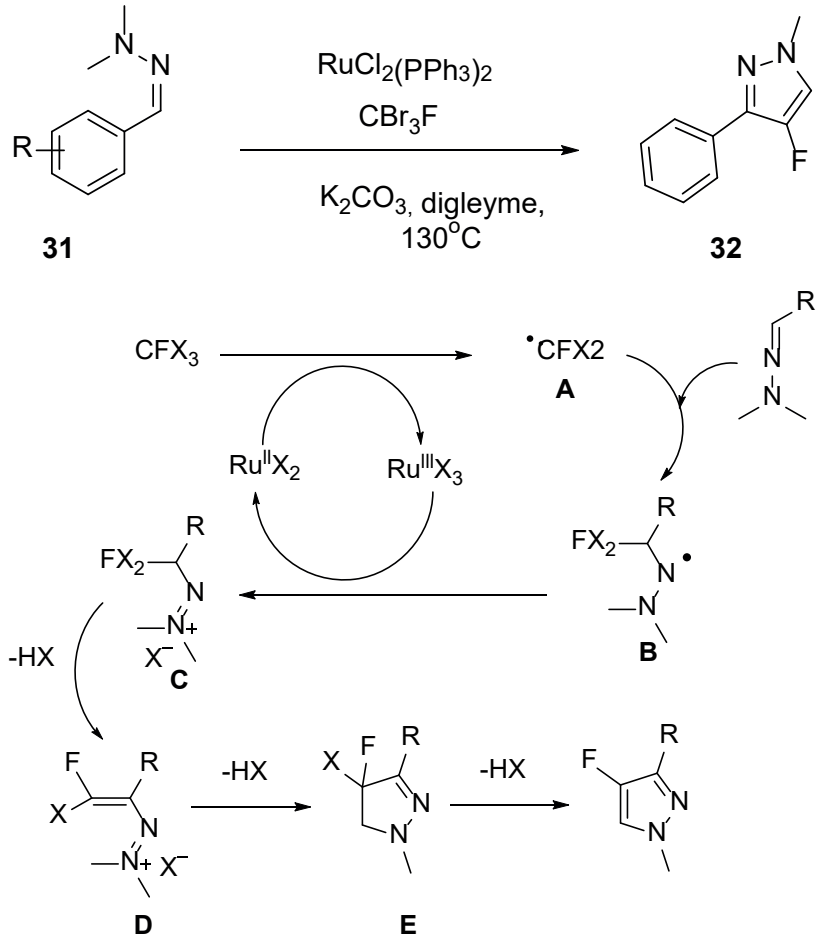

Scheme 9: *Radical synthesis of pyrazole with ruthenium catalyst*

Xu *et al.* reported that pyrazoles were synthesized from reaction the between N-benzylidene tolylsulfonohydrazides and 2,4-dione in the presence of silver salts.[25] The mechanism for the formation of the pyrazole gives in below. Firstly, the interaction of the silver salt with N- tosyl hydrazide would give intermediate A. subsequently, pyrazole **35** is formed from the reaction of the intramolecular nucleophilic addition (**B**) of compound A, and then following cyclization and H-shifting, respectively.

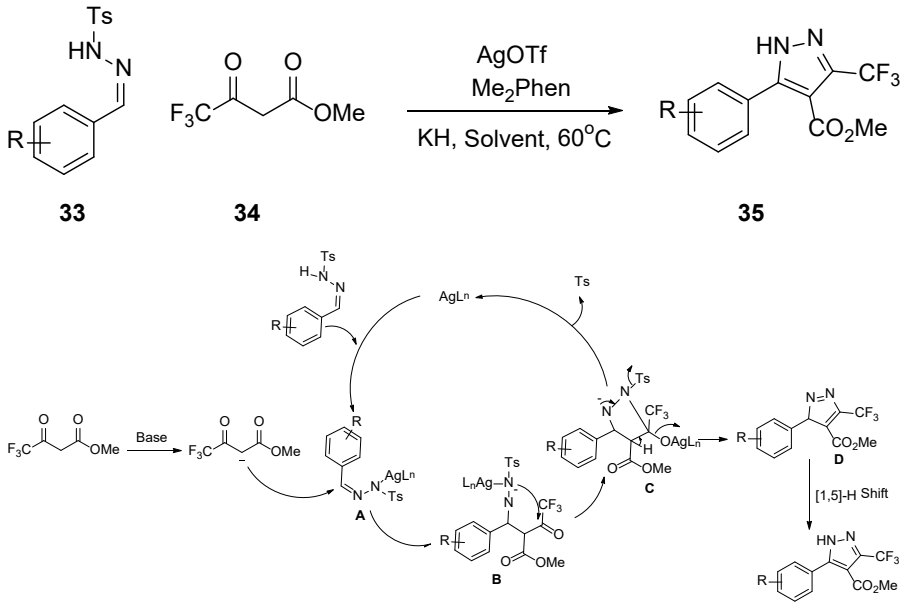

Scheme 10: *Synthesis of pyrazole with silver salt*

Fang *et al*[26] and Chen *et al*[27] reported that the synthesis of pyrazoles using diazo-ester and ketones in the different reaction conditions

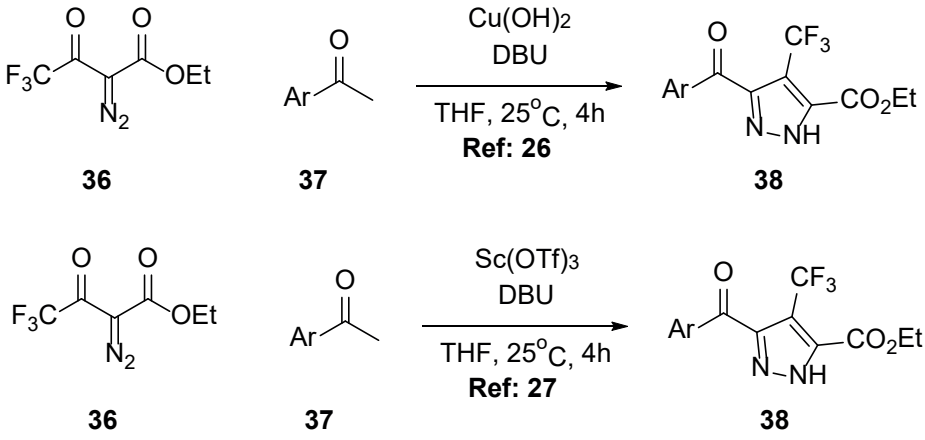

Scheme 11: *Synthesis of pyrazole from diazo-esters*

Meng et al. have reported the synthesis of pyrazoles the visible light-promoted.[28] The different pyrazoles compound were synthesized from the reaction of hydrazine and alkyne visible light-promoted with good yield (Scheme 12).

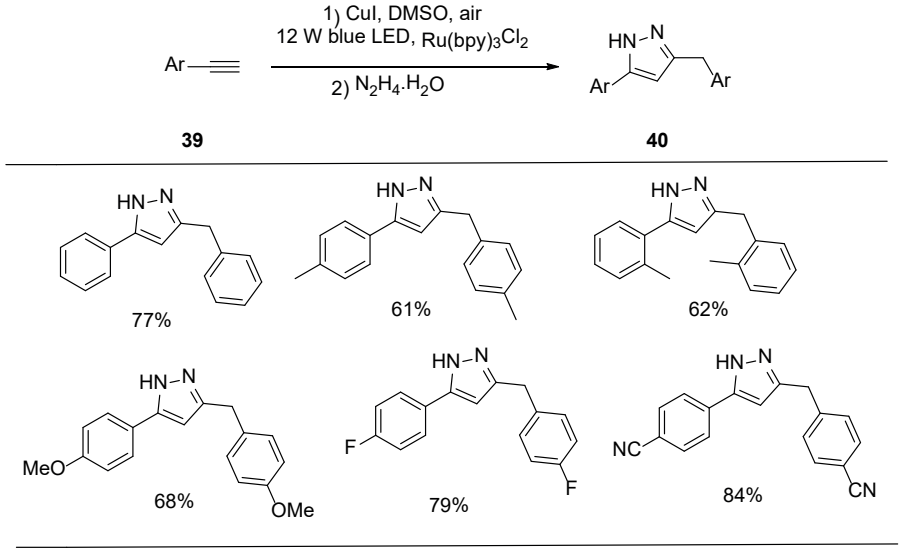

Scheme 12: *Synthesis of pyrazole visible light-promoted*

Fan[29] *et al*. have reported the synthesis of substitute pyrazoles by visible light promoted for preparing pyrazole scaffold using hydrazone and α-bromo ketones. They reported the synthesis of electron-rich and electron-deficient substituted pyrazole compounds with different yields in the scheme 13

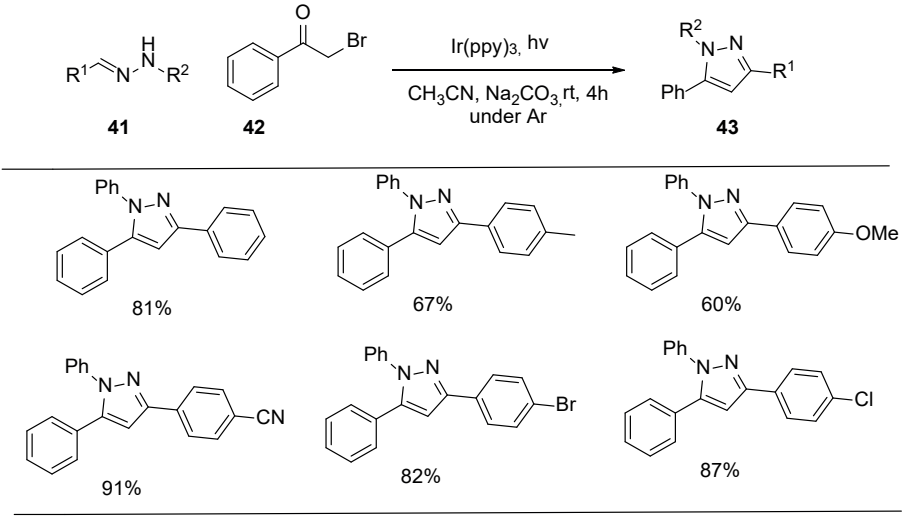

Scheme 13: *Synthesis of substituted pyrazoles with Ir(ppy)$_3$ catalyst*

REFERENCES

1. Kamal, R.; Kumar, A.; Kumar, R., Synthetic strategies for 1,4,5/4,5-substituted azoles: A perspective review. *Journal of Heterocyclic Chemistry* **2022,** *60* (1), 5-17.
2. Li, X.; Yu, Y.; Tu, Z., Pyrazole Scaffold Synthesis, Functionalization, and Applications in Alzheimer's Disease and Parkinson's Disease Treatment (2011-2020). *Molecules* **2021,** *26* (5).
3. Patra, S.; Patra, P., A Brief Review on the Design, Synthesis and Biological Evaluation of Pyrazolo[c]coumarin Derivatives. *Polycyclic Aromatic Compounds* **2023**, 1-42.
4. Bayrak, C., Synthesis and aldose reductase inhibition effects of celecoxib derivatives containing pyrazole linked-sulfonamide moiety. *Bioorg Chem* **2022,** *128*, 106086.
5. Sharshira, E. M.; Hamada, N. M., Synthesis and in vitro antimicrobial activity of some pyrazolyl-1-carboxamide derivatives. *Molecules* **2011,** *16* (9), 7736-45.
6. Rashad, A. E.; Hegab, M. I.; Abdel-Megeid, R. E.; Micky, J. A.; Abdel-Megeid, F. M., Synthesis and antiviral evaluation of some new pyrazole and fused pyrazolopyrimidine derivatives. *Bioorg Med Chem* **2008,** *16* (15), 7102-6.
7. Gul, H. I.; Mete, E.; Taslimi, P.; Gulcin, I.; Supuran, C. T., Synthesis, carbonic anhydrase I and II inhibition studies of the 1,3,5-trisubstituted-pyrazolines. *J Enzyme Inhib Med Chem* **2017,** *32* (1), 189-192.
8. Sharshira, E. M.; Hamada, N. M., Synthesis and antimicrobial evaluation of some pyrazole derivatives. *Molecules* **2012,** *17* (5), 4962-71.
9. Şenol, A. M.; Bayrak, Ç.; Menzek, A.; Onganer, Y.; Yaka, N., Synthesis and photophysical properties of new pyrazolines with triphenyl and ester derivatives. *Journal of Molecular Structure* **2020,** *1214*.
10. Li, Y.; Li, T.; Xiao, L.-Q.; Zhang, Y.-F., Novel Synthesis of Down-/Up-Conversion Fluorescent Oligo(2-pyrazoline)s. *Ind Eng Chem Res* **2018,** *57* (39), 12987-12992.
11. Salim, A. S.; Girgis, A. S.; Basta, A. H.; El-Saied, H.; Mohamed, M. A.; Bedair, A. H., Comparative DFT Computational Studies with Experimental Investigations for Novel Synthesized Fluorescent Pyrazoline Derivatives. *J Fluoresc* **2018,** *28* (4), 913-931.
12. Wang, Y. D.; Han, J.; Chen, J.; Cao, W. G., An efficient route to 3-trifluoromethylpyrazole via cyclization/1,5-H shift and its applications in the synthesis of bioactive compounds. *Tetrahedron* **2015,** *71* (43), 8256-8262.
13. Guo, H.; Zhang, Q.; Pan, W.; Yang, H.; Pei, K.; Zhai, J.; Li, T.; Wang, Z.; Wang, Y.; Yin, Y., One-pot Synthesis of Substituted Pyrazoles from Propargyl Alcohols via Cyclocondensation of in situ-Generated α-Iodo Enones/Enals and

Hydrazine Hydrate. *Asian Journal of Organic Chemistry* **2021,** *10* (8), 2231-2237.

14. Guo, S.; Wang, J.; Guo, D.; Zhang, X.; Fan, X., Synthesis of 3,5-disubstituted pyrazoles via cyclocondensation of 1,2-allenic ketones with hydrazines: application to the synthesis of 5-(5-methyl-pyrazol-3-yl)-2′ -deoxycytidine. *RSC Advances* **2012,** *2* (9).

15. Wang, H.; Sun, X.; Zhang, S.; Liu, G.; Wang, C.; Zhu, L.; Zhang, H., Efficient Copper-Catalyzed Synthesis of Substituted Pyrazoles at Room Temperature. *Synlett* **2018,** *29* (20), 2689-2692.

16. Chen, L. M.; Zhou, C.; Li, J.; Li, J.; Guo, X. Q.; Kang, T. R., Copper-catalyzed reactions of alpha,beta-unsaturated N-tosylhydrazones with diaryliodonium salts to construct N-arylpyrazoles and diaryl sulfones. *Org Biomol Chem* **2022,** *20* (35), 7011-7016.

17. Stokes, B. J.; Vogel, C. V.; Urnezis, L. K.; Pan, M.; Driver, T. G., Intramolecular Fe(II)-Catalyzed N-O or N-N Bond Formation from Aryl Azides. *Organic Letters* **2010,** *12* (12), 2884-2887.

18. Wang, Y. M.; Bi, X. H.; Li, W. Q.; Li, D. H.; Zhang, Q. A.; Liu, Q.; Ondon, B. S., Iron-Catalyzed Aminolysis of beta-Carbonyl 1,3-Dithianes: Synthesis of Stereodefined beta-Enaminones and 3,4-Disubstituted Pyrazoles. *Organic Letters* **2011,** *13* (7), 1722-1725.

19. Zhang, T.; Bao, W., Synthesis of 1H-indazoles and 1H-pyrazoles via FeBr3/O2 mediated intramolecular C-H amination. *J Org Chem* **2013,** *78* (3), 1317-22.

20. Zhao, J.; Qiu, J.; Gou, X.; Hua, C.; Chen, B., Iron(III) phthalocyanine chloride-catalyzed oxidation–aromatization of α,β-unsaturated ketones with hydrazine hydrate: Synthesis of 3,5-disubstituted 1H-pyrazoles. *Chinese Journal of Catalysis* **2016,** *37* (4), 571-578.

21. Panda, N.; Ojha, S., Facile synthesis of pyrazoles by iron-catalyzed regioselective cyclization of hydrazone and 1,2-diol under ligand-free conditions. *Journal of Organometallic Chemistry* **2018,** *861*, 244-251.

22. Panda, N.; Jena, A. K., Fe-catalyzed one-pot synthesis of 1,3-di- and 1,3,5-trisubstituted pyrazoles from hydrazones and vicinal diols. *J Org Chem* **2012,** *77* (20), 9401-6.

23. Schmitt, D. C.; Taylor, A. P.; Flick, A. C.; Kyne, R. E., Jr., Synthesis of pyrazoles from 1,3-diols via hydrogen transfer catalysis. *Org Lett* **2015,** *17* (6), 1405-8.

24. Prieto, A.; Bouyssi, D.; Monteiro, N., Ruthenium-Catalyzed Tandem C-H Fluoromethylation/Cyclization of N-Alkylhydrazones with CBr(3)F: Access to 4-Fluoropyrazoles. *J Org Chem* **2017,** *82* (6), 3311-3316.

25. Xu, Y.; Chen, Q.; Tian, Y.; Wu, W.; You, Y.; Weng, Z., Silver-catalyzed synthesis of 5-aryl-3-trifluoromethyl pyrazoles. *Tetrahedron Lett* **2020,** *61* (5).

26. Fang, Z.; Yin, H.; Lin, L.; Wen, S.; Xie, L.; Huang, Y.; Weng, Z., Collaborative Activation of Trifluoroacetyl Diazoester by a Lewis Acid and Base for the

Synthesis of Polysubstituted 4-Trifluoromethylpyrazoles. *J Org Chem* **2020,** *85* (13), 8714-8722.

27. Chen, H.; Wen, S.; Cui, Y.; Lin, L.; Zhang, H.; Fang, Z.; You, Y.; Weng, Z., A method for synthesis of polysubstituted 4-difluoromethyl and perfluoroalkyl pyrazoles. *Tetrahedron* **2021,** *85*.

28. Meng, Y.; Zhang, T.; Gong, X.; Zhang, M.; Zhu, C., Visible-light promoted one-pot synthesis of pyrazoles from alkynes and hydrazines. *Tetrahedron Lett* **2019,** *60* (2), 171-174.

29. Fan, X. W.; Lei, T.; Zhou, C.; Meng, Q. Y.; Chen, B.; Tung, C. H.; Wu, L. Z., Radical Addition of Hydrazones by alpha-Bromo Ketones To Prepare 1,3,5-Trisubstituted Pyrazoles via Visible Light Catalysis. *J Org Chem* **2016,** *81* (16), 7127-33.

Chapter 6

THE OXIDATIVE STRESS HYPOTHESIS OF ALZHEIMER'S DISEASE

Uğur GÜLLER[1]

1 Doç. Dr. Uğur Güller. ORCID: 0000-0003-0704-5984, Iğdır University, Faculty of Engineering, Food Engineering, Iğdır, Turkey

1. Introduction

Dementia is a cognitive decline that interferes with daily, household, or social functioning in the later years of life (Gale et al., 2018). As mentioned a study performed in 2019, it was predicted that the number of people aged ≥ 65 in Turkey is 6.4 million and 7.1% of people in this age group have dementia. It is predicted that this rate will increase to 14.7% in 2050 (TUIK 2021). Alzheimer's disease (AD) is known as the most frequent form of dementia. Cholinergic neuron degeneration in regions of the brain associated with memory and learning is a hallmark of AD, a progressive neurodegenerative illness. The typical pathology of AD is most pronounced in the hippocampus and neocortex of the brain connected to higher mental actions (Hardy and Selkoe, 2002). According to WHO reports, it was predicted that 50 million people worldwide have AD in 2019. By 2050, this number is likely to increase to 152 million. Dementia and AD are seen as the seventh cause of mortality in the world (WHO 2019).

2. Pathophysiology of Alzheimer's Disease

So many factors have been related to the pathogenesis of AD, including the extracellular stack of β-amyloid (Aβ) plaques, the formation of intracellular oxidative neuronal damage, inflammatory cascades, and neurofibrillary tangles. The pathogenesis of the disease, however, is widely thought to be mainly impacted by an increase in the formation of the Aβ peptide, the principal component of amyloid plaques. Numerous researches have looked at the cellular and molecular diseases caused by Aβ since the peptide's neurotoxic characteristics were first described (Chopra et al., 2011; Imbimbo et al., 2005). Impairments in a variety of mental abilities, including memory, speaking, direction-finding, facial recognition, and problem-solving, are the most prevalent symptoms among AD patients (Blennow et al., 2006; Bartzokis, 2004). Brain atrophy and enlarged cerebral ventricles are morphological features of the disease (Imbimbo et al., 2005). AD is identified histologically by extracellular deposits known as cerebral plaques, which are composed of a thick proteinaceous nucleus containing the Aβ peptide encircled by injured or dead neurons (Speroni, 2005). When AD is investigated biochemically, a cholinergic system deficit is the most glaring and constant discovery.

Acetylcholine, which is released by the cholinergic system, is a neurotransmitter that is crucial for brain nerve cells to communicate with one another. The primary purpose of acetylcholine (ACh) when it is released by nerve cells into the synaptic cleft is to facilitate the transmission of neural signals to muscles or other connected tissues within the nervous system. Its role is to guarantee that neural inputs effectively reach their intended targets (Figure 1). ACh diminishes fast in cases of memory loss (Dhanasekaran, 2015; Geula, 1999). Both acetylcholinesterase (AChE, EC 3.1.1.7) and

butyrylcholinesterase (BuChE, EC 3.1.1.8) are able to hydrolyze ACh. BuChE is expressed and excreted by glial cells in the brain, whereas AChE is mostly linked to neurons and axons. It has also been shown that both cholinesterases can generate Aβ plaques, which can be reduced by using inhibitors. BuChE, rather than AChE, is used by certain neurons to break presynaptic ACh. AChE is existed 4 times more common than BuChE in the healthy human brain. Although BuChE appears to act minimum in regulation, it has been connected to drug metabolism, obesity, cardiovascular disease, hepatic adiposity, and lipoprotein metabolism (Koca et al., 2022; Darvesh et al., 2003; Darvesh et al., 1998). In the brain, AChE levels drop to between 55 and 67% of normal in advanced AD, whereas BuChE levels rise to 120% of normal, indicating that BuChE is crucial for hydrolysis of ACh in this stage of the disease (Carolan et al., 2010; Manoharan et al., 2007; Greig et al., 2001). Due to the role of AChE and BuChE inhibition in the treatment strategy of AD, many studies have been conducted on *in vitro* inhibition of these enzymes (Kılınç et al., 2022; Güller, 2021; Güller et al., 2021).

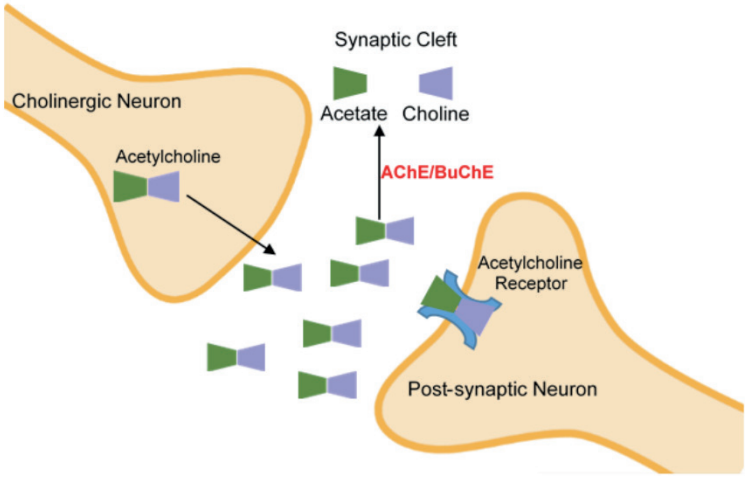

Figure 1. *Acetylcholine in cholinergic system (Koca et al., 2022)*

Most cases of AD are usually the consequences of a combination of environmental agents, the aging process, and genetic risk factors. That is, the effect of a particular genetic mutation in the onset of the disease is less pronounced, with about 5% of patients developing the disease early as a result of fully penetrating autosomal dominant gene mutations (Imbimbo et al., 2005).

There are several hypotheses regarding the pathophysiology of AD. The most common ones are;

• Amyloid hypothesis: AD is caused by a buildup of plaques in the brain termed amyloid beta (Aβ). These plaques impede nerve cell communication, causing inflammation and brain damage.

• Tau hypothesis: According to this hypothesis, tau proteins in the brain develop aberrant formations called neurofibrillary tangles in AD. These formations destroy nerve cells and impede brain communication.

• Oxidative stress hypothesis: The pathogenesis of Alzheimer's disease is linked to increasing oxidative stress in the brain. Oxidative stress causes the accumulation of free radicals and cell damage.

• Inflammation hypothesis: AD is caused by inflammation in the brain. This inflammation causes nerve cells in the brain to become damaged and die.

Each of these hypotheses attempts to explain different aspects of AD, and the exact reason of the disease is not yet totally comprehended.

This section is focused on oxidative stress hypothesis of AD.

3. What is oxidative stress?

Oxidative Stress (OxS) is described as an unbalance between antioxidants and oxidants that favors the oxidants, resulting in redox signaling and control disturbance and molecular damage (Sies et al., 2017; Sies and Jones, 2007) (Figure 2). OxS occurs when the body's antioxidant defense systems fail to neutralize free radicals.

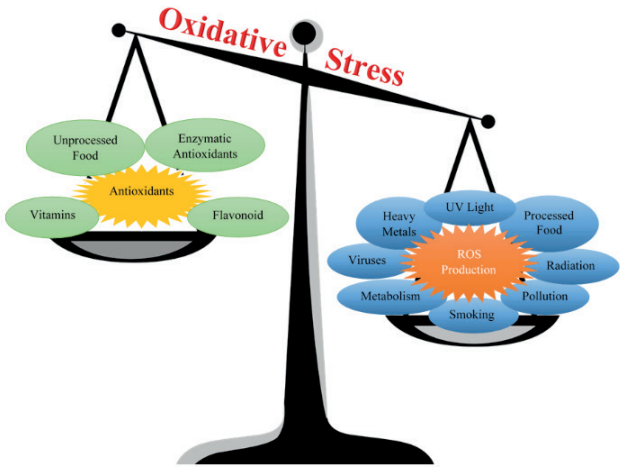

Figure 2. *Oxidative stress occurs when the balance between oxidants and antioxidants is disturbed.*

Free radicals arise within cells as a result of regular metabolic reactions. Nevertheless, the excessive buildup of free radicals beyond the optimal levels

within cells has the potential to inflict harm upon cellular structures and tissues. Free radicals are chemicals commonly known reactive nitrogen and oxygen species (RNS and ROS). ROS and RNS can be broadly classified into two groups, radical species such as hydroxyl ($OH^{\bullet}$), superoxide (O_2^{-}), and oxygen radical ($O_2^{\bullet-}$) and non-radical species such as hypochlorous acid (HOCl), hydrogen peroxide (H_2O_2), and organic peroxides (ROOH). Radical species are more reactive species that are highly electrophilic because of the existence of an unpaired electron (Cheeseman and Slater, 1993). Free radicals combine with oxygen molecules to destroy cell components, which is the main mechanism of OxS. Free radicals can oxidize cell membranes, lipids, proteins, and even DNA. This oxidative damage can impair cell processes, increase cell membrane permeability, modify enzyme activity, and disturb intracellular communication. OxS is known to be activated by a variety of events. These include aging, smoking, starvation, toxic exposure, chronic inflammation, infections, radiation, and stress (Sies, 2017; Ohl, 2016). OxS has numerous impacts and plays an important part in many disorders. OxS is thought to contribute to the development of a variety of diseases and ailments, including cancer, neurological, cardiovascular, and autoimmune diseases, as well as aging, due to cell damage and oxidative DNA damage. Antioxidant defense systems are activated to mitigate the effects of OxS. Antioxidants decrease the impacts of OxS by neutralizing free radicals. Therefore, adopting a healthy lifestyle, including antioxidant-rich foods in the diet, managing stress and reducing exposure to environmental toxins have an important role in reducing the effects of OxS (Wang, 2010; Barnham, 2004).

4. Effects of environmental factors on oxidative stress

Animals, plants, and humans can all experience metabolic alterations as a consequence of environmental stress. These modifications either result in a rise in reactive oxygen and nitrogen species (RONS) formation or a reduction in antioxidant production. Environmental factors can have significant effects on OxS (Babacanoğlu and Güller, 2021; Güller et al., 2020). ROS production can occur from either endogenous or external sources.

The effects of environmental factors on OxS have a strong link with exogenous sources of ROS (Figure 3). UV rays, X-rays, gamma rays, microwave rays, burning of organic materials during forest fires, volcanic activities, air pollutants such as asbestos, carbon monoxide, formaldehyde, ozone and toluene, cleaning products, paint, glue, perfumes, thinner and chemicals such as pesticides, water pollutants, alcohol and smoke can contribute to the formation of free radicals exogenously (Karabulut and Gülay, 2016). Exposure to these factors can cause to increased OxS and oxidative damage to cells. Especially in the case of prolonged exposure, these external factors can boost ROS production, increasing the imbalance in cells. Therefore, controlling environmental factors and reducing exposure are important in terms of mitigating the effects of OxS and protecting health.

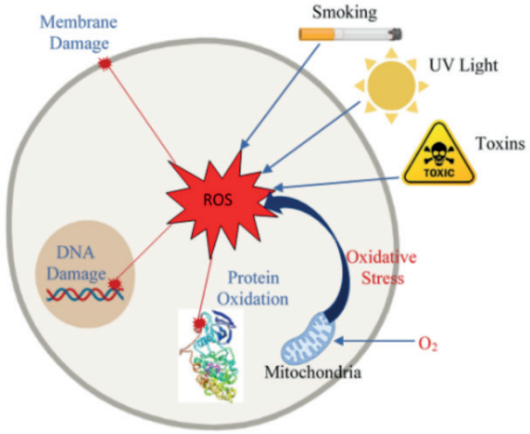

Figure 3. *Exogenous sources of ROS and effects on cells.*

5. The relationship between oxidative stress and aging

Aging is a natural biological process that all living things go through. Individuals' ability to adapt to their surroundings and their ability to balance cell activities deteriorate throughout time (Öğüt and Atay, 2012; Eşer, 1991). This process is caused by molecular changes such as genetic instability, telomere erosion, epigenetic modifications, and proteostasis loss (López-Otín et al., 2013). Aging causes physiological and anatomical changes that influence disease development.

Although life expectancy has lately increased considerably due to advances in medical treatment, immunization, and hygiene measures, the aging process remains an unavoidable natural occurrence (Rappuoli et al., 2014; Eggleston and Fuchs, 2012). The aging process happens when cells' ability to adapt to their surroundings and achieve a balance between internal and external influences declines. This process results in physiological and anatomical alterations as well as the emergence of numerous disorders. Cardiovascular and neurological illnesses, for example, are linked to aging (Wyss-Coray, 2016; Samani and van der Harst, 2008; Finkel et al., 2007).

There is also a relationship between the aging process and OxS. OxS is associated with accumulation of free radicals in cells and increased oxidative damage. This can occur as a result of cellular damage during the aging process. OxS causes changes in cells such as DNA damage, protein dysfunction and cell membrane damage.

ROS production of mitochondria and DNA damage occurs with age, eventually leading to the cell's failure to recognize the essential role of

mitochondria (Son and Lee, 2019). At this point, a relationship emerges between OST (Oxidative Stress Theory) and MFRTA (Mitochondrial Free Radical Theory of Aging). MFRTA is a theory that proposes that during the aging process, increased production of ROS by mitochondria and deposition of mitochondrial DNA damage result in cells failing to recognize the essential role of mitochondria. In this case, the effect of OxS on the aging process suggested by OST is aligned with MFRTA by increasing the production of ROS by mitochondria and contributing to the accumulation of mitochondrial damage. Although still being discussed, two basic expressions in aging are as follows; The first expression is the accumulation of oxidatively damaged macromolecules as a result of oxidative damage and antioxidant imbalance with aging. The second statement is that the accumulated oxidative damage leads to the degenerative aging phenotype (Lara, 2018; Zhang et al., 2015). OxS occurs as a result of cellular damage during the aging process and influences the development of aging-related health problems. Increasing OxS can speed up the progression of aging-related diseases and negatively affect the quality of life.

6. The connection between OxS and the pathophysiology of AD

Different factors contributing to beta-amyloid protein (Aβ) accumulation in aging have been proposed, and intense OxS has been shown as the main cause of this accumulation (Bonda et al., 2010; Butterfield and Lauderback, 2010).

Due to its high oxygen requirement, low antioxidant content, and abundance of easily oxidizable polyunsaturated fatty acids and redox-active metal ions, the brain is particularly sensitive to OxS. (Wang and Michaelis, 2010). ROS have important roles in the pathogenesis of neurological diseases. Therefore, OxS has been suggested as a significant process in neurodegenerative disorders such as Parkinson's disease (PD), AD, multiple sclerosis (MS), and amyotrophic lateral sclerosis (ALS) (Singh et al., 2019; Ohl et al. al., 2016; Barnham et al., 2004).

OxS damages neuronal DNA in the brain, triggering strand breaks, sister chromatid exchange, DNA-protein cross-linking and base modification (Tonnies and Trushina, 2017). In neuropsychiatric diseases, however, a decrease in the levels of antioxidative enzymes is observed and experiments have shown that OxS induces molecular abnormalities that cause psychological states (Bokovic et al., 2011). ROS is closely associated with various pathophysiological processes such as inflammation, mitochondrial dysfunction, hypoactive NMDA receptors, and rapidly increasing GABA interneuron damage (Bitanihirwe et al., 2011). OxS is also tightly associated with other events in neurodegeneration, such as nitric oxide toxicity, excitotoxicity, mitochondrial dysfunction, and inflammation (Jenner, 2003).

Mitochondrial oxidative stress (mOxS) is the main cause of AD. Because increased mitochondrial DNA oxidation is one of the disease's early symptoms, mitochondrial functional abnormalities play a significant part in the etiology of Alzheimer's (Mecocci et al., 2018; Grimm and Eckert, 2017). In fact, age-related mitochondrial regression may play an early role in the pathogenesis of common and advanced age-onset forms of AD. The mitochondrial cascade hypothesis proposes that age-related loss of mitochondrial function leads to the formation of plaques in which Aβ oligomers accumulate, affecting APP (amyloid precursor protein) expression and processing in AD (Cheignon et al., 2018; Swerdlow et al., 2014). Studies have revealed that the hydrophobic 25-35 region of Aβ causes neuronal toxicity and this generates ROS, thus demonstrating that amyloid beta itself is a source of OxS (Hensley et al., 1994; Pike et al., 1992). Subsequent studies revealed that incubating neurons with Aβ 1-42 oligomers triggered protein-dependent lipid peroxidation (Mark et al., 1997). The hydrophobic property of A allows it to accumulate in the lipid bilayer, leading in the development of a lipid termed HNE (4-hydroxynonenal) that covalently bonds to neuronal proteins, causing cell death (Butterfield, 2020; Di Domenico et al., 2017).

NADPH oxidase (NOX), a significant generator of ROS in the central nervous system, catalyzes the electron transport from NADPH to oxygen across the plasma membrane, producing superoxide radicals. NOX is found in various regions of the brain and is widely distributed especially on important structures associated with learning and memory (Tarafdar and Pula, 2018; Ma et al., 2017).

The components of ROS and OxS are important therapeutic targets in the treatment of neuropsychiatric disorders such as depression, diseases such as AD, schizophrenia, PD and anxiety. The effect of OxS becomes more pronounced as we age. An increase in mitochondrial catalase (CAT) effectively attenuates OxS and demonstrates the important function of mitochondria in regulating ROS in the aging process. In this context, the brain is particularly vulnerable to OxS, and ROS is hypothesized to be involved in the etiology of neurological disorders.

Mitochondrial dysfunction is quite common in the aging process, and restoration of mitochondrial function affects age-related ROS. In healthy aging, significant deficiencies in mitochondrial metabolism are observed, especially in the α subunit of mitochondrial F1 ATP synthase, which is dependent on ATP synthesis. This causes an increased ROS production, decreased ATP production, and an increased DNA, lipid, and protein oxidation (Mecocci et al., 2018; Grimm and Eckert, 2017). Mitochondrial degradation causes both mitochondrial DNA damage and genomic DNA damage. Overexpression of enzymes has been reported as a potential method to alleviate the negative effects of aging (Lu et al., 2004). In a study, superoxide dismutase (SOD)

was effective in prolonging the lifespan of overexpressed flies (Tower, 2000). Overexpression of CAT in mitochondria (mCAT) has been found to generally reduce oxidation in mice, protect insulin signaling, and delay the evolution of age-related pathologies such as heart and cataracts (Paglialunga et al., 2015; Dai et al., 2009; Schriner et al., 2005). DNA damage was also reduced in mitochondria in both aged skeletal muscle and asbestos-exposed lungs, resulting in a significant prolongation of the mice's lifespan. (Campisi et al., 2019; Kim et al., 2016; Schriner et al., 2005).

7. The function of oxidative stress in the diagnosis of AD

Studies on the role of OxS in the diagnosis of AD have generally focused on antioxidant components. Many studies show decreased molecular antioxidant levels and increased OxS markers in Alzheimer's patients. For example, in a study conducted, it was determined that there is an accumulation of H_2O_2 in the brain with AD. These findings were consistent across all autopsied Alzheimer's brains from mild to severe (Gsell et al. 1995). It was found that while mitochondrial SOD2 levels decreased in Alzheimer's patients, there was no change in serum SOD1 levels (Thome et al., 1997). Chang et al., (2014) showed in a comprehensive literature review that the level of SOD increases induced by OxS in the early stages of AD and is consumed in the later stages.

When the plasma levels of healthy people over the age of 100 were examined, it was determined that vitamin E (56 μM) was higher than the elderly (42-47 μM) and young people (51 μM) (Mecocci et al., 2000). The same is true for vitamin A. The plasma content of vitamin C and carotenoids showed an inverse relationship with increasing age (Paolisso et al., 1998).

OxS emerges as an increasing factor in the aging process, and this may play an important role in the development of neurodegenerative diseases, especially AD. Low antioxidant levels have been associated with cognitive decline and an increased risk of AD during the aging process. TBARS (Thiobarbituric Acid Reactive Substances) is a biomarker used as a measure of lipid peroxidation. In some studies, serum or plasma TBARS levels were observed to be considerably greater in AD patients compared to the control group. However, this difference was not observed in other studies. Findings on the level of erythrocyte TBARS are also contradictory. According to some research the level of erythrocyte TBARS is increased in AD patients, but there was no difference between AD and control groups among other studies (Casado et al., 2008; Serra et al., 2001; Cristalli et al., 2012; Schrag et al., 2013).

However, it should be noted that OxS is not only associated with AD, but may also be associated with other pathological conditions. Therefore, studies on the use of OxS markers in the diagnosis of AD are ongoing. These studies offer hope for the development of specific and sensitive markers that could aid in the early diagnosis of AD, providing greater understanding and accuracy.

8. Neuroprotection: Antioxidants and Alzheimer's Disease

Although not always consistent, there are studies that show a reduction in AD and cognitive decline with antioxidant intake and inhibition of AChE of some antioxidant agents (Güller et al., 2021; Caglayan et al., 2019).

A study in Southern Italy measured levels of vitamins C and E in plasma of healthy elderly people over the age of 100, higher than 70-99 years old people, but lower than <50 years old adults. In addition, it was observed that individuals over the age of 100 exhibit a better immune profile, metabolic and endocrinologic features and nutritional status compared to elderly individuals. Healthy aging and longevity have been linked with a high dietary consumption of antioxidants in the Mediterranean population (Paolisso et al., 1998). In a seven-year study conducted in France, 1416 people who were at least 68 years old had a significantly lower incidence of dementia with fish and meat consumption (Barberger et al., 2002). The benefits of fish consumption have been confirmed by a study of a much larger population – 6158 people who are at least 65 years old (Morris et al., 2005).

The Mediterranean diet includes high amount of natural antioxidants, such as phenolics, carotenoids and vitamin C. Studies show that a diet similar to the Mediterranean diet reduces cognitive decline, the progression of mild cognitive impairment to AD, and the overall risk of AD. Consumption of dairy products such as fish, olive oil, vegetables, fruits (with a low glycemic index), seeds, legumes, cheese or yogurt is encouraged, while consumption of red meat and products with added sugar is limited. This diet is also effective in reducing the risk of cardiovascular disease, obesity, diabetes and hypertension. Therefore, this diet not only prevents dementia, but also protects general health (Deckers et al., 2015).

High intakes of vitamin C (more than 133 mg daily) and vitamin E (more than 15.5 mg daily) have been shown to reduce the risk of AD (Engelhart et al., 2002). In another research, they did not find a relationship between Alzheimer's risk and dietary intake of carotene, vitamin C and vitamin E supplements (Luchsinger et al., 2003; Laurin et al., 2004).

Curcumin, a phenolic compound, has potent neuroprotective, anti-inflammatory, and antioxidant properties (Bhat et al., 2019; Rajeswari, 2006). Studies in animal models have shown that especially curcumin reverses neurotoxic effects in AD and corrects behavioral changes (Mendonça da Costa et al., 2019). Studies on glioma cells have shown that resveratrol protects these cells from Aβ toxicity by reducing the expression of iNOS and COX-2. Thanks to this effect, resveratrol inhibited the uncontrolled release of prostaglandin E2 and NO. These effects are thought to be related to the capacity of resveratrol to inhibit Aβ-induced nuclear translocation (Kim et al., 2006).

9. Reducing oxidative stress with drug treatments and preventing AD

The contribution of OxS to AD is an important component of neurodegeneration. Therefore, antioxidant treatment strategies aim to reduce oxidative damage by reducing free radical formation and activating endogenous antioxidant systems.

Antioxidant peptides, vitamin E, and antioxidant compounds such as ubiquinone (MitoQ) were directed to specific organelles (eg, mitochondria) that produce high levels of ROS to investigate their neuroprotective properties (Zhao et al. al., 2004; Kelso et al., 2001; Smith et al., 1999). It is proved that MitoQ, which reduces free radical formation, slows the onset of AD by reducing neurodegeneration (Reddy et al., 2012; Augustyniak et al., 2010). Furthermore, the development of catalytic antioxidants and the modification of endogenous antioxidant pathways have been investigated for neuroprotection (Linseman 2009).

Tacrine, the first FDA-approved anticholinesterase inhibitor used in the treatment of AD, has been shown to reduce overall survival in an animal Alzheimer's model (Jhoo et al., 2004). However, when applied at a dose of 50-800 g/kg, it increased FRAP (Ferric Reducing Antioxidant Power) and thus provided "antioxidant activity" (Kracmarova et al., 2012). Another cholinerase inhibitor used in therapy, Donepezil, increased antioxidant capacity and decreased lipid peroxidation when treated with moderate doses in mouse AD models (Wang et al., 2014).

It has been found that galantamine can decrease OxS, increase SOD activity and decrease GSH levels, as well as correct cognitive disorders (Kumar et al., 2011).

New chemical agents that imitate the SOD or CAT activities are also being tested in *in vitro* and *in vivo* animal models of neurodegeneration (Golden and Patel 2009). These compounds are advantageous over most common antioxidants because they act catalytically rather than stoichiometrically to scavenge free radicals. It is thought that catalytic antioxidants show promising effects in animal models with neurodegenerative effects (Linseman 2009).

Endogenous antioxidant pathways are regulated specifically by the transcription factor Nrf2. Nrf2 activates various cytoprotective, detoxification, and antioxidant genes including GSH synthesis. With Nrf2 activation, the synthesis of antioxidant enzymes and production of other protective molecules in cells increases, thus reducing the effects of oxidative damage. This approach is considered a promising strategy for the prevention of AD and other neurodegenerative diseases (Calkins et al., 2009).

10. Conclusion: The oxidative stress hypothesis - New treatment approaches

Oxidation is very common in living metabolism. Under normal conditions, oxidants and antioxidants are in balance in the living body. This situation shifts in favor of oxidant substances as a result of excessive formation of oxidant substances or reduction of antioxidant substances. Increasing the oxidant level is vital for living things. Because the increase in oxidants can cause many diseases such as cardiovascular diseases, gastrointestinal diseases, respiratory and excretory disorders, cancer, diabetes, aging, neurodegenerative diseases. The OxS hypothesis of AD is accepted as a mechanism that plays an important role in the pathophysiology and progression of the disease. It has been observed that OxS is associated with the aging process along with the effect of environmental factors. OxS also plays an important role in the diagnosis of AD, and the use of biomarkers that point to oxidative damage may be a potential helpful tool in the early diagnosis and follow-up of the disease. Antioxidants have an important place among neuroprotection strategies. The use of antioxidant compounds aims to prevent cellular damage and degenerative changes in brain tissue by reducing OxS. However, new approaches targeting OxS with drug treatments are also being actively investigated. Potential drug targets focus on the activation of antioxidant enzymes or regulation of antioxidant systems. These new treatment approaches offer promising strategies for reducing OxS and preventing AD. These OxS -based treatment approaches for AD have promising potential to alleviate or delay the effects of the disease in the future.

REFERENCES

Ansari, M. A., Joshi, G., Huang, Q., Opii, W. O., Abdul, H. M., Sultana, R., & Butterfield, D. A. (2006). In vivo administration of D609 leads to protection of subsequently isolated gerbil brain mitochondria subjected to in vitro oxidative stress induced by amyloid beta-peptide and other oxidative stressors: relevance to Alzheimer's disease and other oxidative stress-related neurodegenerative disorders. Free Radical Biology and Medicine, 41(11), 1694-1703.

Augustyniak, A., Bartosz, G., Čipak, A., Duburs, G., Horáková, L. U., Łuczaj, W., ... & Žarković, N. (2010). Natural and synthetic antioxidants: an updated overview. Free radical research, 44(10), 1216-1262.

Babacanoğlu, E., & Güller, U. (2021). Daily oxygen supplementation to the incubator at different stages of embryonic development alters the activity of antioxidant enzymes in the lung tissue of broiler chicks at a high altitude. British Poultry Science, 62(3), 459-465.

Barberger-Gateau, P., Letenneur, L., Deschamps, V., Pérès, K., Dartigues, J. F., & Renaud, S. (2002). Fish, meat, and risk of dementia: cohort study. Bmj, 325(7370), 932-933.

Barnham, K. J., Masters, C. L., & Bush, A. I. (2004). Neurodegenerative diseases and oxidative stress. Nature reviews Drug discovery, 3(3), 205-214.

Bartzokis, G. (2004). Age-related myelin breakdown: a developmental model of cognitive decline and Alzheimer's disease. Neurobiology of aging, 25(1), 5-18.

Bhat, A., Mahalakshmi, A. M., Ray, B., Tuladhar, S., Hediyal, T. A., Manthiannem, E., ... & Sakharkar, M. K. (2019). Benefits of curcumin in brain disorders. BioFactors, 45(5), 666-689.

Bitanihirwe, B. K., & Woo, T. U. W. (2011). Oxidative stress in schizophrenia: an integrated approach. Neuroscience & Biobehavioral Reviews, 35(3), 878-893.

Blennow, K., de Leon, M. J., & Zetterberg, H. (2006). Alzheimer's disease. The Lancet, 368(9533), 387-403.

Bonda, D. J., Wang, X., Perry, G., Nunomura, A., Tabaton, M., Zhu, X., & Smith, M. A. (2010). Oxidative stress in Alzheimer disease: a possibility for prevention. Neuropharmacology, 59(4-5), 290-294.

Boskovic, M., Vovk, T., Kores Plesnicar, B., & Grabnar, I. (2011). Oxidative stress in schizophrenia. Current neuropharmacology, 9(2), 301-312.

Butterfield, D. A. (2020). Brain lipid peroxidation and alzheimer disease: Synergy between the Butterfield and Mattson laboratories. Ageing research reviews, 64, 101049.

Butterfield, D. A., & Lauderback, C. M. (2002). Lipid peroxidation and protein oxidation in Alzheimer's disease brain: potential causes and consequences involving amyloid β-peptide-associated free radical oxidative stress. Free Radical Biology and Medicine, 32(11), 1050-1060.

Caglayan, C., Demir, Y., Kucukler, S., Taslimi, P., Kandemir, F. M., & Gulçin, İ. (2019). The effects of hesperidin on sodium arsenite-induced different organ toxicity in rats on metabolic enzymes as antidiabetic and anticholinergics potentials: A biochemical approach. Journal of food biochemistry, 43(2), e12720.

Calkins, M. J., Johnson, D. A., Townsend, J. A., Vargas, M. R., Dowell, J. A., Williamson, T. P., ... & Johnson, J. A. (2009). The Nrf2/ARE pathway as a potential therapeutic target in neurodegenerative disease. Antioxidants & redox signaling, 11(3), 497-508.

Campisi, J., Kapahi, P., Lithgow, G. J., Melov, S., Newman, J. C., & Verdin, E. (2019). From discoveries in ageing research to therapeutics for healthy ageing. Nature, 571(7764), 183-192.

Carolan, C. G., Dillon, G. P., Khan, D., Ryder, S. A., Gaynor, J. M., Reidy, S., ... & Gilmer, J. F. (2010). Isosorbide-2-benzyl carbamate-5-salicylate, a peripheral anionic site binding subnanomolar selective butyrylcholinesterase inhibitor. Journal of medicinal chemistry, 53(3), 1190-1199.

Casado, A., Encarnación López-Fernández, M., Concepción Casado, M., & de La Torre, R. (2008). Lipid peroxidation and antioxidant enzyme activities in vascular and Alzheimer dementias. Neurochemical Research, 33, 450-458.

Chang, Y. T., Chang, W. N., Tsai, N. W., Huang, C. C., Kung, C. T., Su, Y. J., ... & Lu, C. H. (2014). The roles of biomarkers of oxidative stress and antioxidant in Alzheimer's disease: a systematic review. BioMed research international, 2014.

Cheeseman, K. H., & Slater, T. F. (1993). An introduction to free radical biochemistry. British medical bulletin, 49(3), 481-493.

Cheignon, C., Tomas, M., Bonnefont-Rousselot, D., Faller, P., Hureau, C., & Collin, F. (2018). Oxidative stress and the amyloid beta peptide in Alzheimer's disease. Redox biology, 14, 450-464.

Chopra, K., Misra, S., & Kuhad, A. (2011). Neurobiological aspects of Alzheimer's disease. Expert Opinion on Therapeutic Targets, 15(5), 535-555.

Cristalli, D. O., Arnal, N., Marra, F. A., de Alaniz, M. J., & Marra, C. A. (2012). Peripheral markers in neurodegenerative patients and their first-degree relatives. Journal of the neurological sciences, 314(1-2), 48-56.

da Costa, I. M., de Moura Freire, M. A., de Paiva Cavalcanti, J. R., de Araújo, D. P., Norrara, B., Moreira Rosa, I. M. M., ... & Guzen, F. P. (2019). Supplementation with Curcuma longa reverses neurotoxic and behavioral damage in models of Alzheimer's disease: a systematic review. Current neuropharmacology, 17(5), 406-421.

Dai, D. F., Santana, L. F., Vermulst, M., Tomazela, D. M., Emond, M. J., MacCoss, M. J., ... & Rabinovitch, P. S. (2009). Overexpression of catalase targeted to mitochondria attenuates murine cardiac aging. Circulation, 119(21), 2789-2797.

Darvesh, S., Grantham, D. L., & Hopkins, D. A. (1998). Distribution of butyrylcholinesterase in the human amygdala and hippocampal formation. Journal of Comparative Neurology, 393(3), 374-390.

Darvesh, S., Hopkins, D. A., & Geula, C. (2003). Neurobiology of butyrylcholinesterase. Nature Reviews Neuroscience, 4(2), 131-138.

Deckers, K., van Boxtel, M. P., Schiepers, O. J., de Vugt, M., Muñoz Sánchez, J. L., Anstey, K. J., ... & Köhler, S. (2015). Target risk factors for dementia prevention: a systematic review and Delphi consensus study on the evidence from observational studies. International journal of geriatric psychiatry, 30(3), 234-246.

Dhanasekaran, S., Perumal, P., & Palayan, M. (2015). In-vitro Screening for acetylcholinesterase enzyme inhibition potential and antioxidant activity of extracts of Ipomoea aquatica Forsk: therapeutic lead for Alzheimer's disease. Journal of Applied Pharmaceutical Science, 5(2), 012-016.

Di Domenico, F., Tramutola, A., & Butterfield, D. A. (2017). Role of 4-hydroxy-2-nonenal (HNE) in the pathogenesis of alzheimer disease and other selected age-related neurodegenerative disorders. Free Radical Biology and Medicine, 111, 253-261.

Eggleston, K. N., & Fuchs, V. R. (2012). The new demographic transition: most gains in life expectancy now realized late in life. Journal of Economic Perspectives, 26(3), 137-156.

Engelhart, M. J., Geerlings, M. I., Ruitenberg, A., van Swieten, J. C., Hofman, A., Witteman, J. C., & Breteler, M. M. (2002). Dietary intake of antioxidants and risk of Alzheimer disease. Jama, 287(24), 3223-3229.

Eşer, İ. (1991). Yaşlılıkta meydana gelen fizyolojik değişiklikler. Ege Üniversitesi Hemşirelik Yüksekokulu Dergisi, 7(1), 52-57.

Finkel, T., Serrano, M., & Blasco, M. A. (2007). The common biology of cancer and ageing. Nature, 448(7155), 767-774.

Gale, S. D. (2018). Acar in KR Daffner. *Dementia. Am. J. Med*, *131*, 1161.

Geula, C. M., & Mesulam, M. M., (1999). Cholinergic Systems in Alzheimer's Disease, Alzheimer Disease. Terry RDea (Ed.), 2nd Ed. PA: Lippincott, Williams and Wilkins, Philadelphia.

Golden, T. R., & Patel, M. (2009). Catalytic antioxidants and neurodegeneration. Antioxidants & Redox Signaling, 11(3), 555-569.

Greig, N. H., Utsuki, T., Yu, Q. S., Zhu, X., Holloway, H. W., Perry, T., ... & Lahiri, D. K. (2001). A new therapeutic target in Alzheimer's disease treatment: attention to butyrylcholinesterase. Current medical research and opinion, 17(3), 159-165.

Grimm, A., & Eckert, A. (2017). Brain aging and neurodegeneration: from a mitochondrial point of view. Journal of neurochemistry, 143(4), 418-431.

Gsell, W., Conrad, R., Hickethier, M., Sofic, E., Frölich, L., Wichart, I., ... & Riederer, P. (1995). Decreased catalase activity but unchanged superoxide dismutase activity in brains of patients with dementia of Alzheimer type. Journal of neurochemistry, 64(3), 1216-1223.

Güller, P., Dağalan, Z., Güller, U., Çalışır, U., & Nişancı, B. (2021). Enzymes inhibition

profiles and antibacterial activities of benzylidenemalononitrile derivatives. Journal of Molecular Structure, 1239, 130498.

Güller, U. (2021). Resorcinol derivatives as human acetylcholinesterase inhibitor: An In Vitro and In Silico study. International Journal of Chemistry and Technology, 5(2), 156-161.

Güller, U., Güller, P. & Çiftci M., (2021). Radical scavenging and antiacetylcholinesterase activities of ethanolic extracts of carob, clove, and linden. Alternative therapies in health and medicine, 27(5), 33-37.

Güller, U., Önalan, Ş., Arabacı, M., Karataş, B., Yaşar, M., & Küfrevioğlu, Ö. İ. (2020). Effects of different LED light spectra on rainbow trout (Oncorhynchus mykiss): in vivo evaluation of the antioxidant status. Fish physiology and biochemistry, 46, 2169-2180.

Hardy, J., & Selkoe, D. J. (2002). The amyloid hypothesis of Alzheimer's disease: progress and problems on the road to therapeutics. *science*, *297*(5580), 353-356.

Hensley, K., Carney, J. M., Mattson, M. P., Aksenova, M., Harris, M., Wu, J. F., ... & Butterfield, D. A. (1994). A model for beta-amyloid aggregation and neurotoxicity based on free radical generation by the peptide: relevance to Alzheimer disease. Proceedings of the National Academy of Sciences, 91(8), 3270-3274.

Imbimbo, B. P., & Speroni, F. (2003). β-Amyloid Therapeutic Strategies for Alzheimer's Disease. Burger's Medicinal Chemistry and Drug Discovery.

Imbimbo, B. P., Lombard, J., & Pomara, N. (2005). Pathophysiology of Alzheimer's disease. Neuroimaging Clinics, 15(4), 727-753.

Jenner, P. (2003). Oxidative stress in Parkinson's disease. Annals of Neurology: Official Journal of the American Neurological Association and the Child Neurology Society, 53(S3), S26-S38.

Jhoo, J. H., Kim, H. C., Nabeshima, T., Yamada, K., Shin, E. J., Jhoo, W. K., ... & Woo, J. I. (2004). β-Amyloid (1–42)-induced learning and memory deficits in mice: involvement of oxidative burdens in the hippocampus and cerebral cortex. Behavioural brain research, 155(2), 185-196.

Karabulut, H., & Gülay, M. Ş. (2016). Serbest radikaller. Mehmet Akif Ersoy Üniversitesi Sağlık Bilimleri Enstitüsü Dergisi, 4(1).

Kelso, G. F., Porteous, C. M., Coulter, C. V., Hughes, G., Porteous, W. K., Ledgerwood, E. C., ... & Murphy, M. P. (2001). Selective targeting of a redox-active ubiquinone to mitochondria within cells: antioxidant and antiapoptotic properties. Journal of Biological Chemistry, 276(7), 4588-4596.

Kılınç, N., Güller, U., & Alım, Z. (2022). Identification of the Inhibition Effects of Some Natural Antiproliferative Agents on CA-I, CA-II, and AChE Activities Isolated from Human Erythrocytes by Kinetic and Molecular Docking Studies. Russian Journal of Bioorganic Chemistry, 48(4), 720-730.

Kim, S. J., Cheresh, P., Jablonski, R. P., Morales-Nebreda, L., Cheng, Y., Hogan, E., ...

& Kamp, D. W. (2016). Mitochondrial catalase overexpressed transgenic mice are protected against lung fibrosis in part via preventing alveolar epithelial cell mitochondrial DNA damage. Free Radical Biology and Medicine, 101, 482-490.

Kim, Y., Lim, S. Y., Rhee, S. H., Park, K. Y., Kim, C. H., Choi, B. T., ... & Choi, Y. H. (2006). Resveratrol inhibits inducible nitric oxide synthase and cyclooxygenase-2 expression in β-amyloid-treated C6 glioma cells. International journal of molecular medicine, 17(6), 1069-1075.

Koca, M., Güller, U., Güller, P., Dağalan, Z., & Nişancı, B. (2022). Design and synthesis of novel dual cholinesterase inhibitors: In Vitro inhibition studies supported with molecular docking. Chemistry & Biodiversity, 19(6), e202200015.

Kracmarova, A., Bandouchova, H., Pikula, J., & Pohanka, M. (2012). Tacrine is implicated in oxidative stress in the laboratory guinea pig model. Neuroendocrinol Lett, 33, 136-144.

Kumar, A., Prakash, A., & Pahwa, D. (2011). Galantamine potentiates the protective effect of rofecoxib and caffeic acid against intrahippocampal Kainic acid-induced cognitive dysfunction in rat. Brain research bulletin, 85(3-4), 158-168.

Laurin, D., Masaki, K. H., Foley, D. J., White, L. R., & Launer, L. J. (2004). Midlife dietary intake of antioxidants and risk of late-life incident dementia: the Honolulu-Asia Aging Study. American journal of epidemiology, 159(10), 959-967.

López-Otín, C., Blasco, M. A., Partridge, L., Serrano, M., & Kroemer, G. (2013). The hallmarks of aging. Cell, 153(6), 1194-1217.

Lu, T., Pan, Y., Kao, S. Y., Li, C., Kohane, I., Chan, J., & Yankner, B. A. (2004). Gene regulation and DNA damage in the ageing human brain. Nature, 429(6994), 883-891.

Luchsinger, J. A., Tang, M. X., Shea, S., & Mayeux, R. (2003). Antioxidant vitamin intake and risk of Alzheimer disease. Archives of neurology, 60(2), 203-208.

Ma, M. W., Wang, J., Zhang, Q., Wang, R., Dhandapani, K. M., Vadlamudi, R. K., & Brann, D. W. (2017). NADPH oxidase in brain injury and neurodegenerative disorders. Molecular neurodegeneration, 12, 1-28.

Manoharan, I., Boopathy, R., Darvesh, S., & Lockridge, O. (2007). A medical health report on individuals with silent butyrylcholinesterase in the Vysya community of India. Clinica chimica acta, 378(1-2), 128-135.

Mark, R. J., Lovell, M. A., Markesbery, W. R., Uchida, K., & Mattson, M. P. (1997). A role for 4-hydroxynonenal, an aldehydic product of lipid peroxidation, in disruption of ion homeostasis and neuronal death induced by amyloid β-peptide. Journal of neurochemistry, 68(1), 255-264.

Mecocci, P., Boccardi, V., Cecchetti, R., Bastiani, P., Scamosci, M., Ruggiero, C., & Baroni, M. (2018). A long journey into aging, brain aging, and Alzheimer's disease following the oxidative stress tracks. Journal of Alzheimer's Disease, 62(3), 1319-1335.

Mecocci, P., Polidori, M. C., Troiano, L., Cherubini, A., Cecchetti, R., Pini, G., ... & Senin, U. (2000). Plasma antioxidants and longevity: a study on healthy centenarians. Free Radical Biology and Medicine, 28(8), 1243-1248.

Mesulam, M., Guillozet, A., Shaw, P., & Quinn, B. (2002). Widely spread butyrylcholinesterase can hydrolyze acetylcholine in the normal and Alzheimer brain. Neurobiology of disease, 9(1), 88-93.

Morris, M. C., Evans, D. A., Tangney, C. C., Bienias, J. L., & Wilson, R. S. (2005). Fish consumption and cognitive decline with age in a large community study. Archives of neurology, 62(12), 1849-1853.

Öğüt, S., & Atay, E. (2012). Yaşlılık ve oksidatif stres. SD Ü. Tıp Fak. Dergisi, 19(2), 68-74.

Ohl, K., Tenbrock, K., & Kipp, M. (2016). Oxidative stress in multiple sclerosis: Central and peripheral mode of action. Experimental neurology, 277, 58-67.

Paglialunga, S., Ludzki, A., Root-McCaig, J., & Holloway, G. P. (2015). In adipose tissue, increased mitochondrial emission of reactive oxygen species is important for short-term high-fat diet-induced insulin resistance in mice. Diabetologia, 58, 1071-1080.

Paolisso, G., Tagliamonte, M. R., Rizzo, M. R., Manzella, D., Gambardella, A., & Varricchio, M. (1998). Oxidative stress and advancing age: results in healthy centenarians. Journal of the American Geriatrics Society, 46(7), 833-838.

Pike, C. J., Cummings, B. J., & Cotman, C. W. (1992). beta-Amyloid induces neuritic dystrophy in vitro: similarities with Alzheimer pathology. Neuroreport, 3(9), 769-772.

Rajeswari, A. (2006). Curcumin protects mouse brain from oxidative stress caused by 1-methyl-4-phenyl-1, 2, 3, 6-tetrahydro pyridine. European Review for Medical and Pharmacological Sciences, 10(4), 157.

Rappuoli, R., Pizza, M., Del Giudice, G., & De Gregorio, E. (2014). Vaccines, new opportunities for a new society. Proceedings of the National Academy of Sciences, 111(34), 12288-12293.

Reddy, P. H., Tripathi, R., Troung, Q., Tirumala, K., Reddy, T. P., Anekonda, V., ... & Manczak, M. (2012). Abnormal mitochondrial dynamics and synaptic degeneration as early events in Alzheimer's disease: implications to mitochondria-targeted antioxidant therapeutics. Biochimica et Biophysica Acta (BBA)-Molecular Basis of Disease, 1822(5), 639-649.

Samani, N. J., & van der Harst, P. (2008). Biological ageing and cardiovascular disease. Heart, 94(5), 537-539.

Schrag, M., Mueller, C., Zabel, M., Crofton, A., Kirsch, W. M., Ghribi, O., ... & Perry, G. (2013). Oxidative stress in blood in Alzheimer's disease and mild cognitive impairment: a meta-analysis. Neurobiology of disease, 59, 100-110.

Schriner, S. E., Linford, N. J., Martin, G. M., Treuting, P., Ogburn, C. E., Emond, M., ... & Rabinovitch, P. S. (2005). Extension of murine life span by overexpression of

catalase targeted to mitochondria. science, 308(5730), 1909-1911.

Serra, J. A., Dominguez, R. O., De Lustig, E. S., Guareschi, E. M., Famulari, A. L., Bartolome, E. L., & Marschoff, E. R. (2001). Parkinson's disease is associated with oxidative stress: comparison of peripheral antioxidant profiles in living Parkinson's, Alzheimer's and vascular dementia patients. Journal of neural transmission, 108, 1135-1148.

Sies, H., Berndt, C., & Jones, D. P. (2017). Oxidative stress. Annual review of biochemistry, 86, 715-748.

Sies, H.; Jones, D.P. (2007). Oxidative stress. In Encyclopedia of Stress, 2nd ed.; Fink, G., Ed.; Elsevier: Amsterdam, The Netherlands, Volume 3, pp. 45–48.

Singh, A., Kukreti, R., Saso, L., & Kukreti, S. (2019). Oxidative stress: a key modulator in neurodegenerative diseases. Molecules, 24(8), 1583.

Smith, R. A., Porteous, C. M., Coulter, C. V., & Murphy, M. P. (1999). Selective targeting of an antioxidant to mitochondria. European Journal of Biochemistry, 263(3), 709-716.

Swerdlow, R. H., Burns, J. M., & Khan, S. M. (2014). The Alzheimer's disease mitochondrial cascade hypothesis: progress and perspectives. Biochimica et Biophysica Acta (BBA)-Molecular Basis of Disease, 1842(8), 1219-1231.

Tarafdar, A., & Pula, G. (2018). The role of NADPH oxidases and oxidative stress in neurodegenerative disorders. International Journal of Molecular Sciences, 19(12), 3824.

Thome, J., Gsell, W., Rösier, M., Kornhuber, J., Frölich, L., Hashimoto, E., ... & Riedcrer, P. (1996). Oxidative-stress associated parameters (lactoferrin, superoxide dismutases) in serum of patients with Alzheimer's disease. Life sciences, 60(1), 13-19.

Tönnies, E., & Trushina, E. (2017). Oxidative stress, synaptic dysfunction, and Alzheimer's disease. Journal of Alzheimer's Disease, 57(4), 1105-1121.

Tower, J. (2000). Transgenic methods for increasing Drosophila life span. Mechanisms of ageing and development, 118(1-2), 1-14.

TUİK, Alzheimer hastalığından ölen yaşlıların cinsiyete göre oranı, 2010-2021.

Wang, D., Liu, L., Zhu, X., Wu, W., & Wang, Y. (2014). Hesperidin alleviates cognitive impairment, mitochondrial dysfunction and oxidative stress in a mouse model of Alzheimer's disease. Cellular and molecular neurobiology, 34, 1209-1221.

Wang, X., & Michaelis, E. K. (2010). Selective neuronal vulnerability to oxidative stress in the brain. Frontiers in aging neuroscience, 12.

World Health Organization. (2018). World health statistics 2019: monitoring hesalth for the sustainable development goals. Geneva, Swizerland: World Health Organization.

Wyss-Coray, T. (2016). Ageing, neurodegeneration and brain rejuvenation. Nature, 539(7628), 180-186.

Zhang, H., Davies, K.J., Forman, H.J. (2015). Oxidative stress response and Nrf2 signaling in aging. Free Radical Biology and Medicine88, 314–336.

Zhao, K., Zhao, G. M., Wu, D., Soong, Y., Birk, A. V., Schiller, P. W., & Szeto, H. H. (2004). Cell-permeable peptide antioxidants targeted to inner mitochondrial membrane inhibit mitochondrial swelling, oxidative cell death, and reperfusion injury. Journal of Biological Chemistry, 279(33), 34682-34690.

Chapter 7

USAGE AREAS, CHEMICAL CONTENTS, MINERAL AND NUTRITIONAL CONTENTS AND BIOLOGICAL ACTIVITIES OF FENNEL

Oğuzhan Koçer[1]
İmran Uysal[2]
Falah Saleh Mohammed[3]
Mustafa Sevindik[4]
Hasan Akgül[5]

1 Department of Pharmacy Services, Vocational School of Health Services, University of Osmaniye Korkut Ata, Osmaniye
2 Osmaniye Korkut Ata University, Bahçe Vocational School, Department of Food Processing, Osmaniye, Turkey
3 Zakho University, Science Faculty, Department of Biology, Duhok, Iraq.
4 Osmaniye Korkut Ata University, Science and Literature Faculty, Department of Biology, Osmaniye, Turkey.
5 Akdeniz University, Science Faculty, Department of Biology, Antalya, Turkey

Introduction

In the scope of traditional medicine, various natural products such as fungi, plants, and animals are utilised. In contrast to modern medicine, traditional medicine has a long history dating back to the origins of human civilization (Mohammed et al., 2022). Numerous studies have demonstrated the significant efficacy of natural products commonly utilised in traditional medicine. Plants are significant natural materials utilised within the scope of traditional medicine (Sevindik et al., 2017). Throughout history, humans have utilised plants for their benefits. Throughout history, humans have utilised plants for various purposes such as shelter, heating, nutrition, spice, tool and equipment production, and combating illnesses (Mohammed et al., 2020a; Korkmaz et al., 2021). Plants contain various essential nutrients such as vitamins, minerals, and proteins that are significant for nourishment. In addition to their nutritional properties, they are also medically significant (Mohammed et al., 2020b). Throughout history, numerous species of plants have been effective in combating and preventing illnesses. Numerous studies have reported that plants exhibit various activities such as anticancer, antimicrobial, anti-inflammatory, antiproliferative, antioxidant, anti-aging, antiallergic, hepatoprotective, and DNA protective effects (Bhawna and Kumar, 2009; Miastkowska and Sikora, 2018; Mohammed et al., 2018; Laxa et al., 2019; Mohammed et al., 2019; Mohammed et al., 2021a; Rahim et al., 2021; Unal et al., 2022; Uysal et al., 2023). In this context, it is highly important to determine the biological activities of various plant species for the purpose of identifying their traditional medicinal uses. In this study, the utilisation areas, general characteristics, nutritional and mineral contents, biological activities, and chemical compositions of *F. vulgare* have been compiled.

Genus *Foeniculum* and Usage Areas

Despite the reporting of various species of *Foeniculum* worldwide, many of these species have become synonymous with one another. The currently accepted species are *Foeniculum scoparium* Quézel, *Foeniculum subinodorum* Maire, Weiller & Wilczek, and *Foeniculum vulgare* Mill. The common names of these species in this category are as follows: French: fenouli; Spanish: hinojo; Italian: finnochio; Russian: fynkhel; Hindi: saunf; German: fenchel and Arabic: shamar. The distribution areas of the *Foeniculum* genus were initially limited to Mediterranean and European countries, but in recent times, cultivation has expanded to regions such as China, India, and North America. Upon examining its historical process, it is evident that the usage of the term can be traced back to ancient Egyptian and Roman periods, as documented in various sources. India ranks first in global production rankings. Upon examining the general morphological structure of the species within the Foeniculum genus, it can be observed that they typically possess an average height of 2 metres, leaves that are approximately 40 cm in length and

filiform in shape, and flowers that are commonly of a bright golden-yellow hue. It blooms during the period of July-August. Fruits are typically ovate in shape. The sowing of seeds occurs in 3-5 rows and the maturation process takes place during the months of September to October (Barros et al., 2010; Gupta, 2010; Krishnamurthy, 2011; Charles, 2012; Khan and Musharaf, 2014; Mehra et al., 2021).

It can be observed that among the species within the *Foeniculum* genus, *F. vulgare* stands out as the most widely used species in terms of its range of applications. As reported in the literature, seeds, leaves, stems, fruits, and the entire plant are commonly utilised. India is the pioneering country in the various utilisation and production of species. The usage of this item is prevalent in countries such as Bolivia, Brazil, Ecuador, Ethiopia, India, Iran, Italy, Jordan, Mexico, Pakistan, Portugal, Serbia, South Africa, Spain, Turkey, and the United States, among others, excluding India. When examining the distribution of application areas, they can be categorised into three main groups: health, nutrition, and the paint industry. In the field of health, plant leaves, fruits, and seeds are commonly utilised. Within this context, it is known that conjunctivitis, gastritis, abdominal pain, common cold, refreshing, stomach bloating, antiemetic, depurative, hypnotic diarrhoea, kidney disorders, colic in children, irritable bowel syndrome, gastralgia, laxative, liver pain, arthritis, fever, fat burning, lactation stimulation in pregnant women (galactagogue), blurred vision and itching in the eyes, gum soreness, and cough treatments are utilised. Fruits, vegetables, leaves, seeds, and all plant-based foods are utilised for nutritional purposes in Portugal, Italy, Spain, and India. In the field of manufacturing, natural light green dye obtained from leaves is utilised in cosmetics, wood colouring, and as a food colouring agent (Akgül and Bayrak, 1988; Uğraş et al., 2003; Ghorbani, 2005; Macia et al., 2005; De Albuquerque et al., 2007; Jarić et al., 2007; Tene et al., 2007; Kaur and Arora, 2009; Lewu and Afolayan, 2009; Neves et al., 2009; Alzweiri et al., 2011; Calvo et al., 2011; Savo et al., 2011; Carrio and Valles, 2012; Oliveira et al., 2012; Polat and Satıl, 2012; Rasul et al., 2012; Bulut and Tuzlaci, 2013; del Carmen Juárez-Vázquez et al., 2013; Guarrera and Savo, 2013; Rahimi and Ardekani, 2013).

Nutritional and Mineral Contents

Plants are natural products that are noteworthy for their nourishing properties. According to Mohammed et al. (2021b), individuals are immutable parameters of their diets. According to the literature, the nutritional and mineral contents of *Foeniculum* species have been compiled and presented in Table 1.

Table 1. Mineral and Nutritional Contents of Foeniculum species

Nutritional Composition	Values
Protein	%9.38 and 1.08-1.37 g/100g
Lipids	%9.76-10.71 and 0.45-1.28 g/100g
Carbohydrate	%40.19 and 18.44-22.82 g/100g
Ash	%12.87-12.97 and 1.62-3.43 g/100g
Mouisture	%6.24-8.04 and 71.31-77.46 g/100g
Caloric energy (kcal/100 g)	97.37-108.23
K	4.241-5.851 mg/kg
Ca	56-363 mg/kg
Mg	82-389 mg/kg
Mn	2093.5-2113.5 mg/kg
Fe	63.3-97.2 mg/kg
Na	77-512 mg/kg
Zn	37-45 mg/kg

It has been reported that *Foeniculum* species have nutritional content values of protein (9.38%), lipids (9.76-10.71%), carbohydrate (40.19%), ash (12.87-12.97%), moisture (6.24-8.04%), and caloric energy (97.37-108.23 kcal/100 g) expressed as percentages. Furthermore, it has been reported that the nutritional content values of protein (1.08-1.37 g/100g), lipids (0.45-1.28 g/100g), carbohydrate (18.44-22.82 g/100g), ash (1.62-3.43 g/100g), and moisture (71.31-77.46 g/100g) are present in g/100g in the literature (Barros et al., 2010; Bukhari et al., 2014; Sabre and Eshra, 2019). It has been reported that *Foeniculum* species have a mineral content of K (4.241-5.851 mg/kg), Ca (56-363 mg/kg), Mg (82-389 mg/kg), Mn (2093.5-2113.5 mg/kg), Fe (63.3-97.2 mg/kg), Na (77-512 mg/kg), and Zn (37-45 mg/kg) (Koudela and Petrikova, 2008; Bukhari et al., 2014; Endalamaw and Chandravanshi, 2015; Sabre and Eshra, 2019).

Biological activities

Plants are natural products with various biological activities. Numerous studies have demonstrated the high biological activities of plants (Pehlivan et al., 2018). In the literature, it has been observed that various extracts such as essential oil, water, ethanol, methanol, and aqueous have been utilised in in vitro and in vivo studies on species belonging to the *F. vulgare*. The literature research conducted is presented in Table 2.

Table 2. Biological activity of Foeniculum vulgare

Plant species	Biological activity	Extraction	Geographic regions	References
Foeniculum vulgare Mill.	Antioxidant, antimicrobial, anticancer, insecticide, larvicidal, anti-inflammatory, antidiabetic, hepatoprotective	essential oil, water, ethanol, methanol, aqueous	Portugal, Algeria, Iran, India, Turkey, China, Pakistan, South Korea, Jordan, Morocco, Egypt	(Oktay et al., 2003; Choi and Hwang, 2004; Özbek et al., 2004; Anwar et al., 2009; Barros et al., 2009; Miguel et al., 2010; Mohamad et al., 2011; Chatterjee et al., 2012; Roby et al., 2013; Senatore et al., 2013; El Ouariachi et al., 2014; Diao et al., 2014; Zoubiri et al., 2014; Abu-Zaiton et al., 2015; Upadhyay, 2015; Bano et al., 2016; Foroughi et al., 2016; Akhbari et al., 2019; Belabdelli et al., 2020; Sanei-Dehkordi et al., 2022)

Antioxidant activity

Reactive oxygen species are routinely generated during metabolic activities. According to Krupodorova and Sevindik's (2020) findings, while oxidant compounds do not exhibit harmful effects at low levels, they can cause cellular damage at high levels. According to Bal et al. (2019), the antioxidant defence system plays a role in suppressing oxidative compounds such as oxidants. When the values of oxidising compounds reach high levels, the antioxidant defence system may become insufficient. In such circumstances, oxidative stress may occur (Eraslan et al., 2021). Numerous serious illnesses such as multiple sclerosis, Alzheimer's disease, cancer, cardiovascular disorders, and Parkinson's disease may arise as a result of oxidative stress (Selamoglu et al., 2020; Saridogan et al., 2021). Supplementary antioxidants can play a role in reducing or suppressing the effects of oxidative stress (Akgül et al., 2022). Within this context, the evaluation of plants as supplementary antioxidants is feasible through the determination of their antioxidant potentials. In our study, we have compiled the literature-reported antioxidant activity studies of Foeniculum vulgare (Table 2). In a study conducted in Portugal, it was reported that the volatile oil obtained from F. vulgare had a DPPH test result of >50% (Miguel et al., 2010). A study conducted in Turkey reported the antioxidant activity of F. vulgare's water and ethanol extracts using total antioxidant, free radical scavenging, superoxide anion radical scavenging, hydrogen peroxide scavenging, and metal chelation tests(Oktay et al., 2003). A study conducted in Pakistan reported that the volatile oil and ethanol extract obtained from F. vulgare plant sample exhibited a DPPH test result of 23.61-26.75 μg/mL(Anwar et al., 2009). A study conducted in India reported significant antioxidant effects of F. vulgare's methanol and aqueous extracts through DPPH, OH- scavenging, and FRAP tests(Chatterjee et al., 2012). The IC50 values of F. vulgare collected from Morocco, as determined

by DPPH assay, were reported to be 6.2 and 1.5 µg/mL for the diethyl ether and ethyl acetate extracts, respectively (El Ouariachi et al., 2014). The DPPH test results of the Shoots, Leaves, Stems, and Inflorescences parts of F. vulgare collected from Portugal were reported as 1.34, 6.88, 12.16, and 7.72 mg/mL, respectively. The results of the reducing power test were reported as 0.48, 1.17, 2.82, and 1.02 mg/mL, while the b-Carotene bleaching inhibition test yielded results of 0.49, 1.14, 2.38, and 1.29 mg/mL. The lipid peroxidation inhibition test results were reported as 0.13, 0.22, 0.27, and 0.25 mg/mL, respectively (Barros et al., 2009). It has been reported that the essential oil of F. vulgare collected from Egypt exhibited 100% efficacy in the DPPH assay(Mohamad et al., 2011).It has been reported that the IC50 value of F. vulgare collected from Egypt, as determined by the DPPH assay, ranges from 0.22-0.47 g/100g for its methanol, ethanol, diethyl ether, and hexane extracts(Roby et al., 2013). The volatile oil of F. vulgare collected from Italy was reported to have a DPPH test result of 0.25-0.33 mmol/L(Senatore et al., 2013). It has been reported that the volatile oil and methanol extract of F. vulgare collected from France exhibited DPPH test results of 444.2 and 52.60 µg/mL, β-carotene test results of 497.92 and 171.23 µg/mL, and Reducing power test results of 2,104.5 and 55.56, respectively (Kalleli et al., 2019). Within this context, it has been determined that F. vulgare exhibits significant antioxidant potential based on the antioxidant activity values reported in the literature.

Antimicrobial activity

In recent years, microorganisms have been identified as a fundamental cause of numerous diseases (Baba et al., 2020). The increase in the number of resistant microorganisms due to the indiscriminate use of antibiotics in contemporary times has rendered the effects of antimicrobial drugs insufficient (Mohammed et al., 2023). Within this scope, researchers have focused on the discovery of new antimicrobial drugs. Plants are significant natural resources within this context. Due to the potential adverse effects of synthetic drugs, numerous natural antimicrobial products have been utilised by individuals (Bal et al., 2017; Islek et al., 2021). Therefore, it is of great importance to conduct research on new antimicrobial drugs. In our study, we have compiled the literature-reported antimicrobial activity studies of F. vulgare (Table 2). In this context, a study conducted in Algeria investigated the antimicrobial activity of the essential oil obtained from F. vulgare on Candida albicans, Aspergillus flavus, Aspergillus niger, Rhizopus sp., Trichophyton rubrum, Trichophyton mentagrophytes, Trichophyton violaceum, Microsporumgypseum, Microsporumcanis, and Rhodotorula sp. According to the research findings, it has been reported that the essential oil of F. vulgare exhibits high activity against C. albicans and Aspergillus species with MIC values of 0.16-0.2 mg/mL (Belabdelli et al., 2020). In a study conducted in India, it was reported that F. vulgare exhibited an

inhibition zone diameter ranging from 19.4-26.4 mm at a concentration of 28 µg/disk against the strains used, and a minimum inhibitory concentration value ranging from 7.0-56 µg/mL (Upadhyay, 2015). A study conducted in Iran reported that Trans-anethole obtained from the essential oil of F. vulgare was effective against Escherichia coli at a concentration of 0.007 g/mL and against Staphylococcus aureus at a concentration of 0.003 g/mL (Foroughi et al., 2016). In a study conducted in China, the antimicrobial effect of the essential oil extracted from F. vulgare was investigated on Bacillus subtilis, S. albus, Shigella dysenteriae, Salmonella typhimurium, and E. coli. According to the study findings, the highest activity was exhibited against S. dysenteriae, with reported MIC and MBC values of 0.125 and 0.25 mg/mL, respectively (Diao et al., 2014). A study conducted in India investigated the antimicrobial activity of the methanol extract of F. vulgare against E. coli, S. aureus, Listeria monocytogenes, B. pumilus, and Enteropathogenic E. coli. According to the research findings, it has been reported that the maximum antibacterial activity was observed against S. aureus with an inhibition zone of 20.00 mm (Bano et al., 2016). The effects of methanol, ethanol, diethyl ether, and hexane extracts of F. vulgare collected from Egypt were investigated against Escherichia coli, Salmonella typhi, Bacillus cereus, Staphylococcus aureus, Candida albicans, and Aspergillus flavus. According to the study findings, it has been reported that the methanol extract exhibited an inhibition zone of 13-22 mm, the ethanol extract exhibited an inhibition zone of 9-19 mm, the diethyl ether extract exhibited an inhibition zone of 11-19 mm, and the hexane extract exhibited an inhibition zone of 13-22 mm (Roby et al., 2013). According to reports, the volatile oil of F. vulgare collected from Italy has been found to be effective against Bacillus subtilis, Staphylococcus aureus, Staphylococcus epidermidis, Streptococcus faecalis, Escherichia coli, Klebsiella pneumoniae, Proteus vulgaris, and Pseudomonas aeruginosa (Senatore et al., 2013). Within this context, it has been determined that F. vulgare may serve as a significant natural resource against reported microorganisms.

Other activities

A study conducted in Iran investigated the anticancer properties of the volatile oil of F. vulgare against human breast cancer (MDA-Mb) and cervical epithelioid carcinoma (Hela) cell lines using the MTT assay. According to the study findings, it has been reported that the compound is a potent anticancer agent with an IC50 lower than 10 µg/mL (Akhbari et al., 2019). A study conducted in Iran reported that the protective duration of F. vulgare's essential oil against Anopheles stephensi was 70 minutes (Sanei-Dehkordi et al., 2022). A study conducted in Algeria investigated the larvicidal effect of the essential oil of F. vulgare on Culex pipiens. The study determined that a mortality rate of 50% was observed in second stage larvae within a concentration of 40 mg/L over a period of 2 hours. According to reports, a

concentration of 60 mg/L resulted in a 90% mortality rate for fourth instar larvae after a 4-hour exposure period (Zoubiri et al., 2014). A study conducted in South Korea investigated the anti-inflammatory effect of F. vulgare's methanol extract. According to the study findings, it has been reported that there was an increase in the activities of superoxide dismutase (SOD) and catalase, as well as high-density lipoprotein cholesterol levels, while the level of malondialdehyde decreased significantly (Choi and Hwang, 2004). A study conducted in Jordan investigated the antidiabetic effect of F. vulgare's methanol extract. According to the study findings, it has been reported that the methanol extract exhibited an 82.43% and 82.26% effect on α-amylase and α-glucosidase, respectively, after an 8-hour duration (Abu-Zaiton et al., 2015). A study conducted in Turkey investigated the hepatoprotective properties of F. vulgare's essential oil in rats with liver damage induced by carbon tetrachloride. According to the research findings, it has been reported that the levels of serum aspartate aminotransferase, alanine aminotransferase, bilirubin, and alkaline phosphatase have decreased (Özbek et al., 2004). The methanolic extract of F. vulgare collected from Egypt has been reported to exhibit effective IC50 values against MCF-7 (15.78 µg/mL), Hepg-2 (27.96 µg/mL), HT-29 (41.87 µg/mL), H460 (50.22 µg/mL), Hela (79.33 µg/mL), and U251 (85.49 µg/mL) cell lines (Mohamad et al., 2011). Literatür verilerine göre F. vulgare'nin biyolojik aktivite bakımından önemli bir kaynak olabileceği tespit edilmiştir.

Essential oil contents

Plants synthesise numerous biologically active compounds within their structures. Bioactive compounds are important from a medical perspective, despite not having any nutritional value (Selamoglu et al., 2017; Akgül et al., 2020). Within this context, it is highly important to determine the compounds present in plants. In our study, the chemical compounds reported in the composition of *F. vulgare* have been compiled. The findings obtained are presented in Table 3.

Table 3. Essential oil contents of Foeniculum vulgare

Plant species	Geographic regions	Used Part	Essential oil content	References
Foeniculum vulgare Mill.	Serbia, China, Portugal, Pakistan, Turkey, Estonia, Italy, Iran, Brazil, Egypt, Morocco, USA	Seed, aerial parts, fruit	α-Farnesene (1.28%), β-Farnesene (3.01%), 2,5-Diethyl phenol (0.78%), Bergamoil (0.63%), Myrcenol (1.02%), 2,4,6,8-Tetrathiatricyclo [3.3.1.13,7]decane (1.77%), Trans-2-caren-4-ol (0.61%), 2-cyclohexen-1-one (2.1%), Endobornyl acetate (0.66%), Trans-3-acetyl-4-methoxy-1-methylenecyclopentane (0.31%), Benzene,1-methoxy-4-(2-propenyl)methylchavicol-estragole (71.1%), Trans-dihydrocarvone (0.57%), 2,6-Octadien-1-ol,2,7-dimethyl (0.26%), P-Menth-3-en-1-ol (0.55-0.72 %), Bicyclo[2.2.1]heptane-2-1 (1.21%), Bicyclo[3.3.1]non-2-en-9-ol,9-methyl (1.94%), Benzene,1-methyl-4-(1-methylethyl) (0.82-1.68%), Nepetalactone (0.7%), Geranyl acetate (0.2%), Piperitenone oxide (12.5%), Piperitenone (1%), Terpinen-4-ol (0.016-2.8%), trans-Pinocarveol (0.2%), Linalool (0.13-0.3%), Terpinolene (2.4%), p-Cymene (1.5%), 3-Carene (0.7%), Sabinene (1%), α-Thujene (0.1%), (E)-anethole (43%–81.10%), fenchone (0.14–34.7%), methyl chavicol (1.5%–7.22%), trans-anethole (3.62%-91.1%), estragole (2.4%-88%), α-pinene (0.82-20%), limonene (0.8%-42.30%), cis-anethole (0.1%–8.6%), β-pinene (17.8%), α-phelandrene (0.9%-10.5%), α-pinene (0.13%-12.4%), myrcene (0.62%-15%), delta-3-carene (2.1%-3.7%), cis-ocimene (0%-0.23%), Ɣ-terpinene (0.22%-2.67%), paracymene (0.68%-5.97%), camphor (0.1%-0.51%), p-allylanisole (71.40%), 1.8-Cineol (0.89 %)	(Akgül and Bayrak, 1988; Marotti and Piccaglia, 1992; Coelho et al., 2003; Mimica-Dukić et al., 2003; Stefanini et al., 2006; Anwar et al., 2009; Miguel et al., 2010; Lahhit et al., 2011; Mohamad et al., 2011; Saharkhiz and Tarakeme, 2011; Raal et al., 2012; Zheljazkov et al., 2013; Diao et al., 2014; El Ouariachi et al., 2014; Mota et al., 2015; Ali et al., 2016; Ahmed et al., 2019; Rezaei-Chiyaneh et al., 2020)

It has been reported that the main components of the essential oil content of F. vulgare species are α-Farnesene (1.28%), 1.8-Cineol (0.89%), β-Farnesene (3.01%), 2,5-Diethyl phenol (0.78%), Bergamoil (0.63%), Myrcenol (1.02%), 2,4,6,8-Tetrathiatricyclo [3.3.1.13,7]decane (1.77%), Trans-2-caren-4-ol (0.61%), 2-cyclohexen-1-one (2.1%), Endobornyl acetate (0.66%), Trans-3-acetyl-4-methoxy-1-methylenecyclopentane (0.31%), Benzene,1-methoxy-4-(2-propenyl)methylchavicol-estragole (71.1%), Trans-dihydrocarvone (0.57%), 2,6-Octadien-1-ol,2,7-dimethyl (0.26%), P-Menth-3-en-1-ol (0.55-0.72 %), Bicyclo[2.2.1]heptane-2-1 (1.21%), Bicyclo[3.3.1]non-2-

en-9-ol,9-methyl (1.94%), Benzene,1-methyl-4-(1-methylethyl) (0.82-1.68%), Nepetalactone (0.7%), Geranyl acetate (0.2%), Piperitenone oxide (12.5%), Piperitenone (1%), Terpinen-4-ol (0.016-2.8%), trans-Pinocarveol (0.2%), Linalool (0.13-0.3%), Terpinolene (2.4%), p-Cymene (1.5%), 3-Carene (0.7%), Sabinene (1%), α-Thujene (0.1%), (E)-anethole (43%–81.10%), fenchone (0.14–34.7%), methyl chavicol (1.5%–7.22%), trans-anethole (3.62%-91.1%), estragole (2.4%-88%), α-pinene (0.82-20%), limonene (0.8%-42.30%), cis-anethole (0.1%–8.6%), β-pinene (17.8%), α-phelandrene (0.9%-10.5%), α-pinene (0.13%-12.4%), myrcene (0.62%-15%), delta-3-carene (2.1%-3.7%), cis-ocimene (0%-0.23%), Ɣ-terpinene (0.22%-2.67%), paracymene (0.68%-5.97%), camphor (0.1%-0.51%), p-allylanisole (71.40%) (Akgül and Bayrak, 1988; Marotti and Piccaglia, 1992; Coelho et al., 2003; Mimica-Dukić et al., 2003; Stefanini et al., 2006; Anwar et al., 2009; Miguel et al., 2010; Lahhit et al., 2011; Saharkhiz and Tarakeme, 2011; Raal et al., 2012; Zheljazkov et al., 2013; Diao et al., 2014; Mota et al., 2015; Ali et al., 2016; Ahmed et al. al., 2019; Rezaei-Chiyaneh et al., 2020). According to the literature data, it has been determined that F. vulgare may be an important natural source in terms of the chemical compounds reported in its body.

Conclusion

In this study, the utilisation areas, general characteristics, biological activities, and chemical contents of *F. vulgare* have been compiled. According to the findings obtained, it has been reported that the plant has many areas of use in the fields of health and food. Furthermore, it has been observed that the antioxidant and antimicrobial activities are particularly high. Upon examination of the reported compounds, it is observed that the primary compound is trans-anethole (3.62%-91.1%). Consequently, according to the literature data, it has been determined that *F. vulgare* could serve as a natural source in pharmacological designs.

REFERENCES

Abu-Zaiton, A., Alu'datt, M., Wafa, M. (2015). Evaluating the effect of Foeniculum vulgare extract on enzymes related with blood pressure and diabetes (in vitro study). International Journal of Advances in Chemical Engineering and Biological Sciences, 2(2), 77-80.

Ahmed, A. F., Shi, M., Liu, C., Kang, W. (2019). Comparative analysis of antioxidant activities of essential oils and extracts of fennel (Foeniculum vulgare Mill.) seeds from Egypt and China. Food Science and Human Wellness, 8(1), 67-72.

Akgul, H., Korkmaz, N., Dayangaç, A., & Sevindik, M. (2020). Antioxidant potential of endemic Salvia absconditiflora. Turkish Journal of Agriculture-Food Science and Technology, 8(10), 2222-2224.

Akgül, A., Bayrak, A. (1988). Comparative volatile oil composition of various parts from Turkish bitter fennel (Foeniculum vulgare var. vulgare). Food Chemistry, 30(4), 319-323.

Akgül, H., Mohammed, F. S., Kına, E., Uysal, İ., Sevindik, M., & Doğan, M. (2022). Total Antioxidant and Oxidant Status and DPPH Free radical activity of Euphorbia eriophora. Turkish Journal of Agriculture-Food Science and Technology, 10(2), 272-275.

Akhbari, M., Kord, R., Jafari Nodooshan, S., Hamedi, S. (2019). Analysis and evaluation of the antimicrobial and anticancer activities of the essential oil isolated from Foeniculum vulgare from Hamedan, Iran. Natural product research, 33(11), 1629-1632.

Ali, S. I., Mohamed, A. A., Sameeh, M. Y., Darwesh, O. M., Abd El-Razik, T. M. (2016). Gamma-irradiation affects volatile oil constituents, fatty acid composition and antimicrobial activity of fennel (Foeniculum vulgare) seeds extract. Research Journal of Pharmaceutical, Biological and Chemical Sciences, 7(1), 524-532.

Alzweiri, M., Al Sarhan, A., Mansi, K., Hudaib, M., Aburjai, T. (2011). Ethnopharmacological survey of medicinal herbs in Jordan, the Northern Badia region. Journal of Ethnopharmacology, 137(1), 27-35.

Anwar, F., Ali, M., Hussain, A. I., Shahid, M. (2009). Antioxidant and antimicrobial activities of essential oil and extracts of fennel (Foeniculum vulgare Mill.) seeds from Pakistan. Flavour and Fragrance Journal, 24(4), 170-176.

Baba, H., Sevindik, M., Dogan, M., & Akgül, H. (2020). Antioxidant, antimicrobial activities and heavy metal contents of some Myxomycetes. Fresenius Environmental Bulletin, 29(09), 7840-7846.

Bal, C., Akgul, H., Sevindik, M., Akata, I., & Yumrutas, O. (2017). Determination of the anti-oxidative activities of six mushrooms. Fresenius Envir Bull, 26(10), 6246-6252.

Bal, C., Sevindik, M., Akgul, H., & Selamoglu, Z. (2019). Oxidative stress index and antioxidant capacity of Lepista nuda collected from Gaziantep/Turkey. Sigma

Journal of Engineering and Natural Sciences, 37(1), 1-5.

Bano, S., Ahmad, N., Sharma, A. K. (2016). Phytochemical investigation and evaluation of anti-microbial and anti-oxidant activity of Foeniculum vulgare (fennel). International Journal of Pharma Sciences and Research, 7(7), 310-314.

Barros, L., Carvalho, A. M., Ferreira, I. C. (2010). The nutritional composition of fennel (Foeniculum vulgare): Shoots, leaves, stems and inflorescences. LWT-Food Science and Technology, 43(5), 814-818.

Barros, L., Heleno, S. A., Carvalho, A. M., & Ferreira, I. C. (2009). Systematic evaluation of the antioxidant potential of different parts of Foeniculum vulgare Mill. from Portugal. *Food and Chemical Toxicology*, *47*(10), 2458-2464.

Belabdelli, F., Piras, A., Bekhti, N., Falconieri, D., Belmokhtar, Z., Merad, Y. (2020). Chemical composition and antifungal activity of Foeniculum vulgare Mill. Chemistry Africa, 3(2), 323-328.

Bhawna, S., & Kumar, S. U. (2009). Hepatoprotective activity of some indigenous plants. Int J Pharm Tech Res, 4, 1330-1334.

Bukhari, H., Shehzad, A., Saeed, K., Sadiq, B. M., Tanveer, S., Iftikhar, T. (2014). Compositional profiling of fennel seed. Pak. J. Food Sci, 24(3), 132-136.

Bulut, G., Tuzlaci, E. (2013). An ethnobotanical study of medicinal plants in Turgutlu (Manisa—Turkey). Journal of Ethnopharmacology, 149(3), 633-647.

Calvo, M. I., Akerreta, S., Cavero, R. Y. (2011). Pharmaceutical ethnobotany in the riverside of Navarra (Iberian Peninsula). Journal of Ethnopharmacology, 135(1), 22-33.

Carrio, E., Valles, J. (2012). Ethnobotany of medicinal plants used in eastern Mallorca (Balearic Islands, Mediterranean Sea). Journal of Ethnopharmacology, 141(3), 1021-1040.

Charles, D. J. (2012). Cinnamon. In Antioxidant Properties of Spices, Herbs and Other Sources (pp. 231-243). Springer, New York, NY.

Chatterjee, S., Goswami, N., Bhatnagar, P. (2012). Estimation of Phenolic Components and in vitro Antioxidant Activity of Fennel (Foeniculum vulgare) and Ajwain (Trachyspermum ammi) seeds. Adv Biores, 3(2), 109-18.

Choi, E. M., Hwang, J. K. (2004). Antiinflammatory, analgesic and antioxidant activities of the fruit of Foeniculum vulgare. Fitoterapia, 75(6), 557-565.

Coelho, J. A. P., Pereira, A. P., Mendes, R. L., Palavra, A. M. F. (2003). Supercritical carbon dioxide extraction of Foeniculum vulgare volatile oil. Flavour and Fragrance Journal, 18(4), 316-319.

De Albuquerque, U. P., De Medeiros, P. M., De Almeida, A. L. S., Monteiro, J. M., Neto, E. M. D. F. L., de Melo, J. G., Dos Santos, J. P. (2007). Medicinal plants of the caatinga (semi-arid) vegetation of NE Brazil: a quantitative approach. Journal of ethnopharmacology, 114(3), 325-354.

del Carmen Juárez-Vázquez, M., Carranza-Álvarez, C., Alonso-Castro, A. J., González-Alcaraz, V. F., Bravo-Acevedo, E., Chamarro-Tinajero, F. J., Solano, E. (2013). Ethnobotany of medicinal plants used in Xalpatlahuac, Guerrero, México. Journal of ethnopharmacology, 148(2), 521-527.

Diao, W. R., Hu, Q. P., Zhang, H., Xu, J. G. (2014). Chemical composition, antibacterial activity and mechanism of action of essential oil from seeds of fennel (Foeniculum vulgare Mill.). Food control, 35(1), 109-116.

El Ouariachi, E., Lahhit, N., Bouyanzer, A., Hammouti, B., Paolini, J., Majidi, L., ... & Costa, J. (2014). Chemical composition and antioxidant activity of essential oils and solvent extracts of Foeniculum vulgare Mill. from Morocco. J. Chem. Pharm. Res, 6(4), 743-748.

Endalamaw, F. D., Chandravanshi, B. S. (2015). Levels of major and trace elements in fennel (Foeniculum vulgari Mill.) fruits cultivated in Ethiopia. SpringerPlus, 4(1), 1-10.

Eraslan, E. C., Altuntas, D., Baba, H., Bal, C., Akgül, H., Akata, I., & Sevindik, M. (2021). Some biological activities and element contents of ethanol extract of wild edible mushroom Morchella esculenta. Sigma Journal of Engineering and Natural Sciences, 39(1), 24-28.

Foroughi, A., Pournaghi, P., Zhaleh, M., Zangeneh, A., Zangeneh, M. M., Moradi, R. (2016). Antibacterial activity and phytochemical screening of essential oil of Foeniculum vulgare. International Journal of Pharmaceutical and Clinical Research, 8(11), 1505-1509.

Ghorbani, A. (2005). Studies on pharmaceutical ethnobotany in the region of Turkmen Sahra, north of Iran:(Part 1): General results. Journal of ethnopharmacology, 102(1), 58-68.

Guarrera, P. M., Savo, V. (2013). Perceived health properties of wild and cultivated food plants in local and popular traditions of Italy: A review. Journal of Ethnopharmacology, 146(3), 659-680.

Gupta, M. (2010). Pharmacological properties and traditional therapeutic uses of important Indian spices: A review. International Journal of Food Properties, 13(5), 1092-1116.

Islek, C., Saridogan, B. G. O., Sevindik, M., & Akata, I. (2021). Biological activities and heavy metal contents of some Pholiota species. Fresenius Environmental Bulletin, 30(6), 6109-6114.

Jarić, S., Popović, Z., Mačukanović-Jocić, M., Djurdjević, L., Mijatović, M., Karadžić, B., Pavlović, P. (2007). An ethnobotanical study on the usage of wild medicinal herbs from Kopaonik Mountain (Central Serbia). Journal of ethnopharmacology, 111(1), 160-175.

Kalleli, F., Bettaieb Rebey, I., Wannes, W. A., Boughalleb, F., Hammami, M., Saidani Tounsi, M., & M'hamdi, M. (2019). Chemical composition and antioxidant potential of essential oil and methanol extract from Tunisian and French fennel (Foeniculum vulgare Mill.) seeds. Journal of food biochemistry, 43(8), e12935.

Kaur, G. J., Arora, D. S. (2009). Antibacterial and phytochemical screening of Anethum graveolens, Foeniculum vulgare and Trachyspermum ammi. BMC complementary and alternative medicine, 9(1), 1-10.

Khan, M., Musharaf, S. (2014). Foeniculum vulgare Mill. A medicinal herb. Medicinal Plant Research, 4(6), 46-54.

Korkmaz, N., Dayangaç, A., Sevindik, M. (2021). Antioxidant, antimicrobial and antiproliferative activities of Galium aparine. J Fac Pharm Ankara, 45(3), 554-564.

Koudela, M., Petrikova, K. (2008). Nutritional compositions and yield of sweet fennel cultivars-Foeniculum vulgare Mill. ssp. vulgare var. azoricum (Mill.) Thell. Hort. Sci, 35(1), 1-6.

Krishnamurthy, K. H. (2011). Medicinal plants: Madhurika, saunf or fennel (Foeniculum vulgare, Gaertn). Journal of New Approaches to Medicine and Health, 19(1), 1-4.

Krupodorova, T., & Sevindik, M. (2020). Antioxidant potential and some mineral contents of wild edible mushroom Ramaria stricta. AgroLife Scientific Journal, 9(1), 186-191.

Lahhit, N., Bouyanzer, A., Desjobert, J. M., Hammouti, B., Salghi, R., Costa, J., Majidi, L. (2011). Fennel (Foeniculum vulgare) essential oil as green corrosion inhibitor of carbon steel in hydrochloric acid solution. Portugaliae Electrochimica Acta, 29(2), 127-138.

Laxa, M., Liebthal, M., Telman, W., Chibani, K., & Dietz, K. J. (2019). The role of the plant antioxidant system in drought tolerance. Antioxidants, 8(4), 94.

Lewu, F. B., Afolayan, A. J. (2009). Ethnomedicine in South Africa: The role of weedy species. African Journal of Biotechnology, 8(6),929-934.

Macia, M. J., Garcia, E., Vidaurre, P. J. (2005). An ethnobotanical survey of medicinal plants commercialized in the markets of La Paz and El Alto, Bolivia. Journal of ethnopharmacology, 97(2), 337-350.

Marotti, M., Piccaglia, R. (1992). The Influence of Distillation Conditions on the Essential Oil Composition of Three Varieties of Foeniculum vulgare Mill. Journal of Essential Oil Research, 4(6), 569-576.

Mehra, N., Tamta, G., Nand, V. (2021). A review on nutritional value, phytochemical and pharmacological attributes of Foeniculum vulgare Mill. Journal of Pharmacognosy and Phytochemistry, 10(2), 1255-1263.

Miastkowska, M., & Sikora, E. (2018). Anti-aging properties of plant stem cell extracts. Cosmetics, 5(4), 55.

Miguel, M. G., Cruz, C., Faleiro, L., Simões, M. T., Figueiredo, A. C., Barroso, J. G., Pedro, L. G. (2010). Foeniculum vulgare essential oils: chemical composition, antioxidant and antimicrobial activities. Natural product communications, 5(2), 1934578X1000500231.

Mimica-Dukić, N., Kujundžić, S., Soković, M., Couladis, M. (2003). Essential oil

composition and antifungal activity of Foeniculum vulgare Mill. obtained by different distillation conditions. Phytotherapy Research: An International Journal Devoted to Pharmacological and Toxicological Evaluation of Natural Product Derivatives, 17(4), 368-371.

Mohamad, R. H., El-Bastawesy, A. M., Abdel-Monem, M. G., Noor, A. M., Al-Mehdar, H. A. R., Sharawy, S. M., & El-Merzabani, M. M. (2011). Antioxidant and anticarcinogenic effects of methanolic extract and volatile oil of fennel seeds (Foeniculum vulgare). Journal of medicinal food, 14(9), 986-1001.

Mohammed, F. S., Akgul, H., Sevindik, M., & Khaled, B. M. T. (2018). Phenolic content and biological activities of Rhus coriaria var. zebaria. Fresenius Environmental Bulletin, 27(8), 5694-5702.

Mohammed, F. S., Günal, S., Pehlivan, M., Doğan, M., Sevindik, M., & Akgül, H. (2020b). Phenolic content, antioxidant and antimicrobial potential of endemic Ferulago platycarpa. Gazi University Journal of Science, 33(4), 670-677.

Mohammed, F. S., Günal, S., Şabik, A. E., Akgül, H., & Sevindik, M. (2020a). Antioxidant and Antimicrobial activity of Scorzonera papposa collected from Iraq and Turkey. Kahramanmaraş Sütçü İmam Üniversitesi Tarım ve Doğa Dergisi, 23(5), 1114-1118.

Mohammed, F. S., Karakaş, M., Akgül, H., & Sevindik, M. (2019). Medicinal properties of Allium calocephalum collected from Gara Mountain (Iraq). Fresen Environ Bull, 28(10), 7419-7426.

Mohammed, F. S., Pehlivan, M., Sevindik, E., Akgul, H., Sevindik, M., Bozgeyik, I., & Yumrutas, O. (2021a). Pharmacological properties of edible Asparagus acutifolius and Asparagus officinalis collected from North Iraq and Turkey (Hatay). Acta Alimentaria, 50(1), 136-143.

Mohammed, F. S., Sevindik, M., Uysal, I., Sevindik, E., & Akgül, H. (2022). A Natural Material for Suppressing the Effects of Oxidative Stress: Biological Activities of Alcea kurdica. Biology Bulletin, 49(Suppl 2), S59-S66.

Mohammed, F. S., Uysal, I., & Sevindik, M. (2023). A review on antiviral plants effective against different virus types. Prospects in Pharmaceutical Sciences, 21(2), 1-21.

Mohammed, F. S., Korkmaz, N., Doğan, M., Şabik, A. E., & Sevindik, M. (2021b). Some medicinal properties of Glycyrrhiza glabra (Licorice). Journal of Faculty of Pharmacy of Ankara University, 45(3), 524-534.

Mota, A. S., Martins, M. R., Arantes, S., Lopes, V. R., Bettencourt, E., Pombal, S., Silva, L. A. (2015). Antimicrobial activity and chemical composition of the essential oils of Portuguese Foeniculum vulgare fruits. Natural product communications, 10(4), 1934578X1501000437.

Neves, J. M., Matos, C., Moutinho, C., Queiroz, G., Gomes, L. R. (2009). Ethnopharmacological notes about ancient uses of medicinal plants in Trás-os-Montes (northern of Portugal). Journal of Ethnopharmacology, 124(2), 270-283.

Oktay, M., Gülçin, İ., Küfrevioğlu, Ö. İ. (2003). Determination of in vitro antioxidant activity of fennel (Foeniculum vulgare) seed extracts. LWT-Food Science and Technology, 36(2), 263-271.

Oliveira, S. G. D., de Moura, F. R. R., Demarco, F. F., da Silva Nascente, P., Del Pino, F. A. B., Lund, R. G. (2012). An ethnomedicinal survey on phytotherapy with professionals and patients from Basic Care Units in the Brazilian Unified Health System. Journal of Ethnopharmacology, 140(2), 428-437.

Özbek, H., Ugras, S., Bayram, I., Uygan, I., Erdogan, E., Öztürk, A., Huyut, Z. (2004). Hepatoprotective effect of Foeniculum vulgare essential oil: A carbon-tetrachloride induced liver fibrosis model in rats. Scandinavian Journal of Laboratory Animal Sciences, 31(1), 9-17.

Pehlivan, M., Mohammed, F. S., Sevindik, M., & Akgul, H. (2018). Antioxidant and oxidant potential of Rosa canina. Eurasian Journal of Forest Science, 6(4), 22-25.

Polat, R., Satıl, F. (2012). An ethnobotanical survey of medicinal plants in Edremit Gulf (Balıkesir–Turkey). Journal of Ethnopharmacology, 139(2), 626-641.

Raal, A., Orav, A., Arak, E. (2012). Essential oil composition of Foeniculum vulgare Mill. fruits from pharmacies in different countries. Natural Product Research, 26(13), 1173-1178.

Rahim, N. A., Jantan, I., Said, M. M., Jalil, J., Abd Razak, A. F., & Husain, K. (2021). Anti-allergic rhinitis effects of medicinal plants and their bioactive metabolites via suppression of the immune system: a mechanistic review. Frontiers in pharmacology, 12, 660083.

Rahimi, R., Ardekani, M. R. S. (2013). Medicinal properties of Foeniculum vulgare Mill. in traditional Iranian medicine and modern phytotherapy. Chinese journal of integrative medicine, 19(1), 73-79.

Rasul, A., Akhtar, N., Khan, B. A., Mahmood, T., Zaman, S. U., Khan, H. M. (2012). Formulation development of a cream containing fennel extract: in vivo evaluation for anti-aging effects. Die Pharmazie-An International Journal of Pharmaceutical Sciences, 67(1), 54-58.

Rezaei-Chiyaneh, E., Amirnia, R., Machiani, M. A., Javanmard, A., Maggi, F., & Morshedloo, M. R. (2020). Intercropping fennel (Foeniculum vulgare L.) with common bean (Phaseolus vulgaris L.) as affected by PGPR inoculation: A strategy for improving yield, essential oil and fatty acid composition. Scientia Horticulturae, 261, 108951.

Saber, J. I., Eshra, D. H. (2019). Using Fennel Seeds and their Oil as a Preservative and Functional Food to Produce Some Food and Drink Products to Alleviate Cough Symptoms. Alexandria Science Exchange Journal, 40(July-September), 406-414.

Saharkhiz, M. J., Tarakeme, A. (2011). Essential oil content and composition of fennel (Foeniculum vulgare L.) fruits at different stages of development. Journal of Essential Oil Bearing Plants, 14(5), 605-609.

Sanei-Dehkordi, A., Abdollahi, A., Safari, M., Karami, F., Ghaznavi, G., & Osanloo, M. (2022). Nanogels Containing Foeniculum vulgare Mill. and Mentha piperita L. Essential oils: mosquitoes' repellent activity and antibacterial effect. Interdisciplinary Perspectives on Infectious Diseases, https://doi.org/10.1155/2022/4510182.

Saridogan, B. G. O., Islek, C., Baba, H., Akata, I., & Sevindik, M. (2021). Antioxidant antimicrobial oxidant and elements contents of Xylaria polymorpha and X. hypoxylon (Xylariaceae). Fresenius Envir Bull. 30(5), 5400-5404.

Savo, V., Giulia, C., Maria, G. P., David, R. (2011). Folk phytotherapy of the amalfi coast (Campania, Southern Italy). Journal of Ethnopharmacology, 135(2), 376-392.

Selamoglu, Z., Dusgun, C., Akgul, H., & Gulhan, M. F. (2017). In-vitro antioxidant activities of the ethanolic extracts of some contained-allantoin plants. Iranian journal of pharmaceutical research: IJPR, 16(Suppl), 92.

Selamoglu, Z., Sevindik, M., Bal, C., Ozaltun, B., Sen, İ., & Pasdaran, A. (2020). Antioxidant, antimicrobial and DNA protection activities of phenolic content of Tricholoma virgatum (Fr.) P. Kumm. Biointerface Research in Applied Chemistry, 10 (3), 5500-5506

Senatore, F., Oliviero, F., Scandolera, E., Taglialatela-Scafati, O., Roscigno, G., Zaccardelli, M., & De Falco, E. (2013). Chemical composition, antimicrobial and antioxidant activities of anethole-rich oil from leaves of selected varieties of fennel [Foeniculum vulgare Mill. ssp. vulgare var. azoricum (Mill.) Thell]. Fitoterapia, 90, 214-219.

Sevindik, M., Akgul, H., Pehlivan, M., & Selamoglu, Z. (2017). Determination of therapeutic potential of Mentha longifolia ssp. longifolia. Fresen Environ Bull, 26(7), 4757-4763.

Stefanini, M. B., Ming, L. C., Marques, M. O. M., Facanali, R., Meireles, M. A. A., Moura, L. S., Sousa, L. A. (2006). Essential oil constituents of different organs of fennel (Foeniculum vulgare var. vulgare). Rev. Bras. Pl. Med., Botucatu, 8, 193-198.

Tene, V., Malagon, O., Finzi, P. V., Vidari, G., Armijos, C., Zaragoza, T. (2007). An ethnobotanical survey of medicinal plants used in Loja and Zamora-Chinchipe, Ecuador. Journal of ethnopharmacology, 111(1), 63-81.

Uğraş, S., Dulger, H., Bayram, İ., Tuncer, İ., Öztürk, G. (2003). Hepatoprotective effect of Foeniculum vulgare essential oil. Fıtoterapıa, 74(3),317-319.

Unal, O., Eraslan, E. C., Uysal, I., Mohammed, F. S., Sevindik, M., & Akgul, H. (2022). Biological activities and phenolic contents of Rumex scutatus collected from Turkey. Fresenius Environmental Bulletin, 31(7), 7341-7346.

Upadhyay, R. K. (2015). GC-MS analysis and in vitro antimicrobial susceptibility of Foeniculum vulgare seed essential oil. American Journal of Plant Sciences, 6(07), 1058.

Uysal, I., Koçer, O., Mohammed, F.S., Lekesiz, Ö., Doğan, M., Şabik, A.E., Sevindik, E., Gerçeker, F.O., Sevindik, M. (2023). Pharmacological and Nutritional Properties: Genus Salvia. Adv Pharmacol, 11(2), 140-155

Zheljazkov, V. D., Horgan, T., Astatkie, T., Schlegel, V. (2013). Distillation time modifies essential oil yield, composition, and antioxidant capacity of fennel (Foeniculum vulgare Mill). Journal of Oleo Science, 62(9), 665-672.

Zoubiri, S., Baaliouamer, A., Seba, N., Chamouni, N. (2014). Chemical composition and larvicidal activity of Algerian Foeniculum vulgare seed essential oil. Arabian Journal of Chemistry, 7(4), 480-485.

Chapter 8

BIOLOGICAL ACTIVITIES, USAGE AREAS AND CHEMICAL CONTENTS OF ECHINACEA SPECIES

Oğuzhan Koçer[1]
İmran Uysal[2]
Falah Saleh Mohammed[3]
Mustafa Sevindik[4]
Hasan Akgül[5]

1 Department of Pharmacy Services, Vocational School of Health Services, University of Osmaniye Korkut Ata, Osmaniye
2 Osmaniye Korkut Ata University, Bahçe Vocational School, Department of Food Processing, Osmaniye, Turkey
3 Zakho University, Science Faculty, Department of Biology, Duhok, Iraq.
4 Osmaniye Korkut Ata University, Science and Literature Faculty, Department of Biology, Osmaniye, Turkey.
5 Akdeniz University, Science Faculty, Department of Biology, Antalya, Turkey

Introduction

Many plants are utilised within the scope of traditional medicine worldwide. Various species of plants are utilised in the treatment or prevention of different ailments within the scope of traditional medicine (Mohammed et al., 2022). In contrast to modern medicine, traditional medicine has a history that is equivalent to that of human civilization and has been transmitted through human experiences up to the present day (Sevindik et al., 2017). Plants are utilised by humans for various purposes. The utilisation of plants by humans has played a significant role in fulfilling various needs such as shelter, warmth, flavouring, nutrition, and medicine, with particular emphasis on the aforementioned purposes (Khan et al., 2019; Mohammed et al., 2020a; Korkmaz et al., 2021). Plants, which are well-known for their nourishing properties, contain essential nutrients such as protein, carbohydrates, vitamins, and minerals. In addition to their nourishing properties, natural sources are also of great medical importance (Mohammed et al., 2020b). Numerous studies have reported the diverse biological activities of plants, including antioxidant, anticancer, DNA protective, antiproliferative, anti-aging, antiallergic, hepatoprotective, and anti-inflammatory effects (Kim et al., 2004; Mohammed et al., 2018; Mohammed et al., 2019; Ahmed et al., 2020; Mohammed et al., 2021; Zulfiqar et al., 2021; Unal et al., 2022; Uysal et al., 2023). Within this context, it is highly important to determine the biological activities of plants. In our study, we have compiled the reported usage areas, biological activities, and chemical contents of *Echinacea* species in the literature.

Genus *Echinacea* and Usage Areas

The genus *Echinacea* belongs to the family Asteraceae. The name of the species is derived from the Greek word echinos. Species belonging to the genus Echinacea are perennial. The majority of these species are naturally found in certain regions of North America. In recent times, the popularity has been steadily increasing worldwide. From a morphological perspective, it can be observed that the plant in question typically emerges from an underground perennial with a basal rosette composed of petioled leaves and a one to several year stem. The disc flowers are conical, hemispherical, or occasionally flattened in shape. The capitulum is surrounded by 3 to 4 rows of bracts. Each disc flower has protrusions beyond the 5-lobed corolla on the receptacle. The flowers can exhibit a range of colours, including white, pink, magenta, and yellow, among others (Bauer, 1991; McKeown, 1999; Binns et al., 2002; Flagel et al., 2008; Karimmojeni et al., 2022). Numerous species within the Echinacea genus are utilised for various purposes. It has been reported that various parts of the plant, including leaves, roots, and flowers, have medicinal properties that can be used to treat a range of ailments, such as the common cold, toothache, snake bites, headaches, and wound infections,

as well as to boost immunity, treat blood poisoning, skin problems, syphilis, and respiratory infections (Mishima et al., 2004; Kumar and Ramaiah, 2011).

Biological activity

Plants are natural products responsible for various biological activities (Pehlivan et al., 2018). This study compiles in vitro and in vivo biological activity studies on species belonging to the *Echinacea* species in the literature. Within this scope, it has been observed that extracts of *Echinacea* species such as ethanol, hydroalcoholic, ethylacetate, hexane, methanol, water, dichloromethane, acetone, and aqueous have been utilised. The findings related to biological activity studies are presented in Table 1.

Table 1. Biological activity of Echinacea species

Plant species	Biological activity	Extraction	Geographic regions	References
Echinacea angustifolia DC.	Antimicrobial, antioxidant, hypoglycaemic, anti-inflammatory, antiproliferative	Ethanol, methanol, hydroalcoholic, ethylacetate, alcohol	Iran, Mexico, China, South Korea, Canada	(Hu and Kitts, 2000; Sloley et al., 2001; Li et al., 2011; Wendakoon et al., 2012; Aarland et al., 2017; Espinosa-Paredes et al., 2021; Moghtaderi et al., 2021; Choi and Choi, 2022)
Echinacea pallida (Nutt.) Nutt.	Antioxidant, antiproliferative, anti-inflammatory	Hexan, methanol, water, lipophilic, alcohol	Switzerland, Turkey, China, Italy, Canada	(Hu and Kitts, 2000; Sloley et al., 2001; Chicca et al., 2007; Pellati et al., 2012; Yaglıoglu et al., 2013; Erenler et al., 2015; Fan et al., 2021)
Echinacea purpurea (L.) Moench	Antimicrobial, antioxidant, antiproliferative, antiviral	Dichloromethane, n-hexane, ethanol ethylacetate, acetone, methanol, water, aqueous, hydroalcoholic, alcohol	Portugal, Turkey, Romania, Mexico, Canada	(Hu and Kitts, 2000; Sloley et al., 2001; Aarland et al., 2017; Coelho et al., 2020; Sharif et al., 2021; Burlou-Nagy et al., 2022)

Antioxidant activity

All living organisms produce free radicals as a result of metabolic activities. The low levels of free radicals with oxidising properties are beneficial, whereas high levels can be highly detrimental (Krupodorova and Sevindik, 2020). As the levels of oxidant compounds increase, the antioxidant defence system is activated and suppresses the oxidant compounds (Bal et al., 2019). However, in cases where the antioxidant defence system is insufficient, oxidative stress occurs. Numerous serious illnesses such as multiple sclerosis, cancer, cardiovascular diseases, neurodegenerative diseases, Parkinson's, and Alzheimer's may manifest in individuals as a result of oxidative stress

(Selamoglu et al., 2020; Saridogan et al., 2021). According to Eraslan et al. (2021), the negative effects caused by oxidative stress can be prevented with the supplementation of antioxidants. Plants are considered significant natural sources of antioxidant supplements (Akgül et al., 2022). In this study, a compilation of antioxidant activity studies conducted on *Echinacea* species in the literature is presented (Table 1). In a study conducted in Turkey, the antioxidant activity of water and methanol extracts obtained from *E. pallida* species was investigated using DPPH, ABTS, and reducing power tests. According to the study findings, the DPHH test yielded an LC50 value of 143 µg/mL, while the ABTS test yielded an LC50 value of 25-30 µg/mL. Additionally, the reducing power test indicated that the aqueous extract demonstrated maximum results at a 700 nm absorbance level (Erenler et al., 2015). In a distinct study, the antioxidant status of *E. pallida*'s hydroalcoholic extract was investigated using DPPH and ABTS assays, sourced from Mexico. According to the research findings, the LC50 values of DPPH and ABTS results were reported to be within the ranges of 0.24-4.8 and 1.26-10.5 µg/mL, respectively (Aarland et al., 2017). A study conducted in South Korea investigated the antioxidant status of extracts obtained from *E. angustifolia* species using DPPH, ABTS, and FRAP tests. The study reports the DPPH and ABTS test results as 27.98 and 20.29%, respectively, while the FRAP test result is reported as 0.412 µg (Choi and Choi, 2022). According to a study conducted in Turkey, it has been reported that the aqueous extract obtained from *E. purpurea* exhibits strong antioxidant activity as determined by DPPH, ABTS, CUPRAC, and FRAP tests (Sharif et al., 2021). According to a study conducted in Canada, the methanol extract of *E. purpurea, E. angustifolia*, and *E. pallida* exhibited reducing power test results of 3.48, 3.84, and 5.07 mg/mL, respectively. Furthermore, it has been reported that the ABTS radical scavenging test yielded results of 11.0, 20.6, and 63.8 mg/mL, respectively (Hu and Kitts, 2000). In a study conducted in Canada, the alcohol extract scavenging capacity results of *E. purpurea, E. angustifolia*, and *E. pallida* were reported as 4.45, 2.83, and 2.79, respectively, for their root parts. Furthermore, the leaf parts have been reported as 1.55, 1.13, and 1.33, respectively (Sloley et al., 2001). According to the literature, it has been observed that *Echinacea* species possess antioxidant potential.

Antimicrobial activity

In recent years, numerous diseases have been found to be caused by microorganisms. The impacts of microorganisms are increasingly prevalent in contemporary times (Baba et al., 2020). The emergence of resistant microorganisms due to indiscriminate use of antibiotics renders current antimicrobial drugs inadequate (Mohammed et al., 2023). Within this scope, researchers have directed their efforts towards the discovery of novel antimicrobial drugs. Natural resources are utilised by humans as a source of

antimicrobial agents. Due to the potential adverse effects of synthetic drugs, individuals have turned to natural resources (Bal et al., 2017; Islek et al., 2021). Within the scope of our study, we have compiled the literature-reported antimicrobial activity studies of *Echinacea* species (Table 1). According to a study conducted in Iran, the antimicrobial activity of ethanol extract obtained from *E. angustifolia* species against multidrug-resistant *Klebsiella pneumoniae* was reported to be 77.1% (Moghtaderi et al., 2021). A study conducted in Mexico investigated the antimicrobial properties of an ethanol extract obtained from the species *E. angustifolia*. According to Wendakoon et al. (2012), the results of the study indicate that the extract obtained from the plant did not exhibit significant antibacterial activity against most of the strains tested, except for a strong activity of 90% against *Staphylococcus epidermis*. A study conducted in China investigated the antimicrobial properties of a supercritical carbon dioxide (SC-CO2) extract obtained from the species *E. angustifolia* against *Botrytis cinerea*. The study reported EC50 and EC90 values of 948 and 1869 µg/mL, respectively (Li et al., 2011). In a study conducted in Portugal, the antimicrobial activity of ethanol, ethyl acetate, and acetone extracts obtained from *E. purpurea* species were investigated against *Escherichia coli, Klebsiella pneumoniae, Morganella morganii, Proteus mirabilis, Pseudomonas aeruginosa, Enterococcus faecalis, Listeria monocytogenes* and *Candida albicans*. According to Coelho et al. (2020), the study results indicate that the microorganisms were inhibited by minimum inhibitory concentration (MIC) values ranging from 2.5 to 20 mg/mL against the strains used. According to a study conducted in Turkey, ethyl acetate, water, and methanol extracts obtained from the leaf and flower parts of *E. purpurea* were reported to possess antimicrobial activity against *Yersinia enterocolitica, Enterococcus durans, Enterococcus faecalis, Enterococcus faecium, Sarcina lutea, Staphylococcus aureus, Staphylococcus epidermidis, Staphylococcus alpha haemolyticus, Streptococcus pneumoniae, Listeria monocytogenes, Escherichia coli, Enterobacter aerogenes, Proteus mirabilis, Proteus vulgaris, Salmonella enteritidis, Salmonella kentucky, Salmonella Typhimurium, Serratia marcescens,* and *Pseudomonas aeruginosa* (Sharif et al., 2021). Within this context, it has been observed in the literature that *Echinacea* species possess significant antimicrobial potentials.

Other activities

In a study conducted in Switzerland, the cytotoxic effect of hexane extract obtained from *E. pallida* species on human pancreatic cancer MIA PaCa-2 and colon cancer COLO320 cell lines was investigated. As a result of the study, it was reported that the LC50 values of E. pallida were 46.41 and 10.55 µg/mL in MIA PaCa-2 and COLO320 cells, respectively (Chicca et al., 2007). In a study conducted in Italy, the cytotoxic effect of the lipophilic extract obtained from the *E. pallida* species was examined. As a result of the study, it

was reported that the LC50 values of isolated (8Z,13Z)-pentadeca-8,13-diene-11-yn-2-one against COLO320 and MCF-7 cancer cell lines were 2.3 µM and 2.5 µm, respectively (Pellati et al., 2012). In a study conducted in Turkey, the antiproliferative effect of methanol extract obtained from *E. pallida* species on rat brain tumor cells (C6) and human uterine carcinoma (HeLa) was investigated. As a result of the research, it was reported that methanol extract significantly inhibited the proliferation of HeLa and C6 cancer cell lines at concentrations of 5-100 µg/mL (Yaglioglu et al., 2013). In a study conducted in China, the anti-inflammatory activity of the extract obtained from *E. pallida* was investigated. As a result of the study, it was reported that *E. pallida* can inhibit the production of pro-inflammatory mediators in mouse peritoneal macrophages and has an anti-inflammatory effect by regulating MAPK signaling pathways (Fan et al., 2021). In a study conducted in Mexico, it was reported that the hydroalcoholic extract obtained from *E. angustifolia* and *E. purpurea* species has hypoglycaemic, anti-inflammatory and antiproliferative effects (Aarland et al., 2017). In another study conducted in South Korea, it was reported that extracts obtained from the E. angustifolia species showed an anti-inflammatory effect of 51.07% at 200 µg/mL (Choi and Choi, 2022). In another study conducted in Mexico, the cytotoxic effect of ethanol ethylacetate extract obtained from *E. angustifolia* species was investigated. As a result of the study, it was reported that the LC50 value of the plant extract on breast cancer MDA-MB-231 cells was 28.18 µg/mL and the LC50 value on MCF-7 cells was 19.97 µg/mL (Espinosa-Paredes et al., 2021). In a study conducted in Portugal, the cytotoxic status of different extracts obtained from *E. purpurea* species was investigated. As a result of the study, it was reported that the best results were 48 µg/mL against NCI H460 cell line, 36.7 µg/mL against HepG2 cell line, 51 µg/mL against HeLa cell line and 21 µg/mL against MCF-7 cell line (Coelho et al., 2020). In a study conducted in Turkey, the lowest LC50 value of *E. purpurea* methanol extract against HeLa cell line was reported to be 73 µg/mL (Sharif et al., 2021). It has been reported that different extracts from *E. purpurea* made in Romania can be effective on herpes simplex virus 1 and 2, human immunodeficiency virus types 1, H7N7 and H5N1, influenza viruses A (H1N1) and H3N2 and pandemic novel swine-borne influenza (H1N1) (Burlou-Nagy et al., 2022). In this context, according to literature data, it has been observed that *Echinacea* species have especially high anticancer activity, apart from antioxidant and antimicrobial activities. In addition, it has been observed to have hypoglycaemic, anti-inflammatory and antiviral effects.

Essential oil content

Plants produce numerous bioactive compounds with varying pharmacological properties in their structures. These bioactive compounds, which lack nutritional properties, possess significant medical potential

(Selamoglu et al., 2017; Akgül et al., 2020). In this study, the reported chemical contents of Echinacea species in the literature have been compiled. The findings obtained are presented in Table 2.

Table 2. Essential oil contents of Echinacea species

Plant species	Geographic regions	Used Part	Essential oil content	References
Echinacea angustifolia DC.	China	stem	trans-9-tetradecenyl (6.55%), cyclopentadecanone (79.12%), 2-pentadecanone (2.34%), 4-hexadecenal-6-yne (4.63%), 6-hexadecenal-4-yne (4.12%)	(Li et al., 2011)
Echinacea pallida (Nutt.) Nutt.	Ukraine	stem	1,8-pentadecadiene (2.64%), pentadecan-2-one (2.66%), cyclopentadecanone (41.28%), 8-cyclopentadecen-2-one (isomer) (2.03%), 8-cyclopentadecen-2-one (18.51%), 8,10-cyclopentadecadien-2-one (1.56%), 6-hexadecene-4-in (1.19%), methylic ester of 7,10-pentadecadiynic acid (8.28%-9.46%)	(Kyslychenko et al., 2008)
Echinacea purpurea (L.) Moench	İtaly, Slovakia, İran, Turkey	aerial, stem	germacrene D (4.8-60.3%), nerolidol (6.6%), α-pinene (5.1-13.1%), α-phelandrene (2.9-4.3%), β-pinene (4.1%), myrcene (15-19.8%), β-caryophyllene (7.2-12.3%), 1-pentadecene (4.4-5.1%), caryophylleneoxide (%8.7), α-cadinol (%6.3), naphthalene (%3.3)	(Hudaib et al., 2002; Holla et al., 2005; Diraz et al., 2012; Ahmadi et al., 2022; Soltanbeigi and Maral, 2022)

In the literature, it has been reported that the main components of the essential oil content of *E. angustifolia* species are 4-hexadecenal-6-yne (4.63%),trans-9-tetradecenyl (6.55%), cyclopentadecanone (79.12%), 2-pentadecanone (2.34%) and 6-hexadecenal-4-yne (4.12%) (Li et al., 2011). It has been reported that the main components in the essential oil content of *E. pallida* species are 6-hexadecene-4-in (1.19%), 1,8-pentadecadiene (2.64%), pentadecan-2-one (2.66%), cyclopentadecanone (41.28%), 8-cyclopentadecen-2-one (isomer) (2.03%), 8-cyclopentadecen-2-one (18.51) %), 8,10-cyclopentadecadien-2-one (1.56%) and 7,10-pentadecadiynic acid (8.28-9.46%) (Kyslychenko et al., 2008). It has been reported that the main components in the essential oil content of *E. purpurea* species are germacrene D (4.8-60.3%), nerolidol (6.6%), α-pinene (5.1-13.1%), α-phelandrene (2.9-4.3%), β-pinene (4.1%), myrcene (15-19.8%), β-caryophyllene (7.2-12.3%), 1-pentadecene (4.4-5.1%), caryophylleneoxide (8.7%), α-cadinol (6.3%) and naphthalene (3.3%) (Hudaib et al., 2002; Holla et al., 2005; Diraz et al., 2012; Ahmadi et al., 2022; Soltanbeigi and Maral, 2022). In this context, it was observed that the highest compound was cyclopentadecanone in *E.*

angustifolia and *E. pallida*. In addition, the highest compound in *E. purpurea* was reported as germacrene D. According to the results of the literature, it has been seen that the reported species may be a natural source in terms of the compounds determined in their body.

Conclusion

In this study, the usage areas, biological activities, and chemical contents of Echinacea species reported in the literature were compiled. As a result of the study, it was seen that the highest chemical compounds in *Echinacea* species was cyclopentadecanone and germacrene D. In addition, it has been determined that *Echinacea* species are important natural sources in terms of anticancer, antimicrobial, and antioxidant activity. In this context, it has been determined that *Echinacea* species can be a natural source in pharmacological designs.

REFERENCES

Aarland, R. C., Bañuelos-Hernández, A. E., Fragoso-Serrano, M., Sierra-Palacios, E. D. C., Díaz de León-Sánchez, F., Pérez-Flores, L. J., Mendoza-Espinoza, J. A. (2017). Studies on phytochemical, antioxidant, anti-inflammatory, hypoglycaemic and antiproliferative activities of Echinacea purpurea and Echinacea angustifolia extracts. Pharmaceutical biology, 55(1), 649-656.

Ahmadi, F., Samadi, A., Sepehr, E., Rahimi, A., Shabala, S. (2022). Morphological, phytochemical, and essential oil changes induced by different nitrogen supply forms and salinity stress in Echinacea purpurea L. Biocatalysis and Agricultural Biotechnology, 43, 102396.

Ahmed, I. A., Mikail, M. A., Zamakshshari, N., & Abdullah, A. S. H. (2020). Natural anti-aging skincare: role and potential. *Biogerontology*, *21*, 293-310.

Akgul, H., Korkmaz, N., Dayangaç, A., & Sevindik, M. (2020). Antioxidant potential of endemic Salvia absconditiflora. *Turkish Journal of Agriculture-Food Science and Technology*, *8*(10), 2222-2224.

Akgül, H., Mohammed, F. S., Kına, E., Uysal, İ., Sevindik, M., & Doğan, M. (2022). Total Antioxidant and Oxidant Status and DPPH Free radical activity of Euphorbia eriophora. *Turkish Journal of Agriculture-Food Science and Technology*, *10*(2), 272-275.

Baba, H., Sevindik, M., Dogan, M., & Akgül, H. (2020). Antioxidant, antimicrobial activities and heavy metal contents of some Myxomycetes. Fresenius Environmental Bulletin, 29(09), 7840-7846.

Bal, C., Akgul, H., Sevindik, M., Akata, I., & Yumrutas, O. (2017). Determination of the anti-oxidative activities of six mushrooms. Fresenius Envir Bull, 26(10), 6246-6252.

Bal, C., Sevindik, M., Akgul, H., & Selamoglu, Z. (2019). Oxidative stress index and antioxidant capacity of Lepista nuda collected from Gaziantep/Turkey. Sigma Journal of Engineering and Natural Sciences, 37(1), 1-5.

Bauer, R. (1991). Echinacea species as potential immunostimulatory drugs. Economic and Medical Plant Research, 253-321.

Binns, S. E., Livesey, J. F., Arnason, J. T., Baum, B. R. (2002). Phytochemical variation in Echinacea from roots and flowerheads of wild and cultivated populations. Journal of agricultural and food chemistry, 50(13), 3673-3687.

Burlou-Nagy, C., Bănică, F., Jurca, T., Vicaș, L. G., Marian, E., Muresan, M. E., Pallag, A. (2022). Echinacea purpurea (L.) Moench: Biological and Pharmacological Properties. A Review. Plants, 11(9), 1244.

Chicca, A., Adinolfi, B., Martinotti, E., Fogli, S., Breschi, M. C., Pellati, F., Nieri, P. (2007). Cytotoxic effects of Echinacea root hexanic extracts on human cancer cell lines. Journal of ethnopharmacology, 110(1), 148-153.

Choi, I. J., & Choi, I. J. (2022). The antioxidant and anti-inflammatory activities of Echinacea angustifolia hot water extract. *Asian Journal of Beauty and Cosmetology*, *20*(3), 373-381.

Coelho, J., Barros, L., Dias, M. I., Finimundy, T. C., Amaral, J. S., Alves, M. J., Ferreira, I. C. (2020). Echinacea purpurea (L.) Moench: chemical characterization and bioactivity of its extracts and fractions. Pharmaceuticals, 13(6), 125.

Diraz, E., Karaman, S., Koca, N. (2012). Fatty Acıd and Essentıal Oıl Composıtıon of Echınacea Purpurea (L.) Moench, Growıng in Kahramanmaras-Turkey. In International Conference on Environmental and Biological Sciences (ICEBS'2012), 21(22), 35-38.

Eraslan, E. C., Altuntas, D., Baba, H., Bal, C., Akgül, H., Akata, I., & Sevindik, M. (2021). Some biological activities and element contents of ethanol extract of wild edible mushroom Morchella esculenta. Sigma Journal of Engineering and Natural Sciences, 39(1), 24-28.

Erenler, R., Telci, I., Ulutas, M., Demirtas, I., Gul, F., Elmastas, M., Kayir, O. (2015). Chemical Constituents, Quantitative Analysis and Antioxidant Activities of E chinacea purpurea (L.) M oench and E chinacea pallida (N utt.) N utt. Journal of Food Biochemistry, 39(5), 622-630.

Espinosa-Paredes, D. A., Cornejo-Garrido, J., Moreno-Eutimio, M. A., Martínez-Rodríguez, O. P., Jaramillo-Flores, M. E., Ordaz-Pichardo, C. (2021). Echinacea Angustifolia DC extract induces apoptosis and cell cycle arrest and synergizes with paclitaxel in the MDA-MB-231 and MCF-7 human breast Cancer cell lines. Nutrition and Cancer, 73(11-12), 2287-2305.

Fan, M. Z., Wu, X. H., Li, X. F., Piao, X. C., Jiang, J., Lian, M. L. (2021). Co-cultured adventitious roots of Echinacea pallida and Echinacea purpurea inhibit lipopolysaccharide-induced inflammation via MAPK pathway in mouse peritoneal macrophages. Chinese Herbal Medicines, 13(2), 228-234.

Flagel, L. E., Rapp, R. A., Grover, C. E., Widrlechner, M. P., Hawkins, J., Grafenberg, J. L., Wendel, J. F. (2008). Phylogenetic, morphological, and chemotaxonomic incongruence in the North American endemic genus Echinacea. American Journal of Botany, 95(6), 756-765.

Holla, M., Vaverkova, S., Farkas, P., Tekel, J. (2005). Content of essential oil obtained from flower heads of Echinacea purpurea L. and identification of selected components. Herba Polonica, 3(51).

Hu, C., & Kitts, D. D. (2000). Studies on the antioxidant activity of Echinacea root extract. *Journal of Agricultural and Food chemistry*, *48*(5), 1466-1472.

Hudaib, M., Cavrini, V., Bellardi, M. G., Rubies-Autonell, C. (2002). Characterization of the essential oils of healthy and virus infected Echinacea purpurea (L.) Moench Plants. Journal of Essential Oil Research, 14(6), 427-430.

Islek, C., Saridogan, B. G. O., Sevindik, M., & Akata, I. (2021). Biological activities and heavy metal contents of some Pholiota species. Fresenius Environmental Bulletin, 30(6), 6109-6114.

Karimmojeni, H., Rezaei, M., Tseng, T. M., Mastinu, A. (2022). Effects of Metribuzin Herbicide on Some Morpho-Physiological Characteristics of Two Echinacea Species. Horticulturae, 8(2), 169.

Khan, T., Ali, M., Khan, A., Nisar, P., Jan, S. A., Afridi, S., & Shinwari, Z. K. (2019). Anticancer plants: A review of the active phytochemicals, applications in animal models, and regulatory aspects. *Biomolecules*, *10*(1), 47.

Kim, H. P., Son, K. H., Chang, H. W., & Kang, S. S. (2004). Anti-inflammatory plant flavonoids and cellular action mechanisms. *Journal of pharmacological sciences*, *96*(3), 229-245.

Korkmaz, N., Dayangaç, A., Sevindik, M. (2021). Antioxidant, antimicrobial and antiproliferative activities of *Galium aparine. J Fac Pharm Ankara*, 45(3), 554-564.

Krupodorova, T., & Sevindik, M. (2020). Antioxidant potential and some mineral contents of wild edible mushroom Ramaria stricta. AgroLife Scientific Journal, 9(1), 186-191.

Kumar, K. M., Ramaiah, S. (2011). Pharmacological importance of Echinacea purpurea. International Journal of Pharma and Bio Sciences, 2(4), 304-314.

Kyslychenko, A. A., Dyakonova, Y. V., Alexandrov, A. N., Darmogray, R. Y. (2008). Gas chromatography with mass-spectrometric detection of the components of the essential oils from Achillea carpatica Błocki ex Dubovik and Echinacea pallida (Nutt.) Nutt. Herba Polonica, 55(4), 63-67.

Li, D., Wang, Z., Zhang, Y. (2011). Antifungal activity of extracts by supercritical carbon dioxide extraction from roots of Echinacea angustifolia and analysis of their constituents using gas chromatography-mass spectrometry (GC-MS). Journal of Medicinal Plants Research, 5(23), 5605-5610.

McKeown, K. A. (1999). A review of the taxonomy of the genus Echinacea. Perspectives on new crops and new uses, 482, 489.

Mishima, S., Saito, K., Maruyama, H., Inoue, M., Yamashita, T., Ishida, T., Gu, Y. (2004). Antioxidant and immuno-enhancing effects of Echinacea purpurea. Biological and Pharmaceutical Bulletin, 27(7), 1004-1009.

Moghtaderi, M., Mirzaie, A., Zabet, N., Moammeri, A., Mansoori-Kermani, A., Akbarzadeh, I., Ren, Q. (2021). Enhanced antibacterial activity of Echinacea angustifolia extract against multidrug-resistant Klebsiella pneumoniae through niosome encapsulation. Nanomaterials, 11(6), 1573.

Mohammed, F. S., Akgul, H., Sevindik, M., & Khaled, B. M. T. (2018). Phenolic content and biological activities of Rhus coriaria var. zebaria. Fresenius Environmental Bulletin, 27(8), 5694-5702.

Mohammed, F. S., Günal, S., Şabik, A. E., Akgül, H., & Sevindik, M. (2020a). Antioxidant and Antimicrobial activity of Scorzonera papposa collected from Iraq and Turkey. Kahramanmaraş Sütçü İmam Üniversitesi Tarım ve Doğa Dergisi, 23(5), 1114-1118.

Mohammed, F. S., Karakaş, M., Akgül, H., & Sevindik, M. (2019). Medicinal properties of Allium calocephalum collected from Gara Mountain (Iraq). Fresen Environ Bull, 28(10), 7419-7426.

Mohammed, F. S., Pehlivan, M., Sevindik, E., Akgul, H., Sevindik, M., Bozgeyik, I., & Yumrutas, O. (2021). Pharmacological properties of edible Asparagus acutifolius and Asparagus officinalis collected from North Iraq and Turkey (Hatay). Acta Alimentaria, 50(1), 136-143.

Mohammed, F. S., Sevindik, M., Uysal, I., Sevindik, E., & Akgül, H. (2022). A Natural Material for Suppressing the Effects of Oxidative Stress: Biological Activities of Alcea kurdica. Biology Bulletin, 49(Suppl 2), S59-S66.

Mohammed, F. S., Günal, S., Pehlivan, M., Doğan, M., Sevindik, M., & Akgül, H. (2020b). Phenolic content, antioxidant and antimicrobial potential of endemic Ferulago platycarpa. Gazi University Journal of Science, 33(4), 670-677.

Mohammed, F. S., Uysal, I., & Sevindik, M. (2023). A review on antiviral plants effective against different virus types. Prospects in Pharmaceutical Sciences, 21(2), 1-21.

Pehlivan, M., Mohammed, F. S., Sevindik, M., & Akgul, H. (2018). Antioxidant and oxidant potential of Rosa canina. *Eurasian Journal of Forest Science*, *6*(4), 22-25.

Pellati, F., Benvenuti, S., Prati, F., Nieri, P. (2012). Isolation, structure elucidation, synthesis, and cytotoxic activity of polyacetylenes and polyenes from echinacea pallida. In Emerging Trends in Dietary Components for Preventing and Combating Disease (pp. 131-149). American Chemical Society.

Saridogan, B. G. O., Islek, C., Baba, H., Akata, I., & Sevindik, M. (2021). Antioxidant antimicrobial oxidant and elements contents of Xylaria polymorpha and X. hypoxylon (Xylariaceae). *Fresenius Envir Bull*. 30(5), 5400-5404.

Selamoglu, Z., Dusgun, C., Akgul, H., & Gulhan, M. F. (2017). In-vitro antioxidant activities of the ethanolic extracts of some contained-allantoin plants. *Iranian journal of pharmaceutical research: IJPR*, *16*(Suppl), 92.

Selamoglu, Z., Sevindik, M., Bal, C., Ozaltun, B., Sen, İ., & Pasdaran, A. (2020). Antioxidant, antimicrobial and DNA protection activities of phenolic content of Tricholoma virgatum (Fr.) P. Kumm. Biointerface Research in Applied Chemistry, 10 (3), 5500-5506

Sevindik, M., Akgul, H., Pehlivan, M., & Selamoglu, Z. (2017). Determination of therapeutic potential of Mentha longifolia ssp. longifolia. Fresen Environ Bull, 26(7), 4757-4763.

Sharif, K. O. M., Tufekci, E. F., Ustaoglu, B., Altunoglu, Y. C., Zengin, G., Llorent-Martínez, E. J., Baloglu, M. C. (2021). Anticancer and biological properties of leaf and flower extracts of Echinacea purpurea (L.) Moench. Food Bioscience, 41, 101005.

Sloley, B. D., Urichuk, L. J., Tywin, C., Coutts, R. T., Pang, P. K., & Shan, J. J. (2001). Comparison of chemical components and antioxidant capacity of different Echinacea species. *Journal of Pharmacy and Pharmacology*, *53*(6), 849-857.

Soltanbeigi, A., Maral, H. (2022). Agronomıc Yıeld and Essentıal Oıl Propertıes of Purple Coneflower (Echinacea purpurea L. Moench) wıth Dıfferent Nutrıent Applıcatıons. Chilean journal of agricultural & animal sciences, 38(2), 164-175.

Unal, O., Eraslan, E. C., Uysal, I., Mohammed, F. S., Sevindik, M., & Akgul, H. (2022). Biological activities and phenolic contents of Rumex scutatus collected from Turkey. Fresenius Environmental Bulletin, 31(7), 7341-7346.

Uysal, I., Koçer, O., Mohammed, F.S., Lekesiz, Ö., Doğan, M., Şabik, A.E., Sevindik, E., Gerçeker, F.O., Sevindik, M. (2023). Pharmacological and Nutritional Properties: Genus Salvia. *Adv Pharmacol*, 11(2), 140-155

Wendakoon, C., Calderon, P., Gagnon, D. (2012). Evaluation of selected medicinal plants extracted in different ethanol concentrations for antibacterial activity against human pathogens. Journal of Medicinally Active Plants, 1(2), 60-68.

Yaglıoglu, A. S., Akdulum, B., Erenler, R., Demirtas, I., Telci, I., Tekin, S. (2013). Antiproliferative activity of pentadeca-(8E, 13Z) dien-11-yn-2-one and (E)-1, 8-pentadecadiene from Echinacea pallida (Nutt.) Nutt. roots. Medicinal Chemistry Research, 22(6), 2946-2953.

Zulfiqar, H., Masoud, M. S., Yang, H., Han, S. G., Wu, C. Y., & Lin, H. (2021). Screening of prospective plant compounds as H1R and CL1R inhibitors and its antiallergic efficacy through molecular docking approach. *Computational and Mathematical Methods in Medicine*, *2021*, 1-9.

Chapter 9

FORECASTING AGRICULTURAL PRODUCTS PRODUCER PRICE INDEX USING FUZZY LINEAR REGRESSION MODELS

Aslı KILIÇ[1]

Özge ELMASTAŞ GÜLTEKİN [2]

1 Lec. Dr., Ege University, Faculty of Science, Department of Statistics, İzmir, TURKEY. asli.kilic@ege.edu.tr, Orcid ID: 0000-0002-3926-8608.
2 Assist. Prof. Dr., Ege University, Faculty of Science, Department of Statistics, İzmir, TURKEY. ozge.elmastas@ege.edu.tr, Orcid ID: 0000-0001-7452-3240.

INTRODUCTION

For a certain period, it is necessary to compare the prices determined by the producers of the products produced and sold in the country according to time and to measure their changes. This measurement is possible with the Producer Price Index (PPI). There are studies in which the short and long term asymmetric effects of PPI on the food and non-alcoholic beverages index included in the consumer price index (CPI) are analyzed (Oral and Eştürk, 2022:32). As of 2014, PPI in our country is divided into 3 sections as domestic producer price index (D-PPI), foreign producer price index (F-PPI) and agricultural products producer price index (Agriculture-PPI) and calculated separately (Emek, Ö.F., 2020). According to the Turkish Statistical Institute definition, Agriculture-PPI is "a proportional indicator of the changes in the first-hand sales prices of the products produced by the farmer and sold to the market over time." When calculating the Agriculture-PPI, agriculture, forestry and fishery products are used.

The volatility in food prices, in other words price instability, may affect the inflation process in the Turkish economy in an undesirable way (Çıplak and Yücel, 2004:04). There are many reasons for the instability in agriculture and food prices, such as the rise in oil prices, global warming, restrictions on product supply, etc. The literature on the relationship between agricultural inputs and food inflation for Turkey as a whole is not very extensive. However, as a result of the researches, although variables such as agricultural input price index, Food Price Index (FPI), oil prices, exchange rate, etc. affected the Agriculture-PPI, no significant relationship was found between the Agriculture-PPI and the exchange rate (Eştürk and Albayrak, 2018:18). There is a relationship between Agriculture-PPI and FPI at the end of the long term and it has been revealed that a 1% increase in Agriculture-PPI will increase FPI by 0.70% at the end of the long term (Demirağ and Sağır, 2022:24). Özyücel et al. (2022) analysed the relationship between Agriculture-PPI, agricultural input price index and FPI by time series methods, applied causality test and found a bidirectional and significant relationship between agricultural input price index, FPI and Agriculture-PPI. While the effect of the change in the food industry price index and oil price on agricultural product producer prices is felt in the short term, the effect of international food price, dollar and euro exchange rates is felt in the long term (Tay Bayramoğlu and Koç Yurtkur, 2015:15). There is a statistically significant co-integration relationship between consumer (CPI), producer (D-PPI) and agriculture (Agriculture-PPI) variables and that there are short-term causality relationships. In the long term, there was a statistically small but significant effect from Agriculture-PPI and D-PPI to CPI, and on the other hand, there was a significant and stronger effect from CPI to Agriculture-PPI and D-PPI (Koçak, 2021:1).

In this study, agricultural input price index, FPI and Brent oil are considered among the variables that are thought to affect the Agriculture-PPI in Turkey. Multivariate linear regression and fuzzy linear regression models were applied in modelling these variables and comparisons were made.

In the first part of the study, information about classical multivariate linear regression models was given. The economic, statistical and econometric assumptions required to investigate whether the forecasts are reliable models are mentioned. In the second part, fuzzy linear regression models are discussed. Among the fuzzy regression techniques frequently used in the literature, standard possibilistic linear regression (PLR) model, revised possibilistic linear regression model and fuzzy least squares regression (LSR) model are included. In the third part, multivariate linear and fuzzy linear regression models for the independent variables affecting the Agriculture-PPI dependent variable are discussed with the estimation of Agriculture-PPI values and comparison of regression models. In the conclusion section, the evaluation of the findings obtained is included.

1. MULTIVARIATE LINEAR REGRESSION ANALYSIS

Multivariate linear regression is an analysis technique used to evaluate the relationship between a dependent variable and at least two independent variables. Regression analysis assumes that the values of the independent variables do not contain error, that is, they are measured without error. Conversely, dependent variable values are assumed to contain random errors. A multivariate linear regression equation is represented as follows:

$$\hat{Y}_i = \beta_0 + \beta_1 x_{1i} + \beta_2 x_{2i} + \cdots + \beta_k x_{ki} + e_i, \;\; i = 1,2,\ldots,n \qquad (1)$$

Although the same β_k coefficients are used to estimate the values of the dependent variable for all values in the sample, the dependent variable values will differ according to different independent variable values. The aim of regression analysis is to estimate the β_k coefficients to minimize the difference between the observed and predicted dependent variable values and to optimise the correlation between the observed and predicted dependent variable values in the data set. The Least Squares (LS) technique is generally used to calculate regression coefficients due to its ease of computation.

Regression analysis provides a mathematical demonstration of the relationship between variables, but does not reveal that these relationships are causal. The demonstration of causality is an experimental and logical problem rather than a statistical problem. However, the regression equation obtained

as a result of the analysis is highly sensitive to the combination of variables included in the model (Tabachnick and Fidell, 2007).

A mathematical expression that represents the relationship between one or more independent quantitative variables and a dependent variable that is thought to be a cause-and-effect relationship is called a regression model. With the help of the functional relationship obtained, depending on the values of the independent variables, the value of the dependent variable is tried to be estimated. In order for this estimation to be a good one, in addition to statistical criteria such as the coefficient and the significance of the regression model obtained and the high coefficient of determination, some basic assumptions such as the distribution of error terms being normal with zero mean and constant σ^2 variance, no multicollinearity between independent variables, no autocorrelation between consecutive error terms, and no changing variance must be met. In cases where one or more of these assumptions cannot be met, and also in cases where precise information about the variables is not available, expert opinions are included, complex systems are handled or sufficient data cannot be reached for analysis, the fuzzy regression method is an alternative method to classical regression. In addition, fuzzy regression analysis is also used when the variable of interest is a vague variable instead of a stochastic or random variable. Fuzzy regression analysis is not based on probability theory, but on possibility and fuzzy set theories. Therefore, the models do not contain error terms. Instead, the error is present at the fuzzy coefficients.

2. FUZZY LINEAR REGRESSION ANALYSIS

Fuzzy logic and fuzzy set theory were developed by Lotfi A. Zadeh in the 1960s. Zadeh proposed the use of the concept of set membership in the decision-making process for systems with uncertainty not caused by random factors. As is known, the boundaries of classical or definite sets are well defined and consist of elements that provide the membership property precisely. In other words, the element is either included in the set or it is not. Fuzzy sets, on the other hand, can contain objects or elements whose membership in that set is not certain. That is, an element that belongs to one fuzzy set can also be an element of another fuzzy set. Each element of a fuzzy set has a degree of belonging to the set, and these degrees are determined by the membership function. Let X be the space of objects with each element denoted by x. A fuzzy set A in X is characterised by a membership function $\mu_A(x)$ that associates each point in X with a real number in the interval [0,1]. The value of the membership function $\mu_A(x)$ in x represents the membership degree of x to the fuzzy set A. The closer the value of $\mu_A(x)$ is to 1, the higher the membership of x to the fuzzy set A (Zadeh, 1965:8). The most well-known types of membership functions in the literature are triangular, trapezoidal,

Gaussian, etc. membership functions. Since triangular fuzzy numbers are used in the fuzzy regression techniques utilised in the study, the triangular membership function is mentioned.

The triangular membership function is defined as follows with three parameters, (a,b,c).

$$\mu_A(x) = \begin{cases} \dfrac{x-a}{b-a}, & if\ a \le x \le b \\ \dfrac{c-x}{c-b}, & if\ b \le x \le c \\ 0, & if\ x < a\ or\ x > c \end{cases}$$

The following graph shows the triangle membership function:

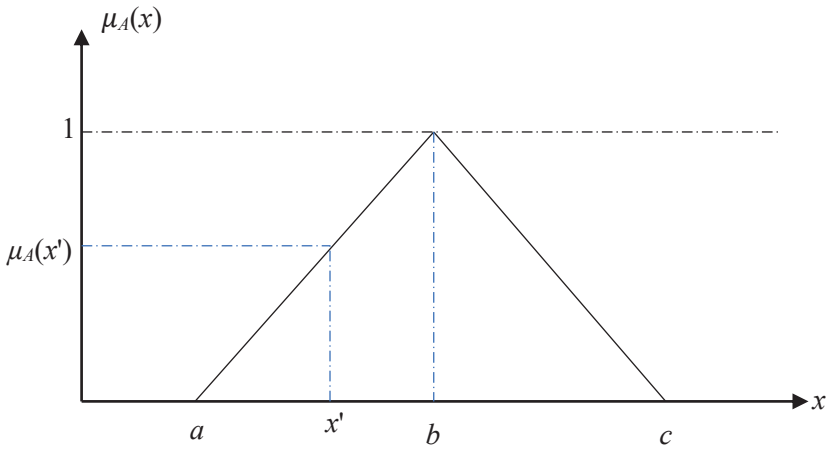

Figure 1. Triangular membership function

In Figure 1, the place where the membership function takes the value 1 is called the modal (centre) value. The part between points a and b is called the left spread, and the part between b and c is called the right spread. A triangular fuzzy number is said to be symmetrical when the right and left spread are equal to each other. The part between points a and c is called support. A fuzzy set $\tilde{A}$ is represented as $\tilde{A} = (X, \mu_{\tilde{A}}(x))$ with the objects belonging to the set and the membership function.

The fuzzy regression method is the method obtained by applying the fuzzy linear function to classical regression analysis. In classical regression analysis, the coefficients of the independent variables are determined as a single value, while in fuzzy regression analysis, these coefficients are estimated as an

interval rather than a single value, and the width of these intervals can vary according to a degree of belief (h). (Tanaka et. al., 1982:12). In fuzzy linear regression, the variables to be included in the regression model must be linear.

There are many studies in which fuzzy linear regression model is applied in economic fields such as unemployment, inflation, municipal waste, etc. in the literature (Özer ve Büyükkeklik, 2022:30; İçen ve Günay, 2015:8; İşbilen Yücel, 2017:27; Erilli vd., 2012:13). In addition to these, fuzzy linear regression is widely used in fields such as textile, engineering, agriculture, meteorology and health (Kar, et.al., 2019:23; Arulchinnappan and Rajendran, 2011:10; Topuz, 2020:12; Sorkheh, et.al, 2018:42; Günay Akdemir ve Tiryaki, 2013:8).

In this study, standard possibilistic linear regression model, revised possibilistic linear regression model and fuzzy least squares regression model, which are frequently used in the literature, are included.

2.1 Standard Possibilistic Linear Regression Model

This technique is the first application of fuzzy set theory in regression analysis. In classical regression analysis, it is assumed that the difference between the observed values and the values predicted by the regression model is due to measurement errors, while in fuzzy regression method, it is assumed that this difference is due to the fuzziness of the system (Tanaka et. al., 1982:12). In the possibilistic regression technique, the spread of the regression coefficients obtained as a result of the analysis is considered as a measure of the fuzziness of the relationship between the dependent variable and the independent variable. In the method, fuzzy parameters are represented by symmetrical triangular membership functions. In a possibilistic regression model, the independent variable values are real-valued numbers. In contrast, regression coefficients are symmetrical triangular fuzzy numbers. In this case, the fuzzy linear regression model can be represented as follows:

$$\tilde{Y}_i = \tilde{A}_0 + \tilde{A}_1 x_{1i} + \tilde{A}_2 x_{2i} + \cdots + \tilde{A}_k x_{ki}\,,\ i = 1,2,\dots,n \qquad (2)$$

Above, $\left(\tilde{A}_0, \tilde{A}_1, \dots, \tilde{A}_k\right)$ is the fuzzy coefficients of k independent variables. Each coefficient $\tilde{A}_j, j = 0,1,\dots,k$ is represented as $\tilde{A}_j = \left(a_j\,, c_j\right)$ with centre a_j and spread c_j. The vector $\boldsymbol{x}_i = (1, x_{1i}, x_{2i}, \dots, x_{ki})$ formed by the independent variables consists of real-valued crisp numbers. Based on the model given above and the definitions made, $\tilde{Y}_i$ can be written as follows:

$$\tilde{Y}_i = \tilde{A}_0 + \sum_{j=1}^{k} \tilde{A}_j x_{ji} = (a_0\,, c_0\,) + \sum_{j=1}^{k} \left(a_j\,, c_j\,\right) x_{ji}\,,\ i = 1,2,\dots,n \qquad (3)$$

$$\tilde{Y}_i = \left((a_0 + a_1 x_{1i} + a_2 x_{2i} + \cdots + a_k x_{ki}), (c_0 + c_1|x_{1i}| + c_2|x_{2i}| + \cdots + c_k|x_{ki}|)\right) \quad (4)$$

In possibilistic linear regression, equation (4) tries to obtain a model that fits the available data set by minimizing the total spread of the fuzzy coefficients to ensure that the observations of the dependent variable are in a suitable range. It is measured by the h index of the degree to which the predicted fuzzy linear model fits into the data. h index is called the degree of belief and is valued in the range [0,1]. In fuzzy linear regression, h value is determined by the decision maker while estimating the parameters. While the solution is obtained by linear programming techniques, the chosen h value has a significant impact on parameter estimation. If you are working with a large data set, h=0, and when the dataset is small, it is appropriate to select larger values. Since the increase in the value of the degree of belief will cause the prediction range to expand, the belonging to the set in question will also increase. In most studies available in the literature, different h values are decided by analysis.

The possibilistic linear regression model for a value h chosen by the decision maker can be formulated as a linear programming problem as follows:

$$Min \sum_{i=1}^{n} \left[c_0 + \sum_{j=1}^{k} c_j |x_{ji}| \right] \quad (5a)$$

$$subject\ to$$

$$a_0 + \sum_{j=1}^{k} a_j x_{ji} + (1-h) \left[c_0 + \sum_{j=1}^{k} c_j |x_{ji}| \right] \geq Y_i, \quad i = 1,2,\dots,n \quad (5b)$$

$$a_0 + \sum_{j=1}^{k} a_j x_{ji} - (1-h) \left[c_0 + \sum_{j=1}^{k} c_j |x_{ji}| \right] \leq Y_i, \quad i = 1,2,\dots,n \quad (5c)$$

$$c_j \geq 0, \qquad j = 0,1,\dots,k$$

Possibilistic regression analysis has been criticized for being infinite in the number of possible solutions, wide prediction intervals, the method being heavily affected by outliers, and the emergence of a multicollinearity problem when the number of independent variables increases (Chukhrova and Johannssen, 2019:84).

2.2 Revised Possibilistic Linear Regression Model

He et. al. (2007) stated that in the possibilistic regression model, the degree of belief depends not only on the spread of the predicted dependent variable, but also on the distance between the predicted centre value of the dependent variable and the observed value of the dependent variable. Therefore, in addition to the objective of minimizing the entire spread, he added the goal of minimizing said distance in order to achieve a higher degree of belief or better pattern fit. Thus the proposed revised possibilistic regression model is expressed as follows in the form of a linear programming problem:

$$Min \sum_{i=1}^{n} \left[c_0 + \sum_{j=1}^{k} c_j |x_{ji}| \right] + \sum_{i=1}^{n} d_i \tag{6a}$$

$$subject\ to$$

$$\frac{d_i}{\left[c_0 + \sum_{j=1}^{k} c_j |x_{ji}|\right]} \leq (1 - h_i), \qquad i = 1,2,\dots,n \tag{6b}$$

$$d_i = y_i - \left[a_0 + \sum_{j=1}^{k} a_j x_{ji} \right], \qquad i = 1,2,\dots,n \tag{6c}$$

$$c_j \geq 0, a_j\ unconstrained, j = 0,1,\dots,k$$

He et. al. (2007) stated that as a result of their application, their proposed model gives better results than standard possibilistic linear regression model due to both the reduction of the fuzziness of the system and obtaining a higher degree of belief.

2.3 Fuzzy Least Squares Regression Model

The fuzzy least squares regression model was proposed by Diamond (1988). In the technique, it is aimed to make the distance between the observed dependent variable values and the estimated fuzzy dependent variable values minimum by using the distance measure. The method requires detailed calculations even in the case of a single independent variable, and in the case of more arguments, the applicability of the technique is adversely affected by the computational load. In this study, a two-stage fuzzy regression technique combining the least squares method and the minimum fuzziness criterion proposed by Savic and Pedrycz (1991) is utilised. In this method, first of all, the center values of the fuzzy regression coefficients are obtained by using the least squares method. In the next stage, the fuzzy widths of the fuzzy coefficients are obtained by using the minimum fuzziness criterion (Chang

and Ayyub, 2001:119). After obtaining the centre values using the least squares technique, the problem to be solved according to the minimum fuzziness criterion can be given as follows:

$$Min \sum_{i=1}^{n} \left[c_0 + \sum_{j=1}^{k} c_j |x_{ji}| \right] \tag{7a}$$

$$subject\ to$$

$$a_0 + \sum_{j=1}^{k} a_j x_{ji} + (1-h) \left[c_0 + \sum_{j=1}^{k} c_j |x_{ji}| \right] \geq Y_i, \quad i = 1,2,\dots,n \tag{7b}$$

$$a_0 + \sum_{j=1}^{k} a_j x_{ji} - (1-h) \left[c_0 + \sum_{j=1}^{k} c_j |x_{ji}| \right] \leq Y_i, \quad i = 1,2,\dots,n \tag{7c}$$

$$c_j \geq 0, \qquad j = 0,1,\dots,k$$

Above, all a_j values which are the centre values of fuzzy coefficients are equal to the coefficients of multivariate linear regression model.

3. ESTIMATION OF AGRICULTURE-PPI WITH MULTIVARIATE LINEAR AND FUZZY LINEAR REGRESSION MODELS

In the literature, there are many variables affecting Turkey's Agriculture-PPI values. In this study, the dependent variable Agriculture-PPI and the independent variables agricultural input price index, food price index and Brent oil are considered and monthly observations are converted into quarterly averages. For the period between 2016:Q1-2021:Q4, multivariate linear regression and fuzzy linear regression models are considered for Agriculture-IPI, FPI and Brent variables affecting the value of Agriculture-PPI. For these variables, firstly, estimation was made with multivariate linear regression model and it was checked whether the necessary assumptions were met. Then, among the fuzzy linear regression models, standard possibilistic linear regression model, revised possibilistic linear regression model and fuzzy least squares regression model are used to make predictions and the results are interpreted for different belief (h) values. Finally, the estimates of fuzzy linear regression models and classical multivariate linear regression models were compared and interpreted. In this study, the margin of error (α) was taken as 0.05, MINITAB 21 statistical software was used to determine multivariate

linear regression model and to check whether all required assumptions were satisfied or not and LINGO 20.0 package program was used for the estimation of fuzzy linear regression models. Information on all variables considered in the study is given in Table 1.

Table 1. Variables considered in the study, their abbreviations and sources

Variables	Abbreviations	Source
Agricultural Products Producer Price Index	Agriculture-PPI	EVDS
Agricultural Input Price Index	Agriculture-IPI	TURKSTAT
Food Price Index	FPI	www.fao.org
Brent Oil (TL per barrel)	Brent	www.eia.gov.tr

3.1 Estimation of Agriculture-PPI with Multivariate Linear Regression Method

In order to apply the multivariate linear regression model for the estimation of the Agriculture-PPI variable, the scatter diagrams between the Agriculture-PPI and each independent variable were first drawn.

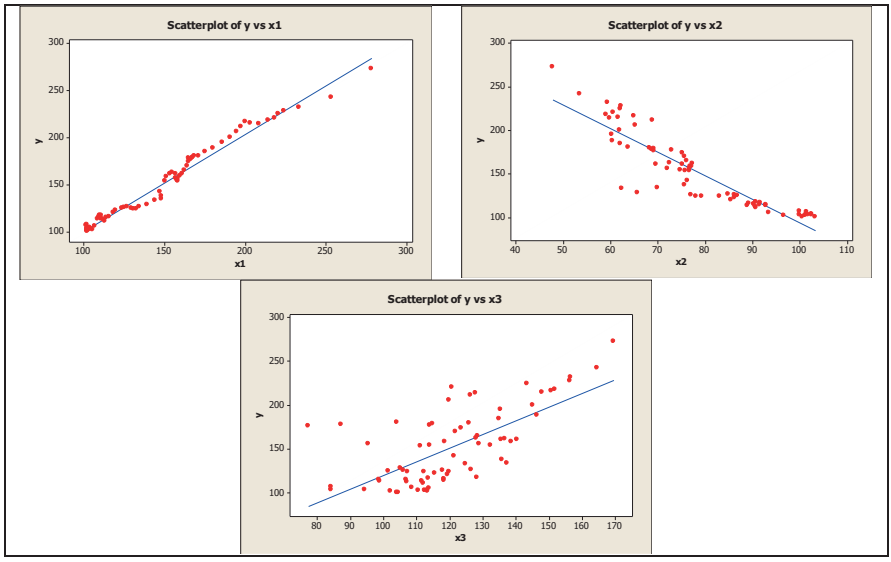

Figure 2. Linear relationship between Agriculture-PPI and independent variables

At Figure 2, the relationship between Agriculture-PPI and each independent variable is in linear structures. As a result of applying the multivariate linear regression model, the predicted model is as follows:

Agriculture-PPI=-36.573+1.28 ×Agriculture-IPI (Input 1+Input 2) + 0.196×FPI-0.0726× Brent (TL per barrel)

$$\hat{Y}_i = -36.573 + 1.28x_{1i} + 0.196x_{2i} - 0.0726x_{3i}$$

According to the results of the analysis, while the coefficients were statistically significant for Agriculture-IPI (p=0.000) and Brent (p=0.000) variables, they were found to be insignificant for FPI (p=0.094). In addition, the model was found to be generally significant (p=0.000) and that 99.3% of the total changes in the dependent variable were explained by the independent variables.

When the econometric criteria are analysed; according to the Kolmogorov Smirnov test, it is determined that the errors are normally distributed (p=0.15) and there is no multicollinearity since the VIF values are less than 10 for all variables. Moreover, the Durbin-Watson d statistic value of 2.18001 indicates that there is no autocorrelation between the consecutive error terms and the scatter diagram for each independent variable against the standardized error terms shows that the errors do not have varying variance.

In conclusion, due to the fact that all the examined assumptions are satisfied, the regression model created is a multivariate linear regression model that can be used to predict Agriculture-PPI values.

3.2 Estimation of Agriculture-PPI with Fuzzy Linear Regression Models

In this study, standard PLR model, revised PLR model and fuzzy LSR model among fuzzy regression models were discussed to estimate Agriculture-PPI variable values.

3.2.1 Estimation with Standard Possibilistic Linear Regression Method

The graph of the Agriculture-PPI estimation values and their actual values for standard possibilistic linear regression model is as shown in Figure 3:

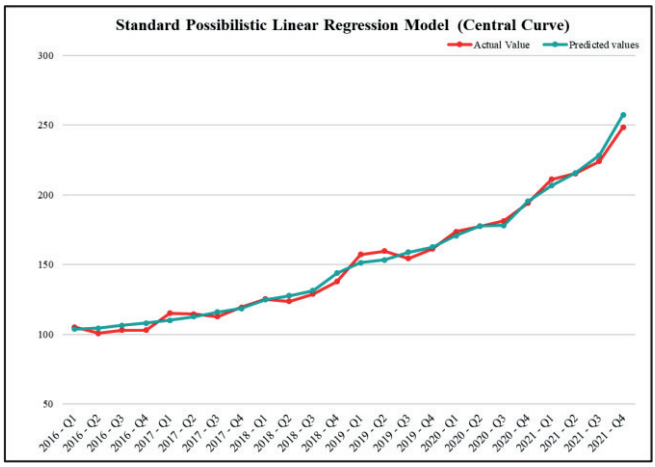

Figure 3. Representation of real and forecast values by standard PLR model

It was observed that the Agriculture-PPI centre forecast values and the actual values for standard PLR model had approximate values over the modeled period. In addition, the mean absolute percentage error (MAPE) was calculated as 2.312 because the center values were the same for all degrees of belief.

When standard PLR model is calculated for different belief (h) values, the fuzzy linear regression models, fuzziness values of the system and average degrees of belief are as follows:

- **Standard possibilistic linear regression model predicted for h=0.0:**

$$\tilde{Y}_i = (-40.86044; 4.010362) + (1.210150; 0)x_{1i} + (0.2930840; 0)x_{2i} + (-0.05639407; 0.005568863)x_{3i}$$

For h=0.0, the calculated system fuzziness is 139.9609 and the average degree of belief is 0.434. In addition, the graphical representation of standard PLR model for h=0.0 is given in Figure 4.

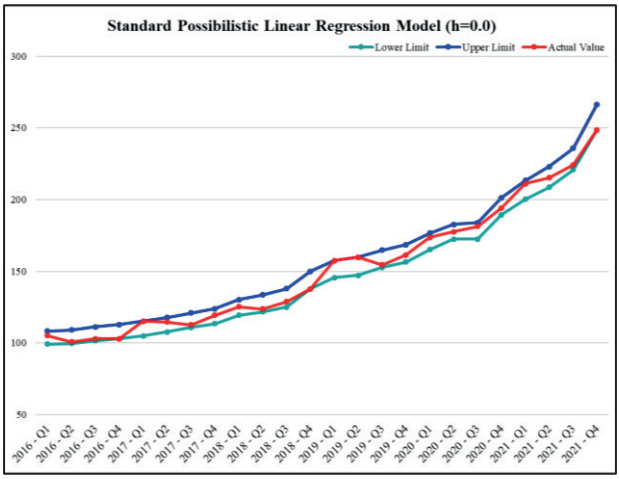

Figure 4. Graphical representation of standard PLR model for h=0.0

- **Standard possibilistic linear regression model predicted for h=0.3 is:**

$$\tilde{Y}_i = (-40.86044; 5.729089) + (1.210150; 0)x_{1i} + (0.2930840; 0)x_{2i} + (-0.05639407; 0.007955519)x_{3i}$$

For h=0.3, the calculated system fuzziness is 199.9442 and the average degree of belief is 0.604. In addition, the graphical representation of standard PLR model for h=0.3 is given in Figure 5.

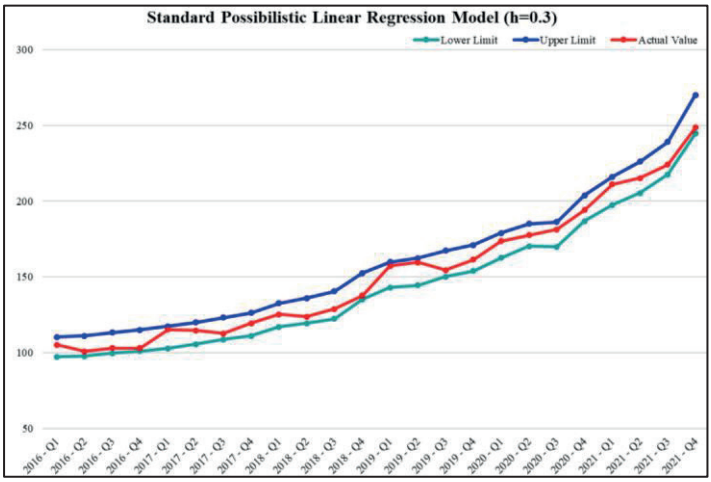

Figure 5. Graphical representation of standard PLR model for h=0.3

- **Standard possibilistic linear regression model predicted for *h*=0.5 is:**

$$\tilde{Y}_i = (-40.86044; 8.020724) + (1.210150; 0)x_{1i} + (0.2930840; 0)x_{2i} + (-0.05639407; 0.01113773)x_{3i}$$

For *h*=0.5, the calculated system fuzziness is 279.9219 and the average degree of belief is 0.717. In addition, the graphical representation of standard PLR model for *h*=0.5 is given in Figure 6.

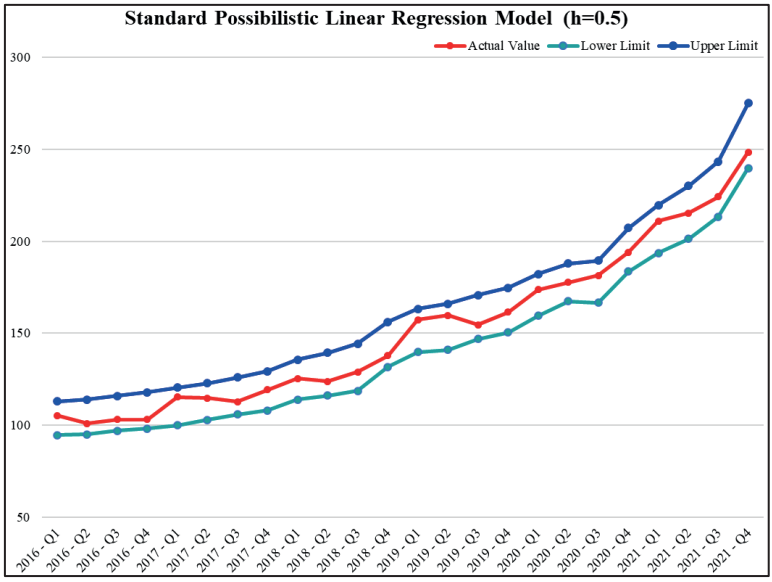

Figure 6. Graphical representation of standard PLR model for *h*=0.5

- **Standard possibilistic linear regression model predicted for *h*=0.7 is:**

$$\tilde{Y}_i = (-40.86044; 13.36787) + (1.210150; 0)x_{1i} + (0.2930840; 0)x_{2i} + (-0.05639407; 0.01856288)x_{3i}$$

For *h*=0.7, the calculated system fuzziness is 466.5364 and the average degree of belief is 0.830. Also, the graphical representation of standard PLR model for *h*=0.7 is given in Figure 7.

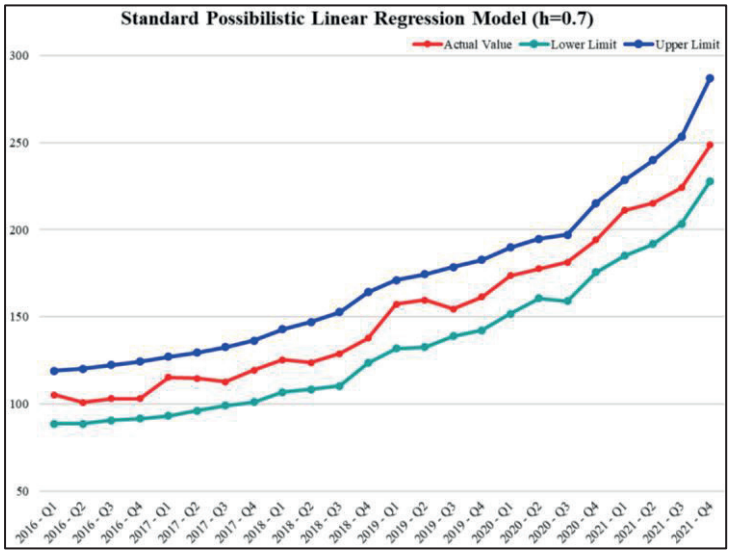

Figure 7. Graphical representation of standard PLR model for h=0.7

3.2.2 Estimation with Revised Possibilistic Linear Regression Model

The graph of Agriculture-PPI forecast values and actual values for the revised possibilistic linear regression model is as shown in Figure 8.

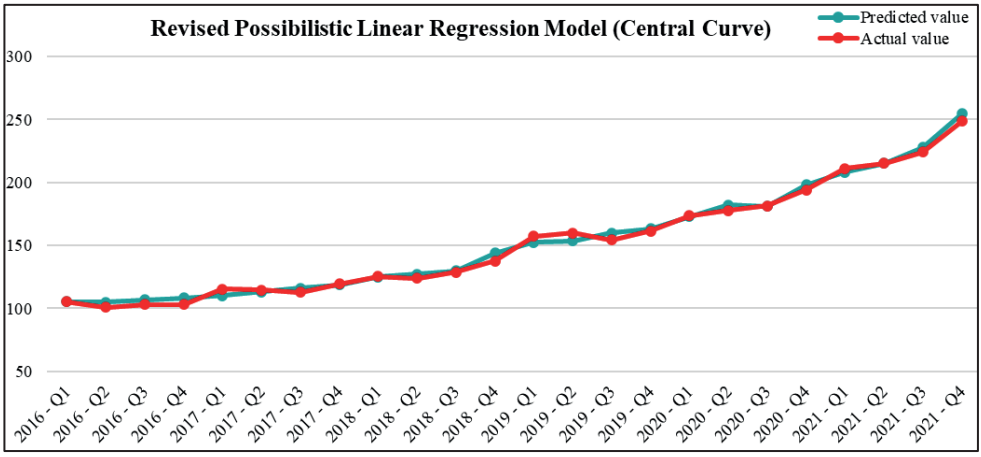

Figure 8. Representation of actual and forecast values by the revised PLR model

It is observed that the Agriculture-PPI centre forecast values and the actual values of the revised possibilistic linear regression model have approximate values within the modelled period. In addition, the mean absolute percentage error (MAPE) was calculated as 2.222 for h=0.0, 0.3 and 0.5 degrees of belief and 2.554 for h=0.7 due to the different centre value.

When the revised PLR model is calculated for different belief (h) values, the fuzzy linear regression models obtained are as follows, the fuzziness values of the system and the mean degrees of belief:

- **Revised possibilistic linear regression model predicted for h=0.0:**

$$\tilde{Y}_i = (-41.26101; 4.260962) + (1.288930; 0)x_{1i} + (0.2458718; 0)x_{2i} + (-0.07484608; 0.005007618)x_{3i}$$

For h=0.0, the calculated system fuzziness is 217.7682 and the average degree of belief is 0.458. In addition, the graphical representation of the revised PLR model for h=0.0 is given in Figure 9.

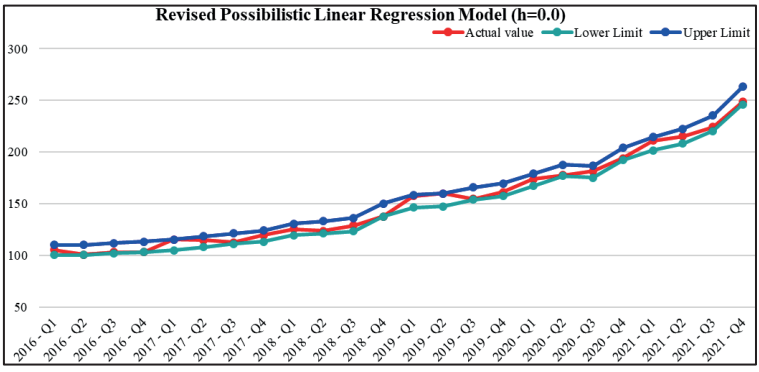

Figure 9. Graphical representation of the revised PLR model for h=0.0

- **Revised possibilistic linear regression model predicted for h=0.3:**

$$\tilde{Y}_i = (-41.26102; 6.087087) + (1.288930; 0)x_{1i} + (0.2458719; 0)x_{2i} + (-0.07484609; 0.007153746)x_{3i}$$

For h=0.3, the calculated system fuzziness is 278.4411 and the average degree of belief is 0.621. In addition, the graphical representation of the revised PLR model for h=0.3 is given in Figure 10.

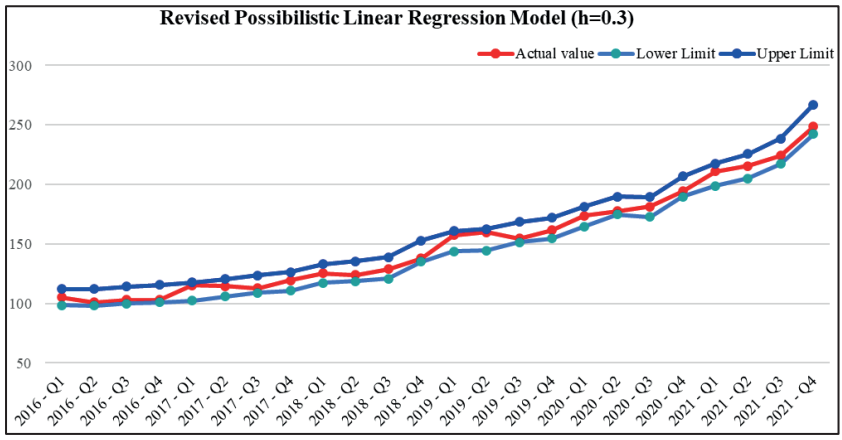

Figure 10. Graphical representation of the revised PLR model for h=0.3

- **Revised possibilistic linear regression model predicted for h=0.5:**

$$\tilde{Y}_i = (-41.26101; 8.521924) + (1.288930; 0)x_{1i} + (0.2458718; 0)x_{2i} + (-0.07484608; 0.01001524\ )x_{3i}$$

For h=0.5, the calculated system fuzziness is 359.3381 and the average degree of belief is 0.729. Furthermore, the graphical representation of the revised PLR model for h=0.5 is given in Figure 11.

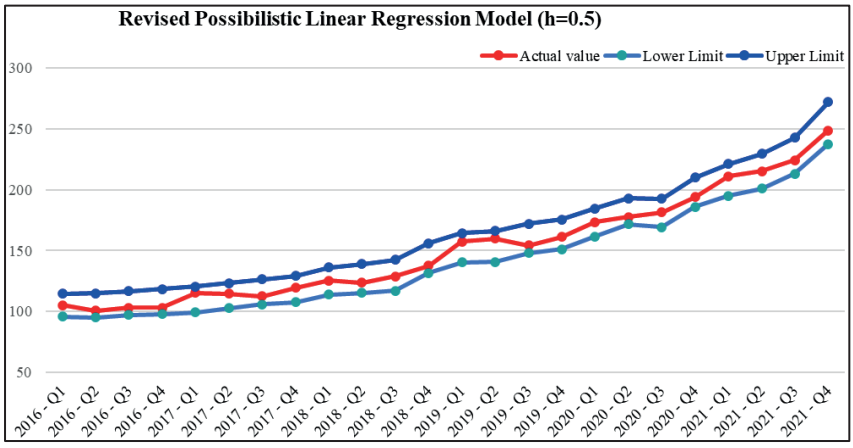

Figure 11. Graphical representation of the revised PLR model for h=0.5

- **Revised possibilistic linear regression model predicted for *h*=0.7:**

$$\tilde{Y}_i = (-40.31449; 22.19324\ ) + (1.299402; 0)x_{1i} + (0.2520130; 0)x_{2i} + (-0.08160821; 0)x_{3i}$$

For *h*=0.7, the calculated system fuzziness is 617.5729 and the average degree of belief is 0.841. Furthermore, the graphical representation of the revised PLR model for *h*=0.7 is given in Figure 12.

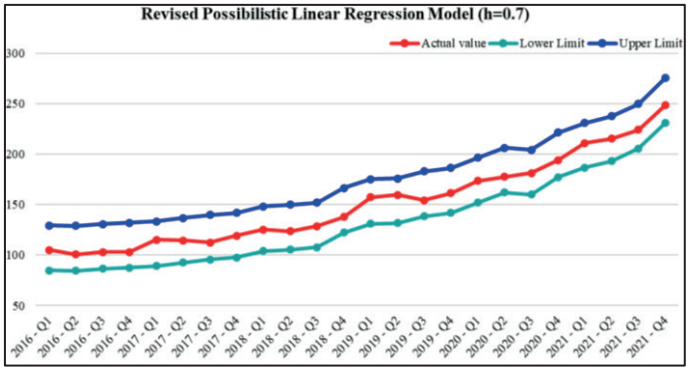

Figure 12. Graphical representation of the revised PLR model for *h*=0.7

3.2.3 Estimation with Fuzzy Least Squares Regression Model

The graph of Agriculture-PPI forecast values and actual values for the fuzzy least squares regression model is as shown in Figure 13.

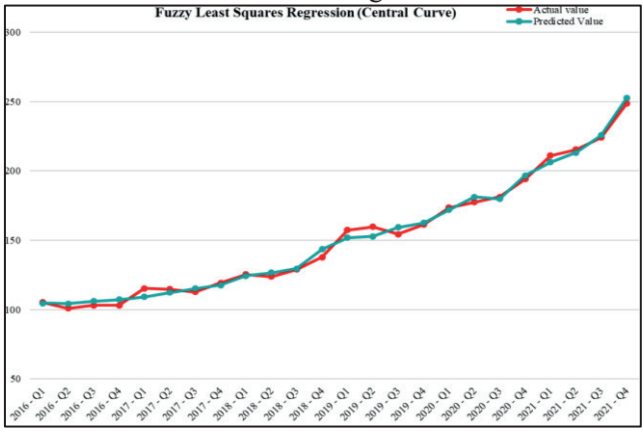

Figure 13. Representation of actual and forecast values with fuzzy LSR model

It is observed that the Agriculture-PPI centre forecast values and the actual values for the fuzzy least squares regression model have approximate values within the modelled period. In addition, the MAPE value was calculated as 2.155 because the center values were the same for all degrees of belief.

When the fuzzy least squares regression model is calculated for different belief (h) values, the fuzzy linear regression models, the fuzziness values of the system and the average degrees of belief are as follows:

- **Fuzzy least squares regression model estimated for h=0.0:**

$$\tilde{Y}_i = (-36.573; 5.497710\ ) + (1.28; 0)x_{1i} + (0.196; 0)x_{2i} + (-0.0726; 0.003896762)x_{3i}$$

For h=0.0, the calculated system fuzziness is 162.5323 and the average degree of belief is 0.544. In addition, the graphical representation of the fuzzy least squares regression model for h=0.0 is given in Figure 14.

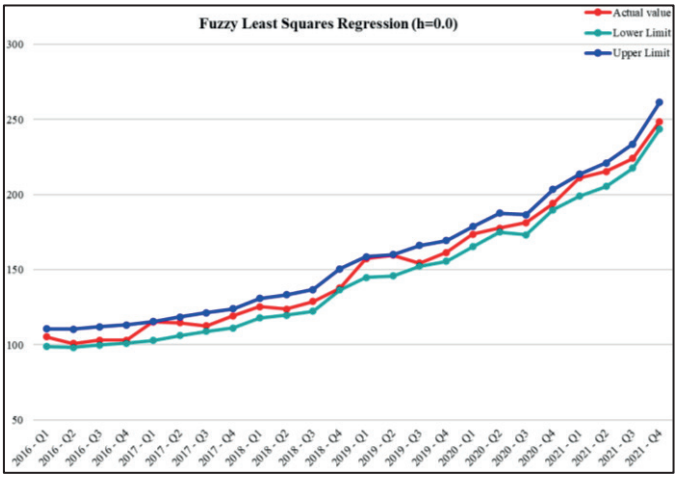

Figure 14. Graphical representation for the fuzzy LSR model for h=0.0

- Fuzzy least squares regression model estimated for h=0.3:

$$\tilde{Y}_i = (-36.573; 7.853871\ ) + (1.28; 0)x_{1i} + (0.196; 0)x_{2i} + (-0.0726; 0.005566803)x_{3i}$$

For h=0.3, the calculated system fuzziness is 232.1890 and the average degree of belief is 0.681. In this regard, the graphical representation of the fuzzy least squares regression model for h=0.3 is given in Figure 15.

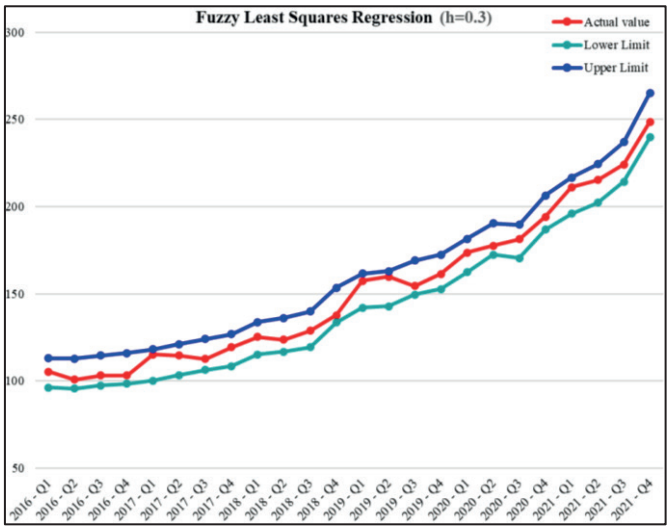

Figure 15. Graphical representation for the fuzzy LSR model for h=0.3

- Fuzzy least squares regression model estimated for h=0.5:

$$\tilde{Y}_i = (-36.573;\ 10.99542) + (1.28; 0)x_{1i} + (0.196; 0)x_{2i} + (-0.0726; 0.007793525)x_{3i}$$

For h=0.5, the calculated system fuzziness is 325.0646 and the average degree of belief is 0.772. In addition, the graphical representation of the fuzzy least squares regression model for h=0.5 is given in Figure 16.

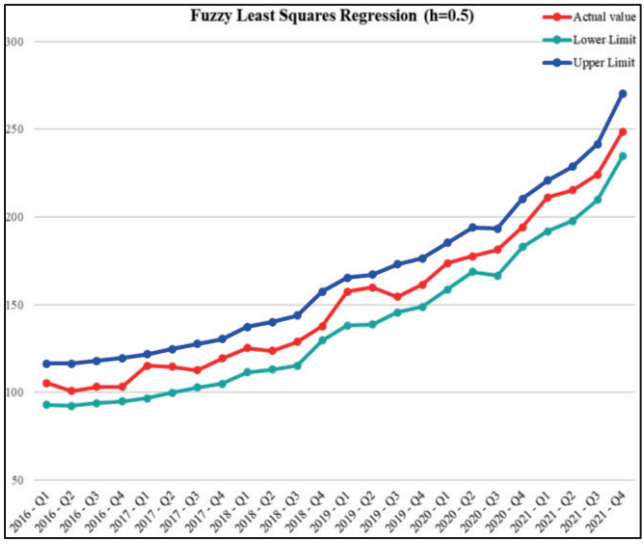

Figure 16. Graphical representation for the fuzzy LSR model for h=0.5

- **Fuzzy least squares regression model estimated for *h*=0.7:**

$$\tilde{Y}_i = (-36.573; 18.32570\ ) + (1.28; 0)x_{1i} + (0.196; 0)x_{2i} + (-0.0726; 0.01298921)x_{3i}$$

For *h*=0.7, the calculated system fuzziness is 541.7743 and the average degree of belief is 0.863. In addition, the graphical representation of the fuzzy least squares regression model for *h*=0.7 is given in Figure 17.

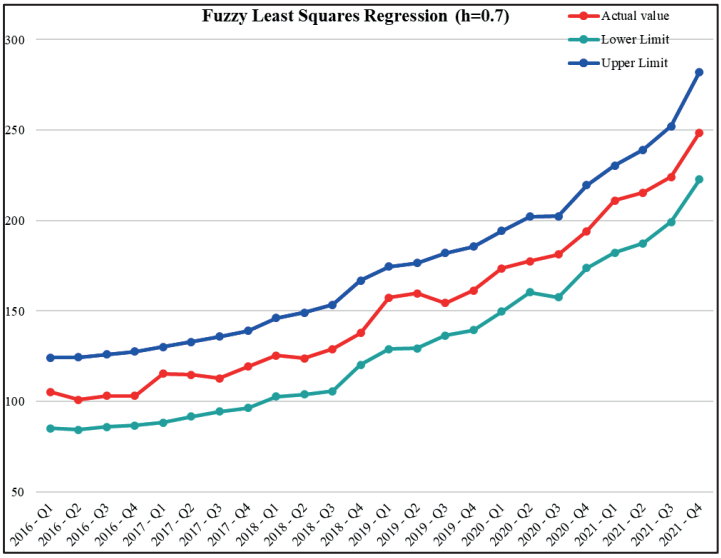

Figure 17. Graphical representation for the fuzzy LSR model for *h*=0.7

3.3 Comparison of Fuzzy Linear Regression Methods with Classical Multivariate Linear Regression Methods

The system fuzziness, average belief levels and MAPE values calculated for different belief levels of the fuzzy linear regression models and multivariate linear regression models applied for the 2016:Q1-2021:Q4 periods used in the forecasting of the Agriculture-PPI variable are shown in Table 2.

Table 2. Comparison of fuzzy linear regression methods and classical multivariate linear regression model for forecasting Agriculture-PPI values

	h	System Fuzziness	$\bar{h}$	MAPE $\left(\frac{\sum_{i=1}^{n}\frac{\lvert Y_i-\hat{Y}_i\rvert}{Y_i}}{n}\times 100\right)$
Classical Multivariate Linear Regression	-	-	-	2.155
Standard PLR model	**0.0**	139.961	0.434	2.312
	0.3	199.944	0.604	
	0.5	279.922	0.717	
	0.7	466.536	0.830	
Revised PLR model	**0.0**	217.768	0.458	2.222
	0.3	278.441	0.621	
	0.5	359.338	0.729	
	0.7	617.573	0.841	2.554
Fuzzy LSR model	**0.0**	162.532	0.544	2.155
	0.3	232.189	0.681	
	0.5	325.065	0.772	
	0.7	541.774	0.863	

According to Table 2, the fuzzy least squares regression model in terms of MAPE values results with a lower percentage of error than other fuzzy linear regression models. In addition, when examined in terms of average degrees of belief, it is seen that the average degrees of belief are higher in the fuzzy least squares regression model for all h levels considered. Finally, in terms of system fuzziness, standard possibilistic linear regression model has the smallest fuzziness for all h levels, while the revised possibilistic linear regression model has the largest fuzziness values. Since the $\bar{h}$ values calculated for all h levels are evaluated as the goodness of fit of the model, it can be said that the fuzzy least squares regression model is the most appropriate model among the fuzzy linear regression models considered in the estimation of the Agriculture-PPI variable since it has a high $\bar{h}$ value and a low average forecast error percentage for the period considered.

RESULTS AND DISCUSSION

Multivariate linear regression and fuzzy linear regression models (standard PLR, revised PLR and fuzzy LSR models) were applied for Agriculture-IPI, FPI and Brent oil variables affecting the Agriculture-PPI variable. As a result of the model estimated after determining that there is a linear relationship between the dependent variable Agriculture-PPI and the independent variables, Agriculture-IPI and Brent oil variables were found statistically significant. In addition, the assumptions of the classical multivariate linear regression model have been found to be satisfied. However, in all of the fuzzy linear regression models, it is determined that the fuzziness in brent oil, which is one of the independent variables, causes fuzziness in the dependent variable Agriculture-PPI and negatively affects the Agriculture-PPI. Among the fuzzy regression models obtained, it can be said that the most appropriate prediction model is the fuzzy LSR model, where the $\overline{h}$ value expressing the goodness of model fit is higher than the other fuzzy regression models for all degrees of belief and the MAPE value is at the lowest value.

As a result, when all models were evaluated, it was found that the Agriculture-PPI value was positively affected by the Agriculture-IPI and FPI variables and the Brent oil variable was negative.

REFERENCES

1. Arulchinnappan, S., Rajendran, G. (2011), A Study on Reverse Osmosis Permeating Treatment for Yarn Dyeing Effluent Using Fuzzy Linear Regression Model, *African Journal of Biotechnology,* 10(78), 17969-17972.

2. Chang, Y.-H.O., Ayyub, B.M. (2001), Fuzzy Regression Methods – A Comparative Assessment, *Fuzzy Sets and Systems*, 119, 187–203.

3. Chukhrova, N., Johannssen, A. (2019), Fuzzy Regression Analysis: Systematic Review and Bibliography, *Applied Soft Computing Journal*, 84, 105708.

4. Çıplak, U., Yücel, M. E. (2004), İthalatta Koruma Önlemleri ile Tarım ve Gıda Fiyatları, *TCMB Çalışma Tebliği,* 04(01), 1-24.

5. Demirağ, İ., Sağır, M. (2022), Türkiye'de Gıda Fiyatları Endeksi ile Tarım Ürünleri Üretici Fiyatları Endeksleri Arasındaki İlişkinin Engle-Granger Yöntemi ile İncelenmesi, *Socrates Journal of Interdisciplinary Social Studies*, 24, 98-105.

6. Diamond, P. (1988), Fuzzy Least Squares, *Information Sciences,* 46 (3), 141-157.

7. Emek, Ö.F. (2020), Enflasyonun Gelir Eşitsizliği Üzerindeki Etkisinin Panel Veri Analizi ile İncelenmesi, *İstanbul Üniversitesi, Sosyal Bilimler Enstitüsü, İktisat ABD,* Doktora Tezi, 166s., İstanbul.

8. Erilli, N.A., Körez, M.K., Öner, Y., Alakuş, K. (2012), Kritik (Kriz) Dönem Enflasyon Hesaplamalarında Bulanık Regresyon Tahminlemesi, *Doğuş Üniversitesi Dergisi,* 13, 239-253.

9. Eştürk, Ö., Albayrak, N. (2018), Tarım Ürünleri-Gıda Fiyat Artışları ve Enflasyon Arasındaki İlişkinin İncelenmesi, *Uluslararası İktisadi ve İdari İncelemeler Dergisi*, 18. EYİ Özel Sayısı, 147-158. DOI: 10.18092/ulikidince.353991.

10. Günay Akdemir, H., Tiryaki, F. (2013), Using Fuzzy Linear Regression to Estimate Relationship Between Forest Fires and Meteorological Conditions, *Applications and Applied Mathematics,* 8(2), 673-683.

11. He, Y. Q.,Chan, L.-K., Wu, M.-L. (2007), Balancing Productivity and Consumer Satisfaction for Profitability: Statistical And Fuzzy Regression Analysis, *European Journal Of Operational Research*, 176, 252–263.

12. İçen, D., Günay, S. (2015), Türkiye'deki İşsizlik Oranının Bulanık Doğrusal Regresyon Analiziyle Tahmini, *İstatistikçiler Dergisi:İstatistik&Aktüerya,* 8, 10-26.

13. İşbilen Yücel, L. (2017), Türkiye'de 2012-1/2016-3 Arası Dönemde 15-64 Yaş Grubu İçin İstihdam Dışı Oranın Bulanık Doğrusal Regresyon Analizi İle Tahmini, *Ekonometri ve İstatistik,* 27, 29-50.

14. Kar, N.B., Das, S., Ghosh, A., Banerjee, D. (2019), Fuzzy Linear Regression Model on Mulberry Silk Cocoon Characteristics, *Research Journal of Textile and Apparel,* 23(3), 201-211.

15. Koçak, N. A. (2021), Türkiye'de Tüketici ve Üretici Fiyatları Arasındaki İlişkinin Alternatif Tahmin Yöntemleri Kullanılarak Analizi, *Business and Economics Research Journal,* 12(1), 33-47.

16. Oral, O., Eştürk, Ö. (2022) Üretici Fiyatından Gıda Tüketici Fiyatına Asimetrik İletim, *Fırat Üniversitesi Sosyal Bilimler Dergisi,* 32(2), 675-683.

17. Özer, F., Büyükkeklik, A. (2022), Doğrusal Bulanık Regresyon Modeli ile Türkiye'deki Belediye Atığı Miktarının Tahmini, *Sosyoekonomi,* 30(52), 473-490.

18. Özyücel, M., Öztürk, M. ve Altıntaş, N. (2022), Türkiye'de Tarımsal Girdi Fiyat Endeksi, Tarım Ürünleri Üretici Fiyat Endeksi ve Gıda Enflasyonu Arasındaki Nedensellik İlişkilerinin Analizi, Editörler: F. Tuna ve M.F. Buğan, *Sosyal Bilimler Üzerine Araştırmalar: Ekonomi&Politika* (s.41-58), Gaziantep: Özgür Yayınları.

19. Savic, D., Pedrycz, W. (1991), Evaluation of Fuzzy Linear Regression Models, *Fuzzy Sets and Systems*, 39, 51-63.

20. Sorkheh, K., Kazemifard, A., Rajabpoor, S. (2018), A Comparative Study of Fuzzy Linear Regression and Multivariate Linear Regression in Agricultural Studies:A Case Study of Lentil Yield Management, *Turkish Journal of Agriculture and Forestry,* 42, 402-411.

21. Tabachnick, B.G., Fidell, L.S. (2007). Using Multivariate Statistics. 5th ed., Pearson Education. Inc., USA, 980 pp.

22. Tanaka, H., Uejima, S., Asai, K. (1982), Linear Regression Analysis with Fuzzy Model*, IEEE Transactions on Systems, Man, and Cybernetics*, 12 (6), 903-907.

23. Tay Bayramoğlu, A., Koç Yurtkur, A. (2015), Türkiye'de Gıda ve Tarımsal Ürün Fiyatlarını Uluslararası Belirleyicileri, *Anadolu Üniversitesi Sosyal Bilimler Dergisi,* 15(2), 63-73.

24. Topuz, D. (2020), Yenidoğanın Ağırlığının Tahminine Yönelik Olarak Elde Edilen Klinik Verilerin Klasik ve Bulanık Doğrusal Regresyon Modelleri ile Analizi, *Türkiye Klinikleri Biyoistatistik Dergisi,* 12(3), 320-334.

25. Zadeh, L. A. (1965), Fuzzy Sets, *Information and Control*, 8, 338-353.

Chapter 10

ORIENTATION OF SPIN SYSTEMS WITH HAARP TECHNOLOGY

Cengiz AKAY[1]
Zafer GÜLTEKİN[2]

1 Cengiz Akay, Dr. Öğretim Üyesi, Bursa Uludağ Üniversitesi, Fen Edebiyat Fakültesi, Fizik Bölümü, 16059, Nilüfer, Bursa, Türkiye cenay.akay@gmail.com https://orcid.org/0000-0002-8037-0364
2 Zafer Gültekin, Araştırma Görevlisi, Bursa Uludağ Üniversitesi, Fen-Edebiyat Fakültesi, Fizik Bölümü, 16059, Nilüfer, Bursa, Türkiye zafergultekin@uludag.edu.tr http://orcid.org/ 0000-0001-8026-0379

1. Introduction

In 2023, a 7.7 magnitude earthquake occurred in the Pazarcık district of Kahramanmaraş on 6 February. After this earthquake, a second earthquake occurred at 13.24. The magnitude of the earthquake, whose epicenter was in the Elbistan district of Kahramanmaraş, was recorded as 7.6. After these two earthquakes, discussions gained momentum that earthquakes were triggered by unnatural ways and artificial techniques. The prevailing view is that the earthquakes were allegedly initiated from HAARP facilities in the US state of Alaska and directed by American aircraft carriers in the bay. This study is about the contention between physics and metaphysics.

There is a profound difference in physics between definite and indefinite integrals. When you assign upper and lower bounds to an indefinite integral, you have made the transition from mathematics to physics. This is actually the very definition of physics. Physics is the optimized version of mathematics. The language of the universe is mathematics and its limits are endless. Physics does not accept this and optimizes it. To give an example, consider an engine. Physics does not accept the suggestion of mathematics, which says that it works with all kinds of fuels such as gasoline, diesel, kerosene, spirit and hydrogen, and optimizes it. It says that this engine will run on gasoline, that engine will run on kerosene, and that engine will run on hydrogen.

Mathematics is beyond physics, and physics is the optimized version of mathematics. From this point of view, metaphysics says that the laws of physics will never be completely true. This definition is also correct. If you add $\pm\infty$ to the lower and upper bounds of an indefinite integral, do you pass physics? The most logical answer depends on what you expect. If you say we pass, you may not be accepted because the terms $\pm\infty$ and 0 are objects in mathematics, but have no equivalent in physics. Zero denotes absence, $\pm\infty$ denotes inaccessibility. Just like accepting that two parallel lines intersect at infinity. This is unnecessary. Fortunately, physics has found a solution to this, the limit state of mathematics. Physics can find solutions that mathematics cannot find directly, based on experimental data, such as reverse engineering.

2. A look at the concept of energy

It is difficult to give a precise definition of energy because its definitions on the macroscopic and microscopic scales are different. These definitions are for us. Energy, defined as the ability to do work on a macroscopic scale, does not have to do work on a microscopic scale. When the force pulling a car does work on a macroscopic scale, the change in internal energy in heating a water predicts its definition according to the laws of thermodynamics. The unified field theory, which states that there is actually only one force in nature and that we perceive it differently in different applications, is not yet incomplete and complete.

The energy transferred from one point to another is called heat energy and this energy can be transferred in three different ways. Each of the physical contact, transport and radiation paths has different processes in itself. The most daring in energy transfer is electromagnetic radiation. Few people, other than experts working in this field, are aware of the transfer of magnetic energy through electromagnetic radiation.

3. Effect of magnetism

Let us give two examples of the transfer of magnetic energy by means of electromagnetic radiation. Induction heating technology, which is widely used in laboratories and industry, has almost entered our homes. The general mechanism of inductive heating can summarized by three successive physical phenomena. It is the creation of eddy currents by transferring the electromagnetic energy to the part to be heated through the coils, the conversion of the eddy currents into heat by the Joule effect, and the heat transfer from the hot region (surface) to the cold regions (deep) heat flow. These processes must completed. The basis of electromagnetic induction is based on Maxwell's laws, which describe the distribution of thermal energy generated by induced currents in the work piece.

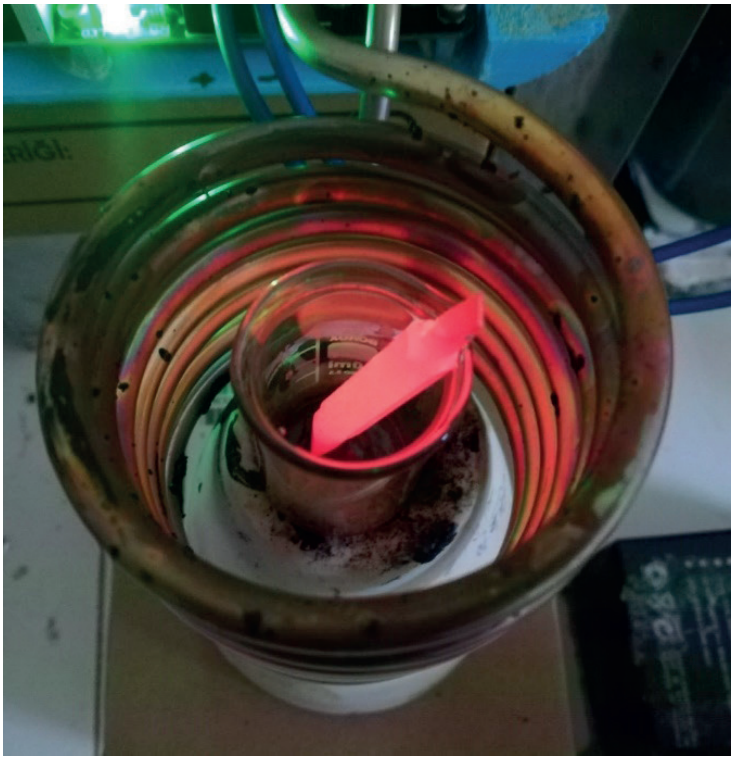

Figure 1. Heating effect of magnetism

Figure 1 shows the state of a piece of steel heated close to its melting temperature with an inductive heater in our laboratory. Due to the ferromagnetic property of the steel workpiece, the hysteresis losses caused by the spins that change direction with the change of the magnetic field cause the material to be heated. The red glow of the steel is similar to the magma layer found underground. Both are susceptible to magnetic influences.

The magma itself, which is located under the layer that forms the earth's crust, is in a molten state because it is very hot. In the structure of the mantle, they are molten rocks, most of which contain some minerals such as highly molten iron, magnesium and calcium, and the part that reaches the earth is called lava [1]. While the surface of the lava, which is under the influence of open air, takes on a dark color, the high-temperature molten mixture continues to spread under the influence of gravity [2].

Figure 2. Exposed lava cools to a deep black color, while the molten rock beneath glows bright orange.

The molten presence of rocks composed largely of ferromagnesium silicates in the Earth's upper mantle leaves the door open to its magnetohydrodynamic effects. This means that magnetic liquids or melts can be directed to flow under the influence of an externally applied magnetic field. Consider that when you want to create an earthquake in a region where there is a fault line with a structure suitable for breaking, it is sufficient to apply magnetic pressure to this molten structure with ferromagnetic feature. Therefore, we can use an aircraft carrier to generate this triggering magnetic field. This aircraft carrier looks like an aircraft carrier but actually has coils with huge coils hidden underneath; let this aircraft carrier have a small atomic battery. Most aircraft carriers actually get their electricity from an atomic battery. The magnetic field oscillations created by these coils fed with tens of

thousands of currents can create magnetic pressure on the fault line and force it to break. According to geologists, at least as much energy as the power of an atomic bomb must be transferred to trigger an earthquake. This is true for the crust near the mantle. In fact, components with magnetic properties also respond to very low magnetic fields. Field strengths do not follow the strict rule. There is not four wheels to an engine, but an engine to all four wheels, and it is long-range. Figure 3 shows the VSM results of a ZnO semiconductor doped with various proportions of Co. While undoped ZnO has diamagnetic property (black curve), its ferromagnetic property increases as it is doped with Co (blue curve). The application of a small magnetic field is sufficient to magnetize this compound [3].

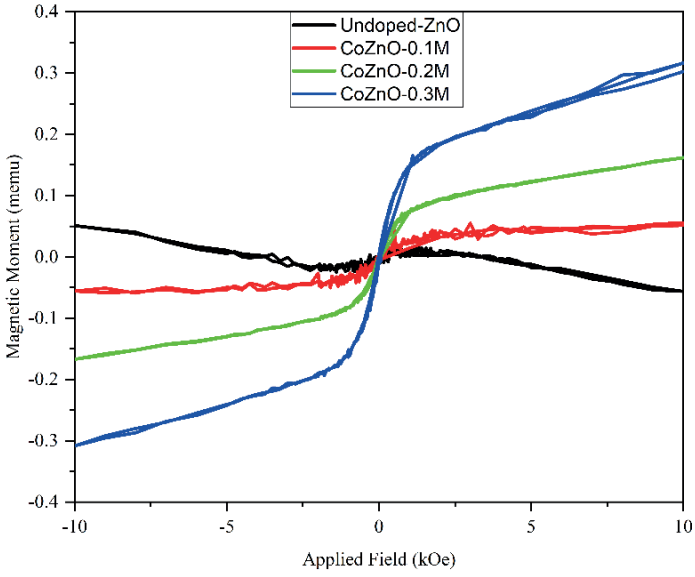

Figure 3. VSM results of Co-doped ZnO semiconductor.

The presence of ferromagnetic components such as Fe, Ni and Co in the earth's crust and molten magma layer means that these molten, liquid-solid rocks will be affected by the applied external magnetic field oscillations. The earth is a gigantic magnet that produces its own magnetic field. These magnetic field oscillations in the VLF, ELF and ULF bands produced in the earth's crust may not be sufficient to trigger artificial earthquakes. Still, there are two more possibilities.

4. NMR phenomenon

The NMR phenomenon can briefly summarized as follows. A collection of spins under the influence of an external magnetic field splits into Zeeman

energy levels. The difference between these energy levels depends on the magnitude of the applied magnetic field. If a radio frequency radiation equal to the difference between the two energy levels applied to the system, a resonance phenomenon called spin reversal takes place. This event is a sign that the sent energy absorbed by the system and notifies us by sending an NMR signal.

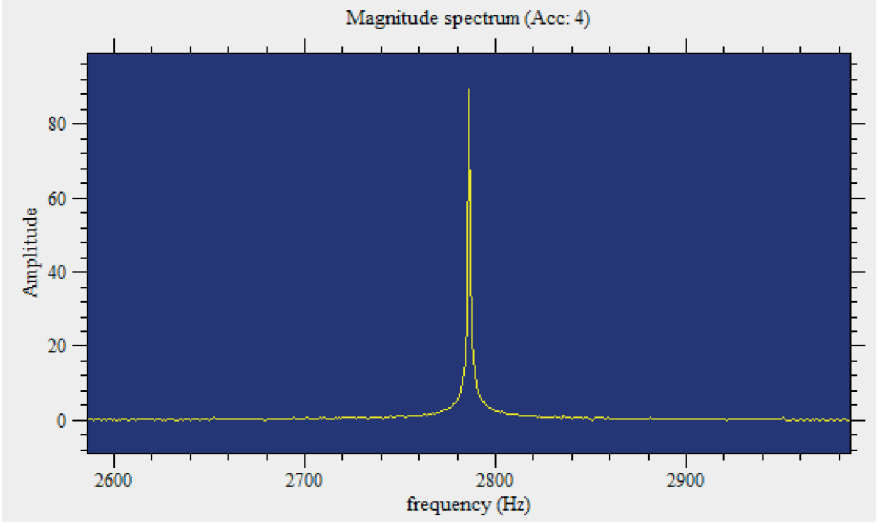

Figure 4. NMR signal of drinking water taken in the earth's magnetic field.

Figure 4 is the pure NMR signal of drinking water obtained in the earth's magnetic field. This signal was obtained from the EFNMR device in our laboratory working in the magnetic field of the earth. The fact that this signal is so pure and clean is due to the good NMR sensitivity of the spins of the hydrogen atoms that make up the spin ensemble. For this reason, the NMR sensitivity of the nuclear spins forming the hydrogen atom is assumed to be one. There is another reason why this signal is good. The higher the number of spins involved in the resonance event, the higher the received signal strength. The signal is the vectorial sum of the signals given by the individual spins, because the field strength acts on each spin individually. In other words, the signal represents the net magnetization vector of the spin ensemble. This is the elegance of the sigma $\sum$ operator in mathematics. Other techniques are used to acquire NMR signals of compounds with very poor NMR sensitivity. For example, in order to receive the weak NMR signals of fluorine compounds, we can also strengthen the NMR signal by stimulating the electrons, which are also spins. This technique is known as the double resonance NMR technique, since the weak NMR signal is more clearly contributed by the electron spins excited by the ESR (electron spin resonance) technique. After all, it has support from one spin community to another spin community. Is

the artificial earthquake triggering of the magnetic field pulses produced by the aircraft carrier with a second radio frequency support directed over the ionosphere from Alaska, similar to the double resonance NMR technique? This works because field strengths are long range and can access individual turns individually. Various sources say that the HAARP technique is used to communicate at very low frequencies with American navy ships navigating the oceans. India protested China, saying its soldiers were being cooked with microwave weapons. China denied this news, who cares. Very low frequency magnetic field oscillations must go beyond HARP technology being a climate weapon. No one but one person knows enough about the capabilities of HAARP technology.

5. Nikola Tesla

The mysterious genius Nikola Tesla is considered the father of alternating current [4]. Thanks to the alternating current motors and machines that he found with his engineering intelligence, we are living the comfort and joy of the current century we live in. Following the death of Tesla, who also pursued the international intelligence services due to his numerous discoveries, his own works, which he had encrypted, were stolen from the hotel room where he stayed. It is said that among the stolen documents, there are documents closely related to HAARP technologies [5]. We do not know if Tesla was aware of the existence of spin and spin waves when listing his numerous discoveries. I could not find any significant information in the publication scans I made. I think the past century has belonged to electrical science, and the next century will be the century of magnetism. Right or wrong, let us focus on the two issues attributed to him, wireless energy transmission and the Philadelphia experiment.

The further away two or more spin particles are from each other, the more they can communicate with each other simultaneously. In other words, two spin particles interact with each other no matter how far apart they are. In the physics world, this topic is known as quantum entanglement. The speed of this interaction is said to be much higher than the speed of light, and the constancy of the speed of light in the universe is still a controversial issue. In Tesla's wireless energy transfer, it is not the electrons transferred, but the activation of the electrons, namely the spins, where they should be. How Nikola Tesla accomplished this is an engineering problem, not a physics one. If a spin that is trillions of light years away can interact with spin regardless of time and space, it means that whoever controls the world of spins can rule us.

The Philadelphia Experiment is an experiment that are said to have been carried out on October 28, 1943 in the state of Pennsylvania by the American navy, based on Tesla's secret projects [6]. In this experiment, the DE173 class 1240-ton USS Eldridge, a naval protection destroyer, returned to the Norfolk

naval base 640 km away in a short time. Although there is no evidence of the existence of the experiment, the dream is beautiful, let us continue. Are you aware, we are talking about a directed mass transfer? A mass transfer to the region where the fault line is to be broken can create enough pressure to trigger an earthquake. This technique is the quantum mechanical equivalent of what geologists call hydraulic fracturing to create artificial earthquakes. We live in a universe where mass and energy are equivalent.

6. Artificial earthquake generation

If magnetic energy can transferred by radiation, then let us produce an artificial earthquake. Let us also decide how we should apply the data we have obtained to the earth. Figure 5 shows the experimental setup used to generate the artificial earthquake. This assembly actually consists of a coil that converts the square wave sent to it into magnetic pulses and a magnet group that converts these magnetic pulses into mechanical vibrations. This magnet group represents the magma layer of the earth.

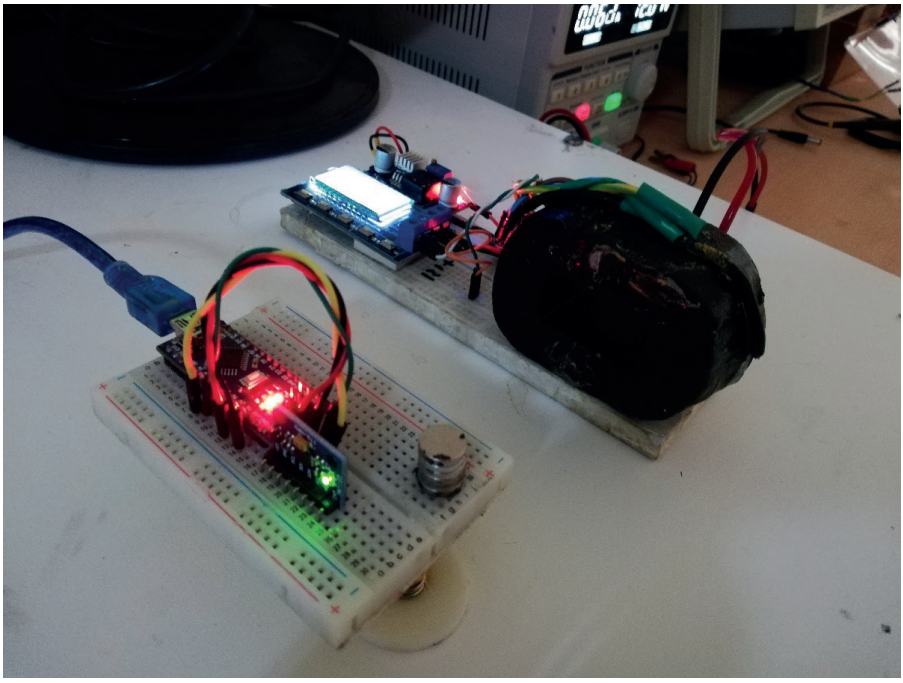

Figure 5. Artificial earthquake generator.

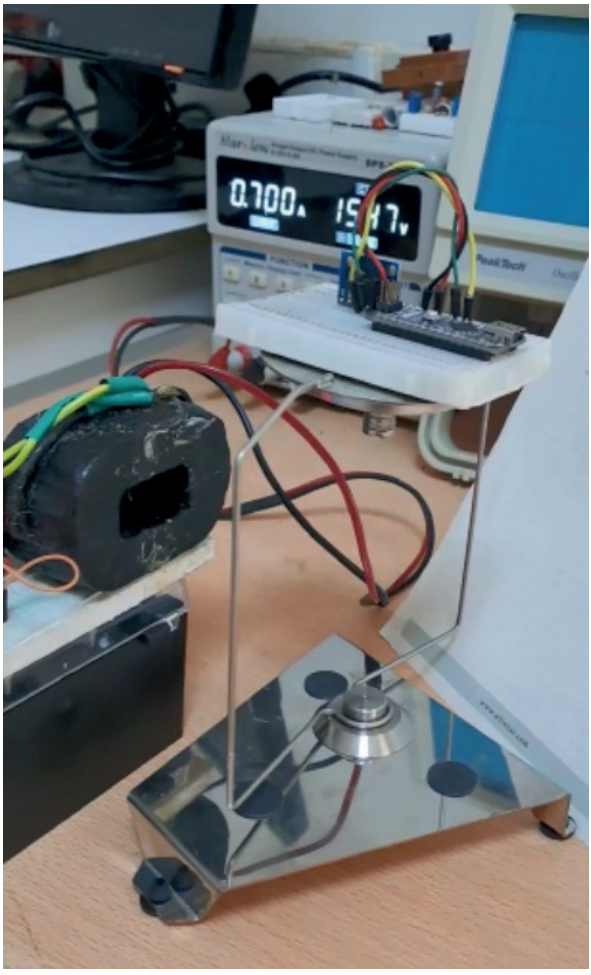

Figure 6. Artificial earthquake simulator.

In a sense, it converts magnetic energy into vibrational energy. An MPU6050 vibration sensor was used to detect these vibrations. The magnet group symbolizing the magma is affixed to the bottom of the mechanical earthquake mechanism. Each magnetic energy pulse is transformed into vibrational energy in this mechanical mechanism.

Figure 6 is the position of this experimental setup placed on the mechanical earthquake setup. As the mechanical earthquake mechanism vibrates, the MPU6050 vibration sensor placed on it converts the vibrations into signals and transfers them to the computer. Graphical interpretations of these transmitted signals are given in Figure 7, Figure 8, Figure 9 and Figure 10.

Magnetic energy pulses are produced at different square wave rates and frequencies. Square wave rates were chosen as 20%, 40%, 60%, and 80% stepwise, for each rate were applied at 1 Hz, 5 Hz, 10 Hz and 20 Hz frequencies, respectively.

Since the MPU6050 vibration sensor simultaneously measures the translational and angular acceleration components in three axes, each of the graphs is grouped in square wave (on/off) ratios.

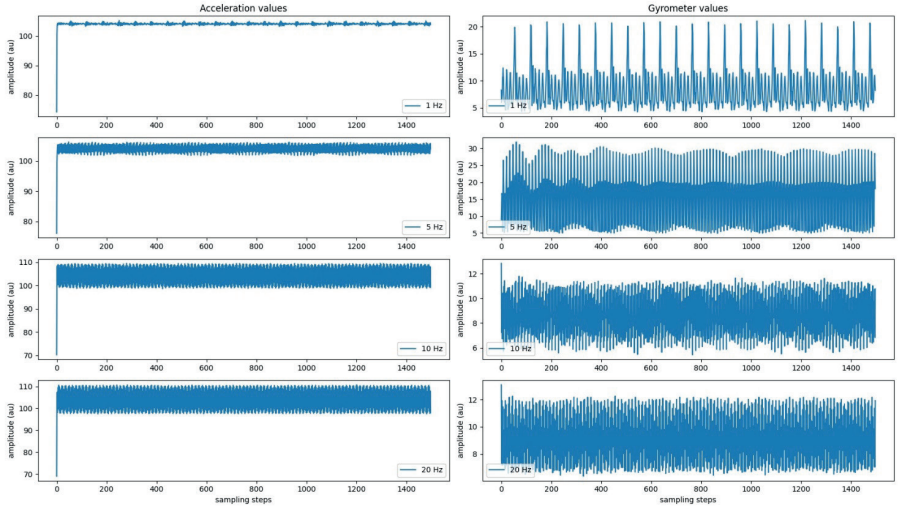

Figure 7. Signals received at 20% square wave rate.

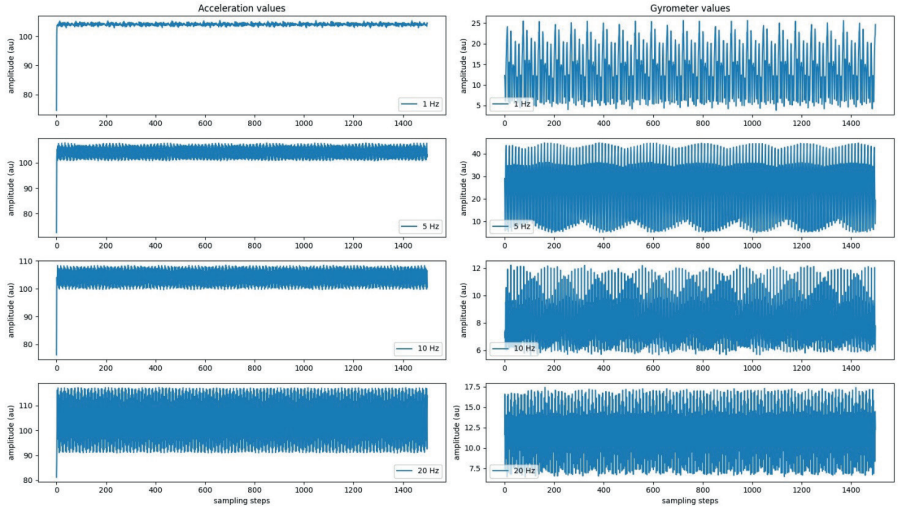

Figure 8. Signals received at 40% square wave rate.

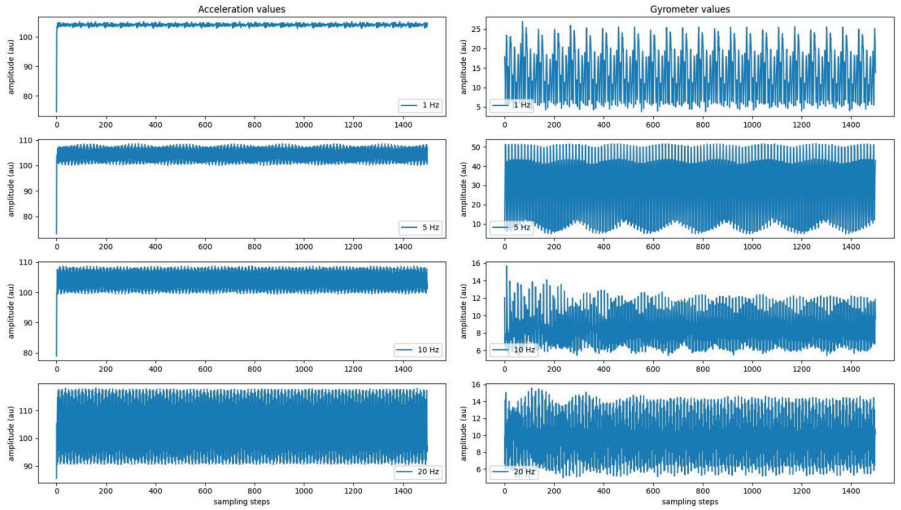

Figure 9. Signals received at 60% square wave rate.

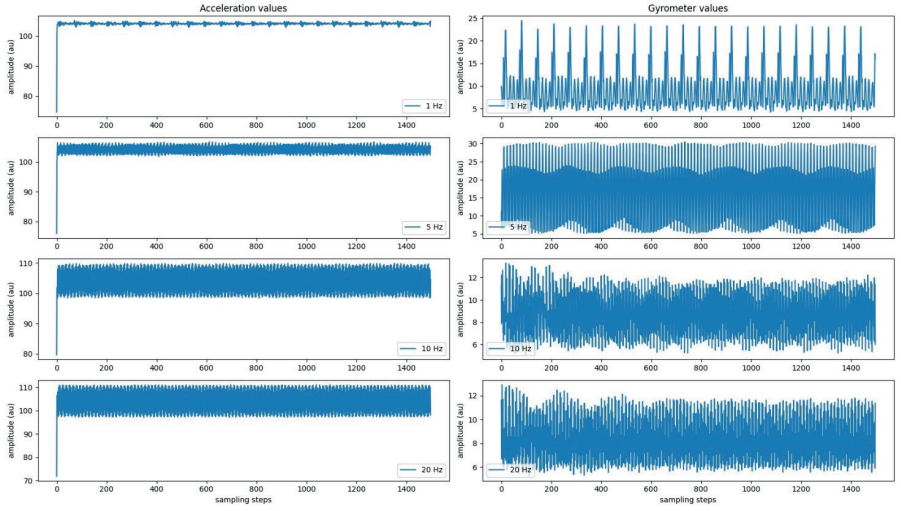

Figure 10. Signals received at 80% square wave rate.

Although each of the graphs above look the same, they are not. The junction point of the mechanical earthquake sensor, which is made by bending a metal wire in the form of a square ring, is not fixed to the ground, but is in a movable position. Therefore, it can also perform rotational motion. The right side of the graphics clearly indicates that the system is also subject to rotation. It is noticed that the amplitudes of translational and rotational vibrations depend on the square wave ratios and the application frequencies.

These charts are not important on their own. However, we can start from the amplitude and period values of the vibrations. Any physics book will say that the energy of a vibrating system is proportional to the square of the amplitude of the vibration.

$$E = \frac{1}{2}kx^2 \qquad (1)$$

In this equation, k is a local constant of the system and x represents the amplitude of the vibrating system. Let us rewrite this equation for a signal with period N in the Python scripting language [7].

$$P = \frac{1}{N}\sum_{n=0}^{N-1} x(n)^2 \qquad (2)$$

This expression gives the average power of a signal with period N. Average power includes the sum of translational and rotational kinetic energies. Figure 11 shows the average power plots obtained. This chart only summarizes the situation for this setup. In this mechanical earthquake mechanism, which represents the earthquake zone, it seen that the most appropriate magnetic pulses to be sent to create an earthquake should be at a frequency of 5 Hz and a square wave rate of 60%. This is also the local, natural vibrational value of that area.

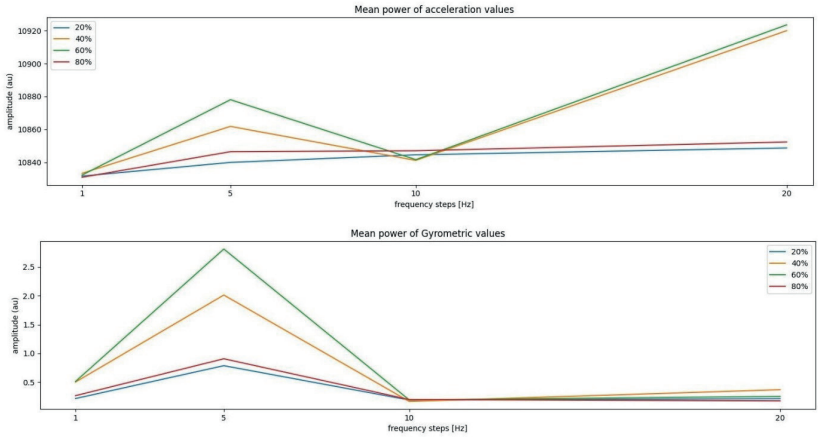

Figure 11. Average power values of vibrations.

7. Conclusion

The lines written by the conspiracy theorists should read. It is a way of understanding which theories of physics they interpret in their own world. The source of those lines they wrote may be the telepathic views of an alien in another corner of space. As FBI agent Fox Molder said, there are aliens among us. Dreams based on mathematical hunches are beyond physical and each one is real. The truth is out there.

REFERANCES

[1] Magma, [Online]. Available: https://tr.wikipedia.org/wiki/Magma (Accessed June 13, 2023).

[2] Lava Flow, [Online]. Available: https://education.nationalgeographic.org/resource/magma/ (Accessed June 13, 2023).

[3] Gültekin, Z., Alper, M., Hacıismailoğlu, M.C. et al. Effect of Mn doping on structural, optical and magnetic properties of ZnO films fabricated by sol–gel spin coating method. J Mater Sci: Mater Electron 34, 438 (2023). https://doi.org/10.1007/s10854-023-09886-7

[4] Nikola Tesla, [Online]. Available: https://en.wikipedia.org/wiki/Nikola_Tesla (Accessed June 13, 2023).

[5] Dalgıç T., "Garip Bir Deha Tesla", 1978, Available: https://www.emo.org.tr/ekler/b4224068a41c5d3_ek.pdf?dergi=7 (Accessed June 13, 2023).

[6] Philadelphia Experiment, [Online]. Available: https://en.wikipedia.org/wiki/Philadelphia_Experiment (Accessed June 13, 2023).

[7] Roberts M. J., "Signals and Systems Analysis Using Transform Methods and MATLAB", pages:99-102, Mc Graw Hill, 2018, ISBN-10. 1260083608 · ISBN-13. 978-1260083606.

Chapter 11

THE IMPORTANCE OF THE HYDROGEN BONDING OF Π-CONJUGATED MOLECULE FOR CHARGE TRANSPORT RATE

***Gül YAKALI*[1]**

***Zeynep TÜRKMEN BULCA*[2]**

1 Nanoscience and Nanotechnology Program, Institute of Science, Izmir Katip Çelebi University, Izmir, 35620, Turkey
2 Department of Engineering Sciences, Faculty of Engineering, Izmir Katip Çelebi University, Izmir, 35620, Turkey
ORCID: 0000-0002-0015-5948

INTRODUCTION

Hydrogen bonding is a powerful and specific noncovalent interaction found in many organic molecules, including those in physical systems where it plays a critical role in supramolecular organization. H-bonding is also important in electrically conducting materials related to biology, such as melanin and indigo [1-5]. The study of H-bonded organic semiconductors is particularly relevant for applications that involve interfacing electronics with biological systems. Moreover, hydrogen bonds play a crucial role in various applications such as biomolecules, dyes, pigments, ionic conductors, and organic semiconductors [6-7]. In the field of organic electronics, which has transitioned from scientific research to mature commercial technologies, the study of the role of hydrogen bonding interactions in organic conducting and semiconducting materials is significant. H-bonding has been demonstrated to be a highly specific tool for self-organizing organic materials. While there have been many studies on the utilization of H-bonding in synthetic materials science, there have been relatively few in the field of organic electronics. H-bond mediated supramolecular semiconducting systems have been demonstrated for field-effect transistor and light-emitting diode applications[8-10].

The charge transfer rate is an important factor in establishing the structure-property relationship of molecules in the supramolecular semiconducting systems. The charge transfer rate depends on parameters such as reorganization energy and charge transfer integral. The charge transfer integral is related to the intensity of the electronic coupling constant, which is influenced by the geometry of the stacking interactions in the solid phase, including the distance between rings, pitch and roll distances and angles, and stacking type [11-14]. Experimental and theoretical studies have shown that a higher electronic coupling, achieved through increased overlap between adjacent rings and favorable stacking, results in a higher charge transfer integral. This is desirable for efficient charge transfer rates, as confirmed by Marcus Electron Theory[15]. Therefore, along with examining the single crystal structure and electronic interactions of molecules, it is necessary to conduct theoretical investigations to predict the charge transport rate of practical materials. The reorganization energy determines the change in energy of the molecule due to the presence of excess charge and the surrounding medium. Minimizing the reorganization energy and maximizing the transfer integral are considered favorable for molecular design[16].

In this study, the effects of molecular packing, noncovalent interactions, and crystal geometry on the charge transport properties of the molecules were analyzed through crystallographic and theoretical studies to fully understand the structure-property relationships and predict charge carrier mobility from a microscopic perspective. The studied molecule behaves as an n-type molecule

having te smaller electron reorganization energy (0.007 eV) which is smaller than reorganization of the pentacene known as the best semiconducting material than that of hole of the studied molecule (0.05 eV) It was envisioned that better n-type transistors could be achieved. Additionally,its electron charge transfer integral (0.8 eV) was found high due to distinct aggregation cluster in its crystal phase. Furthermore, the electron charge transfer rate ($6.02x10^{11}$ 1/s) was predicted to be very high according to the Marcus Electron Transfer Theory, taking into account the reorganization energy and transfer integral.

One of the important goals of this study was to investigate 1,1-Diamino-2,2-dinitroethylene molecule which was studied in terms of crystal structure but charge transfer properties was not investigated for optoelectronic materials, as the use of this derivatives in the optoelectronic field has been relatively rare. Based on the results, the molecule is considered highly suitable for n-type organic semiconducting single crystals with high mobility and preferred clustering modes in the solid phase. This study paves the way for designing new organic semiconductors of the derivatives of the studied molecule with high mobility. In addition this research suggests that this study could lead to the development of novel n-type optoelectronic materials combine low internal electron reorganization energy with high electron affinity.

TEORETICAL METHODOLOGY

The optimized geometry of the molecule in its neutral and charged states were obtained using the B3LYP hybrid functional and 6-31 G (d,p) basis set at the DFT level. These computational methods provide sufficient accuracy for small organic molecules. The electronic and optical properties were analyzed using the B3LYP functionals [17]. The charge transfer rates of the molecule were calculated based on the reorganization energy and charge transfer integral, given by Marcus Electron Theory in the following equation.

$$k = \frac{4\pi^2}{\lambda}\frac{1}{\sqrt{4\pi h k_B T}}t^2 \exp\left(-\frac{\lambda}{4k_B T}\right) \quad (1)$$

The reorganization energy (λ) includes two components: the inner reorganization energy, which accounts for the geometric changes within the molecule upon adding or removing an electron, and the outer reorganization energy, which reflects modifications caused by polarization effects in the surrounding medium. In this study, only the inner reorganization energy was calculated, as the outer reorganization energy is typically challenging to compute due to its requirement for considering both electronic polarization and electron-phonon coupling of the surrounding molecules. The inner reorganization energy (λ) is further divided into two parts: λ^1 represents the

geometry relaxation energy from the neutral to the charged state, and λ^2 represents the geometry relaxation energy from the charged to the neutral state.

$$\lambda = \lambda_{rel}^1 + \lambda_{rel}^2$$

To evaluate λ, the two terms were computed directly from the adiabatic potential energy surfaces. The λ_anion corresponds to the geometry relaxation energy for a molecule transitioning from the neutral state to the charged state, while the λ_cation represents the geometry relaxation energy for a molecule transitioning from the charged state to the neutral state. These calculations involve determining the energies of the neutral and charged states at different molecular geometries [18-20].

$$\lambda_{anion} = \lambda_{rel}^1 + \lambda_{rel}^2 = \left[E^{(0)}(M^-) - E^{(0)}(M)\right] + \left[E^{(1)}(M) - E^{(1)}(M^-)\right] \quad (3)$$

$$\lambda_{cation} = \lambda_{rel}^1 + \lambda_{rel}^2 = \left[E^{(0)}(M^+) - E^{(0)}(M)\right] + \left[E^{(1)}(M) - E^{(1)}(M^+)\right]$$

The ionization energy, both adiabatic (IPa) and vertical (IPv), as well as the adiabatic/vertical electron affinity (EAa)/(EAv) of the molecules, were calculated using the energy differences between the neutral and charged states at various geometries.

$$IPa = E^0(M)^+ - E^0(M) \text{ and } IPv = E^1(M)^+ - E^0(M) \quad (4)$$

$$EAa = E^0(M) - E^0(M)^- \text{ and } EAv = E^0(M) - E^1(M)^-$$

The charge transfer integral of the molecules was determined using the DFT-optimized molecular configurations of the dimeric structures formed by hydrogen bonding interactions. In these dimers, the HOMO (LUMO) levels from each molecule combine to form the HOMO and HOMO-1 (LUMO and LUMO+1) levels. The charge transfer integral (t) is approximated as half the energy difference between the HOMO and HOMO-1 levels for hole transfer or the LUMO and LUMO+1 levels for electron transfer. The accurate calculation of t assumes that the two monomers exhibit symmetric transformation, resulting in equal site energies between them and negligible polarization effects. The hopping integral for intermolecular hole transfer and electron transfer, t_hole and t_electron, respectively, were estimated using the energy splitting between the corresponding electronic levels [21].

$$t_{hole} = \frac{HOMO - HOMO-1}{2} \qquad t_{electron} = \frac{LUMO - LUMO+1}{2} \quad (5)$$

RESULTS&DISCUSSIONS

The arrangement of π-conjugated molecules is of great importance in determining the charge transport properties of organic semiconductors. This is because the molecular organization directly influences the degree of intermolecular orbital overlap, which is critical for efficient charge transport [22]. In small-molecule organic semiconductors, the efficient transfer of charge carriers between individual molecules is essential for proper functionality. The size and arrangement of the molecular crystals play a crucial role in enabling efficient charge transport. Hydrogen bonding offers a means to facilitate the reorganization of molecular packing through self-assembly [23]. However, in hydrogen-bonded small molecules, the charge transfer process often leads to poor solubility in most organic solvents due to the strong hydrogen bonding interactions. This results in the formation of crosslinked network-like materials in the solid state, which are challenging to use for direct fabrication of organic field-effect transistors (OFETs) using solution processing method.[24]

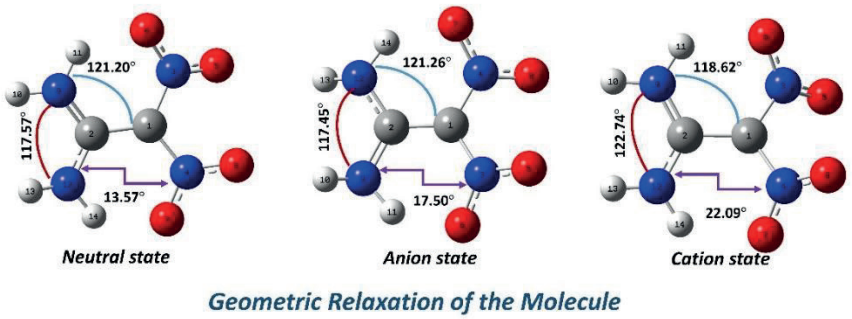

Figure 1. Neutral and charged optimized structures of the molecule

The crystal structure of the molecule (1,1-Diamino-2,2-dinitroethylene) was taken from Cambridge crystallographic database sample 130779 (a = 6.941(1)Å, b =6.659(1) Å , c = 11.315(2) Å, Z = 4 and α=90°,β=90.55(2)°,γ=90°) [25].. The charge transfer and electronic properties of the molecule were examined by analyzing their hole and electron reorganization energies, charge transfer integral, energy gap, ionization potential (IP), and electron affinity (EA), as summarized in Table 1. The optimized structures of the molecule in its neutral and charged states.

The torsional angles between the diamino and dinitroethylene moities in the gas phase is 13.57° which closely match the values observed in the solid phase. When a molecule undergoes charge transfer, it undergoes geometric relaxation to accommodate the new charge distribution. As a result, the torsional angles of molecule change to 17.50° and 22.09° in the anionic and

cationic states, respectively. The change in torsion angles in the cationic state is more high for the molecule compared to the anionic state, indicating that the electron reorganization energy is smaller than that of hole. The same change in the torsisonal angles are observed other fragments of the molecule. This observation is further supported by the calculation of hole and electron reorganization energies listed in Table 1. The calculated reorganization energies for charge transfer are 0.05 eV (μhole) and 0.007 eV (μelectron), respectively. Due to the lower hole reorganization energy, the molecule exhibits a high intrinsic electron transfer rate (6.02×10^{11} s^{-1}), Consequently, The molecule can be identified n-type semiconductors, with the majority carriers being electrons. The presence of nitro groups in the π system contributes to the reduction in electron reorganization energies.

To gain further insight into the charge transfer process and the strength of electronic coupling between adjacent molecules, the charge transfer integrals (t) of the molecule were determined. The value of the transfer integral t is highly dependent on the molecular configuration of the dimer formed through hydrogen bonding interactions. The packing structures of the molecules, as revealed by X-ray diffraction analysis, cluster type stacking interactions along the (001) plane, creating charge transport channels in the solid phases through N-H…O hydrogen bondings (Figure 2). By considering these charge transport channels, the molecular cluster was taken into account for the calculation of charge transfer integrals. The geometries of the cluster were optimized using the B3LYP/6-31G(d,p) method, by freezing the coordinate of the fragments. The LUMO and HOMO levels of the two monomers were combined to create LUMO+1, LUMO, HOMO, and HOMO-1 in the cluster configurations. Along the channel, the energy level splitting between HOMO and HOMO-1 is approximately 0.02 eV while the energy splitting between LUMO and LUMO+1 is 0.004 eV for the molecule. In the charge transport channels of the molecules, the clusters exhibit symmetry, and are equivalent under symmetric transformations. Consequently, the electrostatic polarization effect becomes negligible, with site energies approximately equal [26]. It is worth noting that the highest charge transfer integral in the molecules occurs along the cluster sstacking arrangements with the hydrogen bondings along the (100).

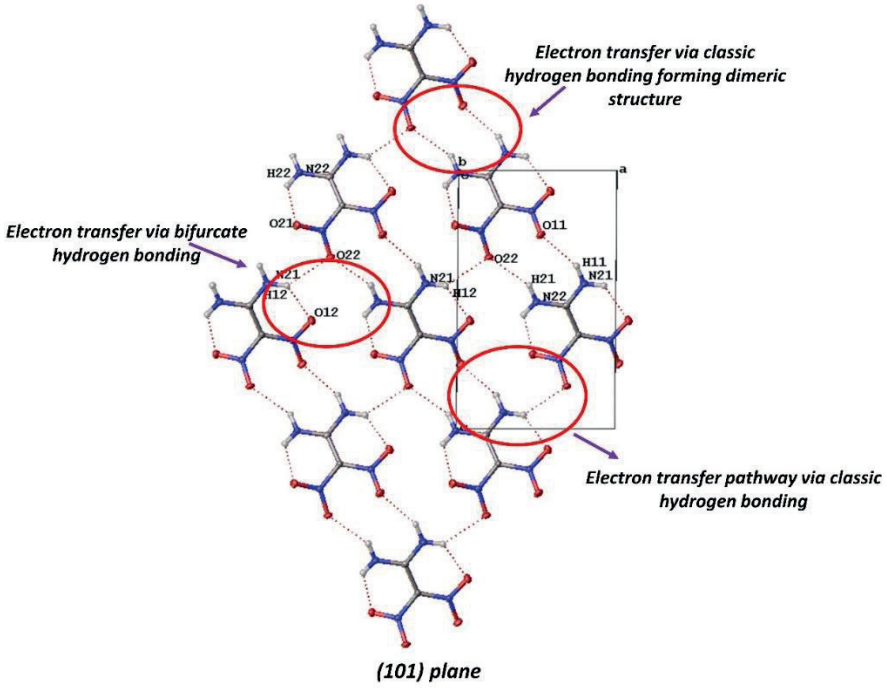

Figure 2. The view of the charge pathways of the molecule in solid phase

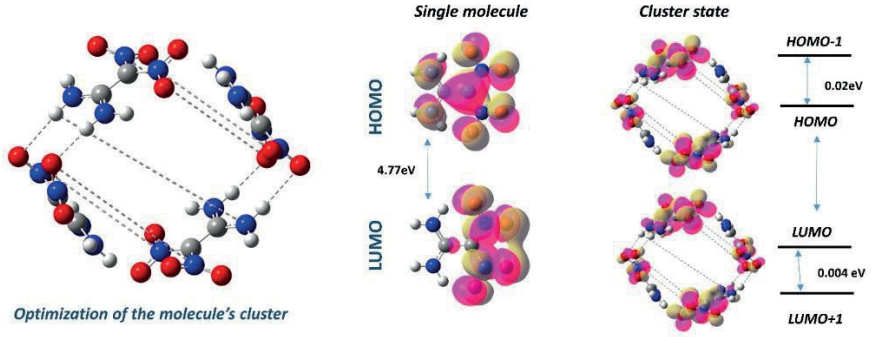

Figure 3. Energy level diagram of the frontier orbitals for cluster state of the molecule in solid phase.

Table 1. The value of parameters determining the charge transfer property of the molecule.

Molecule	λ_{hole} (eV)	λ_{electr} (eV)	t_{elec}	t_{hole}	IPa (eV)	IPv(eV)	Ea (e V)	Ev (e V)	$kt_{hol\ e}$ (s^{-1})	$kt_{electron}$ (s^{-1})
Molecule	0.05	0.007	0.8	0.01	8.80	9.21	0. 53	0.0 4	2.32 x10^{1} ^{1}	6.02x10 ^{11}

MOLECULAR IONIZATION POTENTIAL AND ELECTRON AFFINITY

The injection of holes and electrons is a crucial aspect in the development of optimized electronic devices. Information about the performance and stability of organic devices can be obtained from parameters such as ionization potential (IP) and electron affinity (EA), which determine the energy barrier for hole and electron injection into a molecule [27].

For organic semiconductors, air stability in the environment is a critical feature, along with charge transport characteristics [28]. The ionization energy represents the energy required to remove electrons from a neutral molecule, creating a cationic molecule. Higher IP values indicate that the molecule is less likely to become a cation in the presence of OH- (H2O) or O2- (O2) ions in the atmosphere. Practical applications favor molecules that are more stable and less prone to oxidation [29]. The EA values of the molecule is 0.53 eV (Table 6). In devices, a high EA value implies a small injection energy for electrons, which is desirable when using commonly used metallic electrodes (with an energy level of 3 eV and Lumo of the molecule iss 2.29 eV). Therefore, based on these EA values, molecule exhibits better electron transport feature, as it lowers the energy barrier for electron injection (energy barrier 0.007 eV). Additionally, the HOMO energy level of compound (7.05 eV) does not align well with the work function of the gold electrode (-5.2 eV). Consequently, hole injection from gold to the organic semiconductor is very hard. The molecule can not show p type semiconductor properties.

FRONTIER MOLECULAR ORBITALS

Frontier orbitals are parameters that describe the electron gain or loss state of a molecule. In this study, the incorporation of nitro groups into the terminal sides of the molecule significantly affects the atomic and subatomic orbitals of the compound. The frontier orbitals of the molecule are depicted in Figure 3. The HOMO and LUMO molecular orbital densities primarily arise from the delocalized π-orbitals of the structure. The nitro groups contribute significantly to the HOMO and LUMO, leading to a push-pull effect

commonly observed in D-π-A molecules, [30–31]. In push-pull molecules, the charge is withdrawn from the donor by the acceptor side of the molecule, generating polarization and facilitating the interaction between the donor and acceptor groups known as intramolecular charge transfer (ICT). The ICT process creates low-energy molecular orbitals, as evident in molecule.

HIRSHFELD SURFACE ANALYSIS

Understanding intermolecular interactions is crucial for comprehending the properties and behavior of molecular crystals. Hirshfeld surface analysis has emerged as a powerful tool in the field of crystallography for investigating these interactions. Hirshfeld surface analysis is based on the concept of the Hirshfeld partitioning of the crystal electron density. It involves the construction of a three-dimensional molecular surface that encloses each atom, revealing its associated region of electron density [32-33]. The surface is color-coded to represent the contribution of neighboring atoms to the Hirshfeld surface points. The closer the contacts between atoms, the more significant their contribution to the surface. By analyzing the shape, size, and features of the Hirshfeld surface, valuable information about intermolecular interactions can be obtained. Prominent intermolecular interactions, such as hydrogen bonds, π-π stacking, and van der Waals contacts, can be identified and characterized using Hirshfeld surface analysis. The analysis enables the identification of key interactions governing crystal packing and offers a deeper understanding of the structural stability and properties of the crystal. In materials science, it provides insights into the properties of functional materials, such as organic semiconductors and metal-organic frameworks. The ability to quantify intermolecular interactions using Hirshfeld surface analysis has revolutionized the field of crystallography, facilitating the interpretation and prediction of crystal structures and properties[34].

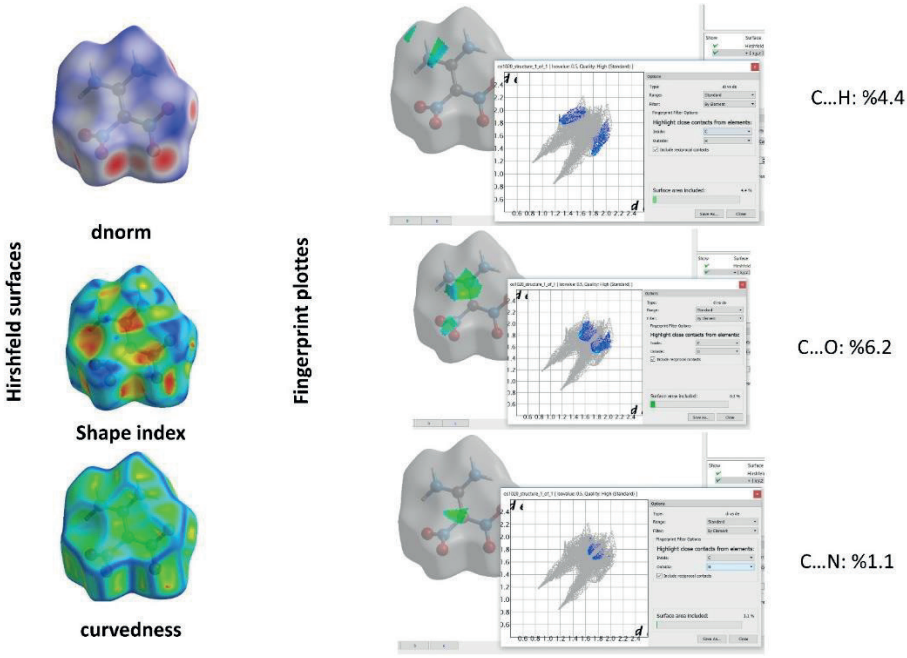

Figure 4. Views of the hirshfeld surfaces mapped with shape-index and curvedness, and fingerprint plotts for compounds.

Hirshfeld surface analysis provided distinct insights into the intermolecular interactions present in the crystal structure of the studied molecule. The analysis revealed that in the molecule, the C···O , C…H and C…N contacts are in the range of 6.2%, 4.4& and 1.1% respectively. These interactions were visualized as spikes in the donor and acceptor regions of the fingerprint plot. These C…H interactions were identified as large red spots on the dnorm surface, indicating its close proximity within the crystal structure and attributes C-H…N hydrohe bonds. A significant feature was the intermolecular c···H contacts, constituting 6.6% of the total Hirshfeld surfaces in the molecule. These contacts were represented by adjacent deep-red regions on the dnorm map.

CONCLUSIONS

In this study, we conducted an investigation into the electronic properties, and charge transport characteristics of studied molecule. This was achieved through techniques including density functional theory calculations, and interpretation using Marcus Electron Theory. We calculated the optimized geometric structures, reorganization energy, charge transfer integral, charge transsfer rate, frontier orbitals, ionization potential (IP), and electronic affinity

(EA) of the molecule. Our aim was to establish the relationship between the molecular structure and properties, considering its crystal geometry, hydrogen bonding interactions, and aggregation modes in the solid phase. The incorporation of nitro groups into the terminal side of the molecular skeleton caused to n-type semiconductor material behavior. From the Marcus Electron Theory calculations, the charge transfer rate for the electron of the molecule was determined to be $6.02x10^{11}s^{-1}$, while that of hole was $2.32x10^{11}$ s^{-1}. Consequently, the studiedd molecule can be considered highly suitable n-type organic semiconducting single crystals, exhibiting high mobility and preferred clusster modes through strong hydrogen bondings in the solid phase.

REFERENCES

[1] Thomas, R., Varghese, S., and Kulkarni, G. U. (2009). The influence of crystal packing on the solid state fluorescence behavior of alkyloxy substituted phenyleneethynylenes. J. Mater. Chem., 19, 4401–4406.

[2] He, L., Duan, L., Qiao,J., Wang, R., Wei, P., Wang, L., and Qiu, Y. (2008). Blue-Emitting Cationic Iridium Complexes with 2-(1*H*-Pyrazol-1-yl) pyridine as the Ancillary Ligand for Efficient Light-Emitting Electrochemical Cells. Adv. Funct. Mater.,18, 2123–2131.

[3] Karabıyık, H., Karabıyık, H. and Ocak İskeleli, N. (2012). Hydrogen-bridged chelate ring-assisted p-stacking interactions. Acta Cryst., B68, 71–79.

[4] Chen, F., Wang, Y., Zhang, W., Tian, T., Bai, B., Wang, H., Bai, F. and Li, M. (2019). Role of Intermolecular Interactions in Molecular Packing of Alkoxy-Substituted Bis-1,3,4-oxadiazole Derivatives. Cryst. Growth Des., 19, 6100−6113.

[5] Kumar, S., Varghese, S., Suresh, C. H., Rath, N., and Das, S. (2009). Correlation between Solid-State Photophysical Properties and Molecular Packing in a Series of Indane-1,3 dione Containing Butadiene Derivatives. J. Phys. Chem., 113, 11927–11935.

[6] Song, K. C., Singh, R., Lee, J., Sin, D. H., Lee, H. and Cho, K. (2013). Propeller-shaped small molecule acceptors containing a 9,9'- spirobifluorene core with imide-linked perylene diimides for nonfullerene organic solar cells. J. Name., 00, 1-3.

[7] Han, L., Li, B., and Ying, J. (2007). (4,4'-Dimethyl-2,2'-bipyridine- κ^2N, N^1)-bis[2-(2-pyridyl) phenyl- κ^2N, C^1]- iridium(III) hexafluoridophosphate. Acta Cryst., E63, m3133.

[8] Gierschner, J., and Park, S. Y. (2013). Luminescent distyrylbenzenes: tailoring molecular structure and crystalline morphology. J. Mater. Chem. C, 1, 5818–5832.

[9] Fu, F., Liao, K., Ma, J., Cheng, Z., Zheng, D., Gao, L., Liu, C., Li, S. and Li, W. (2019). How intermolecular interactions influence electronic absorption spectra: insights from the molecular packing of uracil in condensed phases. Phys. Chem. Chem. Phys.

[10] Yao, Z., Wang, J. and Pei, J. (2018). Control of π−π Stacking via Crystal Engineering in Organic Conjugated Small Molecule Crystals. Cryst. Growth Des.

[11] Lee, E. C., Hong, B. H., Lee, J. Y., Kim, J. C., Kim, D., Kim, Y., Tarakeshwar, P. and Kim, K. S. (2005). Substituent Effects on the Edge-to-Face Aromatic Interactions. J. AM. CHEM. SOC., 127, 4530-4537.

[12] Wang, Z., Shao, H., Ye, J., Zhang, L. and Lu, P. (2007). Substituent Effects on Crosslike Packing of 2',7' -Diarylspiro(cyclopropane-1,9'-fluorene) Derivatives: Synthesis and Crystallographic, Optical, and Thermal Properties. Adv. Funct. Mater., 17, 253–263.

[13] Chen, Y., Lam, J., Kwok, R., Liu, B. and Tang, B.Z. (2019). Aggregation-induced emission: fundamental understanding and future developments. Mater. Horiz., 6, 428—433.

[14] Zhang, H., Zhang, Z., Ye, K., Zhang, J. and Wang, Y. (2006). Organic Crystals with Tunable Emission Colors Based on a Single Organic Molecule and Different Molecular Packing Structures. Adv. Mater., 18, 2369–2372.

[15] Dou, J., Zheng, Y., Yao, Z., Yu, Z., Lei, T., Shen, X., Luo, X., Sun, J., Zhang, S., Ding, Y., Han, G., Yi, Y., Wang,J. and Pei, J. (2015). Fine Tuning of Crystal Packing and Charge Transport Properties of BDOPV Derivatives through Fluorine Substitution. J. Am. Chem. Soc.

[16] Kumar, S., Varghese, S., Suresh, C. H., Rath,N. and Das, S. (2009). Correlation between Solid-State Photophysical Properties and Molecular Packing in a Series of Indane-1,3-dione Containing Butadiene Derivatives. J. Phys. Chem. C, Vol. 113, No. 27.

[17] NBO Version 3.1, E. D. Glendening, A. E. Reed, J. E. Carpenter, and F. Weinhold.

[18] Irfan, A., Al-Sehemi, A., Chaudhry, A. R., Muhammad S. (2018). The structural, electro-optical, charge transport and nonlinear optical properties of oxazole (4Z)-4-Benzylidene-2-(4-methylphenyl)-1,3-oxazol- 5(4H)-one derivative. Journal of King Saud University – Science, 30, 75–82.

[19] Yan, L., Zhao, Y., Yu, H., Hu, Z., He, Y., Li, A., Goto, O., Yan, C., Chen, T., Chen, R., Loo, Y., Perepichka, D., Meng, H. and Huang, W. (2013). Influence of Heteroatoms on the Charge Mobility of Anthracene Derivatives. J. Name., 00, 1-3.

[20] Zhang, Y., Cai, X., Bian, Y., Li, X. and Jiang, J. (2007). Heteroatom Substitution of Oligothienoacenes: From Good p-Type Semiconductors to Good Ambipolar Semiconductors for Organic Field-Effect Transistors. J. Phys. Chem., 112, 5148-5159.

[21] Zhang, M. and Zhao, G. (2012). Heteroatomic Effects on Charge Transfer Mobility of Dianthra[2,3- b:2',3-f] thieno[3,2 b]thiophene (DATT) and Its Derivatives. J. Phys. Chem., 116, 19197−19202.

[22] Chen, F., Wang, Y., Zhang, W., Tian, T., Bai, B., Wang, H., Bai, F. and Li, M. (2019). Role of Intermolecular Interactions in Molecular Packing of Alkoxy-Substituted Bis-1,3,4-oxadiazole Derivatives. Cryst. Growth Des., 19, 6100−6113.

[23] Chang, Y., Lu, Z., An, L. and Zhang, J. (2012). From Molecules to Materials: Molecular and Crystal Engineering Design of Organic Optoelectronic Functional Materials for High Carrier Mobility. J. Phys. Chem., 116, 1195–1199.

[24] XIE, Z., YANG, B., LIU, L. and MA, Y. (2013). J-Type Dipole Stacking and Strong π-π Interactions In The Crystals of Distyrylbenzene Derivatives: The Crystal Structures, High Luminescence Properties and Prediction of High Mobility. Journal of Molecular and Engineering Materials Vol. 1, No. 3 1340002 (13 pages).

[25] Bemm, U. and Ostmark, H. (1998). 1,1-Diamino-2,2-dinitroethylene:t a Novel Energetic Material with Infinite Layers in Two Dimensions. *Acta Cryst*. C54, 1997-1999.

[26] Navamani, K., Saranya, G., Kolandaivel, P. and Senthilkumar, K. (2013). Effect of structural fluctuations on charge carrier mobility in thiophene, thiazole and thiazolothiazole based oligomers. Phys.Chem. Chem. Phys., 15, 17947.

[27] LI, H., WANG, X. and LI, Z. (2012). Theoretical study of the effects of different substituents of tetrathiafulvalene derivatives on charge transport. Chin Sci Bull, 57: 4049-4056.

[28] Siddiqui, S. A., Al-Hajry, A., Al-Assiri, M. S. (2016). Ab Initio Investigation of 2,2'-Bis(4-trifluoromethylphenyl)- 5,5'-Bithiazole for the Design of

Efficient Organic Field-Effect Transistors. International Journal of Quantum Chemistry, 116, 339–345.

[29] Cias, P., Slugovc, C., and Gescheidt, G. (2011). Hole Transport in Triphenylamine Based OLED Devices: From Theoretical Modeling to Properties Prediction. J. Phys. Chem., 115, 14519–14525.

[30] Bure, F. (2014). Fundamental aspects of property tuning in push–pull molecules. RSC Adv., 4, 58826–58851.

[31] Oliva, M. M., Casado, J., Raposo, M., Fonseca, M., Hartmann, H., Hernandez, H. and Navarrete, L. (2006). Structure-Property Relationships in Push-Pull Amino/Cyanovinyl End-Capped Oligothiophenes: Quantum Chemical and Experimental Studies. *J. Org. Chem.*, *71*, 7509-7520.

[32] Spackman, M. A., and Jayatilaka, D. (2009). Hirshfeld surface analysis. CrystEngComm, 11, 19—32.

[33] Spackman, P. R., Turner, M. J., McKinnon, J. J., Wolff, S. K., Grimwood, D. J., Jayatilaka, D. and Spackman, M. A. (2021). CrystalExplorer: a program for Hirshfeld surface analysis, visualization and quantitative analysis of molecular crystals. J. Appl. Cryst., 54.

[34] Psycharis, V., Dermitzaki, D. and Raptopoulou, C. P. (2021). The Use of Hirshfeld Surface Analysis Tools to Study the Intermolecular Interactions in Single Molecule Magnets. Crystals, 11, 1246.

Chapter 12

INVOLUTE CURVES OF ANY NON-UNIT SPEED CURVE IN EUCLIDEAN 3-SPACE

Sümeyye GÜR MAZLUM[1]
Mehmet BEKTAŞ [2]

1 Gümüşhane University, Kelkit Aydın Doğan Vocational School, Department of Computer Technology, Gümüşhane, Türkiye, sumeyyegur@gumushane.edu.tr, ORCID: https://orcid.org/0000-0003-2471-1627
2 Fırat University, Faculty of Science, Department of Mathematics, Elazığ, Türkiye, mbektas@firat.edu.tr, ORCID: https://orcid.org/0000-0002-5797-4944

1. Introduction

The Euclidean space is a comprehensive space that has been discussed with the basic information in the book "Euclid's Elements" written by Euclid in 300 BC, and has been continuously developed by various mathematicians since then, (Sertöz, 2019). Differential geometry studies in Euclidean space focused on the theory of surfaces, lines and curves, (Do Carmo, 2016; Hacısalihoğlu, 2000). The curves theory is one of the topics that is always up to date. Especially special curve types such as helices find a place for themselves in technological and scientific studies. Apart from the special curves recognized as single, there are also some curves referred to as pairs: Bertrand curves, involute-evolute curves, Mannheim curves etc. There are many studies on these curves in Euclidean 3-space, (As and Sarıoğlugil, 2014; Azak, 2021; Bektaş and Yüce, 2013; Çalışkan and Bilici, 2002; Hanif and Hou, 2018; Honda and Takahashi, 2020; Jianu et al., 2021; Kasap et al., 2009; Öztürk et al., 2018; Yılmaz and Erdem, 2021). The curve with the tangential line perpendicular to the tangential line of a curve is called the involute curve of the first curve, in the circumstances the first curve is called the evolute curve. Although these curves are called pairs, it is possible to find more than one evolute curve of an involute curve. This also applies to other curve pairs. On the other hand, studies on curves are generally on unit-speed curves for ease of processing. For this reason, the results obtained for unit speed curves cannot be applied directly to non-unit speed curves. In such cases, the first thing that comes to mind is to convert the curve to a unit speed curve. But instead of repeating this process for each different non-unit speed curve, it is wise to derive the general expressions for well-known theorems and the corollaries of these curves. Some studies on the non-unit speed curves are (Gür Mazlum and Bektaş, 2022; Gür Mazlum et al., 2022; Monterde 2020). One of the most important tools used to determine the geometric properties of a curve is the Frenet frame of the curve. In addition, the curvature and torsion of the curve also have an significant role in specifying the characteristic features of the curve. Zero curvature means the curve is straight and zero torsion means the curve is planar. Derivatives of Frenet vectors are obtained in terms of the curvature, torsion and Frenet vectors. These equations are called Frenet derivative equations. Also, the Darboux vector is known as the axis of motion of the Frenet frame. The unit Darboux vector is called pole vector. This vector can also be expressed in terms of the angle between the binormal and tangent vectors. Calculations of all these elements are given separately for both unit speed and non-unit speed curves, (Hacısalihoğlu, 2000). In the light of these considerations, the relationships of the geometric properties between a non-unit speed curve and its involute curves have been the main subject of this study. Thus, the distance between of these curves has obtained. Besides the relationships between the curvatures, torsions, Frenet vectors, Frenet derivative equations, Darboux vectors and pole vectors of these curves have

attained. In addition, these curves are shown on an example and their graphs are drawn.

2. Preliminaries

Let the curve $\left(\vec{\Im}\right)$ be a differentiable space curve in $\mathbb{E}^3$. If the velocity vector at each point is non-zero, then $\left(\vec{\Im}\right)$ is a regular curve. The tangent vector, the binormal vector and the principal normal vector of the regular curve $\left(\vec{\Im}\right)$ are

$$\begin{cases} \overrightarrow{\Upsilon_1} = \dfrac{\dot{\vec{\Im}}}{\left\|\dot{\vec{\Im}}\right\|}, \\ \overrightarrow{\Upsilon_3} = \dfrac{\dot{\vec{\Im}} \wedge \ddot{\vec{\Im}}}{\left\|\dot{\vec{\Im}} \wedge \ddot{\vec{\Im}}\right\|}, \\ \overrightarrow{\Upsilon_2} = \overrightarrow{\Upsilon_3} \wedge \overrightarrow{\Upsilon_1}, \end{cases} \tag{1}$$

respectively. Here, if $\left\| \dot{\vec{\Im}} \right\| \neq 1$, $\left(\vec{\Im}\right)$ is a non-unit speed curve. So $\left\{\overrightarrow{\Upsilon_1}, \overrightarrow{\Upsilon_2}, \overrightarrow{\Upsilon_3}\right\}$ is Frenet frame of $\left(\vec{\Im}\right)$. Also curvature and torsion of $\left(\vec{\Im}\right)$ are

$$\wp_1 = \frac{\left\|\dot{\vec{\Im}} \wedge \ddot{\vec{\Im}}\right\|}{\left\|\dot{\vec{\Im}}\right\|^3} \tag{2}$$

and

$$\wp_2 = \frac{\left\langle \dot{\vec{\Im}} \wedge \ddot{\vec{\Im}}, \dddot{\vec{\Im}} \right\rangle}{\left\|\dot{\vec{\Im}} \wedge \ddot{\vec{\Im}}\right\|^2} \tag{3}$$

respectively. The Frenet derivative formulae of $\left(\vec{\Im}\right)$ are

$$\begin{bmatrix} \dot{\overrightarrow{\Upsilon}}_1 \\ \dot{\overrightarrow{\Upsilon}}_2 \\ \dot{\overrightarrow{\Upsilon}}_3 \end{bmatrix} = \begin{bmatrix} 0 & \left\| \dot{\vec{\Im}} \right\| \wp_1 & 0 \\ -\left\| \dot{\vec{\Im}} \right\| \wp_1 & 0 & \left\| \dot{\vec{\Im}} \right\| \wp_2 \\ 0 & -\left\| \dot{\vec{\Im}} \right\| \wp_2 & 0 \end{bmatrix} \begin{bmatrix} \overrightarrow{\Upsilon}_1 \\ \overrightarrow{\Upsilon}_2 \\ \overrightarrow{\Upsilon}_3 \end{bmatrix}. \tag{4}$$

The Darboux vector of $\left(\vec{\Im}\right)$ is

$$\vec{\Psi} = \left\| \dot{\vec{\Im}} \right\| \left(\wp_2 \overrightarrow{\Upsilon}_1 + \wp_1 \overrightarrow{\Upsilon}_3 \right) \tag{5}$$

and the norm of this vector is

$$\left\| \vec{\Psi} \right\| = \left\| \dot{\vec{\Im}} \right\| \sqrt{\wp_1^2 + \wp_2^2} \,. \tag{6}$$

The unit pole vector of $\left(\vec{\Im}\right)$ is

$$\vec{\Omega} = \frac{\vec{\Psi}}{\left\| \vec{\Psi} \right\|} = \sin\omega \ \overrightarrow{\Upsilon}_1 + \cos\omega \ \overrightarrow{\Upsilon}_3 \,, \tag{7}$$

here ω is the angle between $\overrightarrow{\Upsilon}_3$ and $\vec{\Psi}$, Figure 1.

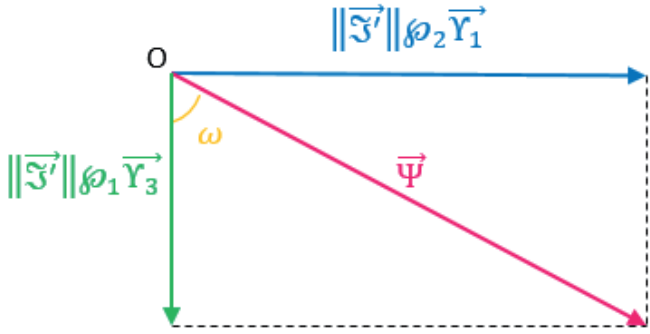

Figure 1. The Darboux vector of $\left(\vec{\Im}\right)$

3. Involute Curves of Any Non-Unit Speed Curve in Euclidean 3-Space

Let $\left(\vec{\Im}\right) = \vec{\Im}(t)$ and $\left(\overrightarrow{\Im^*}\right) = \overrightarrow{\Im^*}\left(t^*\right)$ be two non-unit speed regular curves with the parameters t and t^* in Euclidean 3-space $\mathbb{E}^3$, respectively. Considering (1), there are the following equations for these curves:

$$\xi(t)=\left\|\frac{d\vec{\Im}(t)}{dt}\right\|=\left\|\dot{\vec{\Im}}(t)\right\|, \tag{8}$$

$$\xi^*(t^*)=\left\|\frac{d\vec{\Im}^*(t^*)}{dt^*}\right\|=\left\|\dot{\vec{\Im}}^*(t^*)\right\|. \tag{9}$$

Definition 2.1. Let $\left\{\vec{\Upsilon}_1(t),\ \vec{\Upsilon}_2(t),\ \vec{\Upsilon}_3(t)\right\}$ and $\left\{\vec{\Upsilon}_1^*(t^*),\ \vec{\Upsilon}_2^*(t^*),\ \vec{\Upsilon}_3^*(t^*)\right\}$ be Frenet frames of $\left(\vec{\Im}\right)$ and $\left(\vec{\Im}^*\right)$, respectively. If $\vec{\Upsilon}_1(t)$ at the point $\vec{\Im}(t)$ of $\left(\vec{\Im}\right)$ passes throughout the point $\vec{\Im}^*(t^*)$ of $\left(\vec{\Im}^*\right)$ and $\left\langle\vec{\Upsilon}_1^*(t^*),\ \vec{\Upsilon}_1(t)\right\rangle=0$, then $\left(\vec{\Im}^*\right)$ is called involute curve of $\left(\vec{\Im}\right)$, Figure 2.

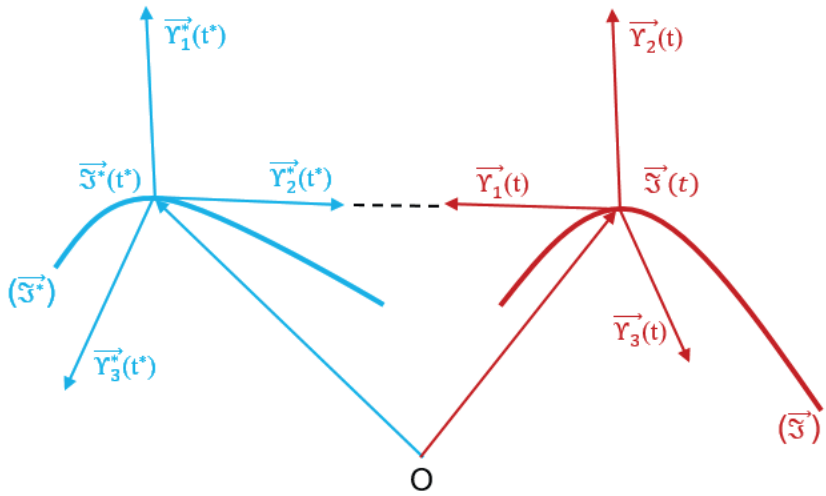

Figure 2. The non-unit speed curve $\left(\vec{\Im}\right)$ and its involute curve $\left(\vec{\Im}^*\right)$

Theorem 3.2. Let $\left(\vec{\Im}^*\right)$ be a involute curve of $\left(\vec{\Im}\right)$. In this case, there is the following equation:

$$\vec{\Im}^*(t^*)=\vec{\Im}(t)-\int\xi(t)dt\ \vec{\Upsilon}_1(t). \tag{10}$$

Proof. Since $\left(\vec{\Im}^*\right)$ is involute curve of $\left(\vec{\Im}\right)$, from Figure 2,

$$\overrightarrow{\Im^*}\left(t^*\right)=\vec{\Im}(t)+\zeta(t)\overrightarrow{\Upsilon_1}(t) \tag{11}$$

is written, where $\zeta(t)$ is a arbitrary function of t. If (11) is derived in terms of t,

$$\dot{\overrightarrow{\Im^*}}\left(t^*\right)\frac{dt^*}{dt}=\dot{\vec{\Im}}(t)+\dot{\zeta}(t)\overrightarrow{\Upsilon_1}(t)+\zeta(t)\dot{\overrightarrow{\Upsilon_1}}(t) \tag{12}$$

is gotten. If expressions (4), (8) and (9) are substituted in (12),

$$\xi^*\left(t^*\right)\frac{dt^*}{dt}\overrightarrow{\Upsilon_1^*}\left(t^*\right)=\left(\dot{\zeta}(t)+\xi(t)\right)\overrightarrow{\Upsilon_1}(t)+\xi(t)\zeta(t)\wp_1(t)\overrightarrow{\Upsilon_2}(t) \tag{13}$$

is obtained. If both sides of (13) are inner multiplied by $\overrightarrow{\Upsilon_1}(t)$,

$$\dot{\zeta}(t)=-\xi(t) \tag{14}$$

and so,

$$\zeta(t)=-\int\xi(t)dt \tag{15}$$

is found. If (13) is substituted in (11), the expression (10) is obtained.

Corollary 3.3. Let $\left(\overrightarrow{\Im^*}\right)$ be a involute curve of $\left(\vec{\Im}\right)$. The distance between of the points $\vec{\Im}(t)$ of $\left(\vec{\Im}\right)$ and $\overrightarrow{\Im^*}\left(t^*\right)$ of $\left(\overrightarrow{\Im^*}\right)$ is as follows:

$$\left|\zeta(t)\right|=\left|\int\xi(t)dt\right|. \tag{16}$$

Proof. From (11),

$$\overrightarrow{\Im^*}\left(t^*\right)-\vec{\Im}(t)=\zeta(t)\overrightarrow{\Upsilon_1}(t) \tag{17}$$

is gotten. If the norm of both sides of (17) is taken, the distance between of the points $\vec{\Im}(t)$ of $\left(\vec{\Im}\right)$ and $\overrightarrow{\Im^*}\left(t^*\right)$ of $\left(\overrightarrow{\Im^*}\right)$ is found as

$$\left\|\overrightarrow{\Im^*}\left(t^*\right)-\vec{\Im}(t)\right\|=\left|\zeta(t)\right|. \tag{18}$$

From (15) and (18), the expression (16) is obtained.

Theorem 3.4. Let $\left(\overrightarrow{\Im^*}\right)$ be a involute curve of $\left(\vec{\Im}\right)$. There is the following equation between the curvatures $\wp_1^*\left(t^*\right)$ of $\left(\overrightarrow{\Im^*}\right)$, $\wp_1(t)\neq 0$ of $\left(\vec{\Im}\right)$ and torsion $\wp_2(t)$ of $\left(\vec{\Im}\right)$:

$$\wp_1^*\left(t^*\right)=\frac{\sqrt{\wp_1^{\,2}\left(t\right)+\wp_2^{\,2}\left(t\right)}}{\wp_1\left(t\right)\left|\int\xi\left(t\right)dt\right|}. \tag{19}$$

Proof. If (14) and (15) are substituted in (13),

$$\xi^*\left(t^*\right)\frac{dt^*}{dt}\overrightarrow{\Upsilon_1^*}\left(t^*\right)=-\wp_1\left(t\right)\xi\left(t\right)\int\xi\left(t\right)dt\ \overrightarrow{\Upsilon_2}\left(t\right) \tag{20}$$

is gotten. If the norm of both sides of (20) is taken,

$$\frac{dt^*}{dt}=\frac{\wp_1\left(t\right)\xi\left(t\right)\left|\int\xi\left(t\right)dt\right|}{\xi^*\left(t^*\right)} \tag{21}$$

is found. So, from (20) and (21), $\overrightarrow{\Upsilon_1^*}\left(t^*\right)=\pm\overrightarrow{\Upsilon_2}\left(t\right)$ is obtained. Here,

$$\overrightarrow{\Upsilon_1^*}\left(t^*\right)=\overrightarrow{\Upsilon_2}\left(t\right) \tag{22}$$

is assumed. If (22) is derived in terms of t,

$$\frac{dt^*}{dt}\overrightarrow{\dot{\Upsilon}_1^*}\left(t^*\right)=\overrightarrow{\dot{\Upsilon}_2}\left(t\right)$$

and so (4) and (21) are considered,

$$\left|\int\xi\left(t\right)dt\right|\wp\left(t\right)\wp^*\left(t^*\right)\overrightarrow{\Upsilon_2^*}\left(t^*\right)=-\wp_1\left(t\right)\overrightarrow{\Upsilon_1}\left(t\right)+\wp_2\left(t\right)\overrightarrow{\Upsilon_3}\left(t\right) \tag{23}$$

is obtained. If the norm of both sides of (23) is taken,

$$\left|\int\xi\left(t\right)dt\right|\wp_1\left(t\right)\wp_2^*\left(t^*\right)=\sqrt{\wp_1^2\left(t\right)+\wp_2^2\left(t\right)}$$

is found. Thus, (19) is obtained.

Theorem 3.5. Let $\left(\overrightarrow{\Im^*}\right)$ be a involute curve of $\left(\vec{\Im}\right)$. There is the following equation between the torsion $\wp_2^*\left(t^*\right)$ of $\left(\overrightarrow{\Im^*}\right)$, curvature $\wp_1\left(t\right)\neq 0$ and torsion $\wp_2\left(t\right)$ of $\left(\vec{\Im}\right)$:

$$\wp_2^*\left(t^*\right)=\frac{\dot{\wp}_1\left(t\right)\wp_2\left(t\right)-\wp_1\left(t\right)\dot{\wp}_2\left(t\right)}{\xi\left(t\right)\wp_1\left(t\right)\left(\wp_1^2\left(t\right)+\wp_2^2\left(t\right)\right)\int\xi\left(t\right)dt}. \tag{24}$$

Proof. If the first, second and third derivatives of (10) in terms of t are taken,

$$\overrightarrow{\Im^*}\left(t^*\right)\frac{dt^*}{dt}=-\xi\left(t\right)\wp_1\left(t\right)\int\xi\left(t\right)dt\ \overrightarrow{\Upsilon_2}\left(t\right), \tag{25}$$

$$\begin{aligned}\dddot{\vec{\mathfrak{I}}}^{*}(t^{*})\frac{dt^{*2}}{dt^{2}} &= \xi^{2}(t)\wp_{1}^{2}(t)\int\xi(t)dt\ \vec{\Upsilon}_{1}(t)\\ &-\left(\xi^{2}(t)\wp_{1}(t)+\left(\xi(t)\dot{\wp}_{1}(t)+\dot{\xi}(t)\wp_{1}(t)\right)\int\xi(t)dt\right)\vec{\Upsilon}_{2}(t)\\ &-\wp_{1}(t)\wp_{2}(t)\xi^{2}(t)\int\xi(t)dt\ \vec{\Upsilon}_{3}(t)\end{aligned} \tag{26}$$

and

$$\begin{aligned}\dddot{\vec{\mathfrak{I}}}^{*}(t^{*})\frac{dt^{*3}}{dt^{3}} &= \left(\xi^{3}(t)\wp_{1}^{2}(t)+\left(2\dot{\xi}(t)\wp_{1}(t)+3\xi(t)\dot{\wp}_{2}(t)\right)\wp_{1}(t)\xi(t)\int\xi(t)dt\right)\vec{\Upsilon}_{1}(t)\\ &+\left(-\xi^{2}(t)\dot{\wp}_{1}(t)+\left(\wp_{1}^{2}(t)+\wp_{2}^{2}(t)\right)\wp_{1}(t)\xi^{3}(t)\int\xi(t)dt\right.\\ &\quad\left.-\left(\dot{\xi}(t)\wp_{1}(t)+\xi(t)\ddot{\wp}_{1}(t)\right)\int\xi(t)dt\right)\vec{\Upsilon}_{2}(t)\\ &-\left(\xi^{3}(t)\wp_{1}(t)\wp_{2}(t)+2\xi(t)\dot{\xi}(t)\wp_{1}(t)\wp_{2}(t)\int\xi(t)dt\right.\\ &\quad\left.+\left(2\dot{\wp}_{1}(t)\wp_{2}(t)+\wp_{1}(t)\dot{\wp}_{2}(t)\right)\xi^{2}(t)\int\xi(t)dt\right)\vec{\Upsilon}_{3}(t)\end{aligned} \tag{27}$$

are gotten, respectively. If the vector product operation is applied to (25) and (26),

$$\dddot{\vec{\mathfrak{I}}}^{*}(t^{*})\wedge\dddot{\vec{\mathfrak{I}}}^{*}(t^{*})=\frac{dt^{3}}{dt^{*3}}\wp_{1}^{2}(t)\wp_{2}(t)\xi^{3}(t)\left(\int\xi(t)dt\right)^{2}\left(\wp_{2}(t)\ \vec{\Upsilon}_{1}(t)+\wp_{1}(t)\ \vec{\Upsilon}_{3}(t)\right) \tag{28}$$

is found. If the inner product operation is applied to the expressions (27) and (28),

$$\left\langle\dddot{\vec{\mathfrak{I}}}^{*}(t^{*})\wedge\dddot{\vec{\mathfrak{I}}}^{*}(t^{*}),\dddot{\vec{\mathfrak{I}}}^{*}(t^{*})\right\rangle=\frac{dt^{6}}{dt^{*6}}\left(\xi^{5}(t)\wp_{2}(t)\wp_{1}^{3}(t)\left(\int\xi(t)dt\right)^{3}\left(\dot{\wp}_{1}(t)\wp_{2}(t)-\wp_{1}(t)\dot{\wp}_{2}(t)\right)\right) \tag{29}$$

is obtained. Also, if the norm of both sides of (28) is taken,

$$\left\|\dddot{\vec{\mathfrak{I}}}^{*}(t^{*})\wedge\dddot{\vec{\mathfrak{I}}}^{*}(t^{*})\right\|=\frac{dt^{6}}{dt^{*6}}\left(\xi^{6}(t)\wp_{1}^{4}(t)\left(\int\xi(t)dt\right)^{4}\left(\wp_{1}^{2}(t)+\wp_{2}^{2}(t)\right)\right) \tag{30}$$

is gotten. If (29) and (30) are substituted in (3), the expression (24) is obtained.

Theorem 3.6. Let $\left(\vec{\mathfrak{I}}^{*}\right)$ be a involute curve of $\left(\vec{\mathfrak{I}}\right)$. There is the following equation between the Frenet frames of $\left(\vec{\mathfrak{I}}^{*}\right)$ and $\left(\vec{\mathfrak{I}}\right)$:

$$\begin{bmatrix}\vec{\Upsilon}_{1}^{*}(t^{*})\\ \vec{\Upsilon}_{2}^{*}(t^{*})\\ \vec{\Upsilon}_{3}^{*}(t^{*})\end{bmatrix}=\begin{bmatrix}0 & 1 & 0\\ -\dfrac{\wp_{1}(t)}{\sqrt{\wp_{1}^{2}(t)+\wp_{2}^{2}(t)}} & 0 & \dfrac{\wp_{2}(t)}{\sqrt{\wp_{1}^{2}(t)+\wp_{2}^{2}(t)}}\\ \dfrac{\wp_{2}(t)}{\sqrt{\wp_{1}^{2}(t)+\wp_{2}^{2}(t)}} & 0 & \dfrac{\wp_{1}(t)}{\sqrt{\wp_{1}^{2}(t)+\wp_{2}^{2}(t)}}\end{bmatrix}\begin{bmatrix}\vec{\Upsilon}_{1}(t)\\ \vec{\Upsilon}_{2}(t)\\ \vec{\Upsilon}_{3}(t)\end{bmatrix}. \tag{31}$$

Proof. If (28) and (30) are substituted in (1),

$$\overrightarrow{\Upsilon_3^*}\left(t^*\right)=\frac{\wp_2\left(t\right)\overrightarrow{\Upsilon_1}\left(t\right)+\wp_1\left(t\right)\overrightarrow{\Upsilon_3}\left(t\right)}{\sqrt{\wp_1^2\left(t\right)+\wp_2^2\left(t\right)}} \tag{32}$$

is gotten. If (22) and (32) are substituted in (1),

$$\overrightarrow{\Upsilon_2^*}\left(t^*\right)=\frac{-\wp_1\left(t\right)\overrightarrow{\Upsilon_1}\left(t\right)+\wp_2\left(t\right)\overrightarrow{\Upsilon_3}\left(t\right)}{\sqrt{\wp_1^2\left(t\right)+\wp_2^2\left(t\right)}} \tag{33}$$

is found. From (22), (32) and (33), the expression (31) is obtained.

Theorem 3.7. Let $\left(\overrightarrow{\Im^*}\right)$ be a involute curve of $\left(\overrightarrow{\Im}\right)$. There is the following equation between the Darboux vectors $\overrightarrow{\Psi^*}\left(t^*\right)$ of $\left(\overrightarrow{\Im^*}\right)$ and $\overrightarrow{\Psi}\left(t\right)$ of $\left(\overrightarrow{\Im}\right)$:

$$\overrightarrow{\Psi^*}\left(t^*\right)=\xi^*\left(t\right)\left(\frac{\overrightarrow{\Psi}\left(t\right)+\dot{\omega}\left(t\right)\overrightarrow{\Upsilon_2}\left(t\right)}{\wp_1\left(t\right)\xi\left(t\right)\int\xi\left(t\right)dt}\right) \tag{34}$$

or

$$\overrightarrow{\Psi^*}\left(t^*\right)=\frac{dt}{dt^*}\left(\overrightarrow{\Psi}\left(t\right)+\dot{\omega}\left(t\right)\overrightarrow{\Upsilon_2}\left(t\right)\right), \tag{35}$$

here $\omega\left(t\right)$ is the angle between $\overrightarrow{\Upsilon_3}\left(t\right)$ and $\overrightarrow{\Psi}\left(t\right)$.

Proof. If (19), (22), (24) and (32) are substituted in (5),

$$\overrightarrow{\Psi^*}\left(t^*\right)=\frac{\xi^*\left(t\right)}{\int\xi\left(t\right)dt}\left(\frac{\wp_2\left(t\right)}{\wp_1\left(t\right)}\overrightarrow{\Upsilon_1}\left(t\right)+\frac{\dot{\wp}_1\left(t\right)\wp_2\left(t\right)-\wp_1\left(t\right)\dot{\wp}_2\left(t\right)}{\xi\left(t\right)\wp_1\left(t\right)\left(\wp_1^2\left(t\right)+\wp_2^2\left(t\right)\right)}\overrightarrow{\Upsilon_2}\left(t\right)+\overrightarrow{\Upsilon_3}\left(t\right)\right) \tag{36}$$

is gotten. Or from (5), the expression (36) is written as

$$\overrightarrow{\Psi^*}\left(t^*\right)=\frac{\xi^*\left(t\right)}{\wp_1\left(t\right)\xi\left(t\right)\int\xi\left(t\right)dt}\left(\overrightarrow{\Psi}\left(t\right)+\frac{\dot{\wp}_1\left(t\right)\wp_2\left(t\right)-\wp_1\left(t\right)\dot{\wp}_2\left(t\right)}{\wp_1^2\left(t\right)+\wp_2^2\left(t\right)}\overrightarrow{\Upsilon_2}\left(t\right)\right). \tag{37}$$

On the other hand, from Figure 1, it is known that

$$\cos\omega\left(t\right)=\frac{\wp_1\left(t\right)}{\sqrt{\wp_1^2\left(t\right)+\wp_2^2\left(t\right)}}, \tag{38}$$

$$\sin\omega\left(t\right)=\frac{\wp_2\left(t\right)}{\sqrt{\wp_1^2\left(t\right)+\wp_2^2\left(t\right)}}. \tag{39}$$

From (38) and (39),

$$\tan\omega\ (t)=\frac{\wp_2(t)}{\wp_1(t)} \tag{40}$$

is gotten. If (40) is derived in terms of t,

$$\left(1+\tan^2\omega\ (t)\right)\dot{\omega}\ (t)=\frac{\dot{\wp}_1(t)\wp_2(t)-\wp_1(t)\dot{\wp}_2(t)}{\wp_1^2(t)}$$

is found. From (40),

$$\dot{\omega}(t)=\frac{\dot{\wp}_1(t)\wp_2(t)-\wp_1(t)\dot{\wp}_2(t)}{\wp_1^2(t)+\wp_2^2(t)} \tag{41}$$

is gotten. If (41) is substituted in (37), the expression (34) is obtained. Or from (21) and (34), the expression (35) is obtained.

Corollary 3.8. Let $\left(\overrightarrow{\Im^*}\right)$ be a involute curve of $\left(\vec{\Im}\right)$. There is the following equation between the Frenet frames of $\left(\overrightarrow{\Im^*}\right)$ and $\left(\vec{\Im}\right)$:

$$\begin{bmatrix}\overrightarrow{\Upsilon_1^*}(t^*)\\ \overrightarrow{\Upsilon_2^*}(t^*)\\ \overrightarrow{\Upsilon_3^*}(t^*)\end{bmatrix}=\begin{bmatrix}0 & 1 & 0\\ -\cos\omega\ (t) & 0 & \sin\omega\ (t)\\ \sin\omega\ (t) & 0 & \cos\omega\ (t)\end{bmatrix}\begin{bmatrix}\overrightarrow{\Upsilon_1}(t)\\ \overrightarrow{\Upsilon_2}(t)\\ \overrightarrow{\Upsilon_3}(t)\end{bmatrix}, \tag{42}$$

here $\omega\ (t)$ is the angle between $\overrightarrow{\Upsilon_3}(t)$ and $\overrightarrow{\Psi}(t)$.

Proof. It is clear that (22), (32), (33), (38) and (39).

Corollary 3.9. Let $\left(\overrightarrow{\Im^*}\right)$ be a involute curve of $\left(\vec{\Im}\right)$. The binormal vector $\overrightarrow{\Upsilon_3^*}(t^*)$ of $\left(\overrightarrow{\Im^*}\right)$ and pole vector $\vec{\Omega}(t)$ of $\left(\vec{\Im}\right)$ are the same.

Proof. It is clear that from (7) and (42).

Corollary 3.10. Let $\left(\overrightarrow{\Im^*}\right)$ be a involute curve of $\left(\vec{\Im}\right)$. If $\left(\vec{\Im}\right)$ with non-zero curvature is a helix,

- the Darboux vectors $\overrightarrow{\Psi}(t)$ of $\left(\vec{\Im}\right)$ and $\overrightarrow{\Psi^*}(t^*)$ of $\left(\overrightarrow{\Im^*}\right)$ is linearly dependent,

- the binormal vector $\overrightarrow{\Upsilon_3^*}(t^*)$ of $\left(\overrightarrow{\Im^*}\right)$ and Darboux vector $\overrightarrow{\Psi^*}(t^*)$ of $\left(\overrightarrow{\Im^*}\right)$ is linearly dependent.

Proof. If $\left(\vec{\Im}\right)$ with non-zero curvature is a helix, it is known that

$$\frac{\wp_2(t)}{\wp_1(t)} = \text{constant}. \tag{43}$$

If (43) is derived in terms of t,

$$\dot{\wp}_1(t)\wp_2(t) - \wp_1(t)\dot{\wp}_2(t) = 0 \tag{44}$$

is gotten. So, from (41) and (44),

$$\dot{\omega}(t) = 0 \tag{45}$$

is obtained. Or, on the other hand, from (40) and (43),

$$\tan\omega(t) = \text{constant} \tag{46}$$

is gotten. If (46) is derived in terms of t,

$$\left(1+\tan^2\omega(t)\right)\dot{\omega}(t) = 0 \tag{47}$$

is found. Thus, from (47), the expression (45) is clearly obtained again. If (45) is substituted in (35),

$$\overrightarrow{\Psi^*}(t^*) = \frac{dt}{dt^*}\vec{\Psi}(t) \tag{48}$$

is gotten. From (7), (48) and Corollary 3.10,

$$\overrightarrow{\Psi^*}(t^*) = \frac{dt}{dt^*}\left\|\vec{\Psi}(t)\right\| \overrightarrow{\Upsilon_3^*}(t^*). \tag{49}$$

Corollary 3.11 is clear, from (48) and (49).

Theorem 3.11. Let $\left(\overrightarrow{\Im^*}\right)$ be a involute curve of $\left(\vec{\Im}\right)$. There is the following equation between the pole vectors $\overrightarrow{\Omega^*}(t^*)$ of $\left(\overrightarrow{\Im^*}\right)$ and $\vec{\Omega}(t)$ of $\left(\vec{\Im}\right)$:

$$\overrightarrow{\Omega^*}(t^*) = \frac{\xi(t)\sqrt{\wp_1^2(t)+\wp_2^2(t)}\,\vec{\Omega}(t) + \dot{\omega}(t)\,\overrightarrow{\Upsilon_2}(t)}{\sqrt{\dot{\omega}^2(t)+\xi^2(t)\left(\wp_1^2(t)+\wp_2^2(t)\right)}}. \tag{50}$$

Proof. If the norm of both sides of (35) is taken,

$$\left\|\overrightarrow{\Psi^*}(t^*)\right\| = \frac{dt}{dt^*}\sqrt{\left\|\vec{\Psi}(t)\right\| + \dot{\omega}^2(t)} \tag{51}$$

is gotten. From (7), (35) and (51),

$$\overrightarrow{\Omega^*}\left(t^*\right)=\frac{\overrightarrow{\Psi}(t)+\dot{\omega}\ (t)\overrightarrow{\Upsilon_2}(t)}{\sqrt{\dot{\omega}^{\,2}(t)+\xi^2(t)\left(\wp_1^2(t)+\wp_2^2(t)\right)}} \tag{52}$$

is found. From (5) and (52), the expression (50) is obtained.

Corollary 3.12. Let $\left(\overrightarrow{\Im^*}\right)$ be a involute curve of $\left(\vec{\Im}\right)$. If $\left(\vec{\Im}\right)$ with non-zero curvature is a helix, the pole vectors $\overrightarrow{\Omega^*}\left(t^*\right)$ of $\left(\overrightarrow{\Im^*}\right)$ and $\vec{\Omega}(t)$ of $\left(\vec{\Im}\right)$ are the same.

Proof. If expression (45) is substituted in (50),

$$\overrightarrow{\Omega^*}\left(t^*\right)=\vec{\Omega}(t) \tag{53}$$

is gotten. So, from (53), Corollary 3.13 is clear.

Theorem 3.13. Let $\left(\overrightarrow{\Im^*}\right)$ with non-zero curvature be a involute curve of $\left(\vec{\Im}\right)$ with non-zero curvature. Let $\omega\ (t)$ be the angle between $\overrightarrow{\Upsilon_3}(t)$ and $\overrightarrow{\Psi}(t)$ of $\left(\vec{\Im}\right)$, and $\omega^*\left(t^*\right)$ be the angle between of the vectors $\overrightarrow{\Upsilon_3^*}\left(t^*\right)$ and $\overrightarrow{\Psi^*}\left(t^*\right)$ of $\left(\overrightarrow{\Im^*}\right)$. There is the following equation between the angles $\omega^*\left(t^*\right)$ and $\omega\ (t)$:

$$\omega^*\left(t^*\right)=\arctan\left(\pm\frac{\dot{\omega}\ (t)}{\xi(t)\sqrt{\wp_1^2(t)+\wp_2^2(t)}}\right). \tag{54}$$

Proof. Similar to (40),

$$\tan\omega^*\left(t^*\right)=\frac{\wp_2^*\left(t^*\right)}{\wp_1^*\left(t^*\right)} \tag{55}$$

is written. If (19) and (24) are substituted in (55),

$$\tan\omega^*\left(t^*\right)=\pm\frac{\dot{\wp}_1(t)\wp_2(t)-\wp_1(t)\dot{\wp}_2(t)}{\xi(t)\left(\wp_1^2(t)+\wp_2^2(t)\right)^{3/2}} \tag{56}$$

is gotten. If (41) is substituted in (56), the expression (54) is obtained.

Corollary 3.14. Let $\left(\overrightarrow{\Im^*}\right)$ be a involute curve of $\left(\vec{\Im}\right)$. There is the following equation between the pole vector $\overrightarrow{\Omega^*}\left(t^*\right)$ of $\left(\overrightarrow{\Im^*}\right)$ and Frenet vectors of $\left(\vec{\Im}\right)$:

$$\begin{aligned}\overrightarrow{\Omega^*}\left(t^*\right) &= \cos\left(\arctan\left(\pm\frac{\dot{\omega}\left(t\right)}{\xi\left(t\right)\sqrt{\wp_1^2\left(t\right)+\wp_2^2\left(t\right)}}\right)\right)\sin\omega\ \overrightarrow{\Upsilon_1}\left(t\right)\\ &+\sin\left(\arctan\left(\pm\frac{\dot{\omega}\left(t\right)}{\xi\left(t\right)\sqrt{\wp_1^2\left(t\right)+\wp_2^2\left(t\right)}}\right)\right)\overrightarrow{\Upsilon_2}\left(t\right)\\ &+\cos\left(\arctan\left(\pm\frac{\dot{\omega}\left(t\right)}{\xi\left(t\right)\sqrt{\wp_1^2\left(t\right)+\wp_2^2\left(t\right)}}\right)\right)\cos\omega\ \overrightarrow{\Upsilon_3}\left(t\right).\end{aligned} \tag{57}$$

Proof. From (7),

$$\overrightarrow{\Omega^*}\left(t^*\right)=\sin\omega^*\left(t^*\right)\ \overrightarrow{\Upsilon_1^*}\left(t^*\right)+\cos\omega^*\left(t^*\right)\ \overrightarrow{\Upsilon_3^*}\left(t^*\right) \tag{58}$$

is written. If (42) and (54) are substituted in (58), the expression (57) is obtained.

Corollary 3.15. Let $\left(\overrightarrow{\Im^*}\right)$ be a involute curve of $\left(\vec{\Im}\right)$. $\left(\vec{\Im}\right)$ with non-zero curvature is a helix if only if $\left(\overrightarrow{\Im^*}\right)$ is planar.

Proof. Since $\left(\vec{\Im}\right)$ is a helix, from (24) and (44),

$$\wp_2^*\left(t^*\right)=0. \tag{59}$$

is gotten. So, from (59), Corollary 3.15 is clear.

Example. Consider the helix curve

$$\left(\vec{\Im}\right)=\vec{\Im}\left(t\right)=\left(\cos t,\sin t,t\right). \tag{60}$$

For this curve, the following equations are obtained:

$$\left\|\vec{\Im}\left(t\right)\right\|=\xi\left(t\right)=\sqrt{2}, \tag{61}$$

$$\zeta\left(t\right)=-\int\xi\left(t\right)dt=-\sqrt{2}t+c. \tag{62}$$

From (1), the Frenet vectors of $\left(\vec{\Im}\right)$ are

$$\begin{cases} \overrightarrow{\Upsilon_1}(t) = \frac{1}{\sqrt{2}}(-\sin t, \cos t, 1), \\ \overrightarrow{\Upsilon_2}(t) = (-\cos t, \sin t, 0), \\ \overrightarrow{\Upsilon_3}(t) = \frac{1}{\sqrt{2}}(\sin t, -\cos t, 1). \end{cases} \tag{63}$$

From (2) and (3), the curvature and torsion of $\left(\vec{\Im}\right)$ are

$$\wp_1(t) = \wp_2(t) = \frac{1}{2}. \tag{64}$$

From (5) and (7), the Darboux vector and pole vector of $\left(\vec{\Im}\right)$ are

$$\vec{\Psi}(t) = \vec{\Omega}(t) = (0,0,1). \tag{65}$$

From (38) and (39), since

$$\cos\omega(t) = \sin\omega(t) = \frac{1}{\sqrt{2}}, \tag{66}$$

the angle between $\overrightarrow{\Upsilon_3}(t)$ and $\vec{\Psi}(t)$ of $\left(\vec{\Im}\right)$ is found as,

$$\omega(t) = \frac{\pi}{4}. \tag{67}$$

On the other hand, from (11), (60), (62) and (63), the involute curve $\left(\overrightarrow{\Im^*}\right)$ of $\left(\vec{\Im}\right)$ is obtained as

$$\left(\overrightarrow{\Im^*}\right) = \overrightarrow{\Im^*}(t^*) = \overrightarrow{\Im^*}(t) = \left(\cos t + \left(t - \frac{c}{\sqrt{2}}\right)\sin t,\ \sin t - \left(t - \frac{c}{\sqrt{2}}\right)\cos t,\ \frac{c}{\sqrt{2}}\right), \tag{68}$$

Figure 3, where c is arbitrary real number. Here, $\left(\vec{\Im}\right)$ has an involute curve at any different point for each different value of c. From (68),

$$\left\|\overrightarrow{\Im^*}(t)\right\| = \xi^*(t) = \frac{\left|\sqrt{2}t - c\right|}{\sqrt{2}} \tag{69}$$

is gotten. Thus, from (21), (61), (62), (64) and (69),

$$\frac{dt^*}{dt} = 1 \tag{70}$$

is found. The Frenet vectors of $\left(\overrightarrow{\Im^*}\right)$ are

$$\begin{cases} \overrightarrow{\Upsilon_1^*}(t) = (-\cos t, -\sin t, 0), \\ \overrightarrow{\Upsilon_2^*}(t) = (\sin t, -\cos t, 0), \\ \overrightarrow{\Upsilon_3^*}(t) = (0,0,1). \end{cases} \tag{71}$$

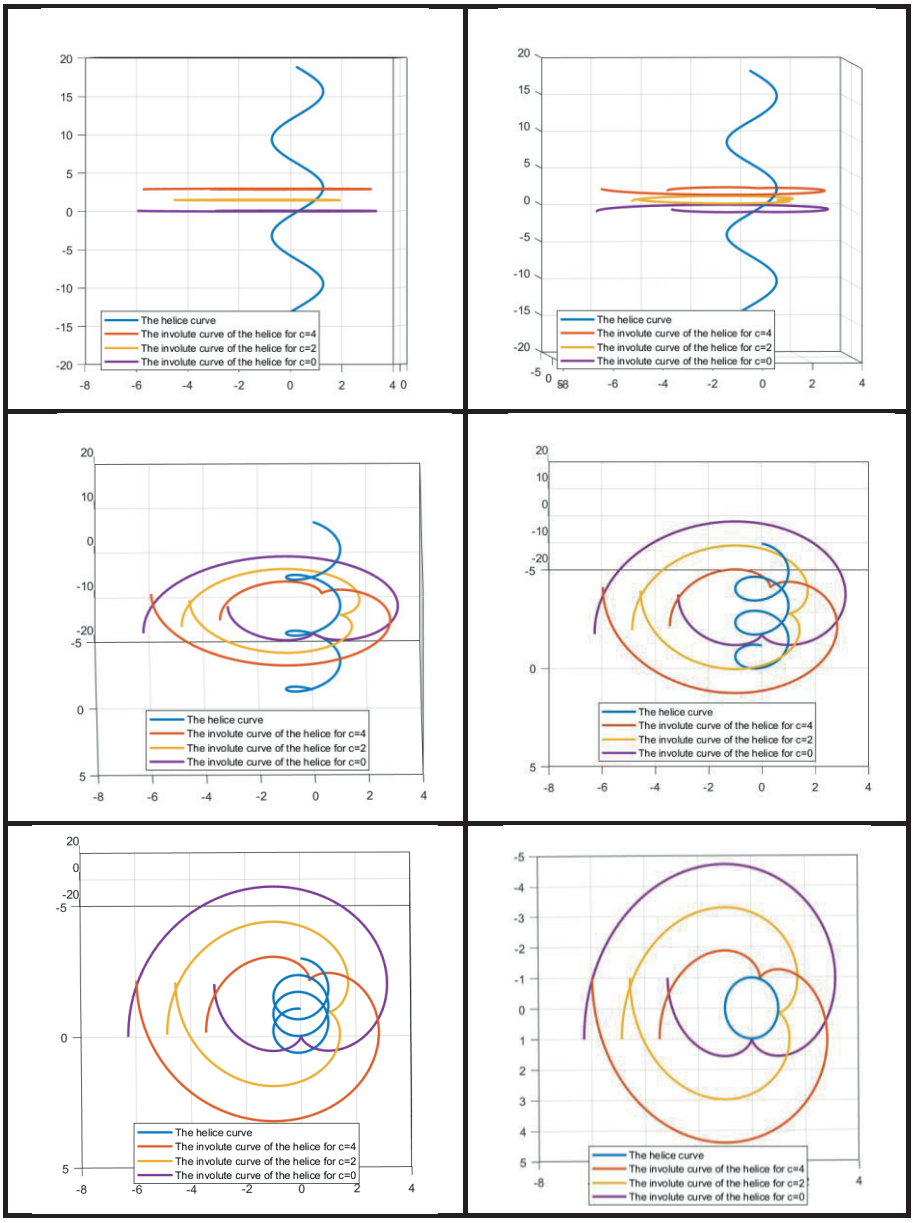

Figure 3. The helix curve $\left(\overrightarrow{\Im}\right)$ and its three involute curves for $c = 0, 2, 4$

Thus, from (63) and (71), it is clear that $\left\langle \overrightarrow{\Upsilon_1^*}(t),\ \overrightarrow{\Upsilon_1}(t) \right\rangle = 0$. Also it is seen that (31) is provided, from (63), (64) and (71), indeed

$$\begin{bmatrix} \overrightarrow{\Upsilon_1^*}(t^*) \\ \overrightarrow{\Upsilon_2^*}(t^*) \\ \overrightarrow{\Upsilon_3^*}(t^*) \end{bmatrix} = \begin{bmatrix} 0 & 1 & 0 \\ -1/\sqrt{2} & 0 & 1/\sqrt{2} \\ 1/\sqrt{2} & 0 & 1/\sqrt{2} \end{bmatrix} \begin{bmatrix} \overrightarrow{\Upsilon_1}(t) \\ \overrightarrow{\Upsilon_2}(t) \\ \overrightarrow{\Upsilon_3}(t) \end{bmatrix}. \tag{72}$$

From (2) and (3), the curvature and torsion of $\left(\overrightarrow{\Im^*}\right)$ are

$$\wp_1^*(t) = \frac{\sqrt{2}}{\left|\sqrt{2}t - c\right|} \quad \text{and} \quad \wp_2^*(t) = 0. \tag{73}$$

It is seen that (19) and (24) are indeed provided, from(62), (64) and (73). Also, as in Corollary 3.15, since $\left(\overrightarrow{\Im}\right)$ is a helix, it is proven that its involute curve $\left(\overrightarrow{\Im^*}\right)$ is planar. From (5) and (7), the Darboux vector and the pole vector of $\left(\overrightarrow{\Im^*}\right)$ are

$$\overrightarrow{\Psi^*}(t) = \overrightarrow{\Omega^*}(t) = (0,0,1). \tag{74}$$

It is seen that (34), (35) and (50) are indeed provided, from (61), (62), (63), (64), (65), (67) and (69). Since $\left(\overrightarrow{\Im}\right)$ is a helix, from (65), (71) and (74), it is seen that, Corollary 3.9 and Corollary 3.12 are provided. It means that, the Darboux vector $\overrightarrow{\Psi^*}(t)$ and binormal vector $\overrightarrow{\Upsilon_3^*}(t)$ of $\left(\overrightarrow{\Im^*}\right)$ is linearly dependent and the pole vector $\overrightarrow{\Omega}(t)$ of $\left(\overrightarrow{\Im}\right)$ and pole vector $\overrightarrow{\Omega^*}(t)$ of $\left(\overrightarrow{\Im^*}\right)$ are same. Moreover, for the involute curve $\left(\overrightarrow{\Im^*}\right)$, from (38), (39) and (73), the following equalities are obtained:

$$\cos\omega^*(t) = 1, \qquad \sin\omega^*(t) = 0. \tag{75}$$

Thus, the angle between $\overrightarrow{\Upsilon_3^*}(t)$ and $\overrightarrow{\Psi^*}(t)$ of this curve is found as

$$\omega^*(t) = 0. \tag{76}$$

It is seen that, (54) is indeed provided, from (61), (64) and (67). Besides, (76) is another proof that $\overrightarrow{\Upsilon_3^*}(t)$ and $\overrightarrow{\Psi^*}(t)$ is linearly dependent.

4. Conclusions

Although studies on unit speed curves provide ease of processing, the results are limited because they do not cover all curves in general. Of course, any curve can be made into a unit speed curve. However, instead of doing this for each curve, it would be wise to obtain general results for non-unit speed curves. In this paper, the involute curves of a non-unit speed curve are studied in Eucliden 3-space. The relationships between some geometric properties of these curves are given and the results are reinforced with an example. Similar studies can be done for other types of curves or in different spaces, similar to (Abdel Aziz et al., 2019; Akyiğit et al., 2010; Almaz and Külahcı, 2021; Bilici and Çalışkan, 2009; Bilici and Çalışkan, 2022; Bükcü and Karacan, 2007; Elsharkawy, 2020; Gür and Şenyurt, 2013; Şenyurt and Gür, 2012).

REFERENCES

Abdel-Aziz H.S., Saad M.K., Abdel-Salam A.A., On involute-evolute curve couple in the hyperbolic and de Sitter spaces, Journal of the Egyptian Mathematical Societ, 27, 1-18, 2019.

Akyiğit M., Azak A.Z., Ersoy S., Involute-evolute curves in Galilean space G_3, Scientia Magna, 6(4), 75-80, 2010.

Almaz F., Külahcı M.A., Involute-evolute d-curves in Minkowski 3-space E_1^3, Boletim da Sociedade Paranaense de Matematica, 39(1), 147-156, 2021.

As E., Sarıoğlugil A., On the Bishop curvatures of involute-evolute curve couple in E^3, Int. J. Phys. Sci., 9(7), 140-145, 2014.

Azak A.Z., Involute-Evolute Curves According to Modified Orthogonal Frame, Journal of Science and Arts, 21(2), 385-394, 2021.

Bektaş Ö., Yüce S., Special involute-evolute partner D-curves in E^3, European Journal of Pure and Applied Mathematics, 6(1), 20-29, 2013.

Bilici M., Çalışkan M., On the Involutes of the Spacelike Curve with a Timelike Binormal in Minkowski 3-Space, Int. Math. Forum, 4(31), 1497-1509, 2009.

Bilici M., Çalışkan M., New Characterizations for Spherical Indicatrices of Involutes of a Spacelike Curve With a Timelike Binormal in Minkowski 3-Space, Journal of Science and Arts, 22(3), 629-638, 2022.

Bükcü B., Karacan M.K., On The Involute and Evolute Curves of The Spacelike Curve with a Spacelike Binormal in Minkowski 3-Space, Int. J. Contemp. Math. Sciences, 2(5), 221-232, 2007.

Do Carmo M.P., Differential Geometry of Curves and Surfaces: Revised and Updated Second Edition, Courier Dover Publications, 2016.

Çalışkan M., Bilici M., Some Characterizations for The Pair of Involute-Evolute Curves in Euclidean Space E^3, Bulletin Pure Appl. Sci., 21E(2), 289-294, 2002.

Elsharkawy A., Generalized involute and evolute curves of equiform spacelike curves with a timelike equiform principal normal in E_1^3, Journal of the Egyptian Mathematical Society, 28(1), 26, 2020.

Gür S., Şenyurt S., Spacelike-timelike involute-evolute curve couple on dual Lorentzian space, J. Math. Comput. Sci., 3(4), 1054-1075, 2013.

Gür Mazlum S., Bektaş M., On the Modified Orthogonal Frames of the Non-Unit Speed Curves in Euclidean Space E^3, Turkish Journal of Science, 7(2), 58-74, 2022.

Gür Mazlum S., Şenyurt S., Bektaş M., Salkowski Curves and Their Modified Orthogonal Frames in E^3, Journal of New Theory, 40, 12-26, 2022.

Hacısalihoğlu H.H., Differantial Geometry, Ankara University Faculty of Science Press, Ankara, Türkiye, 2000.

Hanif M., Hou Z.H., Generalized involute and evolute curve-couple in Euclidean space, Int. J. Open Problems Compt. Math., 11(2), 28-39, 2018.

Honda S.I., Takahashi M., Bertrand and Mannheim curves of framed curves in the 3-dimensional Euclidean space, Turkish Journal of Mathematics, 44(3), 883-899, 2020.

Jianu M., Achimescu S., Daus L., Mihai A., Roman O.A., Tudor D., Characterization of rectifying curves by their involutes and evolutes, Mathematics, 9(23), 3077, 2021.

Kasap E., Yüce S., Kuruoğlu N., The involute-evolute offsets of ruled surfaces, Iranian Journal of Science and Technology, Transaction A, 33(A2), 195-201, 2009.

Monterde J., The Bertrand curve associated to a Salkowski curve, Journal of Geometry, 111(2), 21, 2020.

Öztürk G., Arslan K., Bulca B., A Characterization of Involutes and Evolutes of a Given Curve in E^n, Kyungpook Mathematical Journal, 58(1), 117-135, 2018.

Sertöz A.S., Öklid'in elemanları (in Turkish), TÜBİTAK Publications, Türkiye, 2019.

Şenyurt S., Gür S., Timelike-spacelike involute-evolute curve couple on dual Lorentzian space, J. Math. Comput. Sci., 2(6), 1808-1823, 2012.

Yılmaz M.Y., Erdem E., A characterization of involutes of a given curve in E^3 via directional q-frame, Malaya Journal of Matematik, 9(04), 239-250, 2021.

Chapter 13

A SPECIAL CURVE-PAIR UNDER THE MOBIUS TRANSFORMATION

Serpil ÜNAL[1]

Semra KAYA NURKAN[2]

1 Assistant Professor, Usak University, Faculty of Arts and Sciences, Department of Mathematics, Uşak, Turkey, E-mail:serpil.unal@usak.edu.tr
ORCID: 0000-0002-4043-6832
2 Associate Professor, Usak University, Faculty of Arts and Sciences, Department of Mathematics, Uşak, Turkey, E-mail:semra.kaya@usak.edu.tr
ORCID: 0000-0001-6473-4458

1. Introduction

It is well known that Mobius transformations are important in many fields, especially in complex analysis, geometry and biology. Especially in geometry (Niamsup, 2000; Özgür et al, 2005), it has been used by performing multiple steps such as stereographic projection to the unit two-sphere from the plane, rotating and moving the sphere to a new location, orientation in space, tereographic projection to the plane from the new position of the sphere. Mobius transformations, which are important mappings in complex analysis, are also used in biology as 2D projections from 3D configurations of samples such as humans, fungi and fish (Lundh et al, 2011; Petukhov, 1989). The most basic characteristic property of this transformations, which are also called homographic transformations, linear fractional transformations or bilinear transformations, is that they map circles to circles. In order to apply this idea to other curves in 3D Euclidean space, using quaternions the Poincare expansion was defined in (Beardon, 1983). With the expansion, the mobius transformation studied in the expanded complex plane is actually expanded to quaternions.

Quaternions, introduced by William R. Hamilton in (Hamilton,1844), are non-commutative number systems that are extended by complex numbers. With their useful properties (i.e., homothetic motions especially used in kinematics (Düldül, 2010)), quaternions have recently played an important role in many areas of physical science, such as differential geometry, analysis and synthesis of mechanisms and machines, simulation of particle motion in the theory of relativity (Adler, 1995; Agrawal, 1987). The relationship between quaternions and rotations in 3- and 4-dimensional Euclidean space was completely studied, and the use of quaternions in spherical geometry and mechanics was also considered in (Ward, 1997). Next, the quaternion-based rotational system was defined in (Shoemake, 1985). Kula and Yaylı (2007) studied on split quaternions and rotations in Semi-Euclidean E_2^4 and then Jafari and Yaylı (2015) defined generalized quaternions and gave some algebraic properties of generalized quaternions.

In light of the foregoing, our motivation in this paper is to examine whether the mobius transform, which converts circles to circles, preserves this

property for special curves such as involute-evolute curve pairs. In addition, in this study, the conditions under which the property of being involute-evolute pairs are preserved in E^4 and E_2^4 are also given.

2. Preliminaries

In this part, we discuss mobius transformations, quaternions, Poincare expansion of mobius transformation and a special pair of curves, Involute-Evolute curves, since we study spherical involute-evolute curves under Mobius transformations that expand the complex plane to quaternions with poincare expansion.

2.1. Möbius Transformations

Definition 1. A Möbius transformation M of the complex plane is a rational function of the form

$$M: \hat{\mathbb{C}} \to \hat{\mathbb{C}},\ M(z) = \frac{a_1 z + b_1}{c_1 z + d_1},\quad a_1, b_1, c_1, d_1 \in \mathbb{C},\ \begin{vmatrix} a_1 & b_1 \\ c_1 & d_1 \end{vmatrix} \neq 0$$

where $\hat{\mathbb{C}} = \mathbb{C} \cup \{\infty\}$ is the expanded complex. In case of $c_1 = 0$, the Mobius transformation $S(z) = A_1 z + B_1,\ A_1 \neq 0$ is called a similarity and if $a_1 = d_1 = 0$ and $b_1 = c_1 = 1$, this transformation is called an inversion is given by $J(z) = \frac{1}{z}$. In addition, every Mobius transformation can be written as the composition of similarities and inversions (Jones and Singerman, 1987; Lehner, 1964).

At first glance, it does not appear obvious what the action of these transformations on $\hat{\mathbb{C}}$ looks like. However, the information that follows greatly aids comprehension and visualization (Amer, 2014):

Lemma 1. Any Mobius transformation can be constructed from the following types of maps:

$$(b_1 = c_1 = 0, d_1 = 1),\quad z \mapsto a_1 z$$

$$(c_1 = 0, a_1 = d_1 = 1), \quad z \mapsto z + b_1$$

$$(a_1 = d_1 = 0,\ b_1 = c_1 = 1), \quad z \mapsto \frac{1}{z}$$

Proof. **Case 1:** $c_1 = 0$. By the restriction that $a_1 d_1 - b_1 c_1 \neq 0, d_1 \neq 0,$ so we have

$$G = g_1 \circ g_2$$

where $g_1 : z \mapsto z + \frac{b_1}{d_1}$ and $g_2 : z \mapsto \frac{a_1}{d_1} z$.

Case 2: For $c_1 \neq 0,$ let we choose

$$g_1 : z \mapsto z + \frac{a_1}{c_1}, \quad g_2 : z \mapsto \frac{1}{c_1}, \quad g_3 : z \mapsto \frac{1}{z}, \quad g_4 : z \mapsto z + d_1, \quad g_5 : z \mapsto c_1 z$$

then we have

$$G = g_1 \circ g_2 \circ g_3 \circ g_4 \circ g_5.$$

2.2. Quaternions

Definition 2. A quaternion is the form given by

$$q = x + yi + uj + vk$$

where

a) If $i^2 = -1, j^2 = -1, k^2 = -1, q$ is called a real quaternion and then the product of two real quaternion $q_1 = z_1 + w_1 j$ and $q_2 = z_2 + w_2 j$ is given by

$$q_1 q_2 = (z_1 + w_1 j)(z_2 + w_2 j) = (z_1 z_2 - w_1 \bar{w}_2) + (z_1 w_2 + w_1 \bar{z}_2) j.$$

Besides it can be found that $(z + wj)(\bar{z} - wj) = |z|^2 + |w|^2$ and $jz = \bar{z} j$

for $z, w \in \mathbb{C}$ (Jafari and Yaylı, 2015).

b) If $i^2 = -1, j^2 = 1, k^2 = 1, q$ is a split quaternion and then the product of two split quaternion $q_1 = z_1 + w_1 j$ and $q_2 = z_2 + w_2 j$ is given by

$$q_1 q_2 = (z_1 + w_1 j)(z_2 + w_2 j) = (z_1 z_2 + w_1 \bar{w}_2) + (z_1 w_2 + w_1 \bar{z}_2) j.$$

Besides it can be found that $(z + wj)(\bar{z} - wj) = |z|^2 - |w|^2$ and $jz = \bar{z}j$ for $z, w \in \mathbb{C}$ (Kula and Yaylı, 2007).

2.3. Involute-Evolute Curves

Definition 3. Let $\gamma: I \to E^4$ be a curve with $\gamma'(s) \neq 0$, where $\gamma'(s) = \frac{d\gamma(s)}{ds}$. The arc-lenght s of a curve $\gamma(s)$ is determined such that $\|\gamma'(s)\| = 1$. The curve γ is called evolute of $\tilde{\gamma}$ if the tangent vectors are orthogonal at the corresponding points for each $s \in I \subseteq R$. In this case, $\tilde{\gamma}$ is called involute of the curve γ and there exists a relationship between the position vectors as

$$\tilde{\gamma}(s^*) = \gamma(s) + \lambda T(s)$$

where λ is the distance between the curves γ and $\tilde{\gamma}$ at the corresponding points for each s. The pair of $(\tilde{\gamma}, \gamma)$ is called a involute-evolute pair. λ is not a constant for involute-evolute pairs (Tunçer et al, 2020).

2.4. Poincare Extension of Mobius Transformations in E^4

The image of $q = z + wj$ real quaternion under the Mobius transformation which is called Poincare extension of real quaternions is obtained as

$$T(z + wj) = \frac{(a_1 z + b_1)\overline{(c_1 z + d_1)} + a_1 \bar{c}_1 |w|^2 + |a_1 d_1 - b_1 c_1| wj}{|c_1 z + d_1|^2 + |c_1 w|^2}$$

This extension for similarity transformation $S(z) = A_1 z + B_1,\ A_1 \neq 0$ and inversion transformation $J(z) = \frac{1}{z}$ is denoted respectively by

$$S(z + wj) = A_1 z + B_1 + |A_1| wj$$

$$J(z + wj) = \frac{\bar{z} + wj}{|z|^2 + |w|^2}.$$

It can be found the image of the curve $\gamma: I \to E^4, \gamma(s) = \big(\gamma_1(s), \gamma_2(s), \gamma_3(s), \gamma_4(s)\big)$ under the similarity and inversion transformations through this extension by deciding the quaternion $\gamma = \gamma_1 + \gamma_2 i + \gamma_3 j + \gamma_4 k$. The image of the curve γ for similarity transformation $S(z) = A_1 z + B_1,\ A_1 \neq 0,\ A_1 = (a_{11}, a_{12}),\ B_1 = (b_{11}, b_{12})$ is

$$S\big(\gamma(s)\big) = (a_{11}\gamma_1 - a_{12}\gamma_2 + b_{11}, a_{11}\gamma_2 + a_{12}\gamma_1 + b_{12}, |A_1|\gamma_3, |A_1|\gamma_4)$$

and for inversion transformation $J(z) = \frac{1}{z}$ the image is given by

$$J\big(\gamma(s)\big) = \left(\frac{\gamma_1}{\|\gamma\|^2}, -\frac{\gamma_2}{\|\gamma\|^2}, \frac{\gamma_3}{\|\gamma\|^2}, \frac{\gamma_4}{\|\gamma\|^2}\right)$$

(Beardon, 1983; Brannon et al, 1999).

2.5. Poincare Extension of Mobius Transformations in E_2^4

The image of $q = z + wj$ split quaternion under the Mobius transformation which is called Poincare extension of split quaternions is obtained as

$$T(z + wj) = \frac{(a_1 z + b_1)\overline{(c_1 z + d_1)} - a_1 \bar{c_1} |w|^2 + |a_1 d_1 - b_1 c_1| wj}{|c_1 z + d_1|^2 - |c_1 w|^2}$$

This extension for similarity transformation $S(z) = A_1 z + B_1,\ A_1 \neq 0$ and inversion transformation $J(z) = \frac{1}{z}$ is denoted respectively by

$$S(z+wj) = A_1 z + B_1 + |A_1|wj$$

$$J(z+wj) = \frac{\bar{z}+wj}{|z|^2-|w|^2}.$$

It can be found the image of the curve $\gamma: I \to E_2^4, \gamma(s) = \big(\gamma_1(s), \gamma_2(s), \gamma_3(s), \gamma_4(s)\big)$ under the similarity and inversion transformations through this extension by deciding the split quaternion $\gamma = \gamma_1 + \gamma_2 i + \gamma_3 j + \gamma_4 k$. The image of the curve γ for similarity transformation $S(z) = A_1 z + B_1$, $A_1 \neq 0$, $A_1 = (a_{11}, a_{12})$, $B_1 = (b_{11}, b_{12})$ is

$$S\big(\gamma(s)\big) = (a_{11}\gamma_1 - a_{12}\gamma_2 + b_{11}, a_{11}\gamma_2 + a_{12}\gamma_1 + b_{12}, |A_1|\gamma_3, |A_1|\gamma_4)$$

and for inversion transformation $J(z) = \frac{1}{z}$ the image is given by

$$J\big(\gamma(s)\big) = \left(\frac{\gamma_1}{\|\gamma\|_L^2}, -\frac{\gamma_2}{\|\gamma\|_L^2}, \frac{\gamma_3}{\|\gamma\|_L^2}, \frac{\gamma_4}{\|\gamma\|_L^2}\right)$$

where $\|\gamma\|_L^2 = \gamma_1^2 + \gamma_2^2 - \gamma_3^2 - \gamma_4^2$ (Nurkan, 2011).

3. Spherical Involute-Evolute Curves under Mobius Transformations

3.1. Spherical Involute-Evolute Curves under Mobius Transformations in E^4

The 3-dimensional unit sphere in E^4 is determined by

$$S^3 = \{X = (x_1, x_2, x_3, x_4) \in R^4 : x_1^2 + x_2^2 + x_3^2 + x_4^2 = 1\}$$

with the metric $g(x,x) = \langle x, x\rangle = x_1^2 + x_2^2 + x_3^2 + x_4^2$ and Poincare extension of Mobius transformations in E^4 converts spherical curves to spherical curves.

Lemma 2. Let γ and $\tilde{\gamma}$ be unit speed curves lying on S^3. If $\tilde{\gamma}$ is spherical involute of γ then the image $J(\tilde{\gamma})$ under the inversion transformation $J(z) = \frac{1}{z}$ is spherical involute of $J(\gamma)$.

Proof. Let s be the arc-length parameter of γ and $\tilde{\gamma}$. The Frenet frame of the curves at the points $\gamma(s)$ and $\tilde{\gamma}(s)$ are respectively $\{T(s), N(s), B_1(s), B_2(s)\}$ and $\{\tilde{T}(s), \tilde{N}(s), \tilde{B}_1(s), \tilde{B}_2(s)\}$. Since $\tilde{\gamma}$ is spherical involute of γ there exist the following equation

$$\langle T(s), \tilde{T}(s)\rangle = 0 \tag{1}$$

By putting $T(s) = \gamma'(s)$ and $\tilde{T}(s) = \tilde{\gamma}'(s)$ in (1)

$$\langle \gamma'(s)\ , \tilde{\gamma}'(s)\rangle = 0 \tag{2}$$

is found.

The images of $\gamma(s)$ and $\tilde{\gamma}(s)$ under the inversion transformation J which are expressed by $J(\gamma(s))$ and $J(\tilde{\gamma}(s))$ respectively, are obtained as

$$J\big(\gamma(s)\big) = \left(\frac{\gamma_1}{\|\gamma\|^2}, -\frac{\gamma_2}{\|\gamma\|^2}, \frac{\gamma_3}{\|\gamma\|^2}, \frac{\gamma_4}{\|\gamma\|^2}\right) = \gamma^*$$

$$J\big(\tilde{\gamma}(s)\big) = \left(\frac{\tilde{\gamma}_1}{\|\tilde{\gamma}\|^2}, -\frac{\tilde{\gamma}_2}{\|\tilde{\gamma}\|^2}, \frac{\tilde{\gamma}_3}{\|\tilde{\gamma}\|^2}, \frac{\tilde{\gamma}_4}{\|\tilde{\gamma}\|^2}\right) = \tilde{\gamma}^*$$

By computing the first Frenet vectors of the image curves;

$$T^* = \frac{\gamma^{*\prime}}{\|\gamma^{*\prime}\|}, \quad \tilde{T}^* = \frac{\tilde{\gamma}^{*\prime}}{\|\tilde{\gamma}^{*\prime}\|}$$

are found. So the inner product of $T^*$and $\tilde{T}^*$is obtained as;

$$\langle T^*, \tilde{T}^*\rangle = \frac{1}{\|\gamma^{*\prime}\|\|\tilde{\gamma}^{*\prime}\|}\langle \gamma^{*\prime}, \tilde{\gamma}^{*\prime}\rangle$$

$$= \frac{1}{\|\gamma^{*\prime}\|\|\tilde{\gamma}^{*\prime}\|} \cdot \frac{1}{\|\gamma\|^3\|\tilde{\gamma}\|^3} \cdot \begin{bmatrix} \|\gamma\|\|\tilde{\gamma}\|\langle\gamma',\tilde{\gamma}'\rangle \\ +4\|\gamma\|'\|\tilde{\gamma}\|'\langle\gamma,\tilde{\gamma}\rangle \\ -2\|\gamma\|\|\tilde{\gamma}\|'\langle\gamma',\tilde{\gamma}\rangle \\ -2\|\gamma\|'\|\tilde{\gamma}\|\langle\gamma,\tilde{\gamma}'\rangle \end{bmatrix}$$

By putting $\langle\gamma',\tilde{\gamma}'\rangle = 0$, from equation (2),

$$\langle T^*,\tilde{T}^*\rangle = \frac{1}{\|\gamma^{*\prime}\|\|\tilde{\gamma}^{*\prime}\|} \cdot \frac{1}{\|\gamma\|^3\|\tilde{\gamma}\|^3} \cdot \begin{bmatrix} 4\|\gamma\|'\|\tilde{\gamma}\|'\langle\gamma,\tilde{\gamma}\rangle \\ -2\|\gamma\|\|\tilde{\gamma}\|'\langle\gamma',\tilde{\gamma}\rangle \\ -2\|\gamma\|'\|\tilde{\gamma}\|\langle\gamma,\tilde{\gamma}'\rangle \end{bmatrix} \qquad (3)$$

is found. Since $\gamma,\tilde{\gamma} \subset S^3$, there exists

$$\|\gamma\| = 1 \Rightarrow \|\gamma\|' = 0$$

$$\|\tilde{\gamma}\| = 1 \Rightarrow \|\tilde{\gamma}\|' = 0.$$

By putting these expressions in (3),

$$\langle T^*,\tilde{T}^*\rangle = 0$$

is obtained. This result proves that $J(\tilde{\gamma})$ is spherical involute of $J(\gamma)$.

Lemma 3. Let γ and $\tilde{\gamma}$ be unit speed curves lying on S^3. If $\tilde{\gamma}$ is spherical involute of γ then the image $S(\tilde{\gamma})$ under the similarity transformation $S(z) = A_1 z + B_1;\ A_1 \neq 0$ is spherical involute of $S(\gamma)$.

Proof. The images of $\gamma(s)$ and $\tilde{\gamma}(s)$ under the similarity transformations are

$$S(\gamma(s)) = (a_{11}\gamma_1 - a_{12}\gamma_2 + b_{11}, a_{11}\gamma_2 + a_{12}\gamma_1 + b_{12}, |A_1|\gamma_3, |A_1|\gamma_4)$$
$$= \gamma^{**}$$

$$S(\tilde{\gamma}(s)) = (a_{11}\tilde{\gamma}_1 - a_{12}\tilde{\gamma}_2 + b_{11}, a_{11}\tilde{\gamma}_2 + a_{12}\tilde{\gamma}_1 + b_{12}, |A_1|\tilde{\gamma}_3, |A_1|\tilde{\gamma}_4)$$
$$= \tilde{\gamma}^{**}$$

and the first Frenet vectors of image curves are found as $T^{**} = \frac{\gamma^{**\prime}}{\|\gamma^{**\prime}\|}$, $\tilde{T}^{*} = \frac{\tilde{\gamma}^{**\prime}}{\|\tilde{\gamma}^{**\prime}\|}$

By doing the following calculations

$$\langle T^{**}, \tilde{T}^{**} \rangle = \frac{1}{\|\gamma^{**\prime}\| \|\tilde{\gamma}^{**\prime}\|} \langle \gamma^{**\prime}, \tilde{\gamma}^{**\prime} \rangle$$

$$= \frac{1}{\|\gamma^{**\prime}\| \|\tilde{\gamma}^{**\prime}\|} |A|^2 \langle \gamma', \tilde{\gamma}' \rangle$$

is obtained. Since $\tilde{\gamma}$ and γ are involute-evolute curves, it can be written $\langle \gamma', \tilde{\gamma}' \rangle = 0$. So the below equation is found

$$\langle T^{**}, \tilde{T}^{**} \rangle = 0$$

This result proves that $S(\tilde{\gamma})$ is spherical involute of $S(\gamma)$.

Theorem 1. The Poincare extension of Mobius transformations in E^4 keep being spherical involute-evolute curves.

Proof. From Lemma 2 and Lemma 3, we can say that the spherical involute evolute curves preserve their feature of being spherical involute-evolute under similarity and inverse transformations. We also know from Lemma 1 that mobius transformations can be written as a combination of similarity and inverse transformation. Therefore, we can say that the Mobius transformation, which is written as the composition of these transformations, preserve its spherical involute-evolute.

Example 1. Let the unit speed curve $\gamma: I \to E^4$ defined by

$$\gamma(s) = \left(cos\sqrt{\frac{2}{3}}s, sin\sqrt{\frac{2}{3}}s, cos\sqrt{\frac{1}{3}}s, sin\sqrt{\frac{1}{3}}s \right).$$

Frenet frame vector fields are given by

$$T(s)=\left(-\sqrt{\frac{2}{3}}sin\sqrt{\frac{2}{3}}s,\sqrt{\frac{2}{3}}\,cos\sqrt{\frac{2}{3}}s,-\sqrt{\frac{1}{3}}sin\sqrt{\frac{1}{3}}s,\sqrt{\frac{1}{3}}\,cos\sqrt{\frac{1}{3}}s\right)$$

$$N(s)=\left(\frac{-2}{\sqrt{5}}cos\sqrt{\frac{2}{3}}s\,,\frac{-2}{\sqrt{5}}sin\sqrt{\frac{2}{3}}s,\frac{-1}{\sqrt{5}}cos\sqrt{\frac{1}{3}}s,\frac{-1}{\sqrt{5}}sin\sqrt{\frac{1}{3}}s\right)$$

$$B_1(s)=\left(\frac{1}{\sqrt{3}}sin\sqrt{\frac{2}{3}}s,\frac{-1}{\sqrt{3}}\,cos\sqrt{\frac{2}{3}}s,-\sqrt{\frac{2}{3}}sin\sqrt{\frac{1}{3}}s,\sqrt{\frac{2}{3}}\,cos\sqrt{\frac{1}{3}}s\right)$$

$$B_2(s)=\left(\frac{1}{\sqrt{5}}cos\sqrt{\frac{2}{3}}s\,,\frac{1}{\sqrt{5}}sin\sqrt{\frac{2}{3}}s,\frac{-2}{\sqrt{5}}cos\sqrt{\frac{1}{3}}s,\frac{-2}{\sqrt{5}}sin\sqrt{\frac{1}{3}}s\right)$$

(Deshmukh et al, 2017).

It can easily be seen from here that $T(s)$ and $N(s)$ are spherical involute-evolute curves. According to this, from Lemma 2,

$$J\big(T(s)\big)=\left(-\sqrt{\frac{2}{3}}sin\sqrt{\frac{2}{3}}s,-\sqrt{\frac{2}{3}}\,cos\sqrt{\frac{2}{3}}s,-\sqrt{\frac{1}{3}}sin\sqrt{\frac{1}{3}}s,\sqrt{\frac{1}{3}}\,cos\sqrt{\frac{1}{3}}s\right)$$
$$=\gamma^*$$

$$J\big(N(s)\big)=\left(\frac{-2}{\sqrt{5}}cos\sqrt{\frac{2}{3}}s\,,\frac{2}{\sqrt{5}}sin\sqrt{\frac{2}{3}}s,\frac{-1}{\sqrt{5}}cos\sqrt{\frac{1}{3}}s,\frac{-1}{\sqrt{5}}sin\sqrt{\frac{1}{3}}s\right)=\tilde{\gamma}^*$$

and so,

$$T^*(s)=\left(\frac{-2}{\sqrt{5}}cos\sqrt{\frac{2}{3}}s\,,\frac{2}{\sqrt{5}}sin\sqrt{\frac{2}{3}}s,\frac{-1}{\sqrt{5}}cos\sqrt{\frac{1}{3}}s,\frac{-1}{\sqrt{5}}sin\sqrt{\frac{1}{3}}s\right)$$

$$\tilde{T}^*(s) = \left(\frac{2\sqrt{2}}{3} sin\sqrt{\frac{2}{3}}s, \frac{2\sqrt{2}}{3}\ cos\sqrt{\frac{2}{3}}s, \frac{1}{3} sin\sqrt{\frac{1}{3}}s, \frac{-1}{3} cos\sqrt{\frac{1}{3}}s \right).$$

By putting these expressions,

$$\langle T^*, \tilde{T}^* \rangle = 0$$

is obtained. Therefore, since $N(s)$ is spherical involute of $T(s)$, the image $J\big(N(s)\big)$ under the inversion transformation $J(z) = \frac{1}{z}$ is spherical involute of $J\big(T(s)\big)$.

Similarly, again, since $N(s)$ is spherical involute of $T(s)$, from Lemma 3,

$$S\big(T(s)\big) = \left(-a_{11}\sqrt{\frac{2}{3}} sin\sqrt{\frac{2}{3}}s - a_{12}\sqrt{\frac{2}{3}}\ cos\sqrt{\frac{2}{3}}s + b_{11}, a_{11}\sqrt{\frac{2}{3}} cos\sqrt{\frac{2}{3}}s \right.$$
$$- a_{12}\sqrt{\frac{2}{3}}\ sin\sqrt{\frac{2}{3}}s$$
$$\left. + b_{12}, -|A_1|\sqrt{\frac{1}{3}} sin\sqrt{\frac{1}{3}}s, |A_1|\sqrt{\frac{1}{3}} cos\sqrt{\frac{1}{3}}s \right) = \gamma^{**}$$

$$S\big(N(s)\big) = \left(-\frac{2a_{11}}{\sqrt{5}} cos\sqrt{\frac{2}{3}}s + \frac{2a_{12}}{\sqrt{5}} sin\sqrt{\frac{2}{3}}s + b_{11}, -\frac{2a_{11}}{\sqrt{5}} sin\sqrt{\frac{2}{3}}s \right.$$
$$\left. - \frac{2a_{12}}{\sqrt{5}} cos\sqrt{\frac{2}{3}}s + b_{12}, -\frac{|A_1|}{\sqrt{5}} cos\sqrt{\frac{1}{3}}s, -\frac{|A_1|}{\sqrt{5}} sin\sqrt{\frac{1}{3}}s \right)$$
$$= \tilde{\gamma}^{**}$$

and so,

$$\gamma^{**\prime}(s)=\left(-\frac{2a_{11}}{3}cos\sqrt{\frac{2}{3}}s+\frac{2a_{12}}{3}sin\sqrt{\frac{2}{3}}s,-\frac{2a_{11}}{3}sin\sqrt{\frac{2}{3}}s\right.$$
$$\left.-\frac{2a_{12}}{3}cos\sqrt{\frac{2}{3}}s,-\frac{|A_1|}{3}cos\sqrt{\frac{1}{3}}s,-\frac{|A_1|}{3}sin\sqrt{\frac{1}{3}}s\right)$$

$$\tilde{\gamma}^{**\prime}(s)=\left(\frac{2\sqrt{2}a_{11}}{\sqrt{15}}sin\sqrt{\frac{2}{3}}s+\frac{2\sqrt{2}a_{12}}{\sqrt{15}}cos\sqrt{\frac{2}{3}}s,-\frac{2\sqrt{2}a_{11}}{\sqrt{15}}cos\sqrt{\frac{2}{3}}s\right.$$
$$\left.+\frac{2\sqrt{2}a_{12}}{\sqrt{15}}sin\sqrt{\frac{2}{3}}s,\frac{|A_1|}{\sqrt{15}}sin\sqrt{\frac{1}{3}}s,\frac{-|A_1|}{\sqrt{15}}cos\sqrt{\frac{1}{3}}s\right)$$

By putting these expressions, because of $\left\|\gamma^{**\prime}\right\|\neq 0$ and $\left\|\tilde{\gamma}^{**\prime}\right\|\neq 0$,

$$\langle T^{**},\tilde{T}^{**}\rangle=0$$

is obtained. Therefore, since $N(s)$ is spherical involute of $T(s)$, the image $S\big(N(s)\big)$ is spherical involute of $S\big(T(s)\big)$.

The main curve γ and its spherical indicatrix curves T and N are shown in the following computer-generated graphs.

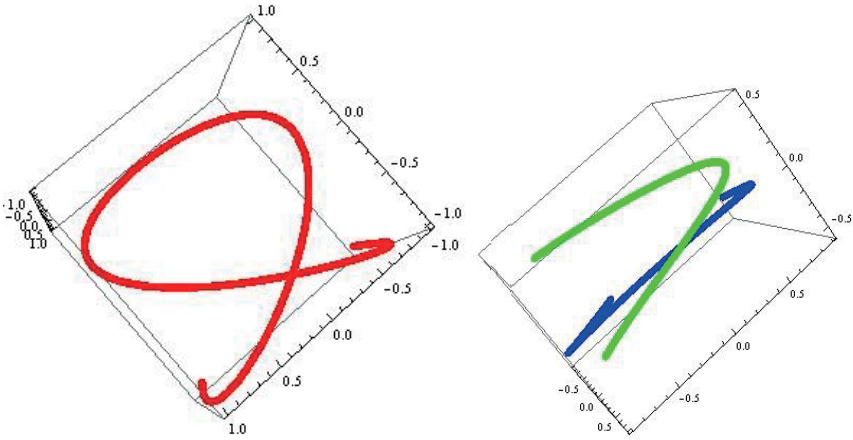

Figure 1. Projections of the main curve (on the left) and its spherical involute-evolute curve pair T (green) and N(blue) (on the right).

The pictures of some projections of the images of spherical involute-evolute curve pair T and N under the inversion and similarity transformation respectively are as follows. Here, yellow and purple curves are γ^* and $\tilde{\gamma}^*$, pink and black curves are γ^{**} and $\tilde{\gamma}^{**}$ respectively.

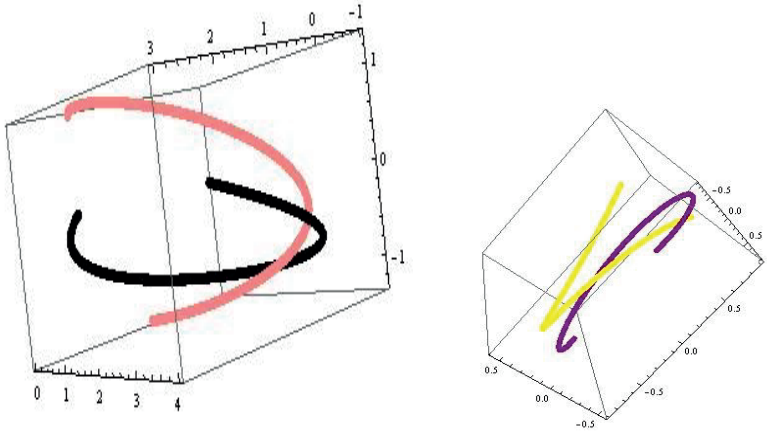

Figure 2. Projections of the images of T and N under the inversion transformation (on the left) and similarity transformation (on the right)

3.2. Spherical Involute-Evolute Curves under Mobius Transformations in E_2^4

The 3-dimensional unit hyperbolic sphere in E_2^4 is determined by

$$H_0^3 = \{X = (x_1, x_2, x_3, x_4) \in R^4 : x_1^2 + x_2^2 - x_3^2 - x_4^2 = 1\}$$

with the metric $g(x,x) = \langle x, x\rangle_L = x_1^2 + x_2^2 - x_3^2 - x_4^2$ and Poincare extension of Mobius transformations in E_2^4 converts spherical curves to spherical curves.

Lemma 4. Let γ and $\tilde{\gamma}$ be unit speed and spacelike curves lying on H_0^3. If $\tilde{\gamma}$ is spherical involute of γ then the image $J(\tilde{\gamma})$ under the inversion transformation $J(z) = \frac{1}{z}$ is spherical involute of $J(\gamma)$.

Proof. Let s be the arc-length parameter of γ and $\tilde{\gamma}$. The Frenet frame of the curves at the points $\gamma(s)$ and $\tilde{\gamma}(s)$ are respectively $\{T(s), N(s), B_1(s), B_2(s)\}$ and $\{\tilde{T}(s), \tilde{N}(s), \tilde{B}_1(s), \tilde{B}_2(s)\}$. Since $\tilde{\gamma}$ is spherical involute of γ there exist the following equation

$$\langle T(s), \tilde{T}(s)\rangle_L = 0 \qquad (4)$$

By putting $T(s) = \gamma'(s)$ and $\tilde{T}(s) = \tilde{\gamma}'(s)$ in (4)

$$\langle \gamma'(s)\ , \tilde{\gamma}'(s)\rangle_L = 0 \qquad (5)$$

is found.

The images of $\gamma(s)$ and $\tilde{\gamma}(s)$ under the inversion transformation J which are expressed by $J(\gamma(s))$ and $J(\tilde{\gamma}(s))$ respectively, are obtained as

$$J(\gamma(s)) = \left(\frac{\gamma_1}{\|\gamma\|_L^2}, -\frac{\gamma_2}{\|\gamma\|_L^2}, \frac{\gamma_3}{\|\gamma\|_L^2}, \frac{\gamma_4}{\|\gamma\|_L^2}\right) = \gamma^*$$

$$J(\tilde{\gamma}(s)) = \left(\frac{\tilde{\gamma}_1}{\|\tilde{\gamma}\|_L^2}, -\frac{\tilde{\gamma}_2}{\|\tilde{\gamma}\|_L^2}, \frac{\tilde{\gamma}_3}{\|\tilde{\gamma}\|_L^2}, \frac{\tilde{\gamma}_4}{\|\tilde{\gamma}\|_L^2}\right) = \tilde{\gamma}^*$$

By computing the first Frenet vectors of the image curves;

$$T^* = \frac{\gamma^{*\prime}}{\|\gamma^{*\prime}\|_L}, \quad \tilde{T}^* = \frac{\tilde{\gamma}^{*\prime}}{\|\tilde{\gamma}^{*\prime}\|_L}$$

are found. So the inner product of $T^*$and $\tilde{T}^*$ is obtained as;

$$\langle T^*, \tilde{T}^* \rangle_L = \frac{1}{\|\gamma^{*\prime}\|_L \|\tilde{\gamma}^{*\prime}\|_L} \langle \gamma^{*\prime}, \tilde{\gamma}^{*\prime} \rangle_L$$

$$= \frac{1}{\|\gamma^{*\prime}\|_L \|\tilde{\gamma}^{*\prime}\|_L} \cdot \frac{1}{\|\gamma\|_L^3 \|\tilde{\gamma}\|_L^3} \cdot \begin{bmatrix} \|\gamma\|_L \|\tilde{\gamma}\|_L \langle \gamma', \tilde{\gamma}' \rangle_L \\ +4\|\gamma\|_L' \|\tilde{\gamma}\|_L' \langle \gamma, \tilde{\gamma} \rangle_L \\ -2\|\gamma\|_L \|\tilde{\gamma}\|_L' \langle \gamma', \tilde{\gamma} \rangle_L \\ -2\|\gamma\|_L' \|\tilde{\gamma}\|_L \langle \gamma, \tilde{\gamma}' \rangle_L \end{bmatrix}$$

By putting $\langle \gamma', \tilde{\gamma}' \rangle_L = 0$, from equation (5),

$$\langle T^*, \tilde{T}^* \rangle_L = \frac{1}{\|\gamma^{*\prime}\|_L \|\tilde{\gamma}^{*\prime}\|_L} \cdot \frac{1}{\|\gamma\|_L^3 \|\tilde{\gamma}\|_L^3} \cdot \begin{bmatrix} 4\|\gamma\|_L' \|\tilde{\gamma}\|_L' \langle \gamma, \tilde{\gamma} \rangle_L \\ -2\|\gamma\|_L \|\tilde{\gamma}\|_L' \langle \gamma', \tilde{\gamma} \rangle_L \\ -2\|\gamma\|_L' \|\tilde{\gamma}\|_L \langle \gamma, \tilde{\gamma}' \rangle_L \end{bmatrix} \tag{6}$$

is found. Since $\gamma, \tilde{\gamma} \subset H_0^3$, there exists

$$\|\gamma\|_L = 1 \Rightarrow \|\gamma\|_L' = 0$$

$$\|\tilde{\gamma}\|_L = 1 \Rightarrow \|\tilde{\gamma}\|_L' = 0.$$

By putting these expressions in (6),

$$\langle T^*, \tilde{T}^* \rangle_L = 0$$

is obtained. This result proves that $J(\tilde{\gamma})$ is spherical involute of $J(\gamma)$.

Lemma 5. Let γ and $\tilde{\gamma}$ be unit speed and spacelike curves lying on H_0^3. If $\tilde{\gamma}$ is spherical involute of γ then the image $S(\tilde{\gamma})$ under the similarity transformation $S(z) = A_1 z + B_1$; $A_1 \neq 0$ is spherical involute of $S(\gamma)$.

Proof. The images of $\gamma(s)$ and $\tilde{\gamma}(s)$ under the similarity transformations are

$$S(\gamma(s)) = (a_{11}\gamma_1 - a_{12}\gamma_2 + b_{11}, a_{11}\gamma_2 + a_{12}\gamma_1 + b_{12}, |A_1|\gamma_3, |A_1|\gamma_4) = \gamma^{**}$$

$$S(\tilde{\gamma}(s)) = (a_{11}\tilde{\gamma}_1 - a_{12}\tilde{\gamma}_2 + b_{11}, a_{11}\tilde{\gamma}_2 + a_{12}\tilde{\gamma}_1 + b_{12}, |A_1|\tilde{\gamma}_3, |A_1|\tilde{\gamma}_4) = \tilde{\gamma}^{**}$$

and the first Frenet vectors of image curves are found as

$$T^{**} = \frac{\gamma^{**\prime}}{\|\gamma^{**\prime}\|_L}, \quad \tilde{T}^{**} = \frac{\tilde{\gamma}^{**\prime}}{\|\tilde{\gamma}^{**\prime}\|_L}$$

By doing the following calculations

$$\langle T^{**}, \tilde{T}^{**}\rangle_L = \frac{1}{\|\gamma^{**\prime}\|_L \|\tilde{\gamma}^{**\prime}\|_L}\langle \gamma^{**\prime}, \tilde{\gamma}^{**\prime}\rangle_L$$

$$= \frac{1}{\|\gamma^{**\prime}\|_L \|\tilde{\gamma}^{**\prime}\|_L}|A|^2\langle \gamma', \tilde{\gamma}'\rangle_L$$

is obtained. Since $\tilde{\gamma}$ and γ are involute-evolute curves, it can be written $\langle \gamma', \tilde{\gamma}'\rangle_L = 0$. So the below equation is found

$$\langle T^{**}, \tilde{T}^{**}\rangle_L = 0.$$

This result proves that $S(\tilde{\gamma})$ is spherical involute of $S(\gamma)$.

Theorem 2. The Poincare extension of Mobius transformations in E_2^4 keep being spherical involute-evolute curves.

Proof. From Lemma 4 and Lemma 5, we can say that the spherical involute evolute curves preserve their feature of being spherical involute-evolute under similarity and inverse transformations. We also know from Lemma 1 that mobius transformations can be written as a combination of similarity and inverse transformation. Therefore, we can say that the Mobius

transformation, which is written as the composition of these transformations, preserve its spherical involute-evolute.

Example 2. Let the unit speed and spacelike curve lying on H_0^3, $\gamma: I \to E_2^4$ defined by

$$\gamma(s) = \left(\frac{3s}{2}, coshs, sinhs, \frac{s}{2}\right)$$

Two of the Frenet frame vector fields $T(s)$ and $N(s)$ are given by

$$T(s) = \left(\frac{3}{2}, sinhs, coshs, \frac{1}{2}\right)$$

$$N(s) = (0, coshs, sinhs, 0)$$

It can easily be seen from here that $T(s)$ and $N(s)$ are spherical involute-evolute curves. According to this, from Lemma 4,

$$J\big(T(s)\big) = \left(\frac{3}{2}, -sinhs, coshs, \frac{1}{2}\right) = \gamma^*$$

$$J\big(N(s)\big) = (0, coshs, -sinhs, 0) = \tilde{\gamma}^*$$

and so,

$$T^*(s) = (0, -coshs, sinhs, 0)$$

$$\tilde{T}^*(s) = (0, sinhs, -coshs, 0)$$

By putting these expressions,

$$\langle T^*, \tilde{T}^* \rangle_L = 0$$

is obtained. Therefore, since $N(s)$ is spherical involute of $T(s)$, the image $J\big(N(s)\big)$ under the inversion transformation $J(z) = \frac{1}{z}$ is spherical involute of $J\big(T(s)\big)$.

Similarly, again, since $N(s)$ is spherical involute of $T(s)$, from Lemma 5,

$$S(T(s)) = \left(\frac{3a_{11}}{2} - a_{12}sinhs + b_{11}, a_{11}sinhs + \frac{3a_{12}}{2} + b_{12}, |A_1|coshs, \frac{|A_1|}{2}\right) = \gamma^{**}$$

$$S(N(s)) = (-a_{12}coshs + b_{11}, a_{11}coshs + b_{12}, |A_1|sinhs, 0) = \tilde{\gamma}^{**}$$

and so,

$$\gamma^{**\prime}(s) = (-a_{12}coshs, a_{11}coshs, |A_1|sinhs, 0)$$

$$\tilde{\gamma}^{**\prime}(s) = (-a_{12}sinhs, a_{11}sinhs, |A_1|coshs, 0)$$

By putting these expressions, because of $\left\|\gamma^{**\prime}\right\|_L \neq 0$ and $\left\|\tilde{\gamma}^{**\prime}\right\|_L \neq 0$,

$$\langle T^{**}, \tilde{T}^{**}\rangle_L = 0$$

is obtained. Therefore, since $N(s)$ is spherical involute of $T(s)$, the image $S(N(s))$ is spherical involute of $S(T(s))$.

4. Conclusions

Transformations defined in the expanded complex plane are called mobius transformations. This transformation can operate in four-dimensional spaces with the help of quaternions. This article was inspired by the question of whether curve pairs have access to the Mobius transformations property of converting circles into circles. The problem revealed in this study specifically for the involute-evolute curve pair under consideration. It has been demonstrated that a spherical curve pair is all that is necessary for Mobius transformations to keep their characteristic of being an involute-evolute curve pair. Future research will focus on the characteristics of other curve pairs whose properties are preserved by the Mobius transformations.

REFERENCES

Adler S. L. (1995). Quaternionic quantum mechanics and quantum Oelds. Oxford university press inc., New York.

Agrawal O. P. (1987). Hamilton operators and dual-number-quaternions in spatial kinematics. Mech. Mach. theory 22 (6), 569-575.

Amer R. B. M. (2014). Lecture Notes of Möbius Transformation in Hyperbolic Plane. Applied Mathematics, 5: 2216-2225.

Beardon, A. (1983). The Geometry of Discrete Groups. Springer-Verlag, Berlin.

Brannon, A. D., Esplen, M. F. and Gray, J. J. (1999). Geometry. Cambridge Uni. Press, Australia.

Deshmukh, S., Al-Dayel, I. and Ilarslan, K. (2017). Frenet Curves in Euclidean 4-Space. International Electronic Journal of Geometry, 10 (2): 56-66.

Düldül, M. (2010). Two and three dimensional regions from homothetic motions. Appl. Math. ENotes. 10, 86–93.

Jafari, M. and Yaylı, Y. (2015). Generalized quaternions and their algebraic properties. Communications Faculty of Sciences University of Ankara Series A1, 64 (1): 15-27.

Jones, G. A. and Singerman, D. (1987). Complex Functions, An Algebratic Geometric Viewpoint, Cambridge Uni. Press, Australia.

Hamilton, W. R. (1844). On quaternions; or on a new system of imagniaries in algebra. Lond. Edinb. Dublin Philos. Magn. J. Sci. 25(3), 489–495.

Kula, L. and Yaylı, Y. (2007). Split quaternions and rotations in semi-Euclidean E_2^4. J. Korean Math. Soc., 44 (6): 1313-1327.

Lehner, J. (1964). Discontinuous Groups and Autoformic Functions. Mathematical Surveys, 8. Providence, R.I.: American Mathematical Society.

Lundh, T., Udagawa, J., Hanel, S.E. and Otani, H. (2011). Cross- and Triple-Ratios of Human Body Parts During Development. Anatomical Record, 294(8), 1360-1369.

Niamsup, P. (2000). A note on the characteristics of Mobius transformations. J. Math. Anal. Appl., 248 (1): 203-215.

Nurkan, S. K. (2011). Mobius transformations in different geometries and Motions, Ankara University, Dissertation, Ankara.

Özgür, N. Y., Özgür, C. and Bulut, S. (2005). On the images of the helix under the Mobius ¨ Transformations. Nonlinear Func. Anal.& Appl., 10 (5), 743-749.

Petukhov, S. V. (1989). Non-euclidean geometries and algorithms of living bodies. Computers & Mathematics with Applications, 17(4-6):505–534.

Shoemake, K. (1985). Animating rotation with quaternion curves. In: Proceedings of the 12th Annual Conference on Computer Graphics and Interactive Techniques (SIG-GRAPH'85). ACM New York, USA, 19, 245–254.

Tunçer, Y., Ünal, S. and Karacan, M. K. (2020). Spherical Indicatrices of Involute of a Space Curve in Euclidean 3-Space. Tamkang Journal of Mathematics, 51(2), 113–121.

Ward, J.P. (1997). Quaternions and Cayley Numbers. Kluwer Academic Publishers, Boston.

Chapter 14

STATISTICAL INFERENCE FOR THE KUMARASWAMY WEIBULL DISTRIBUTION UNDER DOUBLY TYPE II CENSORING

Gamze GÜVEN[1]
Birdal ŞENOĞLU[2]

1 Dr. Öğr. Üyesi, Eskisehir Osmangazi University,
ORCID: 0000-0002-8821-3179, gamzeguven@ogu.edu.tr
2 Prof. Dr., Ankara University,
ORCID: 0000-0003-3707-2393, senoglu@science.ankara.edu.tr

1 INTRODUCTION

The Weibull distribution is one of the most widely used probability distribution in life testing experiments and reliability theory, see Weibull (1939). Therefore, different forms of the Weibull distribution, such as exponentiated Weibull, inverse Weibull, transmuted inverse Weibull, etc., have received tremendous attention in recent years. For example, Cordeiro et al. (2010) proposed another generalization of the Weibull distribution called as Kumaraswamy Weibull which is very flexible for modelling data sets in various different research areas, see Kumaraswamy (1980) in the context of Kumaraswamy distribution. In the rest of the paper, Kumaraswamy Weibull distribution is denoted as Kw-Weibull for brevity.

It should be noted that the experimenter may not always observe all observations in the fields of reliability analysis, survival analysis and life testing, etc. If the r_1 smallest and the r_2 largest observations are censored from the data, then the resulting data set is termed as doubly Type II censored. Complete samples ($r_1 = r_2 = 0$), left Type II censored samples ($r_1 = 0$) and right Type II censored samples ($r_2 = 0$) are the special cases of the doubly Type II censored samples.

There exists a vast literature about Type II censored samples in the context of parameter estimation. For example, Tiku (1967a) derived modified maximum likelihood (MML) estimators of the mean and standard deviation of the normal distribution, Balakrishnan and Varadan (1991) derived approximate maximum likelihood estimators for the extreme value distribution, Wu (2007) and Wu (2008) proposed joint confidence region for the parameters of two-parameter exponential distribution and Pareto distribution under Type II doubly censoring, respectively. Volterman et al. (2012) discussed nonparametric inferential methods and Feroze and Aslam (2012) considered Bayesian analysis of inverse Rayleigh distribution for the situation of doubly Type II censored samples. Pak et al. (2013) studied maximum likelihood (ML) estimation of the scale parameter of the Rayleigh distribution under doubly Type II censoring scheme when the lifetime observations are fuzzy. Çelik and Şenoğlu (2018) estimated the one-way ANOVA model parameters when the underlying distribution is Azzalini's skew normal and Yalçınkaya et al. (2021) used ML and maximum product of spacings (MPS) methods to estimate the parameters of the skew normal distribution for Type II censored samples.

In this paper, ML and MML estimators of the unknown parameters of the Kw-Weibull distribution are derived under doubly Type II censoring when the shape parameters are assumed to be known. Then the efficiencies of the estimators are investigated in terms of mean square error (MSE) criterion

using a Monte Carlo simulation study. At the end of the study, simulated data is analyzed for illustrative purposes.

2 METHODOLOGY

In this section, Kw-Weibull distribution is presented and then the ML and MML estimators of μ and σ are obtained for doubly Type II censored samples under the assumption of known shape parameters.

2.1 Kw-Weibull Distribution

Inserting the cumulative distribution function (cdf) of the Weibull distribution into the cdf of the Kumaraswamy distribution, Kw-Weibull cdf is obtained as follows

$$F(x) = 1 - \left\{1 - \left[1 - exp\left\{-\left(\frac{x-\mu}{\sigma}\right)^p\right\}\right]^a\right\}^b \quad x \geq \mu,\ p, \sigma > 0. \tag{1}$$

Then, the corresponding probability density function (pdf) of Kw-Weibull distribution is derived as

$$f(x) = \frac{abp}{\sigma}\left(\frac{x-\mu}{\sigma}\right)^{p-1} exp\left\{-\left(\frac{x-\mu}{\sigma}\right)^p\right\}\left[1 - exp\left\{-\left(\frac{x-\mu}{\sigma}\right)^p\right\}\right]^{a-1}\left\{1 - \left[1 - exp\left\{-\left(\frac{x-\mu}{\sigma}\right)^p\right\}\right]^a\right\}^{b-1} \tag{2}$$

Therefore, a random variable X with density function $f(x)$ is denoted as Kw-Weibull(a, b, p, σ, μ), see Cordeiro et al. (2010) for the moments and other mathematical features of the Kw-Weibull distribution.

Plots of the Kw-Weibull density function for different shape parameter values a, b and p are displayed in Figure 1.

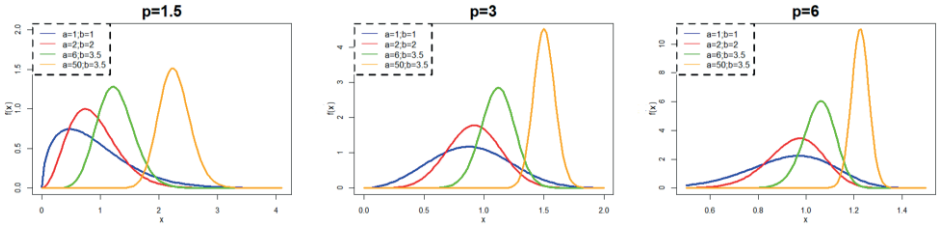

Figure 1: Kw-Weibull probability density functions for different shape parameter values.

The simulated skewness and kurtosis values of the Kw-Weibull distribution are presented below for better understanding the shape of the Kw-Weibull probability density functions.

$(a,b)=$	$(1,1)$	$(2,2)$	$(6,3.5)$	$(50,3.5)$
		$p=1.5$		
Skewness	1.072	0.715	0.331	0.287
Kurtosis	4.392	3.641	3.179	3.220
		$p=3$		
Skewness	0.168	0.041	-0.053	0.102
Kurtosis	2.728	2.899	3.041	3.093
		$p=6$		
Skewness	-0.374	-0.340	-0.257	0.009
Kurtosis	3.038	3.188	3.191	3.074

It can easily be seen from Figure 1 that Kw-Weibull distribution reduces to the Weibull, Exponential and Rayleigh distributions when $(a,b)=(1,1)$, $(a,b,p)=(1,1,1)$ and $(a,b,p)=(1,1,2)$, respectively.

2.2 Parameter Estimation

In this subsection, estimators of the location and scale parameters of the Kw-Weibull distribution are derived using ML and MML methodologies when the shape parameters a, b and p are known, see Tiku (1967b, 1968) in the context of MML methodology.

Let $x_{(r_1+1)}, \ldots, x_{(n-r_2)}$ be a doubly Type II censored sample of size $n-r_1-r_2$ from $X \sim$Kw-Weibull(a,b,p,σ,μ) distribution, then the likelihood (L) function is given by

$$L = \frac{n!}{r_1!r_2!}\left(\frac{1}{\sigma}\right)^{n-r_1-r_2}\left(\prod_{i=r_1+1}^{n-r_2} f\left(z_{(i)}\right)\right)\left\{F\left(z_{(r_1+1)}\right)\right\}^{r_1}\left\{1-F\left(z_{(n-r_2)}\right)\right\}^{r_2}. \quad (3)$$

Here, r_1 and r_2 denote the number of left and right censored observations, respectively. Also,

$$z_{(i)}=\frac{x_{(i)}-\mu}{\sigma},\ z_{(r_1+1)}=\frac{x_{(r_1+1)}-\mu}{\sigma} \text{ and } z_{(n-r_2)}=\frac{x_{(n-r_2)}-\mu}{\sigma}.$$

By taking logarithm of the likelihood function, the log likelihood $(\ln L)$ function is obtained as follows

$$\ln L = ln\left(\frac{n!}{r_1!r_2!}\right) - (n - r_1 - r_2)\ln\sigma + \sum_{i=r_1+1}^{n-r_2}\ln\left(f\left(z_{(i)}\right)\right) + r_1\ln\left(F\left(z_{(r_1+1)}\right)\right) + r_2\ln\left(1 - F\left(z_{(n-r_2)}\right)\right). \quad (4)$$

ML estimators of μ and σ are obtained by setting the derivatives of the $\ln L$ function to zero and then solving the following system of equations

$$\frac{\partial \ln L}{\partial \mu} = -\frac{1}{\sigma}\left(\sum_{i=r_1+1}^{n-r_2} g_1\left(z_{(i)}\right) + r_1 g_2\left(z_{(r_1+1)}\right) - r_2 g_3\left(z_{(n-r_2)}\right)\right) = 0 \quad (5)$$

and

$$\frac{\partial \ln L}{\partial \sigma} = -\frac{1}{\sigma}\left(n - r_1 - r_2 + \sum_{i=r_1+1}^{n-r_2} z_{(i)} g_1\left(z_{(i)}\right) + r_1 z_{(r_1+1)} g_2\left(z_{(r_1+1)}\right) - r_2 z_{(n-r_2)} g_3\left(z_{(n-r_2)}\right)\right) = 0. \quad (6)$$

Here,

$g_1\left(z_{(i)}\right) = \frac{f'\left(z_{(i)}\right)}{f\left(z_{(i)}\right)}$, $g_2\left(z_{(r_1+1)}\right) = \frac{f\left(z_{(r_1+1)}\right)}{F\left(z_{(r_1+1)}\right)}$ and $g_3\left(z_{(n-r_2)}\right) = \frac{f\left(z_{(n-r_2)}\right)}{1-F\left(z_{(n-r_2)}\right)}$.

It can easily be seen that this system of equations has no analytic solution and so numerical methods should be used. However, using numerical methods may cause to some problems such as non-convergence of iterations, convergence to wrong root, etc. Therefore, MML methodology which obtains explicit estimators of the parameters μ and σ is used by applying the following steps.

Step 1: The nonlinear functions $g_1(.)$, $g_2(.)$ and $g_3(.)$ in Eqs. (5) and (6) are linearized employing the Taylor series around $t_{(i)} = E(z_{(i)})$ $(i = r_1 + 1, \ldots, n - r_2)$, $t_1 = E(z_{(r_1+1)})$ and $t_2 = E(z_{(n-r_2)})$, respectively. The linearized forms of the $g_1(.)$, $g_2(.)$ and $g_3(.)$ functions are defined as follows

$$g_1\left(z_{(i)}\right) \cong \alpha_{1i} - \beta_{1i} z_{(i)}, \quad (7)$$

$$g_2\left(z_{(r_1+1)}\right) \cong \alpha_2 - \beta_2 z_{(r_1+1)} \quad (8)$$

and

$$g_3\left(z_{(n-r_2)}\right) \cong \alpha_3 + \beta_3 z_{(n-r_2)}, \quad (9)$$

respectively. Here,

$$\alpha_{1i} = \frac{f'(t_{(i)})}{f(t_{(i)})} + \beta_{1i} t_{(i)}, \quad \beta_{1i} = -\left(\frac{f''(t_{(i)}) f(t_{(i)}) - ((f'(t_{(i)})))^2}{\left(f(t_{(i)})\right)^2} \right), \quad \alpha_2 = \frac{f(t_1)}{q_1} + \beta_2 t_1, \quad \beta_2 = -\left(\frac{f'(t_1)}{q_1} - \frac{(f(t_1))^2}{q_1^2} \right), \alpha_3 = \frac{f(t_2)}{q_2} - \beta_3 t_2, \quad \beta_3 = \frac{f'(t_2)}{q_2} + \frac{(f(t_2))^2}{q_2^2},$$
$q_1 = r_1/(n+1)$ and $q_2 = 1 - r_2/(n+1)$.

Note that $t_{(i)}$, t_1 and t_2 cannot be obtained exactly, therefore their approximate values are obtained by solving the following equalities

$$\int_0^{t_{(i)}} f(z)dz = \frac{i}{n+1} \quad (i = r_1 + 1, \dots, n - r_2), \; F(t_1) = q_1 \text{ and } F(t_2) = q_2,$$

respectively. Here, $f(z) = abpz^{p-1} exp\{-z^p\}[1 - exp\{-z^p\}]^{a-1}\{1 - [1 - exp\{-z^p\}]^a\}^{b-1}$ is the standard Kw-Weibull distribution.

Step 2: Modified likelihood equations are obtained as follows by incorporating the equalities in Eqs. (7)-(9) into the Eqs. (5) and (6)

$$\frac{\partial \ln L^*}{\partial \mu} = -\frac{1}{\sigma}\left(\sum_{i=r_1+1}^{n-r_2} (\alpha_{1i} - \beta_{1i} z_{(i)}) + r_1(\alpha_2 - \beta_2 z_{(r_1+1)}) - r_2(\alpha_3 + \beta_3 z_{(n-r_2)}) \right) = 0 \tag{10}$$

and

$$\frac{\partial \ln L^*}{\partial \sigma} = -\frac{1}{\sigma}\left((n - r_1 - r_2) + \sum_{i=r_1+1}^{n-r_2} z_{(i)}(\alpha_{1i} - \beta_{1i} z_{(i)}) + r_1 z_{(r_1+1)}(\alpha_2 - \beta_2 z_{(r_1+1)}) - r_2 z_{(n-r_2)}(\alpha_3 + \beta_3 z_{(n-r_2)}) \right) = 0 \tag{11}$$

Step 3: Solutions of the Eqs. in (10) and (11) are called as MML estimators and obtained as follows

$$\hat{\mu} = K - D\hat{\sigma} \quad \text{and} \quad \hat{\sigma} = \frac{-B + \sqrt{B^2 + 4AC}}{2\sqrt{A(A-1)}} \tag{12}$$

Where

$$K = \left\{ \sum_{i=r_1+1}^{n-r_2} \beta_{1i} x_{(i)} + r_1 \beta_2 x_{(r_1+1)} + r_2 \beta_3 x_{(n-r_2)} \right\}/m, \; D = \left\{ \sum_{i=r_1+1}^{n-r_2} \alpha_{1i} + r_1 \alpha_2 - r_2 \alpha_3 \right\}/m,$$

$m = \sum_{i=r_1+1}^{n-r_2} \beta_{1i} + r_1\beta_2 + r_2\beta_3,\ A = n - r_1 - r_2,$

$B = \sum_{i=r_1+1}^{n-r_2} \alpha_{1i}\left(x_{(i)} - K\right) + r_1\alpha_2\left(x_{(r_1+1)} - K\right) - r_2\alpha_3\left(x_{(n-r_2)} - K\right)$
and

$C = \sum_{i=r_1+1}^{n-r_2} \beta_{1i}\left(x_{(i)} - K\right)^2 + r_1\beta_2\left(x_{(r_1+1)} - K\right)^2 + r_2\beta_3\left(x_{(n-r_2)} - K\right)^2.$

MML estimators of the parameters μ and σ are asymptotically equivalent to the corresponding ML estimators. Hence, they are asymptotically unbiased and efficient. They are also known to be robust against to the outliers in the direction(s) of the long tail(s). It is obvious that if $r_1 = r_2 = 0$, then $\hat{\mu}$ and $\hat{\sigma}$ in (12) reduce to the MML estimators of μ and σ for the complete samples, see Ergenç et al. (2022) in the context of complete samples.

3 MONTE CARLO SIMULATION

In this section, MSE's of the ML and MML estimators of the unknown parameters are compared under different sample sizes, shape parameters and number of censored observations using Monte-Carlo simulation. MSE values in Tables 1 and 2 are calculated using the following formula

$$MSE(\hat{\theta}) = Var(\hat{\theta}) + Bias^2(\hat{\theta})$$

where $\hat{\theta}$ represents the estimator of the parameter θ.

Note that without loss of generality the values of μ and σ are taken to be 0 and 1, respectively. The true shape parameter values, sample sizes and number of censored observations used in the simulation study are reported as follows:

Simulation setup

	(a, b)	n	(r_1, r_2)
p=1.5	(1, 1)	10 20 50	(0, 1) (0, 2)
	(2, 2) (6, 3.5) (50, 3.5)	10 20 50	(1, 1) (1, 2)
p=3	(1, 1) (2, 2) (6, 3.5) (50, 3.5)	10 20 50	(1, 1) (2, 2)

Random number generation: Random numbers are generated from the Kw-Weibull distribution via inverse transformation method. In other words, first uniform random variate from $U(0,1)$ is generated and then it is equated to the inverse of the cdf of the Kw-Weibull distribution as follows

$$X = \left(-\log\left[1-\left(1-[1-U]^{1/b}\right)^{1/a}\right]\right)^{1/p}\sigma+\mu\,. \tag{13}$$

Since μ and σ are taken to be 0 and 1, respectively, as said earlier Eq. (13) reduces to

$$X = \left(-\log\left[1-\left(1-[1-U]^{1/b}\right)^{1/a}\right]\right)^{1/p}.$$

Note that ML equations have no explicit solutions as mentioned before. Therefore, BFGS (Broyden-Fletcher-Goldfarb-Shanno) maximization method in the R Statistical Software (v4.1.2; R Core Team 2021) is used to solve them.

The simulation results presenting mean, variance and MSE values of the MML and ML estimators of the parameters μ and σ are based on 10,000 random samples, see Tables 1 and 2.

Table 1. Simulated mean, variance and MSE values for the location and scale parameters μ and σ; p=1.5.

		MML						ML					
		Mean	Variance	MSE	Mean	Variance	MSE	Mean	Variance	MSE	Mean	Variance	MSE
n	(r_1, r_2)		$\hat{\mu}$			$\hat{\sigma}$			$\hat{\mu}$			$\hat{\sigma}$	
						$(a, b) = (1, 1)$							
10	(0,1)	0.1730	0.0174	0.0473	0.8825	0.0581	0.0719	0.1139	0.0187	0.0317	0.8766	0.0562	0.0714
	(0,2)	0.1736	0.0177	0.0478	0.8651	0.0670	0.0852	0.1148	0.0193	0.0325	0.8596	0.0648	0.0845
20	(0,1)	0.1028	0.0068	0.0174	0.9280	0.0268	0.0320	0.0632	0.0072	0.0112	0.9334	0.0266	0.0310
	(0,2)	0.1019	0.0068	0.0172	0.9240	0.0285	0.0343	0.0621	0.0071	0.0109	0.9307	0.0283	0.0331
50	(0,1)	0.0517	0.0020	0.0046	0.9631	0.0106	0.0119	0.0300	0.0020	0.0029	0.9702	0.0105	0.0114
	(0,2)	0.0512	0.0019	0.0045	0.9623	0.0105	0.0119	0.0295	0.0019	0.0028	0.9700	0.0105	0.0114
						$(a, b) = (2, 2)$							
10	(1,1)	0.0713	0.0492	0.0543	0.9466	0.0769	0.0798	0.1034	0.0459	0.0566	0.8862	0.0674	0.0804
	(1,2)	0.0757	0.0527	0.0584	0.9372	0.0883	0.0922	0.1121	0.0484	0.0610	0.8703	0.0761	0.0930
20	(1,1)	0.0364	0.0191	0.0204	0.9754	0.0311	0.0317	0.0461	0.0187	0.0208	0.9497	0.0294	0.0320
	(1,2)	0.0393	0.0195	0.0211	0.9696	0.0331	0.0340	0.0495	0.0191	0.0215	0.9433	0.0313	0.0345
50	(1,1)	0.0170	0.0062	0.0065	0.9893	0.0105	0.0106	0.0174	0.0062	0.0065	0.9813	0.0103	0.0107
	(1,2)	0.0192	0.0063	0.0067	0.9866	0.0108	0.0110	0.0196	0.0063	0.0067	0.9788	0.0106	0.0111
						$(a, b) = (6, 3.5)$							
10	(1,1)	0.0614	0.1169	0.1207	0.9580	0.0750	0.0768	0.1322	0.1041	0.1215	0.8962	0.0657	0.0764
	(1,2)	0.0726	0.1358	0.1410	0.9460	0.0908	0.0937	0.1510	0.1187	0.1415	0.8772	0.0781	0.0932
20	(1,1)	0.0273	0.0477	0.0484	0.9816	0.0309	0.0313	0.0575	0.0454	0.0487	0.9541	0.0292	0.0313
	(1,2)	0.0305	0.0506	0.0515	0.9792	0.0335	0.0339	0.0617	0.0481	0.0519	0.9510	0.0316	0.0340
50	(1,1)	0.0125	0.0163	0.0165	0.9923	0.0107	0.0108	0.0228	0.0160	0.0166	0.9824	0.0105	0.0108
	(1,2)	0.0127	0.0164	0.0166	0.9909	0.0109	0.0110	0.0230	0.0162	0.0167	0.9811	0.0107	0.0110

						$(a,b)=(50,3.5)$							
10	(1,1)	0.0957	0.3869	0.3961	0.9602	0.0776	0.0791	0.2340	0.3391	0.3938	0.8969	0.0677	0.0783
	(1,2)	0.1307	0.4424	0.4595	0.9435	0.0902	0.0934	0.2827	0.3809	0.4608	0.8738	0.0774	0.0933
20	(1,1)	0.0379	0.1592	0.1607	0.9845	0.0320	0.0323	0.1001	0.1504	0.1604	0.9557	0.0302	0.0321
	(1,2)	0.0477	0.1661	0.1684	0.9803	0.0335	0.0339	0.1113	0.1567	0.1691	0.9509	0.0315	0.0340
50	(1,1)	0.0119	0.0570	0.0572	0.9951	0.0114	0.0114	0.0353	0.0559	0.0571	0.9841	0.0112	0.0114
	(1,2)	0.0160	0.0570	0.0573	0.9936	0.0115	0.0116	0.0391	0.0559	0.0574	0.9828	0.0113	0.0116

Table 2. Simulated mean, variance and MSE values for the location and scale parameters μ and σ; p=3.0.

		MML			ML			MML			ML		
		Mean	Variance	MSE	Mean	Variance	MSE	Mean	Variance	MSE	Mean	Variance	MSE
n	(r_1, r_2)		$\hat{\mu}$			$\hat{\sigma}$			$\hat{\mu}$			$\hat{\sigma}$	
						$(a, b) = (1,1)$							
10	(1,1)	0.0621	0.0594	0.0632	0.9361	0.0673	0.0714	0.1068	0.0541	0.0655	0.8813	0.0596	0.0737
	(2,2)	0.0794	0.0917	0.0980	0.9153	0.1056	0.1128	0.1459	0.0790	0.1003	0.8378	0.0885	0.1148
20	(1,1)	0.0337	0.0239	0.0250	0.9673	0.0265	0.0275	0.0498	0.0231	0.0256	0.9456	0.0253	0.0282
	(2,2)	0.0304	0.0296	0.0305	0.9695	0.0326	0.0335	0.0532	0.0283	0.0311	0.9417	0.0308	0.0342
50	(1,1)	0.0168	0.0080	0.0083	0.9853	0.0089	0.0091	0.0196	0.0079	0.0083	0.9798	0.0088	0.0092
	(2,2)	0.0125	0.0088	0.0090	0.9894	0.0097	0.0098	0.0180	0.0087	0.0090	0.9814	0.0095	0.0098
						$(a, b) = (2,2)$							
10	(1,1)	0.0514	0.0677	0.0704	0.9460	0.0744	0.0773	0.1057	0.0601	0.0713	0.8866	0.0653	0.0782
	(2,2)	0.0710	0.0969	0.1020	0.9230	0.1089	0.1148	0.1442	0.0818	0.1026	0.8434	0.0909	0.1154
20	(1,1)	0.0215	0.0275	0.0280	0.9774	0.0300	0.0305	0.0448	0.0262	0.0282	0.9516	0.0284	0.0308
	(2,2)	0.0209	0.0325	0.0329	0.9777	0.0358	0.0363	0.0484	0.0307	0.0330	0.9476	0.0336	0.0363
50	(1,1)	0.0076	0.0096	0.0096	0.9922	0.0104	0.0104	0.0154	0.0094	0.0097	0.9833	0.0102	0.0105
	(2,2)	0.0069	0.0103	0.0103	0.9934	0.0112	0.0112	0.0159	0.0101	0.0103	0.9834	0.0109	0.0112
						$(a, b) = (6, 3.5)$							
10	(1,1)	0.0437	0.0997	0.1016	0.9600	0.0773	0.0789	0.1140	0.0874	0.1004	0.8975	0.0676	0.0781
	(2,2)	0.0720	0.1414	0.1466	0.9354	0.1114	0.1156	0.1635	0.1181	0.1449	0.8539	0.0928	0.1142
20	(1,1)	0.0158	0.0401	0.0403	0.9857	0.0310	0.0312	0.0475	0.0379	0.0401	0.9574	0.0293	0.0311
	(2,2)	0.0240	0.0472	0.0478	0.9776	0.0367	0.0372	0.0591	0.0443	0.0478	0.9463	0.0344	0.0373
50	(1,1)	0.0052	0.0140	0.0140	0.9954	0.0109	0.0109	0.0172	0.0137	0.0140	0.9848	0.0106	0.0109
	(2,2)	0.0066	0.0154	0.0155	0.9940	0.0120	0.0120	0.0190	0.0151	0.0155	0.9829	0.0117	0.0120
						$(a, b) = (50, 3.5)$							
10	(1,1)	0.0597	0.1770	0.1805	0.9607	0.0786	0.0801	0.1537	0.1547	0.1783	0.8978	0.0686	0.0791
	(2,2)	0.0986	0.2525	0.2622	0.9345	0.1121	0.1164	0.2207	0.2105	0.2592	0.8529	0.0934	0.1150
20	(1,1)	0.0225	0.0707	0.0712	0.9855	0.0314	0.0316	0.0653	0.0666	0.0709	0.9568	0.0296	0.0315
	(2,2)	0.0288	0.0818	0.0827	0.9812	0.0363	0.0366	0.0760	0.0767	0.0825	0.9496	0.0340	0.0365
50	(1,1)	0.0102	0.0252	0.0253	0.9933	0.0112	0.0113	0.0264	0.0247	0.0254	0.9824	0.0110	0.0113
	(2,2)	0.0094	0.0269	0.0269	0.9939	0.0119	0.0120	0.0261	0.0263	0.0269	0.9826	0.0117	0.0120

According to the Tables 1 and 2, simulation results are summarized as follows.

According to Bias: MML estimators have smaller bias than the corresponding ML estimators for all values of the shape parameters a, b, p and sample sizes except for (a, b, p) = (1, 1, 1.5) and $n = 20$ and 50. However, ML estimator of μ has better performance than MML estimator in terms of bias criterion when (a, b, p) = (1, 1, 1.5) and $n = 10$.

According to MSE: Except for the case of (a, b, p) = (1, 1,1.5), MML and ML estimators show similar performances in terms of MSE criteria. For (a, b, p) = (1, 1,1.5), ML estimators (especially for $\hat{\mu}$) are superior to the corresponding MML estimators.

Also note that bias and MSE values of the MML and ML estimators decrease rapidly with increasing sample size as expected.

4 APPLICATION

In this section, simulated data set $n = 20$ is used to show the implementation of the theoretical results. Random sample of size $n = 18$ is generated from the Kw-Weibull(2,2,3,1,0) distribution. The remaining two observations are generated from the Kw-Weibull(2,2,3,3,0) and Kw-Weibull(2,2,3,0.1,0) distributions to create outliers defined as the observations lying far away from the bulk of the data. The data set is ordered in ascending way, see Table 3 given below.

Table 3. The simulated data set; $n = 20$.

0.0820564	0.5401349	0.5480824	0.6392717
0.7668069	0.7949512	0.8687057	0.8939567
0.8958074	0.9359419	0.9490846	0.9611112
1.0231863	1.0989476	1.1856698	1.1966247
1.2057479	1.2674934	1.3021582	2.4616920

Kw-Weibull quantile-quantile (Q-Q) plot of the simulated data is given in Figure 2.

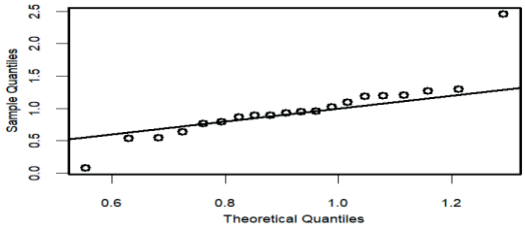

Figure 2. Kw-Weibull Q-Q plot of the simulated data.

It can be seen from Figure 2 that the largest and smallest observations (i. e., 2.4616920 and 0.0820564, respectively) deviate from the straight line as expected. Therefore, they are censored by taking $r_1 = r_2 = 1$ and the MML and ML estimates are obtained as follows:

MML		ML	
$\hat{\mu}$	$\hat{\sigma}$	$\hat{\mu}$	$\hat{\sigma}$
-0.201	1.247	-0.171	1.214
(0.610)	(0.716)	(0.597)	(0.701)

*The bootstrap standard errors of the estimates are given in parenthesis.

Although, the standard errors of the MML and ML estimates of the parameters μ and σ are close to each other, standard errors of the ML estimates are just a little bit smaller than those of the MML estimates as expected. These results are in agreement with the simulation results given in Table 2.

It should be noted that the values of A, B, C, D, K, m in Eq. (12) are obtained as follows in calculating the MML estimates.

$A = 18, \quad B = -1.177179, \quad C = 25.01047, \quad D = 0.9158486, \quad K = 0.9408173$ and $m = 400.3191$.

5 CONCLUDING REMARKS

In this paper, we derive the MML estimators of the unknown parameters of the Kw-Weibull distribution based on doubly Type II censored data. Efficiencies of these estimators are compared with the corresponding ML estimators via Monte Carlo simulation using R Statistical Software (v4.1.2; R Core Team 2021) in terms of MSE criterion. Monte-Carlo simulation results indicate that ML and MML estimators show similar performances except for the case of $(a, b, p) = (1, 1, 1.5)$. ML estimators show improved performance than MML estimators in the mentioned case. It should also be noted that estimating the parameters of the Kw-Weibull distribution under doubly Type II censoring using the MML method overcomes the drawbacks of the iterative methods. Therefore, it can comfortably be used as an alternative to the iterative ML method.

REFERENCES

Balakrishnan, N., & Varadan, J. (1991). Approximate MLEs for the location and scale parameters of the extreme value distribution with censoring. *IEEE Transactions on Reliability*, *40*(2), 146-151.

Cordeiro, G. M., Ortega, E. M., & Nadarajah, S. (2010). The Kumaraswamy Weibull distribution with application to failure data. *Journal of the Franklin Institute*, *347*(8), 1399-1429.

Çelik, N., & Şenoğlu, B. (2018). Robust estimation and testing in one-way ANOVA for Type II censored samples: skew normal error terms. *Journal of Statistical Computation and Simulation, 88*(7), 1382-1393.

Ergenç C., Güven G., & Şenoğlu B. (2022). "Estimating Parameters of Kumaraswamy Weibull Distribution" 6th International Conference on Mathematics "*An Istanbul Meeting for World Mathematicians*" 21-24 June, 2022, Istanbul, Turkey.

Feroze, N., & Aslam, M. (2012). On posterior analysis of inverse Rayleigh distribution under singly and doubly type II censored data. *International Journal of Probability and Statistics*, *1*(5), 145-152.

Kumaraswamy, P. (1980). A generalized probability density function for double-bounded random processes. *Journal of hydrology*, *46*(1-2), 79-88.

Pak, A., Parham, G. A., & Saraj, M. (2013). On estimation of Rayleigh scale parameter under doubly type-II censoring from imprecise data. *Journal of Data Science, 11*(2), 305-322.

Tiku, M. L. (1967a). Estimating the mean and standard deviation from a censored normal sample. *Biometrika, 54*(1-2), 155-165.

Tiku, M. (1967b). A note on estimating the location and scale parameters of the exponential distribution from a censored sample. *Australian Journal of Statistics, 9*(2), 49-54.

Tiku, M. L. (1968). Estimating the parameters of log-normal distribution from censored samples. *Journal of the American Statistical Association, 63*(321), 134-140.

Volterman, W., Balakrishnan, N., & Cramer, E. (2012). Exact nonparametric meta-analysis for multiple independent doubly Type-II censored samples. *Computational Statistics & Data Analysis, 56*(5), 1243-1255.

Weibull, W. (1939). A statistical theory of the strength of material. Ingen. Vetensk. Acad. Handl. 151, 1–45.

Wu, S. F. (2007). Interval estimation for the two-parameter exponential distribution based on the doubly type II censored sample. *Quality & quantity*, 41, 489-496.

Wu, S. F. (2008). Interval estimation for a Pareto distribution based on a doubly type II censored sample. *Computational statistics & data analysis, 52*(7), 3779-3788.

Yalçınkaya, A., Yolcu, U., & Şenoğlu, B. (2021). Maximum likelihood and maximum product of spacings estimations for the parameters of skew-normal distribution under doubly type II censoring using genetic algorithm. *Expert Systems with Applications*, *168*, 114407.